DISS. ETH NO. 14801

UNSTABLE ALPINE PERMAFROST: A POTENTIALLY IMPORTANT NATURAL HAZARD – VARIATIONS OF GEOTECHNICAL BEHAVIOUR WITH TIME AND TEMPERATURE

A dissertation submitted to the

SWISS FEDERAL INSTITUTE OF TECHNOLOGY ZURICH

for the degree of

Doctor of Technical Sciences

presented by

LUKAS URS ARENSON

Dipl. Bauingenieur ETH

born December 14, 1972

citizen of Zurich and Basle

accepted on the recommendation of

Prof. Dr. Sarah M. Springman, examiner

Prof. Dr. Michael C.R. Davies, co-examiner

Prof. Dr. Andrew C. Palmer, co-examiner

Zurich, 2002

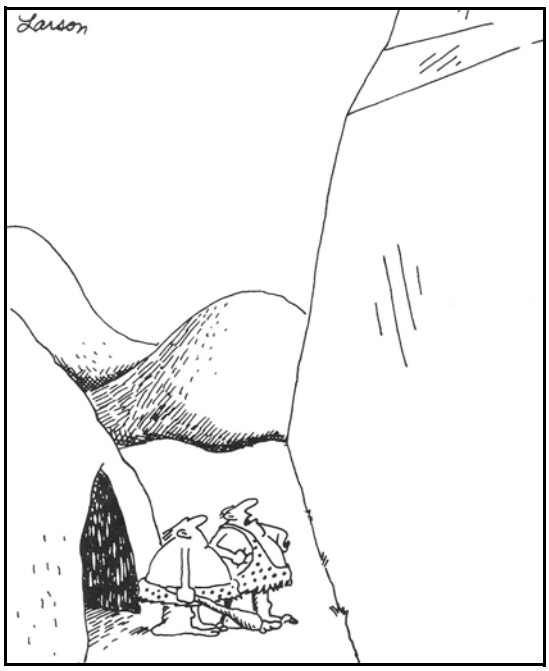

“Say, Thag ... wall of ice closer today?”

Contents

Abstract

In Switzerland, degrading or thawing permafrost has been identified as being an issue of national importance with respect to its potential for causing severe damage or even loss of life in densely populated Alpine regions due to climate change. On this basis, a joint project was initiated between three Institutes of the Swiss Federal Institute of Technology, Zurich: Institute for Geotechnical Engineering, Institute for Geophysics and the Laboratory for Hydraulics, Hydrology and Glaciology. This thesis deals with the variations of the geotechnical behaviour of Alpine permafrost with time and temperature. However, input from several other sub-projects have been used in order to interpret and analyse the geotechnical results.

Permafrost may be found in Alpine regions at elevations from about 2500 m above sea level, depending on the location and the exposure. A special geomorphological feature within permafrost is called a rock glacier. Active rock glaciers are composed of ice, solids, water and air. They tend to be covered with boulders and to creep down-slope due to gravitational forces. Six boreholes were drilled within two active rock glaciers in the Engadin, Swiss Alps, in order to study the behaviour of this special type of frozen soil. Cores were analysed and tested in the laboratory, and several field investigations were carried out in the boreholes.

The stratigraphy of the two rock glaciers could be determined from the drillings and additional geophysical investigations in the boreholes and from the surface. Both rock glaciers show high volumetric ice content, or even pure ice, underneath the 2 – 4 m thick active layer that consists mainly of large boulders. Volumetric air content in the frozen soil was found to be more than 20% within some layers and during the drilling, the flushing air completely disappeared into the ground. These observations corroborate evidence that several open channels have to be expected within the rock glaciers, allowing air and water circulation through the frozen body. Temperature measurements confirm the existence of a thermal disturbance within the permafrost at the Murtèl-Corvatsch rock glacier. Underneath the permafrost base, there is a highly permeable layer, which facilitates the drainage of melt water from the permafrost layer. Furthermore, seasonal temperature changes were observed at the Muragl rock glacier in the permafrost, indicating that this layer must be connected to the atmosphere. Air

circulation underneath the permafrost may result in an acceleration of the permafrost degradation. The deformation measurements within the rock glaciers reveal that a distinct shear zone exists, where more than 60% of the total deformation was observed. This shear zone was determined to correspond with the permafrost base for the Muragl rock glacier, indicating that the frozen soil at the location of the drillings only exists because it has been carried down-slope within the rock glacier. The shear zone within the Murtèl-Corvatsch rock glacier is situated at a depth in-between the ice-rich part and layers with frozen boulders, cobbles and gravel. Seasonal changes were observed in the deformation for the Muragl rock glacier, whereas the Murtèl-Corvatsch rock glacier creeps about nine times slower at a rate that is more or less constant throughout the year.

Triaxial creep and shear tests at temperatures between -4.5 and -1.0°C on artificially frozen and natural permafrost samples from the two rock glaciers resulted in new insight into the behaviour of frozen soils. A Glen type creep law was used in order to describe the steady state creep conditions. The creep parameters are strongly dependent on the structure and the temperature. Close to the melting point of the ice, an exponential increase of the unfrozen water results in a rapid change of the activation energy and therefore, large creep strains. Low volumetric ice content increases structural hindrance between the solid particles, resulting in a decreasing creep susceptibility. However, even though samples with low volumetric ice content creep generally less than samples with high volumetric ice content, the increase of creep deformation with an increasing load is much more significant for the first composition. No tertiary creep, i.e. creep failure, may be expected under the stress conditions that are anticipated within the two rock glaciers under investigation. The sample response during shear tests allowed interpretation on a micro-structural level. It seems, that depending on the volumetric air, solid and ice content, and the applied strain rate, the behaviour changes from brittle to dilatant (or ductile). Compression of the sample resulting in a ductile response occurs due to air cavities, whereas the existence of solid particles increases structural hindrance and dilatant behaviour has to be expected. Volume changes were recorded during the test due to the compression of air voids, even though the tests were performed without permitting drainage to take place.

The experimental work in the laboratory and the field investigations have allowed statements concerning the stability of the two rock glaciers to be made. Permafrost degradation is a gradual process and therefore, sudden failure of the whole rock glacier may not be expected. However, in combination with increasing active layer thickness and water run-off on the permafrost table, debris flows can be triggered at the tongue and within the top layer. Depending on the environment of the rock glacier forefield, these debris flows could be enlarged. Due to the air and water permeability through cavities within the rock glacier, thermal disturbances can occur that result in faster movements and accelerate the degradation of the permafrost.

However, further investigations are necessary into the volumetric behaviour of frozen soils during creep and shear, as well as a better knowledge about the hydrology within rock glaciers is required. This awareness might help for future numerical modelling of rock glacier response on climate change with a method that allows to model the interaction between the different phases.

Zusammenfassung

Aufgrund des Gefährdungspotentiales im dicht besiedelten alpinen Raum in der Schweiz, wurde im Zusammenhang mit einer Klimaveränderung, degradierender, d.h. auftauender Permafrost als ein Problem von nationaler Bedeutung angesehen. Drei Institute der Eidgenössischen Technischen Hochschule in Zürich (Institut für Geotechnik, Institut für Geophysik und die Versuchsanstalt für Wasserbau, Hydrologie und Glaziologie) haben im Anschluss daran ein gemeinsames Projekt injiziert. Die vorliegende Arbeit befasst sich mit der Veränderung des geotechnischen Verhaltens von alpinem Permafrost über die Zeit und veränderlichen Temperaturen. Für die Interpretation dieser geotechnischen Ergebnisse wurden aber auch die Resultate der Partnerprojekte miteinbezogen.

Je nach Lage und Exposition können Dauerfrostböden (Permafrost) im alpinen Raum in Höhenlagen ab etwa 2500 m über Meer vorgefunden werden. Eine geomorphologisch spezielle Vorkommensart von Permafrost ist ein sogenannter Blockgletscher. Aktive Blockgletscher bestehen aus Eis, Feststoffen, Wasser und Luft, sind meist mit Geröll bedeckt und kriechen aufgrund der Schwerkraft talwärts. Um das Verhalten von Blockgletschern zu untersuchen, wurden insgesamt sechs Bohrlöcher in zwei aktive Blockgletscher im Oberengadin, Schweiz, abgetäuft. Die gewonnenen Bohrkerne wurden im Labor analysiert und mechanisch getestet. In den Bohrlöchern wurden zusätzlich verschiedene Untersuchungen durchgeführt und mit den Laborergebnissen verglichen.

Der Schichtaufbau der Blockgletscher konnte aufgrund der Bohrungen, sowie geophysikalischen Messungen in den Bohrlöchern aber auch von der Oberfläche aus bestimmt werden. Beide Blockgletscher zeigen sehr hohe Eisgehalte und reines Eis unterhalb einer 2 – 4 m dicken aktiven Zone, welche aus groben Blöcken besteht und im Sommer jeweils auftaut. Es wurde ein volumetrischer Luftgehalt von teilweise mehr als 20% gemessen und während den Bohrungen ging die Spülluft teilweise komplett im Untergrund verloren. Diese Beobachtungen erhärten die Vermutung, dass verschiedene offene Verbindungen in einem Blockgletscher vorhanden sein können, in welchen Wasser und Luft zirkulieren kann. Zusätzlich Temperaturmessungen bestätigen diese Vermutung und zeigen thermische Unregelmässigkeiten im Blockgletscher Murtèl-Corvatsch. Unterhalb der Permafrostbasis wurde eine sehr durchlässige Schicht festgestellt, welche eine gute Drainage des geschmolzenen Wassers aus der

Permafrostschicht zulässt. Im Muragl Blockgletscher sind in dieser Schicht saisonale Schwankungen in der Temperatur gemessen worden, welche auf eine Verbindung zur Atmosphäre hindeuten und zu einem beschleunigten Auftauen des Permafrostes führen können. Die Deformationsmessungen in den Blockgletschern zeigen, dass mehr als 60% der gesamten Verformung in einer konzentrierten Scherschicht stattfindet. Im Blockgletscher Muragl lag diese Scherschicht direkt über der Permafrostbasis, während sie im Blockgletscher Murtèl-Corvatsch in einer Schicht zwischen dem eisreichen Teil und den Schichten mit mehr Blöcken, Steinen und Kies zu finden ist. Für den ersten Fall bedeutet dies, dass dort der Permafrost nur existiert, weil er innerhalb des Blockgletschers von weiter oben nach unten transportiert wurde. Im Blockgletscher Muragl wurden aufgrund der höher gelegenen Scherschicht saisonale Schwanken in den Deformationen gemessen, während der Blockgletscher Murtèl-Corvatsch etwa neunmal langsamer, aber konstant talwärts kriecht.

Triaxiale Kriech- und Scherversuche an künstlichen und original Permafrostproben der beiden Blockgletscher bei Temperaturen zwischen -4.5°C und -1.0°C ergaben neue Einsichten in das Verhalten von gefrorenen Böden. Das Kriechen kann mit einer Glen'schen Kriechfunktion beschrieben werden, wobei die Parameter sowohl temperatur-, als auch eisgehaltsabhängig sind. Nahe dem Schmelzpunkt nimmt die Aktivierungsenergie aufgrund des hohen Anteils an Wasser exponentiell zu, und dies führt zu erhöhten Kriechdehnraten. Ein niedriger Eisgehalt fördert eine gegenseitige Verkeilung der festen Körner und deshalb ist die Kriechempfindlichkeit geringer. Mit einer Beschleunigung der Kriechdeformationen, d.h. Kriechversagen, muss für die untersuchten Spannungszustände, welche in den Blockgletschern angenommen wurden, nicht gerechnet werden. Das Verhalten der Proben während den Scherversuchen lässt zudem Interpretationen auf der Ebene der Mikrostruktur zu. Je nach Verformungsgeschwindigkeit, Eis- und Luftgehalt, tritt ein sprödes, duktiles oder dilatantes Verhalten ein. Eine grosse Anzahl von Luftporen erlauben ein Zusammendrücken der Probe, so dass diese sich duktil verhält. Demgegenüber führt eine grosse Anzahl an Bodenkörnern zu einer Dilatanz, da die Körner sich gegenseitig behindern. Obwohl die Versuche undrainiert durchgeführt wurden, wurde ein Volumenveränderung während dem Abscheren gemessen.

Aufgrund der Feld- und Laborexperimente können Aussagen über die Stabilität der beiden Blockgletscher gemacht werden. Da das Auftauen ein sehr langsamer aber stetiger Prozess ist, muss nicht mit einem dramatischen Versagen eines Blockgletschers gerechnet werden. Durch eine Vergrösserung der aktiven Zone an der Oberfläche, können durch Starkniederschläge oder Schmelzwasser Murgänge ausgelöst werden, welche sich je nach Umgebung, im Vorfeld stark vergrössern können. Wasser- und Luftzirkulationen unterhalb und im Blockgletscher führen durch die thermische Störung zu einem beschleunigten Schmelzen des Permafrostes und zu einer Zunahme der Kriechdeformationen.

Um das Verhalten der Blockgletscher besser zu verstehen, sind jedoch noch weitere Untersuchungen bezüglich deren Hydrologie, aber auch in Bezug auf das Volumenverhalten von gefrorenen Böden unter Belastung erforderlich. Diese Erkenntnisse sollten dazu helfen in Zukunft Blockgletscher numerisch zu modellieren. Am erfolgversprechendsten dürften Methoden sein, welche die Interaktion zwischen den einzelnen Phasen richtig erfassen können.

List of Tables

List of Figures

List of Symbols

A	creep parameter: $\dot{\varepsilon} = A \cdot \sigma^n$	
-	strain rate at time t_1 and $q = 0$	*(Eq. 2-8)*
-	cross sectional area	
-	amplitude of TDR signal	
-	creep parameter for primary creep approach (pressuremeter test): $\varepsilon_{vp} = A\left(\frac{\sigma_e}{\sigma_c}\right)^{n_1} t^b$	
B	creep parameter: $\dot{\varepsilon} = B \cdot exp\left(\frac{-Q}{RT}\right) \cdot \sigma^n$	
-	length of signal during TDR calibration test	
C	heat capacity [J/m^{3}K]	
C_0	amplitude in velocity	
D	diameter	
-	spacing between two supports during TDR calibration test	
D_r	relative soil density	
E	Young's modulus [MPa]	
F	area	
ΔF	Height of energy barrier that has to be surmounted for a deformation λ	*(Fig. 2-6)*
G	shear modulus [MPa]	
H	height	
$H_{1,2}$	minimum and maximum mean normal stress for shear stress $\tau_i = 0$ kPa	*(Fig. 2-23)*
I_1	first invariant of the strain tensor	
I_{2D}	second invariant of the strain tensor	
J_1	first invariant of the stress tensor	
J_{2D}	second invariant of the stress tensor	
K	earth-pressure coefficient: ratio between horizontal and vertical effective stress	
-	flexibility ratio	*(Eq. 3-3)*
-	creep parameter: $t_m = K / \sigma^n$	*(Fig. 2-30)*
-	thermal conductivity [W/mK]	
K_{Ic}	fracture toughness (or stress intensity factor) mode I [kNm$^{-3/2}$]	
M	mass	
-	inclination of the critical state line in *p'-q* space (critical state soil mechanics)	
N	Avogadro's number: $6.022 \cdot 10^{23}$ mole^{-1}	
Q	activation energy [kJ/mole]	
Q_p	activation energy for the soil skeleton [kJ/mole]	

Q_u activation energy for the unfrozen water [kJ/mole]

R universal gas constant: $N \cdot k$ = 8.314 $J \cdot K^{-1} \cdot mole^{-1}$

- appropriate confining ratio *(Eq. 2-48)*

R^2 correlation coefficient

S specific surface area of frozen soil

T temperature

T_m melting temperature *(Fig. 2-29)*

T_M mean annual surface temperature *(Fig. 2-1)*

T_n normalised temperature: 273.16 °K

T_t temperature at triple point

V volume

V_{ext} ice volume - voids volume, *ice-rich* soil: $V_{ext} > 0$

W work that has to be input in order to re-break bonds in shear

X parameter, relating activation frequency to strain rate:

$$A = X \cdot \frac{kT}{h}$$

a soil parameter: $\varepsilon = \frac{1}{b} sinh(a\sigma)$ *(Eq. 2-18)*

- soil parameter to link CSR with CSC tests: $\varepsilon_{min} = a \cdot e^{b \cdot q_{res}}$ *(Eq. 5-11)*

- adjustable coefficient

$$p_m = p_t \left\{ 1 + a \left[1 - \left(\frac{T}{T_t} \right)^n \right] \right\} \quad \textit{(Eq. 2-24)}$$

- regression parameter: $lnw_u = a + b\,lnS + cS^d\,lnT$ *(Eq. 2-27)*

- axis intercept of q-axis (p-q diagram, critical state soil mechanics)

- creep parameter for steady state creep approach (pressuremeter test):

$$\dot{\varepsilon}_{vp,\,min} = a\sigma_e^{\,n_2}$$

b creep parameter (pressuremeter test):

$$\varepsilon_{vp} = A \left(\frac{\sigma_e}{\sigma_c} \right)^{n_1} t^b$$

- soil parameter: $\varepsilon = \frac{1}{b} sinh(a\sigma)$ *(Eq. 2-18)*

- = tan ϕ

- soil parameter to link CSR with CSC tests:

$$\varepsilon_{min} = a \cdot e^{b \cdot q_{res}} \quad \textit{(Eq. 5-11)}$$

- regression parameter: $lnw_u = a + b\,lnS + cS^d\,lnT$ *(Eq. 2-27)*

c cohesion

- regression parameter: $lnw_u = a + b\,lnS + cS^d\,lnT$ *(Eq. 2-27)*

- specific heat capacity

d diameter

- regression parameter: $lnw_u = a + blnS + cS^d lnT$ *(Eq. 2-27)*

- crack length

dh length of inclinometer probe (61 cm)

dt time in-between two readings (slope inclinometer)

du horizontal deformation in-between two readings (slope inclinometer)

e voids ratio

f $= \frac{r}{2a}$

$2a$: length of parent, sliding crack
r: creep zone radius to be determined after Riedel-Rice (1980) model

h Planck's constant: $6.626 \cdot 10^{-34}$ J/s

- length of secondary crack

$h_{1,2}$ absolute value of minimum and maximum mean normal stress for shear stress $\tau_i = 0$ kPa *(Fig. 2-23)*

k Boltzmann's constant: $1.380 \cdot 10^{-23}$ J/K

l length of pile

m slope of a straight line representing logarithmic strain rate versus logarithmic time *(Eq. 2-17)*

n creep parameter: $\dot{\varepsilon} = A \cdot \sigma^n$

- exponent:

$$p_m = p_t\left\{1 + a\left[1 - \left(\frac{T}{T_t}\right)^n\right]\right\} \quad \textit{(Eq. 2-24)}$$

- porosity

n_1 creep parameter for primary creep approach (pressuremeter test):

$$\varepsilon_{vp} = A\left(\frac{\sigma_e}{\sigma_c}\right)^{n_1} t^b$$

n_2 creep parameter for steady state creep approach (pressuremeter test)

$$\dot{\varepsilon}_{vp,\,min} = a\sigma_e^{\,n_2}$$

p hydrostatic pressure: $\frac{J_1}{3} = \frac{1}{3}(\sigma_1 + \sigma_2 + \sigma_3)$

- pressure acting at the borehole wall during pressuremeter test

*p** melting pressure of ice

p_n normalised pressure: 0.000611657 kPa

p_m melting pressure

p_t pressure at triple point

q second invariant of stress:

$$\sqrt{3J_{2D}} = \frac{3}{\sqrt{2}}\tau_{oct} = \sqrt{\frac{1}{2}[(\sigma_1-\sigma_2)^2+(\sigma_2-\sigma_3)^2+(\sigma_3-\sigma_1)^2]}$$

under conditions of triaxial compression, $\sigma_c = \sigma_2 = \sigma_3$,
q = deviator stress: $\sigma_1 - \sigma_3$

- heat flow per unit area

q_{max} peak deviatoric stress

q_{res} residual deviatoric stress

r radius

t time

- thickness of coaxial cable

t_m time until inflection between primary and tertiary creep *(Fig. 2-30)*

t_r pulse generation time

t_v constant phase shift

u displacement

- pore pressure

$v_{surface}$ surface velocity

v_0 initial velocity

w width between secondary cracks

w_i volumetric ice content

Δw_{res} relative movement needed between pile and soil for the value of skin friction to reduce from peak to residual in a strain-softening soil

w_u gravimetric unfrozen water content

x distance of crimp from origin during TDR calibration test

y deflection of coaxial cable during TDR calibration test

y_i original value

$\bar{y}_i$ calculated value

α value of the slope of the mid-range linear portion of a plot of logarithmic strain rate versus deviator stress, all points corresponding to the same time after load application

- soil parameter: $w_u = \alpha \cdot T^{\beta}$ *(Eq. 2-26)*

- thermal diffusivity [m^2/K]: K/C

β soil parameter: $w_u = \alpha \cdot T^{\beta}$ *(Eq. 2-26)*

- slenderness ratio of microcolumn *(Eq. 2-48)*

Γ surface energy *(Eq. 2-48)*

γ coefficient of volume change due to temperature [K^{-1}]

- surface free energy [J/m^2] *(Eq. 2-49)*

γ_{oct} octahedral shear strain

Δ increment

δ	elastic distortion of the material structure under a shear force	
-	time hardening parameter	
ε	strain	
ε_{ij}	deviatoric strain tensor: $I_1 = (\varepsilon_1 + \varepsilon_2 + \varepsilon_3)$	
ε	equivalent strain: $\sqrt{3I_{2D}} = \frac{3}{\sqrt{2}}\gamma_{oct} = \sqrt{\frac{1}{2}[(\varepsilon_1-\varepsilon_2)^2 + (\varepsilon_2-\varepsilon_3)^2 + (\varepsilon_3-\varepsilon_1)^2]}$	
$\dot{\varepsilon}$	strain rate	
$\bar{\dot{\varepsilon}}$	equivalent strain rate	*(Fig. 2-29)*
$\dot{\varepsilon}_c$	arbitrary reference creep strain rate (pressuremeter tests)	
$\dot{\varepsilon}_t$	transition strain rate under biaxial compression	*(Eq. 2-50)*
θ_u	volumetric unfrozen water content	
λ	distance between two equilibrium (stable) positions	
μ	friction coefficient	
μ_σ	viscosity	
ν	Poisson's ratio	
π	= 3.14159	
ρ	density	
ρ_b	bulk density	
ρ_d	dry density	
σ	stress	
σ	equivalent stress: $\frac{1}{2}[(\sigma_1-\sigma_2)^2 + (\sigma_2-\sigma_3)^2 + (\sigma_3-\sigma_1)^2]$	*(Fig. 2-29)*
σ_c	confining pressure in triaxial apparatus	
-	reference stress corresponding to $\dot{\varepsilon}_c$ (pressuremeter tests)	
σ_e	*von Mises* equivalent stress: $\frac{1}{2}\sqrt{(\sigma_1-\sigma_2)^2 + (\sigma_2-\sigma_3)^2 + (\sigma_3-\sigma_1)^2}$	
σ_m	mean normal stress	
σ_{0H}	horizontal total stress at rest	
σ_{0V}	vertical total stress at rest	
τ	shear stress	
-	normalised time t/t_m, normalised strain $\varepsilon/\varepsilon_m$	*(Fig. 2-30)*
τ_{oct}	octahedral shear stress	
τ_s	shaft shear stress	*(Eq. 3-3)*
ϕ	angle of friction	
ψ	integration factor for creep strain	
ψ_m	integration constant for creep strain at failure ε_m	
ω_0	multiplier for the time	*(Eq. 3-2)*
$Ø_i$	inner diameter	
$Ø_o$	outer diameter	

subscripts

a	axial
f	failure
g	gas
h	horizontal
i	ice
	i = 1, 2, 3, ... n
ij	tensor
p	pile
r, rr	radial
s	solid
uw	unfrozen water
v, zz	vertical
v	voids
w	water
H	Hookean element
$\theta\theta$	circumferential
σ	Newtonien element
∞	at infinity
0	initial state
1, 2, 3	principal directions

superscript:

e	elastic
ie	instantaneous elastic
ve	viscoelastic
vp	viscoplastic

Abbreviations

A.D.:	Anno Domini
BTS:	Bottom Temperature of the Snow cover
cf.:	*confer* (compare)
CSC:	constant stress (creep)
CSR:	constant strain rate
e.g.:	for example
etc.	*etcetera*
ETH:	Eidgenössische Technische Hochschule: Swiss Federal Institute of Technology
GM:	silty gravels, gravel-sand-silt mixtures
GPR:	ground penetrating radar
GW:	well graded gravels, gravel-sand mixtures, or sand-gravel-cobble mixtures
i.e.:	*id est* (that is)
IG:	Institute of Geophysics: Institut für Geophysik
IGT:	Institute for Geotechnical Engineering: Institut für Geotechnik
IPA:	International Permafrost Association
LVDT:	linear variable differential transformer
m asl:	metres above sea level
MSP:	multiple sieve pluviation
n/a:	not available
N-Nl:	Neutron – Neutron, long
N-Ns:	Neutron – Neutron, short
PACE	Permafrost and Climate in Europe (EU Programme)
PE:	polyethylene
PERMOS:	Permafrost monitoring Switzerland
PU:	polyurethane
PVC:	polyvinyl chloride
PW:	porewater
PWP:	porewater pressure
SN:	Swiss code
SZ:	shear zone
TDR:	time domain reflectometry
temp.:	temperature
USCS:	unified soil classification system
VAW:	Laboratory for Hydraulics, Hydrology and Glaciology: Versuchsanstalt für Wasserbau, Hydrologie und Glaziologie
WR:	wet rodding
ZAA:	zero annual amplitude

^{14}C: radiocarbon

Introduction

Research on *Geocryology*, as defined below, began with early reports on permafrost in the USSR at the beginning of the 20th century. The term *Geocryology* is highly generalised and was defined by Brown and Kupsch (1974) as '*The study of earth materials having a temperature below 0°C*'. This definition is entirely based on the temperature and is therefore independent of the water and the ice content of the soil or the rock. Beside the temperature, the definition of *Permafrost* contains a boundary condition relating to the time. According to Brown and Kupsch (1974), the ground must have temperatures below zero degrees centigrade over at least two consecutive winters and the intervening summer. Depending on the source, between 20% (Brown, 1997) and 25% (Yershov, 1998) of the Earth's surface is underlain by permafrost or perennially frozen ground.

Scientifically based permafrost research in Switzerland started only about 30 years ago and has focused primarily on permafrost evolution, geomorphological mapping, photogrammetrical studies, and borehole temperatures as well as deformation monitoring of soils containing ice. This relatively short research history is more astonishing, since the risk potential of permafrost has been mentioned already in the fifties by Jäckli (1957): *'In der Permafrostzone ist auch der klüftigste Fels kompakt, zähe, wasserdicht und im Stollenbau standfest. …Das seit 100 Jahren beobachtete Ansteigen der Klimagrenze hat ein Auftauen des Permafrostes in seinen tiefsten Lagen zur Folge, wodurch sich Steine und Felspartien, die früher durch Permafrost zusammengehalten wurden, loslösen und abstürzen: ein Grund zu Steinschlag und Felsstürzen an warmen Sommertagen.'*[1]

Degradation of permafrost in thickness and geographic extent might have different significance depending on the location and stratigraphy. Warming of rocks may lead to rockfalls as mentioned by Jäckli. Within areas where the permafrost contains ice, major damage to engineering structures may be expected

1. 'Within permafrost, even a very jointed rock is compact, tough, impermeable and self-supporting within gallery construction. ...The noted rise in the climate boundary, which is observed since 100 years, results in melting of permafrost within the lower regions and stones as well as parts of rocks, that had previously been held together by permafrost, may detach and fall down: a reason for rockfall on warm summer days.'

as a consequence of long-term temperature increase at the surface. This might be of particular importance when the ice content by volume is larger than the theoretically available pore space within the soil matrix (ice-rich permafrost). The permafrost is usually covered by an active layer, which is delineated by annual freezing and thawing above the permafrost table. This layer may undergo hydrological, geomorphological and environmental changes, affecting the stability of steep mountain slopes (Lewkowicz, 1992). Potential hazards related to permafrost degradation as a function of the slope inclination have been assessed by Harris *et al*. (2001a). Johnson (1984a) states that the periglacial landscape is dominated by mass movement phenomena, the majority of which do not conform to steady or dynamic equilibrium models of a landscape evolution. The potential threat posed by global warming to man made structures across northern regions associated with thawing permafrost, on the other hand, has recently been highlighted by Nelson *et al*. (2001).

Engineering approaches are demanded in order to solve these geomechanical problems, since geomorphological models (e.g. Olyphant, 1983; Konrad *et al.*, 1999) have failed to answer some of the important questions posed in periglacial mountain environments.

1.1 Objectives of the Project

On the basis of some catastrophic events, such as those occurring within Alpine environments in 1987 (Haeberli *et al.*, 1990a; Zimmermann, 1990; Haeberli, 1992; Zimmermann and Haeberli, 1992; Dramis *et al.*, 1995) potential instabilities of Alpine permafrost in Switzerland have been identified as being an issue of national importance (Haeberli *et al.*, 1997; Haeberli, 1999). The melting of permafrost slopes at elevations above 2500 metres above sea level (m asl) induced by climate change might cause massive damage in the valleys below, due to triggering of debris flow slides.

In order to establish plans for protecting populated mountain areas, it is necessary to understand the mechanical behaviour of frozen soils and their response with time to changing temperatures. Constitutive models with the requisite physical parameters are therefore necessary. Within an ETH mini-poly-project, the following three institutes of the Swiss Federal Institute of Technology, Zurich (ETH) have been working together:

- Institute for Geotechnical Engineering (IGT),
- Institute of Geophysics (IG),
- Laboratory for Hydraulics, Hydrology and Glaciology (VAW).

The principal goals of this project are:

- to understand the mechanical behaviour of Alpine permafrost by determining
  - the structure (content, origin and extent),
  - the physical properties and state (density, stiffness, strength, *in situ* stress),

- a representative constitutive model,
- the deformation (creep) mechanisms,

• to delineate how physical parameters vary with time and temperature, and

• to carry out preliminary numerical modelling of glaciological features.

Generally, three main thrusts have been made in order to reach these goals, which are not only suitable for the individual sub projects, but also for the mini-poly-project as a whole. Details are illustrated in Figure 1-1.

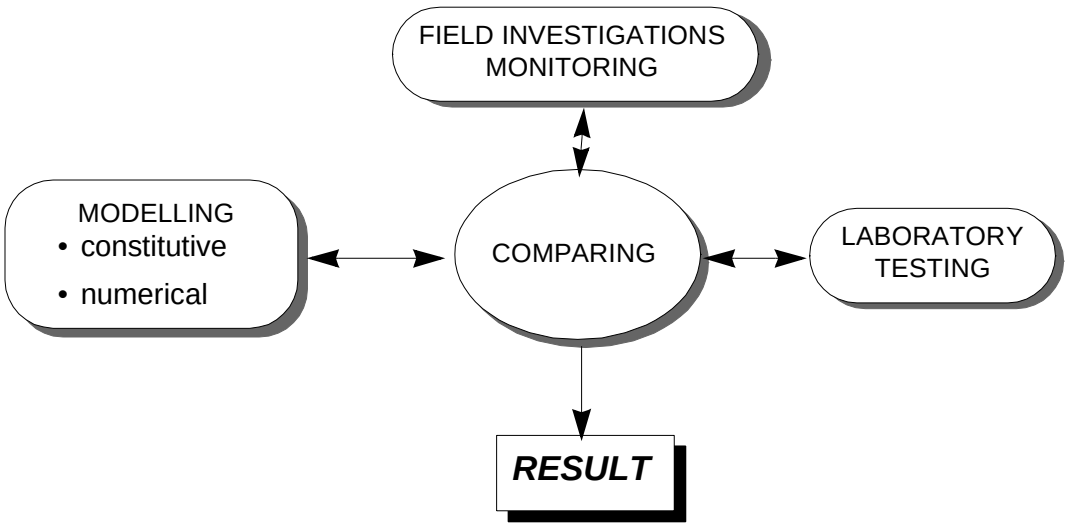

Figure 1-1: *Approach in solving the problem within the ETH Mini-Poly-Project 'Unstable Alpine Permafrost: a potentially important natural hazard'.*

The different responsibilities and contributions to this mini-poly project are summarised in Table 1-1.

Multi disciplinary project	**IGT**	**IG**	**VAW**
jointly shared six boreholes drilled through two rock glaciers, some into bedrock	undisturbed core sampling	surface geophysics	borehole geophysics
	in situ and laboratory testing	crosshole geophysics	temperature measurements
two doctoral theses, follow up project was funded to deliver a third doctoral thesis	deformation measurements		
	constitutive modelling	joint data inversion	preliminary numerical modelling

Table 1-1: *Outline of the ETH mini-poly-project: 'Unstable Alpine Permafrost: a potentially important natural hazard'.*

The specific goals for the geotechnical part within this ETH mini-poly-project, which is described herein, are:

- to investigate frozen soils in the laboratory to understand the influences of the soil-ice content, particle size, confining pressure, strain rate and temperature on the creep, strength and stiffness response,
- to obtain equivalent creep, strength and stiffness data from *in situ* field tests and cored, soil samples and to compare these with those from artificially frozen soils,
- to establish a mechanical relationship between key parameters for both artificial and real permafrost,
- to obtain relevant parameters for future input to a coupled constitutive model and subsequent numerical analysis,
- to test existing constitutive equations that may represent the thermo-mechanical behaviour of Alpine permafrost,
- to judge the stability of active rock glaciers based on the laboratory and field investigations.

1.2 Organisation of the Thesis

The thesis is organised as a series of eight main chapters with an additional reference section and several minor chapters, such as the abstract, list of symbols, *etc*. Every chapter is formed as a unit so that it can be read individually with a brief abstract at the beginning. Cross references will guide the reader directly to important sections, tables or figures within cited chapters.

The thesis starts with an introduction that outlines the framework, goals and objectives of the project, which is reported in the current work.

An extensive literature review within chapter two introduces the *state of the art* on permafrost and frozen soil research. This chapter is divided into two main sections and presents general features as well as aspects from engineering and natural sciences. At the beginning, literature concerning permafrost research is presented. This literature has been based mainly on field investigations and monitoring, and explains the natural phenomena and interpretations thereof. The second part focuses more on the stress-strain response of frozen and unfrozen soils, as well as of ice. Several constitutive equations for creep and shear are presented, together with some ideas from fracture mechanics. The literature chapter ends with a judgement of the content in terms of suitability for the problems presented by the current project.

The field investigations and subsequent monitoring of rock glacier temperatures and deformations are summarised and discussed briefly within chapter three. The two locations chosen in the Swiss Alps form the two main sections of this chapter, following an introduction that focuses on the drilling techniques for undisturbed core extraction in Alpine permafrost.

The laboratory tests are presented within chapter four. Constant stress (creep) tests and constant strain rate tests on samples from the two rock glaciers as well as from artificially frozen samples are described including the varying boundary conditions. In addition, the specifications of the purpose built triaxial testing equipment are given.

Chapter four focuses mainly on the test procedures and the presentation of test results, but without further analysis. Chapter five, however, gives interpretations of the results and cross-comparisons between the various samples and test conditions. A constitutive equation for creep is presented that accounts for temperature, stress and volumetric ice content. Strength and volumetric behaviour during shearing is also discussed and analysed.

The results of the laboratory tests are then compared with the results of the field investigations and monitoring programmes within chapter six. The solution presented in chapter five will be used for the description of phenomena observed in the field.

The subsequent discussion within chapter seven focuses on the deformation mechanisms at a microstructural level. The main processes that are responsible for the creep and strength response of ice-rich frozen soils are presented with regard to rock glacier behaviour. Possible instability processes of rock glaciers that arise from this are discussed within a sub-chapter. The two locations under investigation are compared with each other and extraneous rock glacier sites that are also presented in the literature review. The limitations of the testing equipment and the constitutive approach adopted are also discussed with respect to their very different relevance to the general problem.

The main results of the thesis are presented in a dense form in chapter eight. Furthermore, a final view regarding general rock glacier deformation processes is given, as well as recommendations for future investigations in the field of permafrost and rock glacier research. These recommendations are divided into field and laboratory examinations.

All references used within the thesis are summarised in an individual chapter at the end of this thesis.

Chapter 2

Literature Review

There is an extensive body of literature available in the field of permafrost and frozen soil research. Many attempts can be found to describe the phenomenon, to discuss the environmental impact, in particular of climate change, or to examine how this material can be used in construction. Its morphology, distribution, past and future evolution has also been a source for many investigations. Much of this work has been published by scientists of the former USSR and China, some of which has been translated and published. Since this review is confined to publications in English or German and therefore the contributions that have not been translated may be missing.

The most important publications are summarised in this chapter with respect to their origins. General permafrost research is presented first. In the second part, the focus lies on Alpine permafrost, and in particular on rock glaciers. Since this geomorphological phenomenon is not restricted to the Alpine region, some research is also included from other permafrost sites. In the third part, research on frozen ground is explored. Some aspects concerning mechanisms of unfrozen soils, as well as mechanisms of ice, are also covered.

2.1 Permafrost

Natives from the northern regions probably have known of the existence of permafrost since they settled there. The first data and publications, however, appear in the beginning of the sixteenth century. It was Michail Vasilievic Lomonosov (1711 - 1765) who offered the first known scientific explanation, which was based on the heat exchange between the ground and the environment (Yershov, 1998). Large expeditions studied the northern hemisphere during the eighteenth and first half of the nineteenth century. At that time, a 116 m deep shaft was dug, allowing the first hypothesis to be made about the thickness of permafrost. Dur-

ing the next hundred years, the industrial revolution brought many scientists into the region of perennially frozen soils, and in 1895, a committee of four people published a first work on the problems of engineering geocryology: *'The instructions for studying the soil permafrost of Siberia'*. Climatological, soil science and agricultural studies began at the beginning of the twentieth century. A landmark publication was published by M.I. Sumgin in 1927, who accumulated the knowledge of geocryology by that time and presented it in a book. Within the next decades, institutes were founded and research was carried out, covering many aspects of frozen ground resulting in a rapid increase in number of publications.

Some milestone publications are mentioned from the early days, but the main focus is on recent research.

2.1.1 Definition

The term *permafrost*, also known as pergelisol and perennially frozen ground, was first defined by Muller (1947): *'Permanently frozen ground or permafrost is defined as a thickness of soil or other superficial deposit, or even of bedrock, at a variable depth beneath the surface of the earth, in which a temperature below freezing has existed continually for a long time (from two [years] to tens of thousands of years). Permanently frozen ground is defined exclusively on the basis of temperature, irrespective of texture, degree of induration, water content or lithological character'*. Further definitions, which are illustrated in Figure 2-1, can be based on this crucial statement.

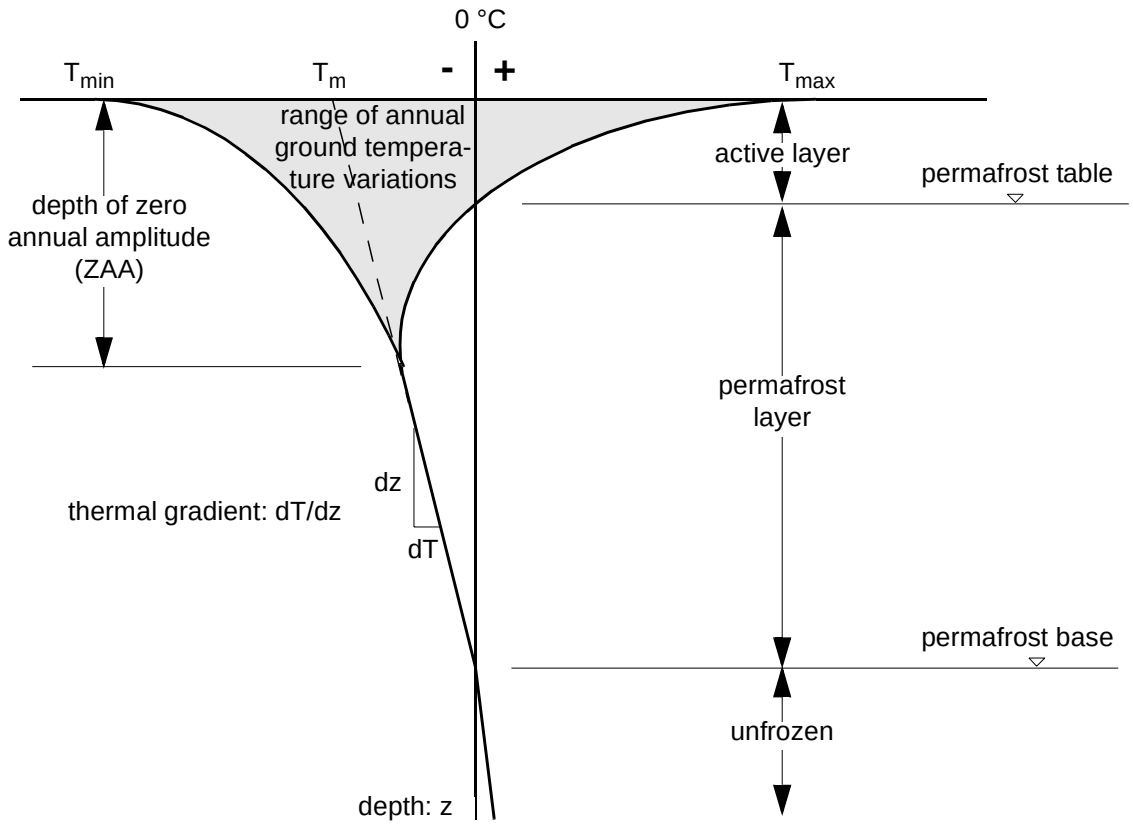

Figure 2-1: *Temperature profile in permafrost.*

The *thermal gradient* is a function of the mean annual surface temperature T_M and the heat flow from the earth's interior, and it varies from 1°C per 22 m to 1°C per 160 m (Brown *et al.*, 1981). Since the definition is just based on temperature and time, moisture, in the form of frozen *and* unfrozen water may or may not be present. If there is no ice in the permafrost body, it is called *dry permafrost*.

The temperature within the frozen ground, and in particular the geothermal gradient, reveals useful information concerning past climatic conditions (e.g. French, 1999). Temperature anomalies can be determined following for example analysis of Lachenbruch *et al.* (1988).

2.1.2 Distribution

About one fifth to one fourth of the Earth's land area is currently underlaid by permafrost, according to the *Circum-Arctic Map of Permafrost and Ground Ice Conditions*, which was prepared under the auspices of the International Permafrost Association (IPA) (Heginbottom *et al.*, 1993; Brown *et al.*, 1998). Depending on the model applied, a 25–44% reduction in total area is expected for the next century (Anisimov and Nelson, 1996) assuming a 2°C increase in mean global temperature. In particular, this retreat happens in regions with small permafrost thicknesses and areas of discontinuous permafrost. As a consequence, the lower limit of permafrost will move up to higher altitudes in regions of high-elevation or to more extreme latitudes mainly around the northern hemisphere.

Awareness of the presence of perennially frozen grounds is mainly limited to the northern hemisphere, where large areas are covered by it. Some permafrost can be found also in the southern circumpolar regions, even though further investigations are necessary (Bockheim, 1995). In contrast to this so called *arctic, antarctic or polar permafrost*, *mountain permafrost* can be found under moderate climatic conditions at higher elevations. According to Stearns (1966), about 6–7% of the permafrost is mountain permafrost. Of that, however, only about 0.2% is in the European Alps, whereas the main part (80.4%) can be found in Asia. Another 19.4% are in the American mountains (after Fujii and Higuchi, 1972). Those figures have to be applied with caution since they may change with the ongoing trend of global warming.

In Switzerland, permafrost may be present from elevations of about 2100 m asl[1], depending on the exposure of the location (Haeberli, 1975). Recent modelling of the permafrost distribution, using the PERMAKART approach (Keller, 1992), estimates that 4–6% of the Swiss territory is covered by permafrost (Keller *et al.*, 1998; Vonder Mühll, 1999), which is significantly higher than the estimated area of Switzerland covered by glaciers in 1960 (3.5%).

The occurrence of the permafrost distribution was determined for 33 glacier regions in the Swiss Alps, indicating also larger permafrost occurrences in the Alpine regions of the three cantons Berne, Wallis and Graubünden (Figure 2-3, Maisch *et al.*, 1998).

1. m asl: metres above sea level

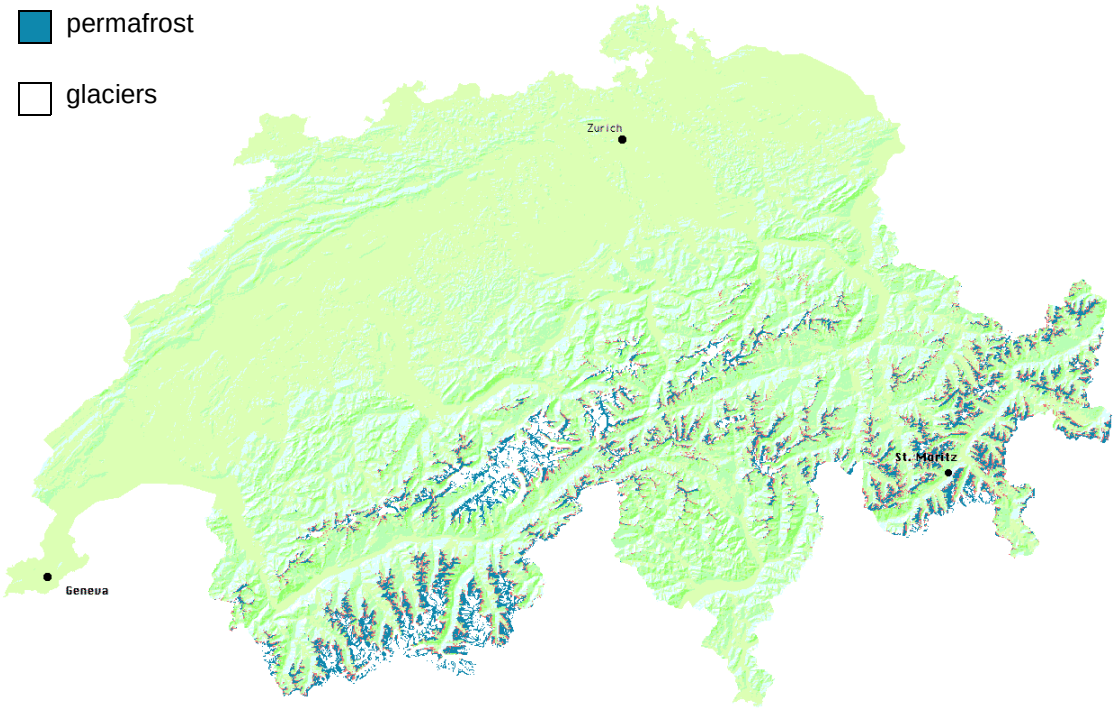

Figure 2-2: *Permafrost map of Switzerland (Keller et al., 1998).*

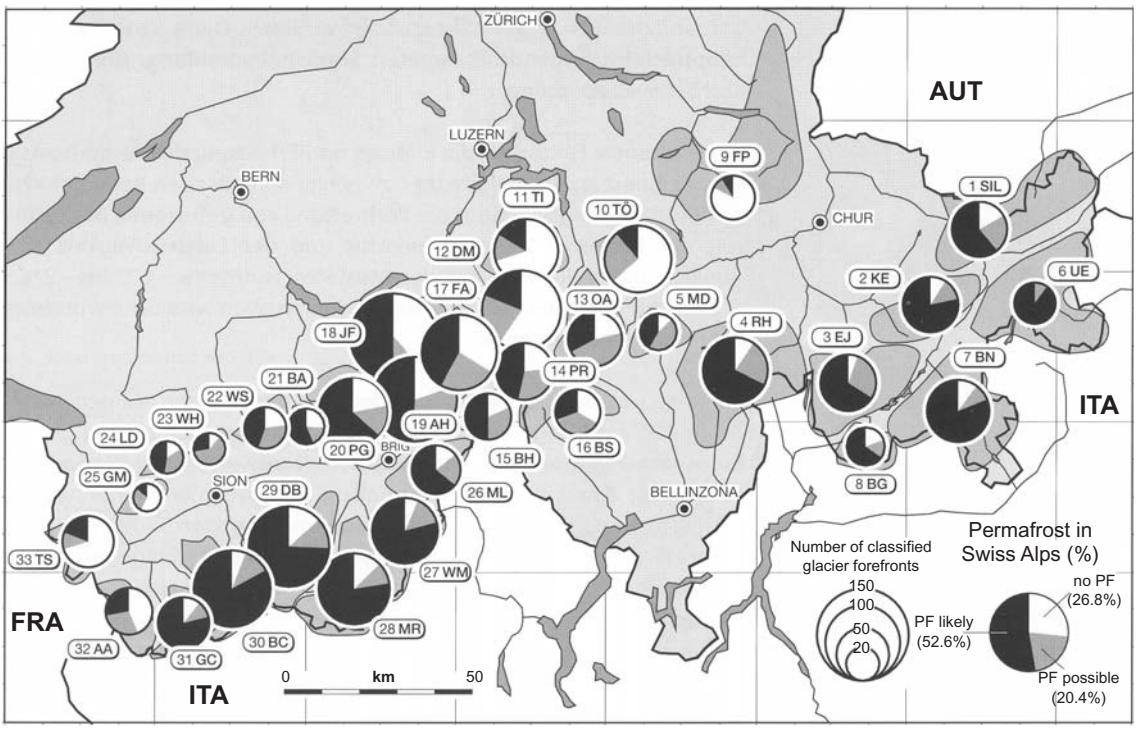

26	**ML**	Monte Leone	17	**FA**	Finsteraarhorn	11	**TI**	Titlis	6	**UE**	Unterengadin	1	**SIL**	Silvretta
27	**WM**	Weissmies	18	**JF**	Jungfrau	12	**DM**	Damma	7	**BN**	Bernina	2	**KE**	Kesch
28	**MR**	Monte Rosa	19	**AH**	Aletschhorn	13	**OA**	Oberalp	8	**BG**	Bergell	3	**EJ**	Err-Julier
29	**DB**	Dent Blanche	20	**PG**	Petersgrat	14	**PR**	Piz Rotondo				4	**RH**	Rheinwald
30	**BC**	Mont Bl. de Cheilon	21	**BA**	Balmhorn	15	**BH**	Blinnehorn	9	**FP**	Flims-Pizol	5	**MD**	Medel
31	**GC**	Grand Combin	22	**WS**	Wildstrubel	16	**BS**	Basódin	10	**TÖ**	Tödi			
32	**AA**	Aig. d'Argentière	23	**WH**	Wildhorn									
33	**TS**	Tour Salliere	24	**LD**	Les Diablerets									
			25	**GM**	Grand Muveran									

Figure 2-3: *Permafrost distribution for glacier forefronts in the Swiss Alps (Maisch et al., 1998).*

Special geomorphological features can be found, which are only present due to the steep environment within mountain permafrost regions, such as *rock glaciers* (cf. Chapter 2.2), *solifluction* (cf. Chapter 2.1.3*)* or *ice core moraines* (e.g. Washburn, 1979; Guodong and Dramis, 1992).

2.1.3 Interactions

Since permafrost is a thermal state, determination of the energy balance to the ground is very important for its modelling and prediction of future changes. Many different factors and effects have major influence on the thermal regime in the ground. The heat transfer between the ground and the surface can be summarised as shown in Figure 2-4.

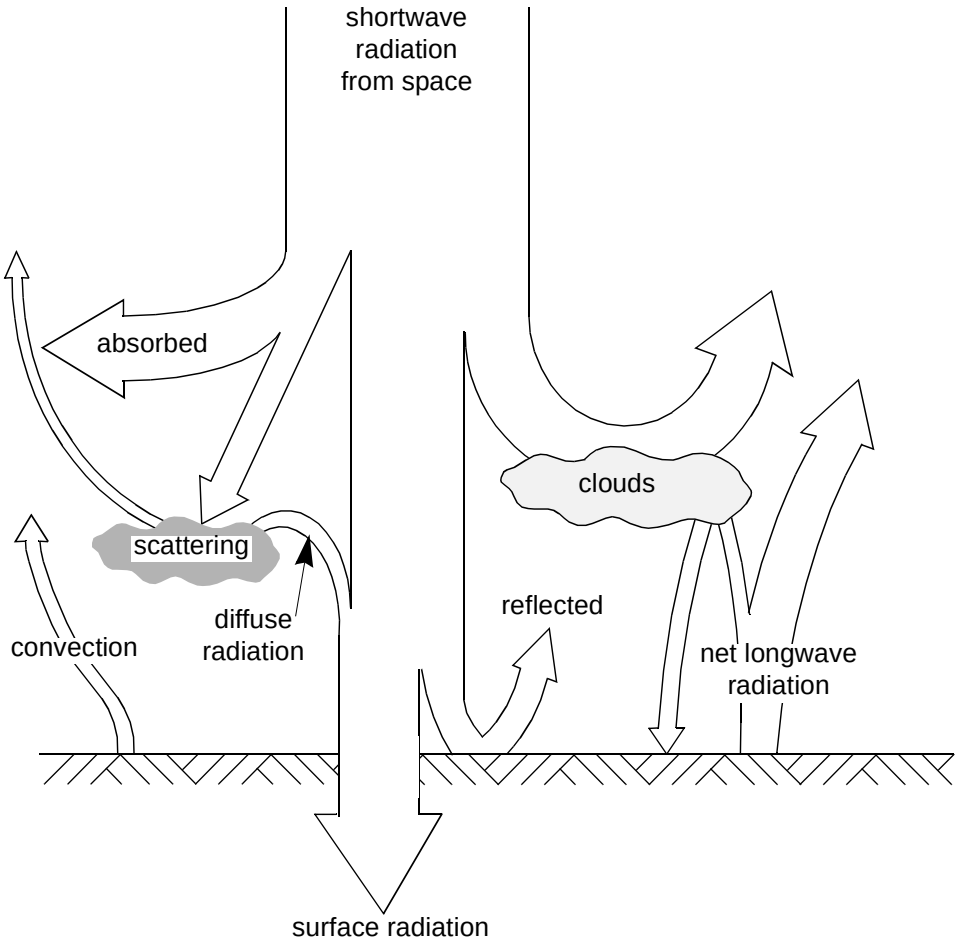

Figure 2-4: *Heat transfer between ground surface and air on a sunny day (after Aldrich, 1956).*

Hoelzle *et al.* (2001) outline the typology of models for European mountain permafrost, which are currently available and involve various levels of sophistication at different spatio-temporal scales, with special emphasis on aspects of energy exchange at the surface and within the active layer. The complexity of the interactions between the atmosphere and the active layer, and their influences on the permafrost are shown in Figure 2-5. A central factor in high mountain permafrost is the effect between the snow cover and the active layer, which has already been described by Keller and Gubler (1993). Furthermore, attempts have been

made to model the influence of the snow cover on soil freezing (Osokin *et al.*, 2000) as well as analysing the effect on the soil temperature and the energy balance (Sokratov and Barry, 2001).

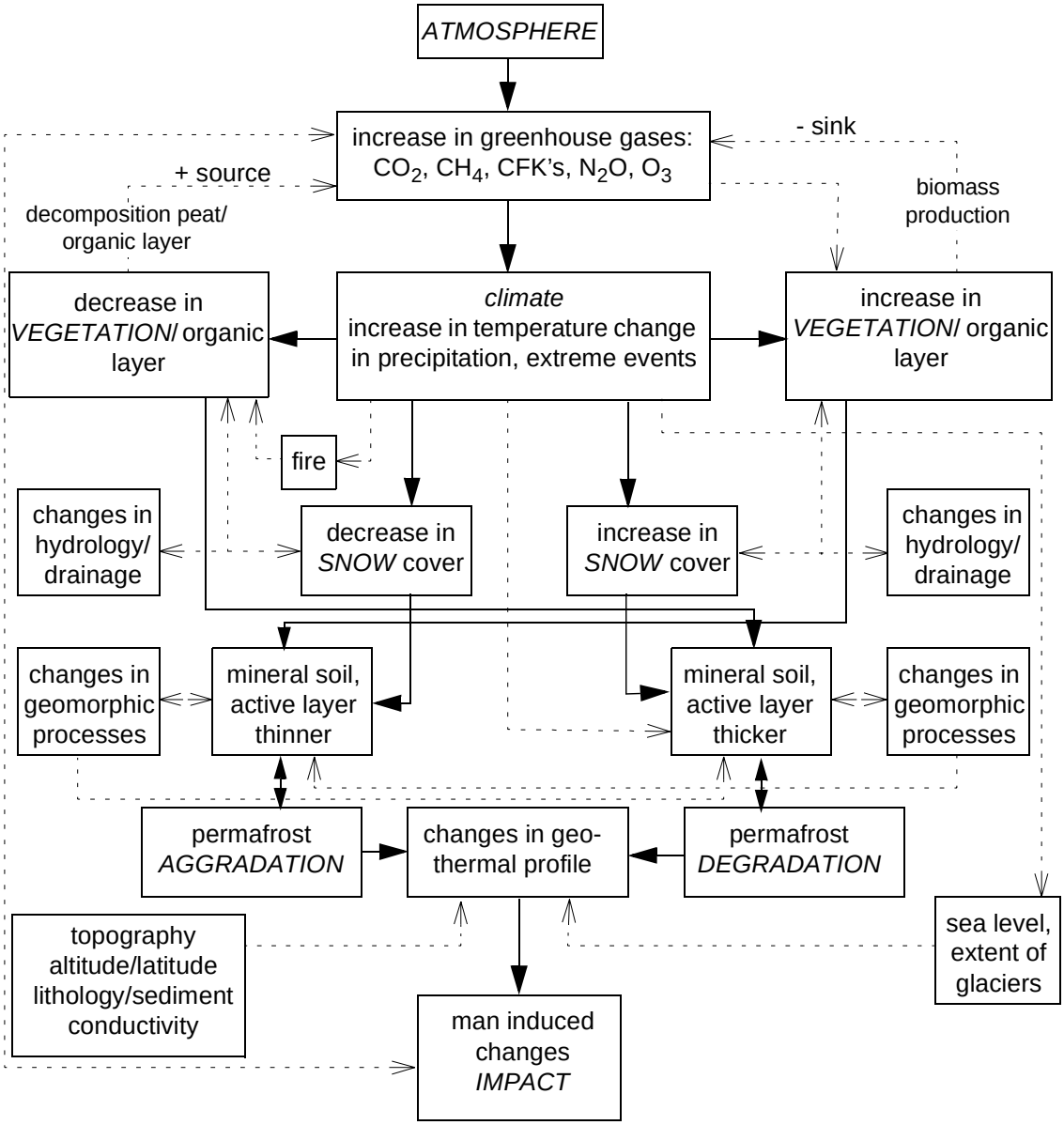

Figure 2-5: *Schematic representation of the complex interaction of the active layer and the permafrost with the atmosphere including biological, hydrological and geomorphic processes (after Koster and Nieuwenhuijzen, 1992).*

However, several processes are important for the thermal regime of Alpine permafrost (after Vonder Mühll *et al.*, 1998):

- First major snowfall: a thin snow cover at the beginning of the winter allows the cold air to penetrate into the ground, and rapid heat loss from the ground can be observed. On the other hand, thick snow cover acts as an insulating layer and the heat will be retained.

- Duration of positive or negative temperatures: as long as snow covers the ground, the temperature at the ground surface is below or at zero centigrade and the heat penetration is impeded.
- Zero-curtain effect (Outcalt *et al.*, 1990): A zero curtain in autumn shortens the duration, in which temperatures are negative in the following winter, and in spring, the zero curtain causes a shorter period of positive temperatures in the following summer.

The effect of avalanche-defence snow supporting structures on the ground temperature has been studied related to steep Alpine slopes, focusing on the temperature penetration through the structure and the influence of the accumulated snow above, and less snow below, the construction (Phillips *et al.*, 2000; Thalparpan, 2000). They concluded that no significant geotechnical problems have to be expected due to artificial modification of the snow cover.

In addition, there are effects of unfrozen water on the active layer and the permafrost, which have to be considered when modelling thermal effects (Romanovsky and Osterkamp, 2000). The unfrozen water brings in a spatially distributed latent heat and therefore changes the thermal properties of the active layer and, if the water has the possibility to flow through the permafrost body (e.g. Vonder Mühll *et al.*, submitted), also of the frozen soil. Due to the formation of a strong thermal gradient at the permafrost table, the heat flux out of the ground increases. Despite the heat flux, effective stresses within the active layer are reduced due to an increase in the porewater pressure and therefore, stability problems of the thawing slope, usually known as *gelifluction* or *solifluction*, occur (Bennett and French, 1991; Harris *et al*., 1995; Harris and Davies, 2000; Harris and Lewkowicz, 2000). Centrifuge modelling showed (Harris *et al*., 2002) that gelifluction reflects elasto-plastic soil behaviour and not viscosity-controlled flow.

Another interaction was noted by Wegmann *et al.* (1998) between glaciers and permafrost in adjacent rock walls. Numerical calculations showed that permafrost is penetrating into the rock wall as a consequence of glacier retreat. The response at the permafrost base, however, may be delayed by the order of millennia.

2.1.4 Permafrost and Climate Change

Concern over the sensitivity of perennially frozen ground to climate changes has instigated many research programmes (e.g. Koster and Nieuwenhuijzen, 1992; Guodong and Dramis, 1992; Haeberli *et al.*, 1993; Harris *et al.*, 2001a). This is of particular interest in the context of the predicted rise of the mean annual air temperature as a consequence of global warming (e.g. Deque *et al.*, 1998; Hulme *et al.*, 1999; Knutti *et al*., 2002). Due to the retarded response of permafrost to cycles of air temperature, permafrost temperatures have been used to examine past climate changes. An overview can be found in Lunardini (2000).

Osterkamp and Romanovsky (1999) compared the air temperature and the snow cover with the permafrost temperatures for permafrost in Alaska and found that permafrost will persist at depth a long time after thawing begins, with time scales of centuries to millennia required to thaw even relatively thin discontinuous permafrost. The thickness of the active layer, however, will increase and may cause problems, in particular related to nearby structures (Williams, 1995).

In addition, climate change may result in new different ground freezing conditions, thereby influencing the surface velocity and the maximum depth of solifluction processes (Matsuoka, 2001).

A rise in elevation of the lower permafrost boundary has to be expected within mountain permafrost areas, causing local degradation of frozen slopes (Haeberli *et al.*, 1993) and loss of stability within ice-filled rock discontinuities, even at temperatures still below the freezing point (Davies *et al.*, 2001). A widespread loss of permafrost will trigger erosion or subsidence of ice-rich landscapes and in addition, the thawing will have a severe impact on infrastructure due to excessive settlements and exploration, and will result in rapid coastal erosion (IPCC, 2001).

2.1.5 Alpine Permafrost Research

Due to the steep slopes, weathered rocks and warmer mean annual air temperatures, mountain permafrost shows different geomorphological features to arctic permafrost. In particular, gravity driven forms, such as (creeping) rock glaciers or solifluction processes are much more common for this environment.

Ice found during the construction of dams, power or cable car stations in Alpine regions, was often attributed to remains from the frost during the winter (Keller, 1990; Haeberli, 1992), and the existence of permafrost was usually denied.

Permafrost research was initiated in Switzerland by Prof. Dietrich Barsch, who worked at the University of Basle at the beginning of the seventies. In those beginnings, refraction seismic and geoelectric methods were used for the determination of permafrost (Barsch, 1973; Fisch *et al.*, 1977). These methods allowed an estimation of the horizontal and vertical spread of a frozen body due to differing geophysical properties between frozen and unfrozen ground. At that time, the BTS-method (BTS: Bottom Temperature of the Snow cover) was developed (Haeberli, 1973; 1975). In contrast with the classical geophysical methods, the thermal characteristics of the soil are used while measuring the temperature under the winter snow cover during spring. Since the snow cover acts as an insulating layer, assuming that it is thick enough, the temperature at the bottom of the snow cover is generated by the temperatures within the ground. BTS-values cooler than -3°C indicate that permafrost is possible. This relatively easy, fast, empirical method allowed large areas in the Swiss Alps to be mapped for permafrost.

In the meantime, many other institutes and scientists have worked in the field of permafrost, with sensitivity to climatic changes forming a major focus (Cheng and Dramis, 1992; Haeberli *et al.*, 1993). It must be assumed that the lower boundary of the permafrost in Alpine regions may shift in altitude as a consequence of the warming during the twentieth century. Formally frozen slopes will thaw and cause local degradation. With an ongoing trend of global warming, it must be further assumed that the degradation of the frozen ground within high mountain regions might even accelerate.

However, only since the dramatic events during summer 1987, where several debris flows caused severe damage and even loss of life (Haeberli *et al.*, 1990a; Zimmermann, 1990; Zimmermann and Haeberli, 1992; Dramis *et al.*,

1995), the risk potential of Alpine permafrost had been obvious to the public. Several research projects investigated the causes of the events and concluded that the melting of permafrost at elevations above 2500 m asl represent the most severe consequences of global warming for Switzerland, since the resulting debris flow slides are likely to cause massive damage in the valleys below (Haeberli *et al.*, 1999a).

In December 1997, a European EU-funded project called PACE (Permafrost and Climate in Europe) started to enhance understanding of permafrost in the context of global warming (Harris *et al.*, 2001b). The project was divided into six work packages:

- geothermal monitoring of mountain permafrost (e.g. Sollid *et al.*, 2000; Isaksen *et al.,* 2001),
- mapping of permafrost distribution, depth and character using geophysical techniques (e.g. Hauck, 2001; Hauck *et al.*, 2001; Vonder Mühll *et al.*, 2001a),
- mapping and monitoring of temporal and spatial changes in mountain permafrost (e.g. Etzelmüller *et al.*, 2001),
- energy balance measurements and numerical modelling of permafrost distribution (e.g. Mittaz *et al.*, 2000; Gruber and Hoelzle, 2001; Hoelzle *et al.*, 2001),
- thermally-controlled geotechnical centrifuge modelling of permafrost degradation (e.g. Davies *et al.*, 2000; Harris *et al.*, 2000a; Davies *et al.*, 2001), and
- process-based geotechnical hazard prediction in the context of global warming (Harris *et al.*, 2001b).

In addition, progress has been made in photogrammetrical investigations due to digital image analyses (e.g. Kääb and Vollmer, 2000) and higher resolutions of various geophysical techniques. New tomographic inversion methods have been applied as well (Musil *et al.*, submitted, a; b).

2.2 Rock Glaciers

Rock glaciers are special geomorphological phenomena of mountain permafrost. The term rock glacier may be attributed to Capps (1910). He described the fundamental behaviour of rock glaciers:

- which have neither a real accumulation or an ablation region, in contrast to ‘ice’ glaciers,
- which cannot retreat, even if the ice melts out and movements cease,
- for which the ice content must be high, or even massive ice must be present, and
- that water must have an important influence on the morphology of the rock glacier.

However, seven years earlier, Cross and Howe (1903) described the phenomenon as: '*The larger rock streams, however, must owe their origin to glaciers; no other agencies could transport such vast quantities of rock waste so far from their sources.'* They also recognised the transport mechanisms of rock glaciers, but they connected it directly to glaciers.

More than fifty years later, Jäckli (1957) in Switzerland and Wahrhaftig and Cox (1959) in Alaska, stated, that rock glaciers are down-hill creeping frozen soil masses, and compared them to lava streams.

About a 1000 active rock glaciers are known to exist in the Swiss Alps (Haeberli, 1985). Even though no figures are available, it must be assumed that several millions of rock glaciers exists world wide, which explains why they have been described extensively in the literature. The term rock glacier has caused confusion ever since and different authors have tried to include more details relating to morphology or genesis in the name: *talus rockglacier*, *debris rockglacier, lobate rock glacier, tongue-shaped rock glacier, moraine rock glacier, protalus lobe,* just to name a few (Hamilton and Whalley, 1995). Details of the historical development of the term rock glacier and various definitions can be found in Barsch (1996). Milestones in the rock glacier research were the work by Fisch *et al.* (1977), who performed geoelectrical measurements on rock glacier and moraine material for the Grande Dixence hydro-power station in the Swiss Alps, and the seismic studies on various rock glaciers in Switzerland done by Barsch (1969; 1973).

In contrast to temperate glaciers, ice cores from rock glaciers may represent much larger time spans and therefore have been recognised as important sources of ice at temperate latitudes (Clarke *et al.*, 1996, Haeberli *et al.*, 1999b). The age of the rock glaciers could be estimated from organic remains within the ice cores, and it was discovered that the rock glaciers are relatively old (Haeberli *et al.*, 1999b, Konrad *et al.*, 1999), in that most of the larger rock glacier date from times before the Little Ice Age, the period between about 1450 and 1890 A.D., in which many regions of the world experienced cooling.

The deformation behaviour of rock glaciers has always been of particular interest (Wahrhaftig and Cox, 1959). Since measurements of internal deformation are expensive, only limited studies are available. With the exception of the study by Johnson and Nickling (1979), these few measurements showed that in contrast to temperate glaciers, the investigated rock glaciers have a shear horizon, where most of the deformation takes place (Wagner, 1992; Hoelzle *et al.*, 1998, Arenson *et al.*, 2002).

A detailed overview of rock glacier literature, rock glacier formation models and internal structure studies is given in Burger *et al.* (1999). However, some important contributions are summarised in Table 2-1.

Reference	general / overview	genesis	geophysics	internal structure	dynamics	geomorphology	engineering	natural hazards	climate	age
Ackert, 1998		x			x	x				x
Arenson *et al.*, 2002				x	x					
Barsch, 1977		x			x					
Barsch, 1996	x									
Berthling *et al.*, 1998; 2000			x	x	x	x				
Burger *et al.*, 1999	x		x			x	x			
Calkin *et al.*, 1998		x			x					x
Elconin and LaChapelle, 1997				x	x					
Giardino, 1979		x			x					
Giardino and Vick, 1985						x	x	x		
Giardino *et al.*, 1987	x									
Haeberli and Vonder Mühll, 1996		x		x		x				
Haeberli, 1985					x					
Haeberli *et al.*, 1998		x			x	x				
Haeberli *et al.*, 1999										x
Haeberli, 2000	x									
Harris *et al.*, 2001a							x	x	x	
Humlum, 1982						x				
Humlum, 1998						x			x	
Ikeda and Matsuoka, 2002	x					x				
Isaksen *et al.*, 2000			x		x					
Johnson and Nickling, 1979					x					
Johnson, 1984a, b		x				x				
Kääb *et al.*, 1997					x					x
Kääb *et al.*, 1998					x					
Kääb *et al*., 2002					x	x				x
Kääb and Vollmer, 2000					x					
King *et al.*, 1987			x	x						
Konrad *et al.*, 1999		x		x	x					x
Martin and Whalley, 1987	x	x				x				
Musil *et al.*, submitted, a; b			x	x						
Nicholas and Butler, 1996			x	x						x
Sollid and Sørbel, 1992	x				x					
Vonder Mühll and Holub, 1992			x	x						
Vonder Mühll and Klingelé, 1994			x	x						
Wagner, 1992				x	x					
Wagner, 1996a; b			x	x						
Wahrhaftig and Cox, 1959		x			x	x				
Whalley and Martin, 1992	x	x		x	x	x				

Table 2-1: *Summary of 'recent' important rock glacier literature.*

One of the main problems with permafrost research, and in particular with rock glacier research, is that the frozen soil is not exposed. Therefore, direct observations are very rare. There are a few sites, where large rock glacier exposures were recorded and described (Fisch *et al.*, 1977; Moore and Friedman, 1991; Elconin and LaChapelle, 1997). In addition to exposures, some observations could be made within a tunnel through the Hurricane Basin rock glacier (Brown, 1925) and from cores, which were obtained from various drillings. Further details about drilling in rock glaciers can be found in Chapter 3.1.2.

One of the central goals of all this research is the description of this very obscure phenomenon *rock glacier*. Even though many investigations add a tiny stone to the whole mosaic, the genesis of rock glaciers is still being debated and allows ongoing speculations to be made (e.g. Konrad *et al.*, 1999). The claim that rock glaciers represent a landform continuum, for example, has originally been presented by Wahrhaftig and Cox (1959) and was further developed by Giardino and Vitek (1988) (Figure 2-6), Johnson (1978) and Corte (1987) on the basis of different classification schemes (continuum, dynamic, form). Johnson (1984a; b) presented possible rock glacier origins and movement processes that can be summarised schematically (Figure 2-7). Rock glaciers with glacial origins, i.e. rock covered glaciers consist of massive ice and behave also like glaciers, whereas different movement mechanisms have to expected for rock glaciers with a non-glacial origin depending on the ice content. Primary movements are mainly controlled by current climate conditions resulting in steady state creep for icy rock glaciers and sudden or catastrophic movements, such as mud flows for environments without ice. Continuous flow mechanisms (‘concrete’ flow) can also be expected, in particular for icy rock glaciers due to gravity, but can, depending on the internal soil composition and the slope angle, also occur for dry rock glaciers.

Haeberli *et al.* (1998) focus more on a process oriented characterisation of the problem and describe initial condition that are necessary for the evolution of layered rock glaciers and their further advance. Possible origins of the ice within rock glacier permafrost is presented in Haeberli and Vonder Mühll (1996). Depending on the ice resistivity, two origins were determined: i) sedimentary ice from temperate firn zones of mountain glaciers, and ii) meteoric water during percolation/circulation in ground material and refreezing at the permafrost table, the permafrost base or within the permafrost (secondary frost heave).

However, clear concepts about rock glacier dynamics, origin and development are still lacking. Despite the major challenge of modelling the inhomogeneity of a rock glacier, such knowledge of past geomorphological processes may help in better predicting their future behaviour.

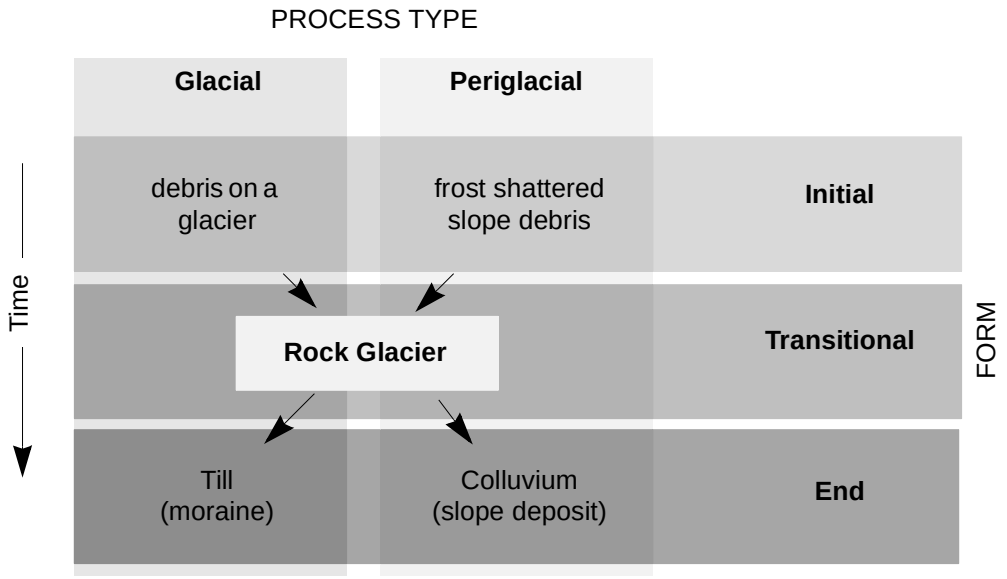

Figure 2-6: *Diagram illustrating the Alpine landscape continuum (after Giardino and Vitek, 1988 and Burger et al., 1999). Rock glaciers are transitional forms that can develop from two processes and can progress to two end-phases. The rate of movement is related to process, not form.*

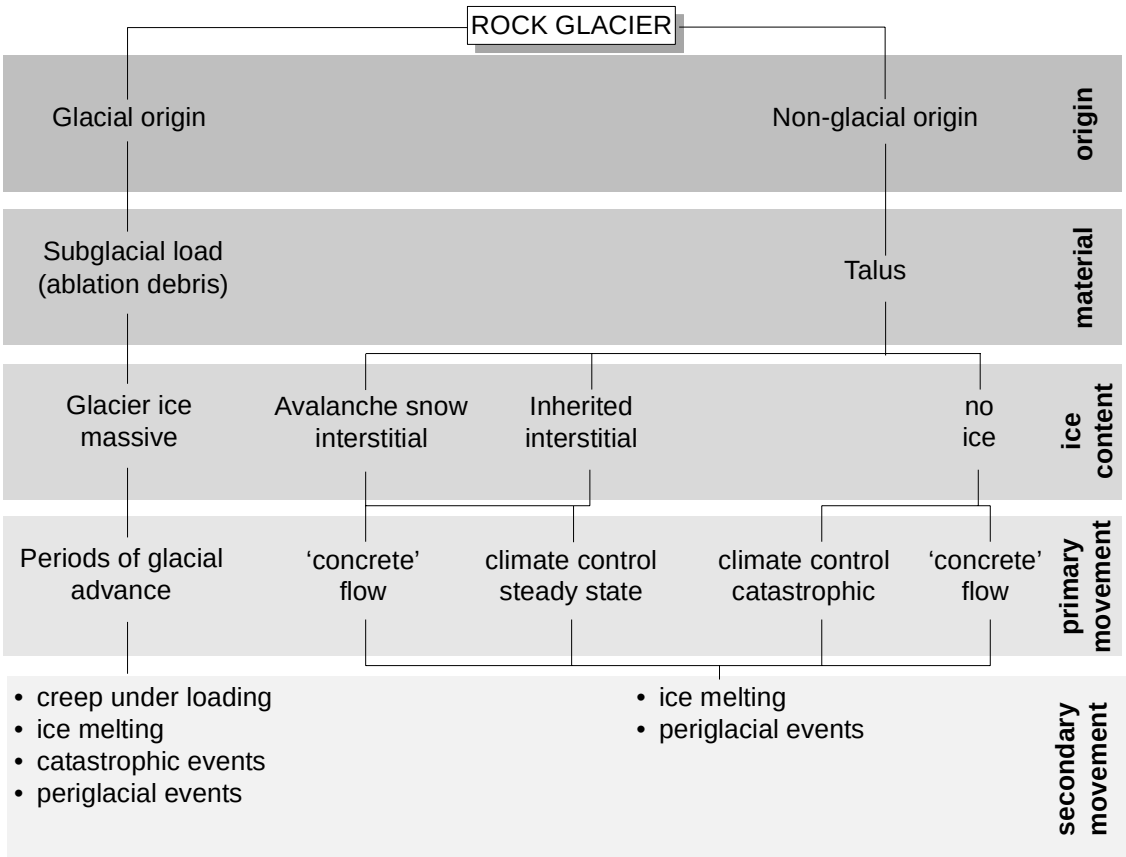

Figure 2-7: *Chart of possible rock glacier origins (after Martin and Whalley, 1987; Johnson, 1984a; b).*

2.3 Material Behaviour of Frozen Soils

2.3.1 Unfrozen 'Normal' Soils

Some important aspects of unfrozen soils are presented within this first sub-chapter in order to understand the stress-strain-time-temperature response of frozen materials.

In general, there are two different types of time dependent deformations of a soil under a constant load: (i) the deformation of soils, which have a small permeability, due to the time dependent reduction of excess porewater pressures caused by a sudden load, following Darcy's law and known as *consolidation*, and (ii) the viscous deformation of the soil within the microscopic structure of the material, known as *creep*, *relaxation*, *rate sensitivity* or *secondary compression*.

Different approaches have been used in order to model this phenomenon. In addition to the rate process theory, three other approaches for the modelling of time dependent behaviour from a microscopic point of view are well known: the empirical approach, the visco-elastic approach and the viscoplastic approach.

Rate Process Theory

Time dependent creep of soils, mainly clays, has been described since the sixties (e.g. Murayama and Shibata, 1961; Mitchell, 1964) using the theory of absolute reaction rates (Glasstone *et al.*, 1941). The basis of this theory is that so called *flow units* (particles, molecules, atoms, *etc*.) are constrained from movements relative to each other by virtue of energy barriers separating adjacent equilibrium positions. The displacement of a flow unit from one equilibrium to another equilibrium position requires an *activation energy* ΔF. This value depends on the material and on the type of process. The effect of a shear force on the energy barriers is shown in Figure 2-8.

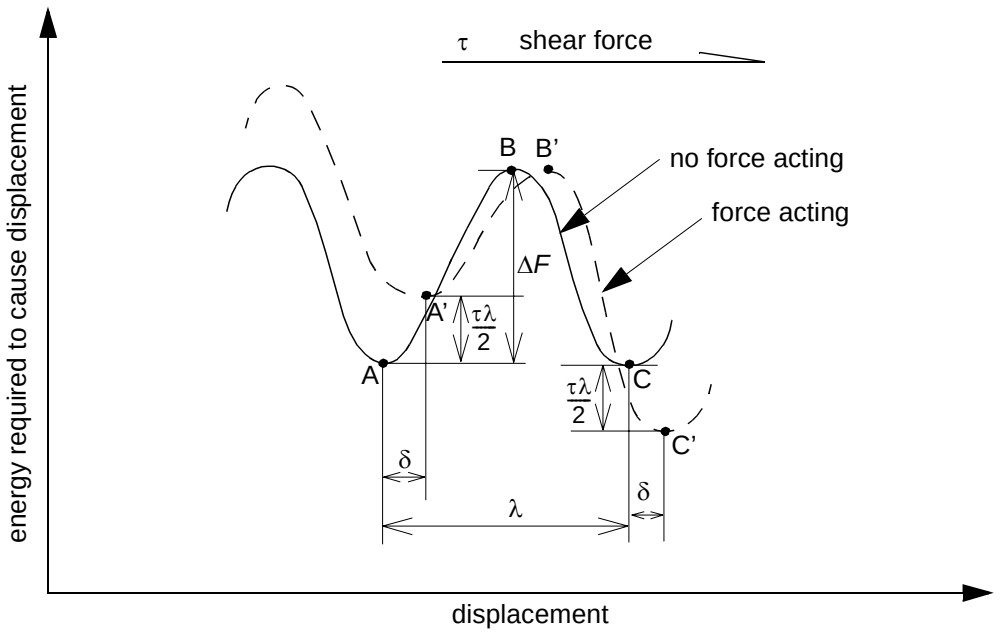

Figure 2-8: *The effect of a shear force acting on the energy balance.*

A strain rate equation can be derived based on this theory, if the rate of movement is expressed as a function of a unit length:

$$\dot{\varepsilon} = 2X\frac{kT}{h}exp\left(-\frac{\Delta F}{RT}\right)sinh\left(\frac{\tau\lambda}{2kT}\right) \qquad [2\text{-}1]$$

where X is a parameter relating activation frequency to strain rate and may be both time and structure dependent, k is the Boltzmann's constant ($1.380\cdot10^{-23}$ J K^{-1}), T is the absolute temperature in °K, h is the Planck's constant ($6.624\cdot10^{-34}$ J s^{-1}), N is the Avogadro's number ($6.022\cdot10^{23}$ mole^{-1}), whereas R (the universal gas constant) is equal to $N\cdot k$ (= 8.314 J·K^{-1} mole^{-1}), λ is the distance between two equilibrium positions (see Figure 2-8) and τ is the acting shear force.

If $(\tau\lambda/(2kT)) < 1$, then $sinh\left(\frac{\tau\lambda}{2kT}\right) \approx \left(\frac{\tau\lambda}{2kT}\right)$, and the rate is directly proportional to τ.

This is the case for a Newtonian fluid.

However, this is not the case for most soil deformation problems (Mitchell and Campanella, 1968), and therefore with

$$sinh\left(\frac{\tau\lambda}{2kT}\right) \approx \frac{1}{2}\cdot exp\left(\frac{\tau\lambda}{2kT}\right) \text{ equation [2-1] changes to} \qquad [2\text{-}2]$$

$$\dot{\varepsilon} = X\frac{kT}{h}exp\left(-\frac{\Delta F}{RT}\right)exp\left(\frac{\tau\lambda N}{2RT}\right). \qquad [2\text{-}3]$$

The equation [2-3] may be written as

$$\dot{\varepsilon} = X\frac{kT}{h}exp\left(-\frac{Q}{RT}\right), \qquad [2\text{-}4]$$

where

$$Q = \Delta F - \frac{\tau\lambda N}{2} \qquad [2\text{-}5]$$

is termed the *experimental activation energy*. For conditions, in which everything is constant except for the temperature T ($X(kT/h) \approx constant$), the *Arrhenius equation* can be written, which was proposed by Arrhenius around 1900:

$$\dot{\varepsilon} = A\,exp\left(-\frac{Q}{RT}\right), \qquad [2\text{-}6]$$

for which the material parameter

$$A = X \cdot \frac{kT}{h}. \qquad [2\text{-}7]$$

Some values for the experimental activation energy Q are given in Table 2-2 (from Mitchell, 1976, Tab. 14.1).

	Material	activation energy* [kJ/mole]
1	remoulded illite, saturated, water contents of 30-40%	104 – 167
2	dried illite: sample air-dried from saturation, then evacuated	155
3	San Francisco Bay mud, undisturbed	104 – 134
4	Dry Sacramento River sand	~104
5	Water	16 – 21
6	Montmorillonite-water paste, dilute	84 – 109
7	Lake clay, undisturbed and remoulded	96 – 113
8	Osaka clay, overconsolidated	121 – 134
9	Concrete	121 – 134
10	Metals	> 209
11	Frozen soils	394
12	Sault Ste. Marie clay, suspensions, discontinuous structures	17 – 21
13	Sault Ste. Marie clay, Li^+, Na^+, K^+ forms, in H_2O and CCl_4, consolidated	117

* The first four values are experimental activation energies Q. Whether the remainder are values of effective (ΔF) or experimental (Q) activation energies is not always clear from the reference.

Table 2-2: *Activation energies for creep of several materials (after Mitchell, 1976).*

A statistical model that embodies the changes in the structure of the material during creep, by applying the concept of a time-dependent spectrum of energy barriers to shear, has been presented by Pusch and Feltham (1980).

Empirical Approach

In order to determine the creep potential, the strain rate $\dot{\varepsilon}$ can be expressed for any time t with

$$\dot{\varepsilon} = A\,exp(\alpha q)\left(\frac{t_0}{t}\right)^m \quad \text{(Singh and Mitchell, 1968; 1969)} \qquad [2\text{-}8]$$

where

A = strain rate at time t_1 and q = 0 (projected value)

α = value of the slope of the mid-range linear portion of a plot of logarithmic strain rate versus deviator stress, all points corresponding to the same time after load application

q = deviator stress (σ_1 - σ_3)

t_0 = unit time

m = slope of a straight line representing logarithmic strain rate versus logarithmic time

The parameter m in [2-8] is the key factor in defining the creep potential of the soil. The lower the value of m the larger are the creep strains and the greater is the probability of creep rupture. According to Singh and Mitchell (1969), creep rupture appears only with values of $m \leq 1$.

This type of relation is only relevant to states of one-dimensional deformation and is not applicable to general loading conditions.

Viscoelastic Approach

This approach, which has also been called the method of rheological models (Feda, 1992), has been widely applied to many materials, not only soils. Three different rheological models are usually used: the *Maxwell model*, the *Kelvin model* and the combined *Burger model*. All these models use springs and dashpots, which represent the elementary constitutive relationship. The ideally elastic (Hookean) behaviour can be modelled by

$$\sigma = E \cdot \varepsilon, \qquad [2\text{-}9]$$

with E as the Young's modulus of the material, and the ideally viscous (Newtonian) behaviour is modelled by

$$\sigma = \mu_\sigma \cdot \dot{\varepsilon}. \qquad [2\text{-}10]$$

where μ_σ is the viscosity of the material.

• Maxwell's model

For a Maxwell material (Figure 2-9), these two equations can be combined. The strain rate is assumed to be constant and a simple equation (eq. 2-11) can be formulated for the strain rate.

$$\dot{\varepsilon} = \frac{\sigma}{\mu_\sigma} + \frac{\dot{\sigma}}{E}. \qquad [2\text{-}11]$$

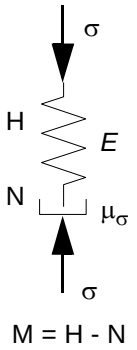

H Hookean material
N Newtonian material
M Maxwell material: M = H - N
E Young's modulus
μ_σ normal viscosity

Figure 2-9: *Rheological model of a Maxwell material.*

• Kelvin's / Voigt's model

For a Kelvin or a Voigt material (Figure 2-10), the stress can be expressed as

$$\sigma = E\varepsilon + \mu_\sigma\dot{\varepsilon}. \qquad [2\text{-}12]$$

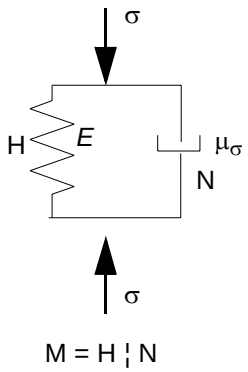

H Hookean material
N Newtonian material
K Kelvin material: K = H ¦ N
E Young's modulus
μ_σ normal viscosity

Figure 2-10: *Rheological model of a Kelvin / Voigt material.*

• Poynting-Thompson model (standard model)

If Maxwell's model truly reflects the stress relaxation effects, and Kelvin's model represents the creep behaviour reasonably well then a combination of the two models should be able to model the soil response. The Poynting-Thompson model (Figure 2-11) is formed by placing a spring element in series with a Kelvin / Voigt element. The stress and strain for the spring and the Kelvin / Voigt

element is shown in Figure 2-11 on the right. The upper spring (E_{H1}) responds immediately to a load σ_0 whereas retarded response occurs in the spring and the dashpot of the Kelvin / Voigt element.

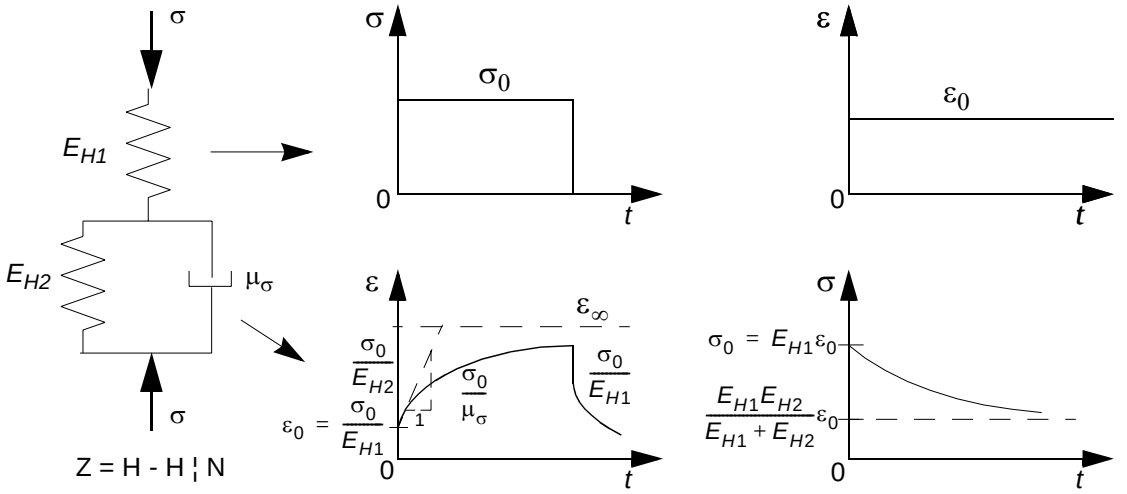

Figure 2-11: *Rheological model of a standard (Poynting-Thompson) material.*

The constitutive relationship for a Poynting-Thompson model is

$$\dot{\sigma} + \frac{E_{H1} + E_{H2}}{\mu_\sigma}\sigma = E_{H1}\dot{\varepsilon} + \frac{E_{H1}E_{H2}}{\mu_\sigma}\varepsilon \qquad [2\text{-}13]$$

and then the strain ε and the stress σ can be calculated as (see also Figure 2-11)

$$\varepsilon = \frac{\sigma_0}{E_{H1}} + \frac{\sigma_0}{E_{H2}}\left[1 - exp\left(-\frac{E_{H2}}{\mu_\sigma}t\right)\right], \text{ and} \qquad [2\text{-}14]$$

$$\sigma = E_{H1}\varepsilon_0 - \frac{E_{H1}^2}{E_{H1} + E_{H2}}\varepsilon_0\left[1 - exp\left(-\frac{E_{H1} + E_{H2}}{\mu_\sigma}t\right)\right], \text{ respectively.} \qquad [2\text{-}15]$$

- Burger's model

Burger's model is an extension of the Poynting-Thompson model, adding an extra viscosity term (dashpot) (Figure 2-12). The general equation for this model is given in Equation [2-16] so that this represents a Maxwell element in series with a Kelvin / Voigt element.

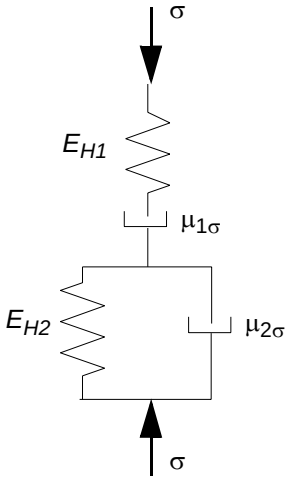

Figure 2-12: *Rheological model of Burger material.*

$$\ddot{\sigma} + \left(\frac{E_{H1}}{\mu_{1\sigma}} + \frac{E_{H1}}{\mu_{2\sigma}} + \frac{E_{H2}}{\mu_{2\sigma}}\right)\dot{\sigma} + \frac{E_{H1}E_{H2}}{\mu_{1\sigma}\mu_{2\sigma}}\sigma = E_{H1}\ddot{\varepsilon} + \frac{E_{H1}E_{H2}}{\mu_{2\sigma}}\dot{\varepsilon} \qquad [2\text{-}16]$$

Some attempts have been made to model non-linear material response, which can be classified as follows:

- geometrical non-linearity
- physical non-linearity
  - magnitude or parametric non-linearity
  - interaction or deformation non-linearity
  - inter-mode or tensorial non-linearity.

Only the isochronic non-linearity can be described by the method of rheological models (Feda, 1992). The non-linearity can also be introduced for the Hookean material (eq. 2-17) and/or the Newtonian material (eq. 2-18: *Eyring rate-process theory;* Joly, 1970).

$$\varepsilon = \varepsilon_0\left(\frac{\sigma}{\sigma_0}\right)^{1-m} \qquad (m < 1) \qquad [2\text{-}17]$$

$$\varepsilon = \frac{1}{b}sinh(a\sigma) \qquad [2\text{-}18]$$

m, *a* and *b* are soil parameters.

Plastic and viscous features of the material behaviour are important and therefore viscoplastic solutions are often more appropriate for larger strains.

Viscoplastic Approach

An important assumption for the viscoplastic approach is that the viscous effects become pronounced only after the material undergoes yielding, and that the viscous effects are assumed not to be significant in the elastic domain. As a consequence, the strain rate is composed of an elastic (*e*) and a viscoplastic (*vp*) part (Perzyna, 1963):

$$\dot{\varepsilon} = \dot{\varepsilon}^{e} + \dot{\varepsilon}^{vp} \qquad [2\text{-}19]$$

Different models have been developed during the last decades in order to determine the viscoplastic strain rate $\dot{\varepsilon}^{vp}$. Adachi *et al.* (1996) offers a review of these, such as the *Adachi and Oka model*, the *modified overstress model*, *Yin and Graham model* or the *Liang and Ma model*. It is clear that only a combination of the viscoelastic and the viscoplastic models results in effective modelling of the time-dependent behaviour of a soil. However, the experimental identification of the viscoplastic and the viscoelastic strain, which is necessary in order to determine all the parameters for these models, is very difficult. In addition, the temperature dependency has to be taken into account and therefore a thermo-viscoplastic model might be necessary for the future.

2.3.2 Frozen Soil Composites

Frozen soil is a very complex geomaterial, whose mechanical and thermal properties are coupled and dependent on numerous factors. Generally, it is a composite of four different constituents: (i) solid grains (mineral or organic) of different size and shape, (ii) ice, of different grain size and orientation, (iii) unfrozen water (e.g. Williams, 1967a) and (iv) gas or air (Figure 2-13).

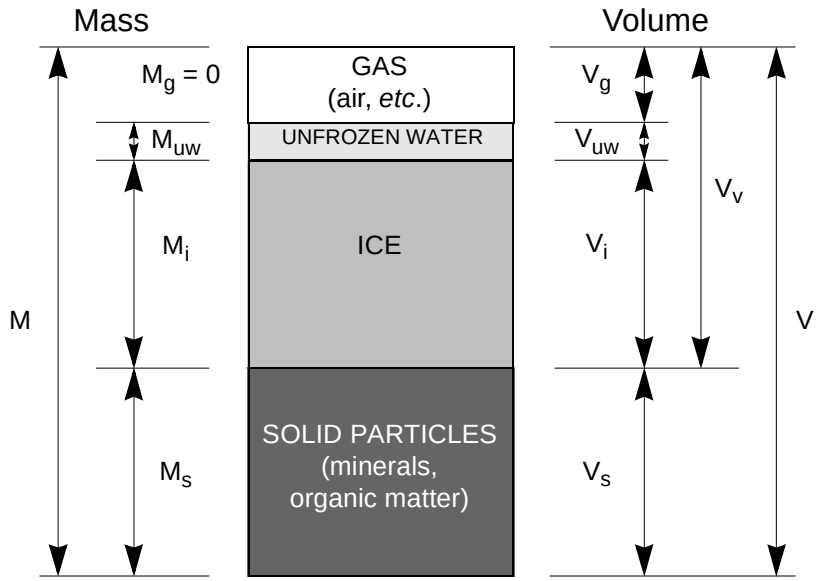

Figure 2-13: *Mass-Volume relationship for frozen soils (after Andersland and Ladanyi, 1994).*

Different phase relationships can be defined using the notation of Figure 2-13. The *voids ratio e* is defined as

$$e = \frac{V_v}{V_s} = \frac{\rho_s}{\rho_d} - 1, \qquad [2\text{-}20]$$

with V_v and V_s as the volume of voids (filled with air, water and ice) and solids, respectively. The voids ratio can also be expressed as a function of the specific density ρ_s and the dry density ρ_d. The *porosity n*, which is usually expressed in percentages, compares the volume of the voids with the total volume *V*.

$$n = \frac{V_v}{V} = \frac{e}{1+e} = 1 - \frac{\rho_d}{\rho_s} \qquad [2\text{-}21]$$

In ice and permafrost research, the ice content is usually defined by the volumes:

$$w_i = \frac{V_i}{V} \qquad [2\text{-}22]$$

The soil is *ice-rich*, sometimes also called *ice oversaturated*, when the volumetric ice content w_i is larger than the maximum possible voids ratio in the unfrozen state: $V_i > V_v$ and $V_{ext} > 0$, respectively (Figure 2-14).

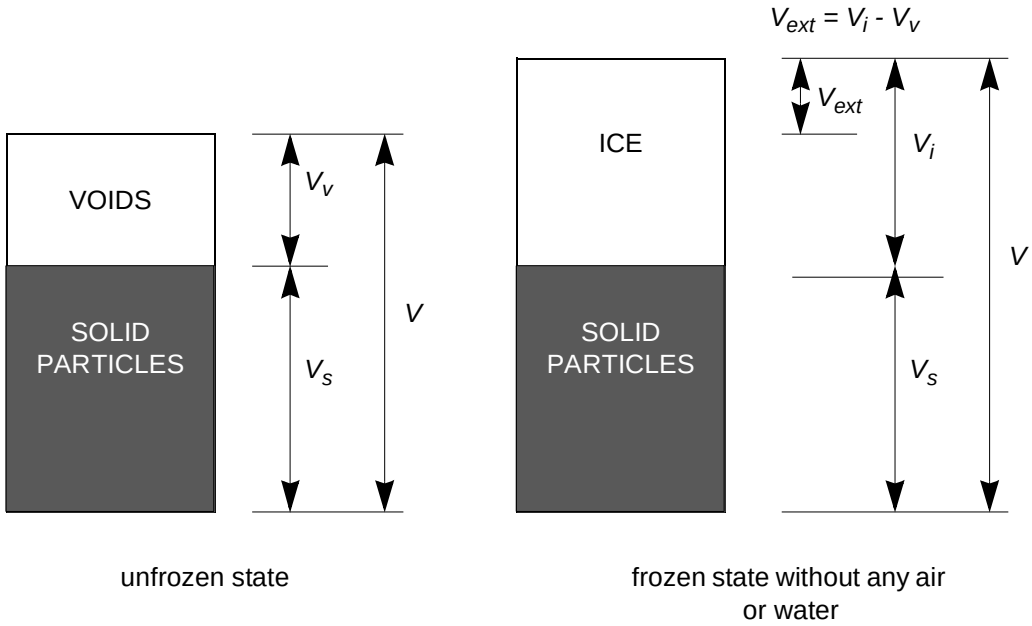

Figure 2-14: *Definition of ice-rich soils.*

Combining masses *M* and volumes *V*, the density ρ of the samples can be determined:

$$\rho = \frac{M}{V} = \frac{M_s + M_i + M_{uw}}{V_s + V_i + V_{uw} + V_g}, \quad \rho_i = \frac{M_i}{V_i}, \quad \rho_s = \frac{M_s}{V_s} \qquad [2\text{-}23]$$

ρ is the bulk density (frozen or unfrozen), ρ_i is the ice density and ρ_s is the density of the solids.

Structure of Ice

There are different forms of stable ice, which differ in the crystal structure and their orientation depending on the temperature and the pressure. A detailed description of all the known forms can be found in Petrenko and Whitworth (1999). The ice phase Ih is the form of ice that is usually found in frozen soils. This ice phase is formed under normal conditions, with temperatures above -100°C and atmospheric pressure. The number 'I' is attributed to Tammann (1900) and the 'h' represents the hexagonal rings of the crystals (Figure 2-15).

The particles within the soil are also influencing the growth of the crystals, irrespective of temperature, temperature gradient or pressure. Usually, the crystals start freezing from a solid particle until reaching the next ice crystal. Therefore, crystals within a frozen soil are usually smaller than in a pure ice sample. In addition, the freezing process attracts free water from below the ice fringe and therefore also additional water freezes within the soil matrix, resulting in a volume increase in V_i, which can be larger than 9% caused by the phase change of the water. This segregation is also the reason for the formation of ice lenses.

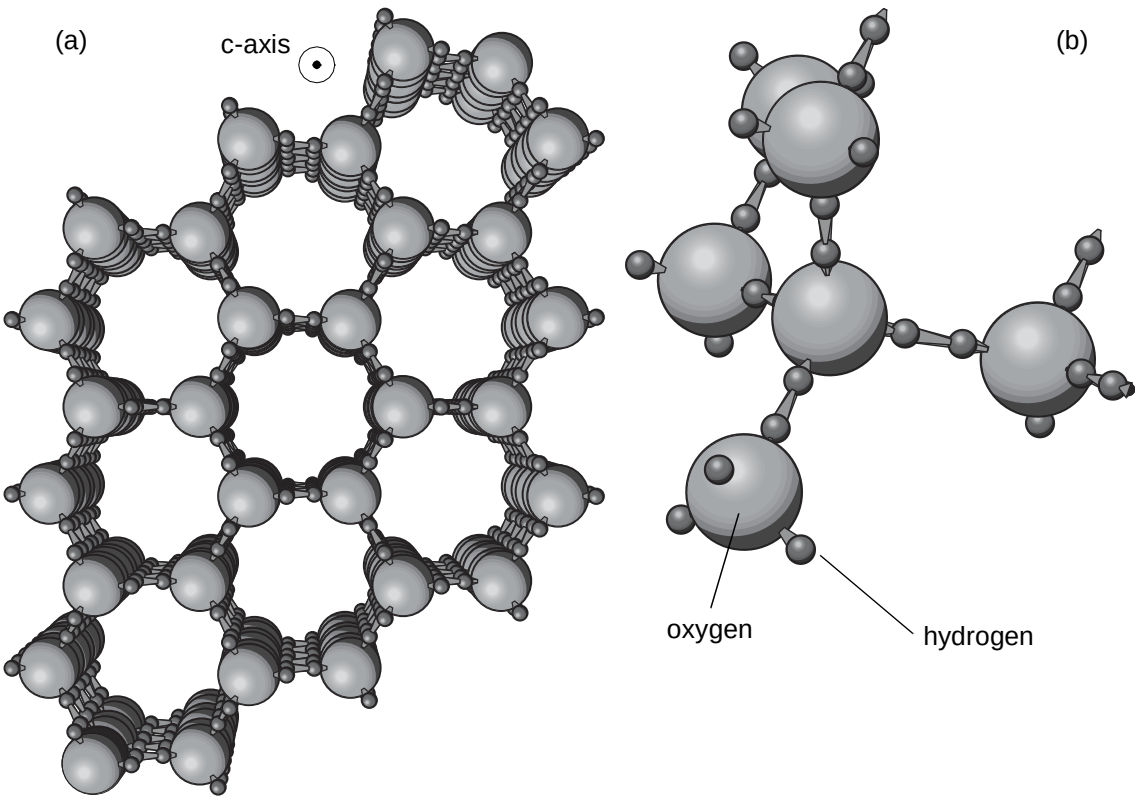

Figure 2-15: *Crystal structure of ice Ih. There is actually only one hydrogen atom between the oxygen atom, but it may change its position in-between the two hydrogen atoms shown in the figure (ice coordinates: Madura, 1994).*
a) hexagonal rings along c-axis.
b) close-up of the tetrahedral structure.

The density of ice depends on the temperature. An ice density of 0.9168 g/cm^3 can be assumed fractionally below zero centigrade.

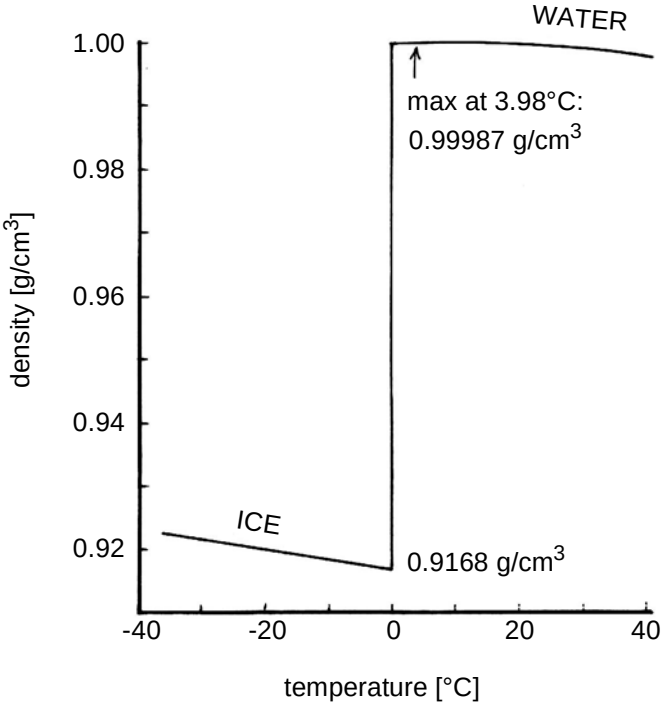

Figure 2-16: *Density variation of water and ice as a function of temperature (after Andersland and Ladanyi, 1994).*

The melting point of the ice can be expressed by the Simon equation as a function of the pressure (Wagner *et al.*, 1994):

$$p_m = p_t\left\{1 + a\left[1 - \left(\frac{T}{T_t}\right)^n\right]\right\} \quad [2\text{-}24]$$

p_m melting pressure in kPa

p_t pressure at the triple point in kPa (for ice Ih–ice III–L: p_t = 209.9 kPa, Bridgman, 1912)

a adjustable coefficient (dimensionless)

T absolute temperature in °K

T_t temperature at triple point in °K (for ice Ih–ice III–L: T_t = 251.165°K, Bridgman, 1912)

n exponent

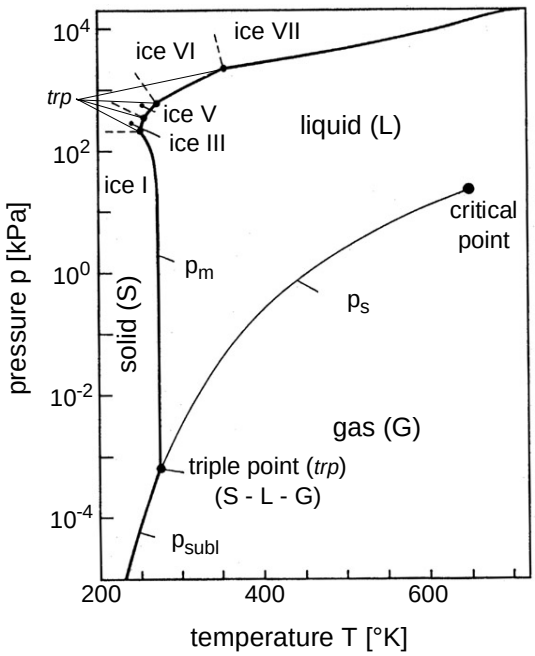

Figure 2-17: *The phase – boundary curves of water in a pressure - temperature diagram (after Wagner et al., 1994).*

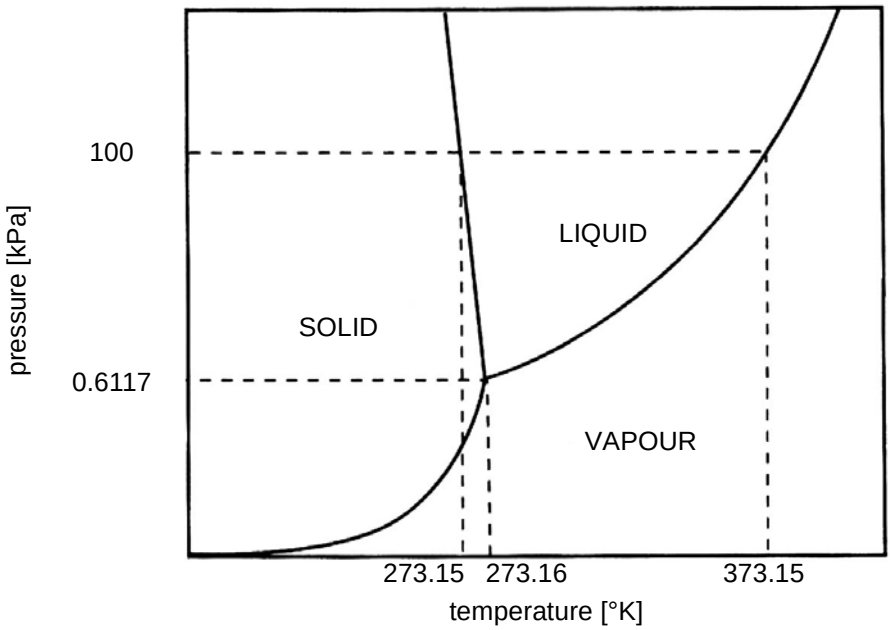

Figure 2-18: *Schematic diagram of the phase change of ice Ih, not to scale (after Wagner et al., 1994; Petrenko and Whitworth, 1999).*

Another approach is shown in Equation (2-25), which is based on numerous experimental data (for more detail, see Wagner *et al.*, 1994):

$$\frac{p_m}{p_n} = 1 - 0.626000 \cdot 10^6 \left[1 - \left(\frac{T}{T_n}\right)^{-3}\right] + 0.197135 \cdot 10^6 \left[1 - \left(\frac{T}{T_n}\right)^{21.2}\right] \quad [2\text{-}25]$$

The parameters for ice Ih within a temperature range from 273.16°K to 251.165°K and a pressure range from 0.000611657 MPa to 209.9 MPa are:

p_n normalised pressure: p_n = 0.000611657 MPa

T_n normalised temperature: T_n = 273.16°K

Unfrozen Water

Frozen soil is a composite material containing solid particles, ice, air and unfrozen water. There are two states in which unfrozen water exists: as strongly bonded and as weakly bonded water. The former is the water film around the solid particles and is held to it by high intermolecular forces that suppress freezing, even at low temperatures. As a result of this strongly adsorbed water film, probably no direct ice – sand grain contact exists (Ting *et al.*, 1983). The rest of the water is weakly bonded to the particles and can freeze more easily. The amount of unfrozen water is dependent on the temperature, stress, the size and shape of the grains, i.e. the specific grain surface within the frozen soil (e.g. Williams, 1967b) and of the solute in the water. Even though many studies have

been performed on the presence of unfrozen water in a frozen soil at temperatures below the phase equilibrium, there is still a need for research into the interaction between these components (e.g. Watanabe and Mizoguchi, 2002).

A possible composite structure of a frozen soil is shown in Figure 2-19 (after Ting *et al.*, 1983).

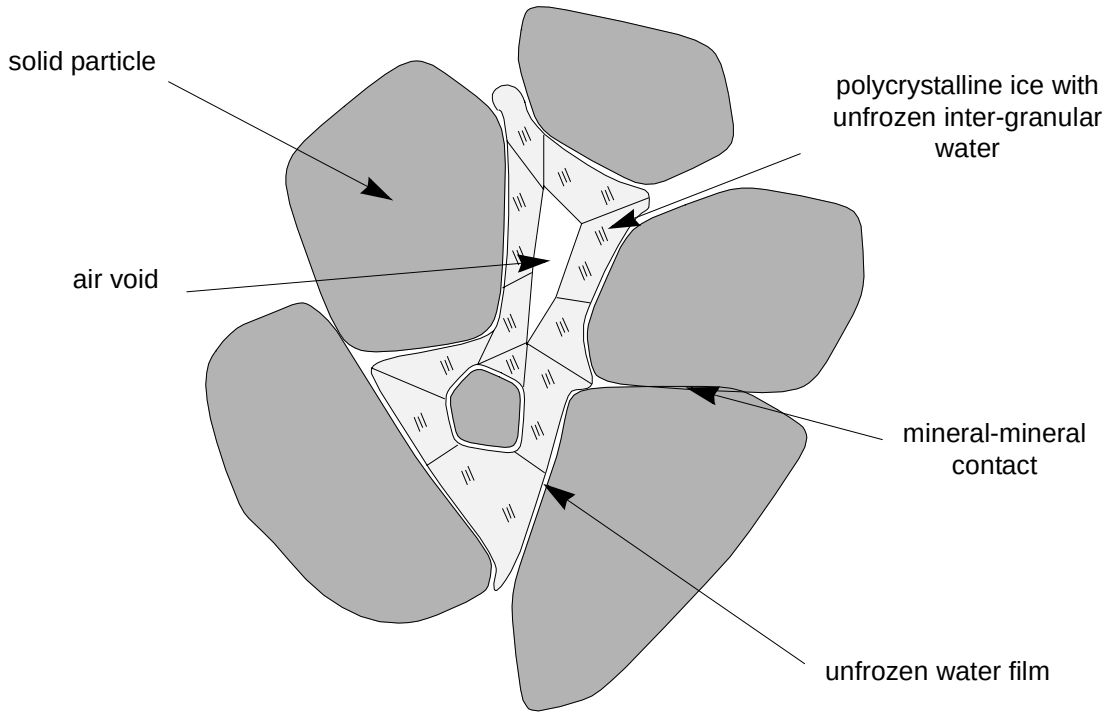

Figure 2-19: *Two dimensional schematic of the structure of frozen soils (after Ting et al., 1983).*

In order to calculate the unfrozen water content w_u, a simple power law was first introduced by Lovell (1957), and is often used in the form proposed by Anderson *et al.* (1973):

$$w_u = \alpha \cdot T^{\beta}, \qquad [2\text{-}26]$$

with α and β representing soil parameters, which are found to relate to the specific surface area S of the frozen soil and are determined experimentally, and T is the temperature below zero centigrade in °C. A general water phase composition equation emerged from regression analyses (Anderson *et al.*, 1973):

$$\ln w_u = a + b \ln S + c S^{d} \ln T, \text{ where} \qquad [2\text{-}27]$$

a, b, c and d are regression parameters to be determined from laboratory tests. Usually the volumetric unfrozen water content θ_u is measured in the field, which depends on the bulk density of the soil ρ_b and the density of the water ρ_w:

$$\theta_u = \left(\frac{\rho_b}{\rho_w}\right) \cdot w_u \qquad [2\text{-}28]$$

Anderson and Morgenstern (1973) showed the dependency of the particle size and soil density on the unfrozen water content (Figure 2-20).

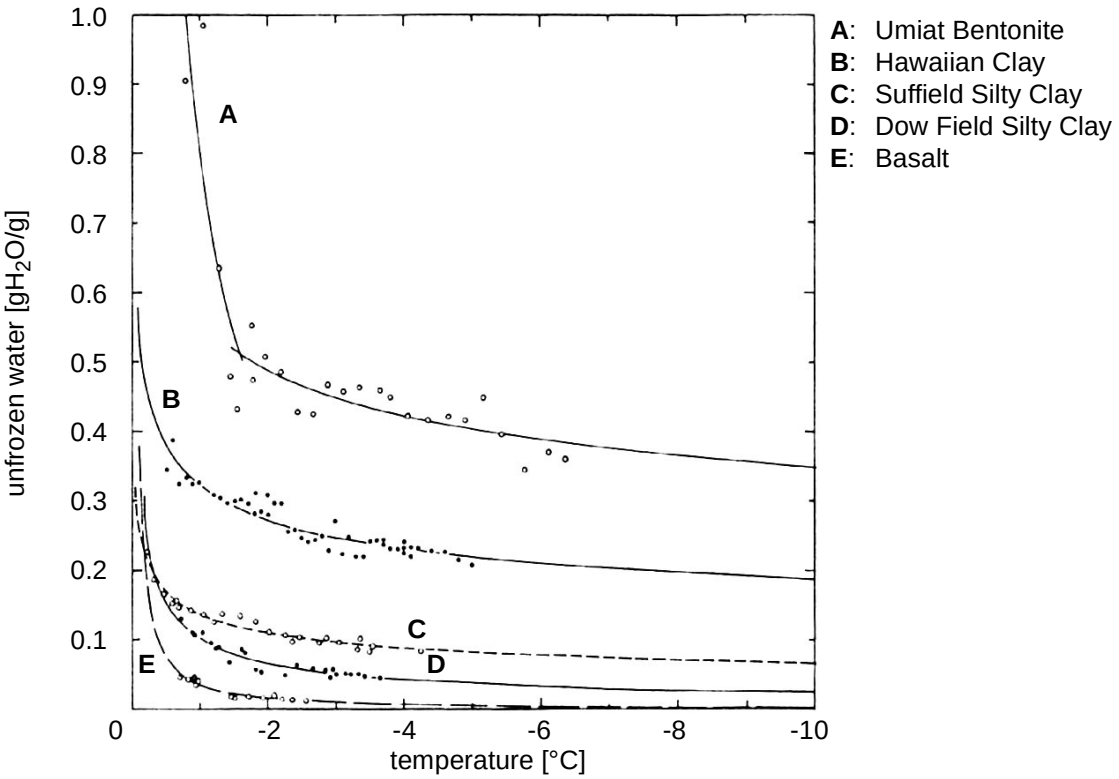

Figure 2-20: *Phase composition curve for five representative soils (after Anderson and Morgenstern, 1973).*

Equation [2-25] for pressure melting and equation [2-26] show that the amount of unfrozen water increases with increasing temperature and confining pressure. Some authors concluded that higher unfrozen water contents lower the strength and increase the creep rate (Chamberlain *et al.*, 1972; Fish, 1984; 1991; Zhu *et al.*, 1997). However, the unfrozen water within the frozen soil, influences the effective stresses not only in a negative sense (decrease of effective stresses due to increase of the porewater pressure), but also *vice versa*. Suction (negative porewater pressure) developed during the freezing of saturated silt and clay samples at temperatures between 0°C and -3°C (Williams, 1967c) can strengthen the soil due to an increase in effective stresses. The measured suction was larger as temperatures decreased, and can reach values of more than 0.1 MPa for various clays (Williams, 1967b). Schofield (1935) already showed that as the moisture content of soil samples is reduced, the freezing point is depressed further below 0°C. He carried out investigations on the suction with which water is held in the soil sample and argued that this suction or *pressure deficiency* of the soil water around solid particles is mainly responsible for the freezing point depression observed.

This depression occurs because the attraction force between the unfrozen water and the wall of the pore is greater per liquid molecule in a small pore than in a big one, as the wall area per liquid molecule is greater. This adhesive attraction force keeps the liquid molecules from forming an orderly solid crystal structure. The low temperature is acting as a driving force for freezing, and at a certain point, this force is great enough to cause freezing. However, there will be

an adsorbed, liquid-like layer nearest the wall that will never freeze. (Also free ice has a liquid-like layer, a few hundred molecules thick, that exists between the ice crystals at temperatures well below 0°C (Hobbs, 1974)).

The existence of such strongly bonded liquid water at temperatures and pressures below the normal phase boundary is often called *premelting* (e.g. Dash *et al.*, 1995). The effect is driven by the tendency to reduce the interfacial free energy. For, if the state of the system slightly below the bulk melting temperature were to be initially dry, the system could lower its free energy by converting a layer of the solid to liquid. The cost of this conversion involves free energy change due to melting, but if the layer is thin enough and the temperature sufficiently close to the bulk melting point the cost will not be prohibitive. This competition between surface and conversion terms establishes the actual thickness of the liquid: it is the value at which the free energy of the system is a minimum. The determination of a theoretical thickness-temperature relationship and its dependence on the nature of the molecular interactions is described in Dash *et al.* (1995).

Differences in the unfrozen water content exists between thawing and freezing and had been illustrated by Stähli and Stadler (1997). This hysteresis is relatively minor for the coarser materials (Figure 2-21). Organic materials that have large specific surfaces, also show hysteresis between thawing and freezing and have higher unfrozen water contents at similar temperatures than non-organic soils (Nyberg *et al.*, 2001).

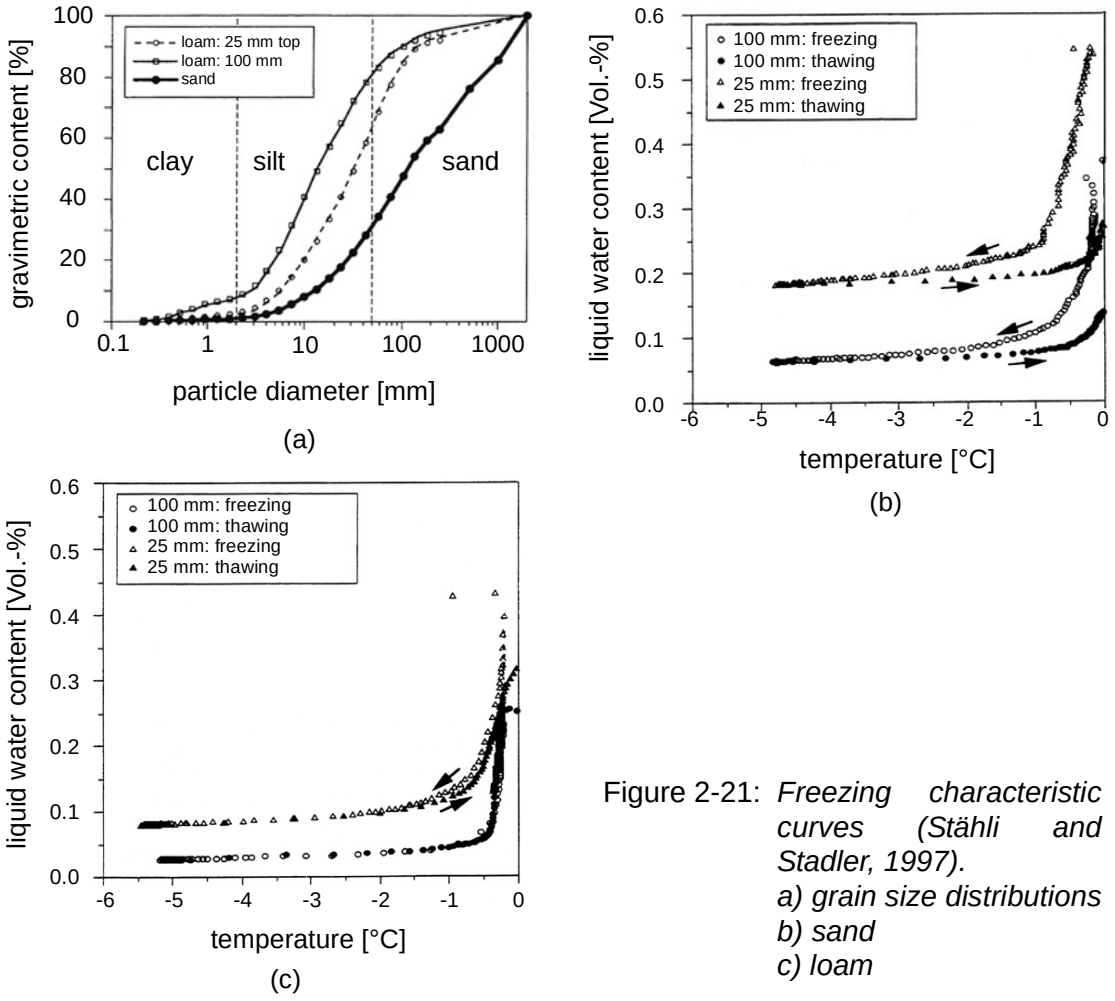

Figure 2-21: *Freezing characteristic curves (Stähli and Stadler, 1997).*
a) grain size distributions
b) sand
c) loam

2.3.3 General Behaviour of Frozen Soils

Most of the research on frozen soils has been performed within the background of engineering problems due to construction. This was necessary for the development and exploitation of the northern regions in the early 1960's, and for construction within artificially frozen soils, for example for tunnels or shafts to be built within saturated granular materials (e.g. Jessberger, 1996). The mechanical behaviour of Alpine permafrost soils, where the solid particles are much coarser than in the polar regions, has not been studied previously. In contrast to the frozen ground, which originates from artificial freezing of a saturated material, for example for tunnelling (Herzog and Ramholt, 1979), the volumetric ice content is much higher in naturally frozen grounds.

Under standard situations with constant ground water conditions, time effects are often neglected in 'normal' soil mechanics with granular, relatively stiff geomaterials, since they only play a minor role in the material behaviour and have nearly no influence on the strength of the soil. Frozen material on the other hand, exhibits pronounced time dependency, which is often described as a creep phenomenon. However, it is not so easy to separate the strength and deformation processes. The strength of the material is very much dependent on the loading strain, and therefore on the test duration, i.e. on the time until a certain strain is reached. Sayles (1968) and Sayles and Haines (1974) have already shown for frozen sands and for frozen silts, respectively, that the long-term strength is less than 45% and can be as low as 10% of the instantaneous strength in unconfined compression. In addition, Fish (e.g. 1985; 1991) showed that creep tests and strain-rate compression tests are coupled, and therefore similar parameters can be derived from both tests.

Some general summaries of progress in modelling frozen soil behaviour can be found in the state-of-the-art paper presented by Sayles (1988) at the Fifth International Symposium on Ground Freezing or in an earlier work by Anderson and Morgenstern (1973), which was presented at the Second International Conference on Permafrost.

However, the author distinguishes between strength and creep literature within this review, being fully aware that it is not easy to separate the two interlocking mechanisms of behaviour. Therefore the following two chapters contain research that focuses more on one or the other point.

2.3.4 Strength and Stiffness

An overview of Youngs' moduli of ice and frozen sands are given in Yasufuku *et al*. (2001). The initial secant modulus G_{max} is strongly dependent on the axial strain as well as on the temperature and the composition of the material. Therefore the values range from 0.05 GPa up to 35 GPa.

Strength and stiffness of ice

Numerous compression tests have been performed in order to study the failure processes of polycrystalline ice. Temperature, strain rates, confining pressure, grain size or inclusions have provided the focus during early research projects.

According to Gold (1977), the maximum unconfined compression strength of polycrystalline ice with randomly oriented grains of about 1 mm grain size at a temperature of -10°C is reached at a strain rate between 10^{-3} s^{-1} and 10^{-4} s^{-1} and is about 10 MPa. The dependency of the compressive strength on strain rate and confining pressure was shown among others by Chamberlain *et al.* (1972), Alkire and Andersland (1973) and Jones (1982). The second study demonstrated an increase in long-term strength with increasing confining pressure and the latter paper indicated that below strain rates of 10^{-6} s^{-1}, there was little effect of the confining pressure in contrast to strain rates above $5 \cdot 10^{-3}$ s^{-1}, where an increase in the compressive strength with increasing confining pressure was found.

Mellor and Cole (1982) found an *initial yield point* for fine-grained isotropic ice in uniaxial compression, at which internal cracks began to form before a peak stress was reached.

The different failure modes of ice, depending on these boundary conditions (temperature, confining pressure, *etc*.), have also been studied extensively. Mizuno (1998), for example, showed that a higher confining pressure was required to inhibit brittle failure for columnar ice and coarse-grained ice than for fine-grained granular ice at the same strain rate. More studies dealing with microcracking and strength have been conducted among others by Kalifa *et al.* (1992), Rist and Murrell (1994), Rist *et al.* (1994), Meglis *et al.* (1999) or Melanson *et al.* (1999). The latter two publications show that the most dramatic microstructural changes occur during the first few percentages of axial strain deformation.

Fish and Zaretsky (1997a; 1997b) describe a simple parabolic yield criterion for ice in a multiaxial stress state under high hydrostatic pressures. Only three parameters, which have a defined physical meaning, are required. With those temperature dependent parameters the octahedral ice shear stress τ_i can be calculated:

$$\tau_i(p, T) = (c + bp) - (c + bp^*)\left(\frac{p}{p^*}\right)^2 \qquad [2\text{-}29]$$

b = $\tan \phi$

ϕ internal angle of friction (temperature dependent)

c ice cohesion (temperature dependent)

T temperature

p hydrostatic pressure

p^* ice melting pressure (temperature dependent)

The temperature effect on the strength of ice under triaxial conditions was studied by Rist and Murrell (1994) and Gagnon and Gammon (1995) using the Arrhenius approach. The second study also showed that the uniaxial strength at a constant temperature and constant strain rate correlates with the mean number of air bubbles per unit volume. The strength increases with increasing bubble density for the glacial ice that has been investigated by Gagnon and Gammon

(1995), which is in contrast to studies performed on laboratory ice (e.g. Toope *et al.*, 1991; Ebinuma and Maeno, 1992) the presence of bubbles at grain boundaries weakens the ice. Gagnon and Gammon (1995) conclude that *intragranular* bubbles, which were found in the iceberg samples, have a strengthening effect since they can accommodate more strain for a given stress, whereas *intergranular* bubbles, i.e. bubbles at grain boundaries, have a weakening effect and this may explain why uniaxial compressive strength of iceberg and glacial ice is generally greater than laboratory-grown ice of similar grain size. Andrews (1985) partly attributes the low fracture toughness of glacier ice recorded during his investigations to the presence of air bubbles.

Sinha (1989a) determined Young's moduli and Poisson's ratios of 8.9 to 9.4 GPa and about 0.31, respectively for granular ice at temperatures from 0 to -38°C.

Triaxial tests on crushed ice showed that unlike polycrystalline ice, its behaviour is very sensitive to the hydrostatic pressure due to the porosity of the composition (Singh and Jordaan, 1996). However, the sample showed no rate dependency in the axial strain rate range applied, which was between $5 \cdot 10^{-3}$ s^{-1} and $2 \cdot 10^{-2}$ s^{-1} with a confining pressure up to 20 MPa and a temperature of -10°C.

Many of the above mentioned studies showed that the microstructure and therefore the type of the ice has a major influence on the mechanical properties. A good overview of these influences is given by Cole (2001).

Strength and stiffness of frozen soils

Different 'mixture' theories are available (cf. Yasufuku *et al.*, 2001) in order to determine elastic properties of saturated ice-sand mixtures at a constant temperature.

Comparisons between frozen and unfrozen high-pressure triaxial tests on Manchester fine sand (Swan, 1996) showed that a stiffer material behaviour was achieved in the frozen state and that the Young's modulus as well as the upper yield stress, in contrast to the peak strength, were now independent of the confining stress. This has also been shown by Andersen *et al.* (1995). After reaching the upper yield region, the formerly intact frozen material transforms to a damaged composite of solid particles and ice grains. The study of mechanisms presented in the literature (Kaplar, 1963; Parameswaran and Jones, 1981; Baker and Kurfurst, 1985) and summarised in Andersen *et al.* (1995), shows that the mineralogy of the solid particles, the density of the material and, in particular, the bond strength of the ice-silicate interface are the most significant factors that affect the Young's modulus. On the other hand, various authors (Chamberlain *et al.,* 1972; Sayles, 1973; Bragg and Andersland, 1980; Parameswaran and Jones, 1981; Bourbonnais and Ladanyi, 1985; Sayles, 1988) presented discussions of possible mechanisms influencing the upper yield point reaching a general consensus that the upper yield behaviour of sand-ice mixtures is dominated by the ice matrix and therefore dominated by the volumetric ice content.

Direct shear test on frozen sand with various volumetric ice contents (Yasufuku *et al.*, submitted) demonstrated that during initial phases of shearing, the shear zone extends primarily from particle to particle over a depth of approximately 1-2 mm. However, as shearing proceeds, the shear zone increases in thickness due to mobilisation of the ice granules and particles acting and dilating together, which can be described as a '*rubbleisation*'. The schematic shear response of a relatively dense sample, resulting from this mechanism is given in Figure 2-22 and is similar to results obtain from triaxial compression (e.g. Andersen *et al.*, 1995). Low density results in a more ductile behaviour without strain softening after the peak value.

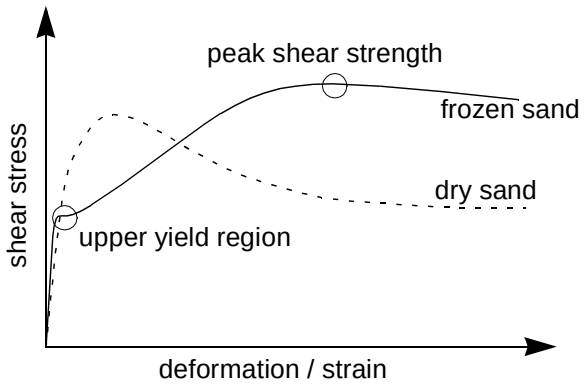

Figure 2-22: *Schematic shear response of frozen and dry sand under direct shear.*

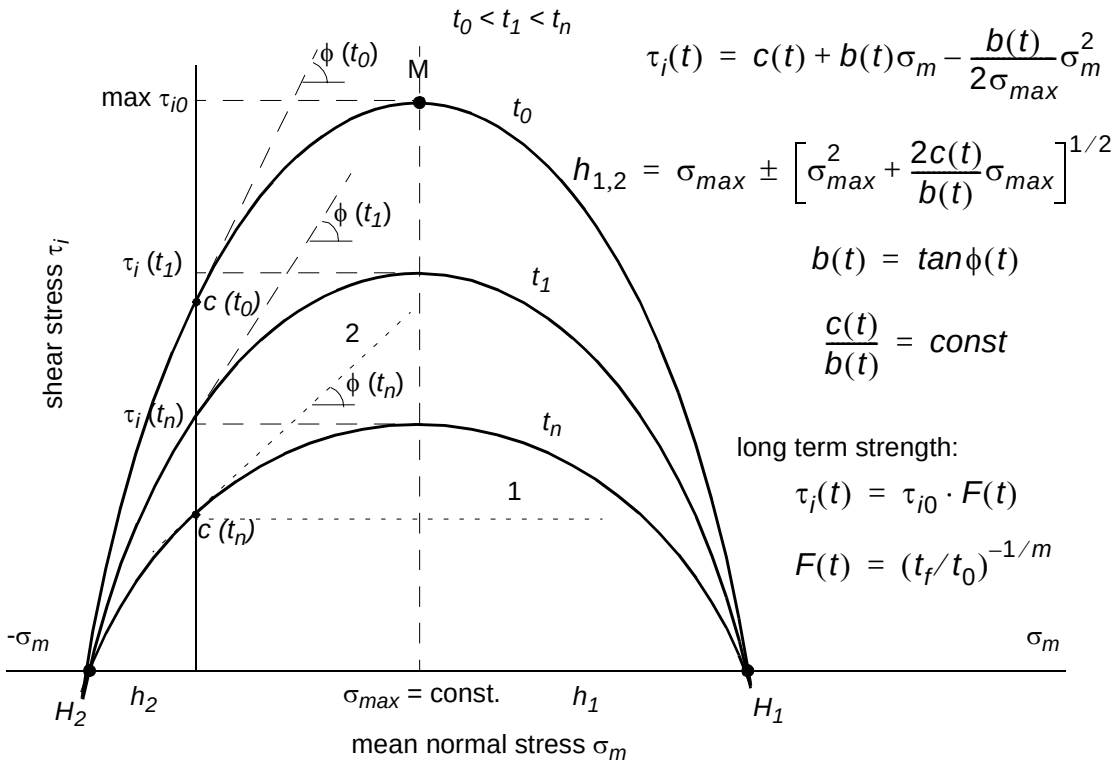

Figure 2-23: *Parabolic criterion for creep strength of frozen soils (from Fish, 1985; 1991).*
1: Tresca criterion
2: Mohr-Coulomb criterion

A parabolic yield and long-term strength criteria for frozen soils has been presented and applied for frozen Ottawa sand under combined stress state by Fish (1991; 1994) that use a cohesion *c*, a friction angle ϕ, mean normal stress σ_{max} at maximal shear stress τ_{i0} , time to failure t_f and two long-term strength parameters *m* and t_0 (Figure 2-23). The shape of the long-term strength curves are similar and therefore the maximum shear stress τ_i will always be attained for the same mean normal stress σ_{max}, which can be considered to be a fundamental parameter of frozen soil or ice.

Figure 2-23 also shows two additional criteria for the determination of the shear strength: i) Tresca criterion (1869) and ii) Mohr-Coulomb / Drucker-Prager criterion (1952). The first criterion simply assumes ideal plasticity, i.e. no change in strength with increasing normal stress and the second criterion incorporates a linear increase of the shear strength with increasing normal stress.

The strength of the frozen sand is strongly dependent of the volumetric fraction of ice, or sand, respectively (e.g. Sayles and Carbee, 1981; Jones and Parameswaran, 1983; Ting *et al.*, 1983). Different mechanisms play different roles with increasing volume fraction of sand (e.g. Goughner and Andersland, 1968). Based on earlier works on sand/ice mixtures (Goughner and Andersland, 1968; Hooke *et al*., 1972) Ting *et al.* (1983) propose four mechanisms (Figure 2-24):

i) ice strength and strengthening,

ii) soil strength,

iii) dilatancy effects, and

iv) structural hindrance between soil and ice matrix.

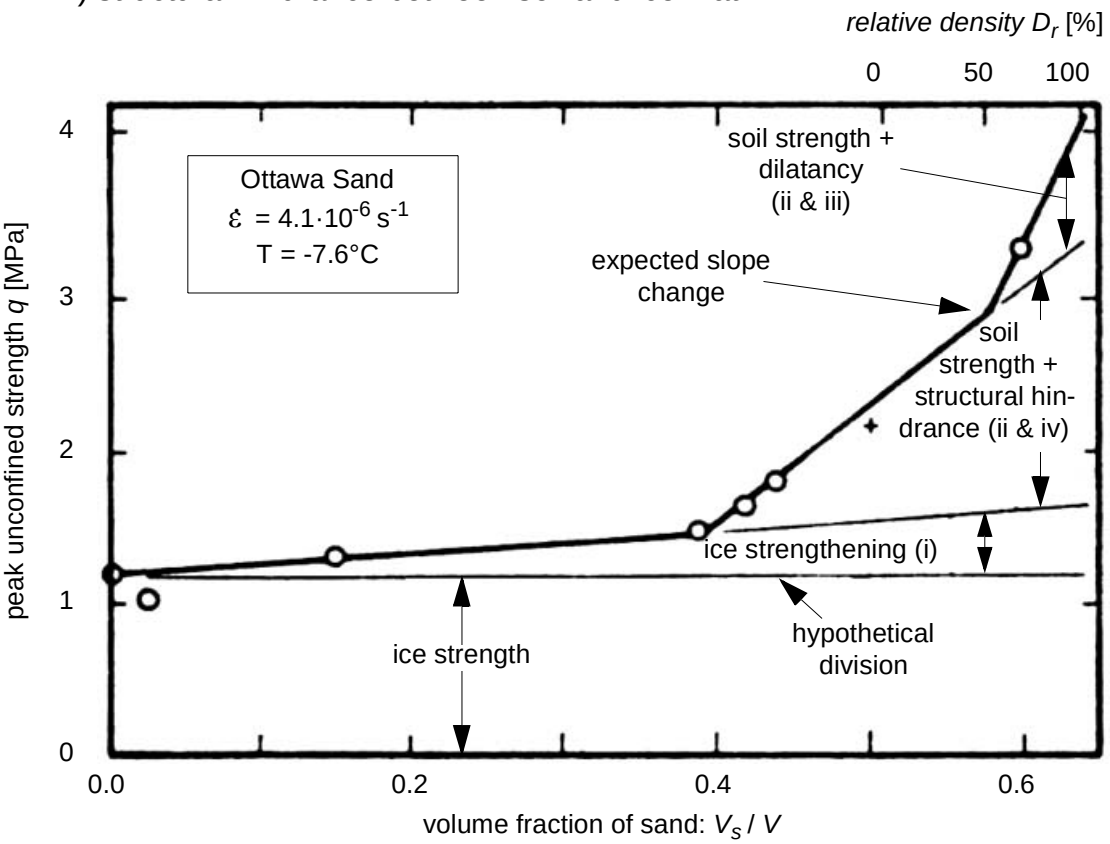

Figure 2-24: *Mechanism map for unconfined strength of frozen sand (after Ting et al., 1983) with test data from Goughner and Andersland (1968).*

The shear behaviour of frozen sand, however, is strain rate, temperature and normal pressure dependent. Chamberlain *et al.* (1972) have shown that for a constant temperature, the frozen mixture starts to behave similarly to a saturated sand for high confining pressures, when the pore ice melts under high stresses. This general behaviour was summarised by Ladanyi (1981) and is presented as a schematic plot of the failure envelope for frozen sand at various normal pressures (Figure 2-25).

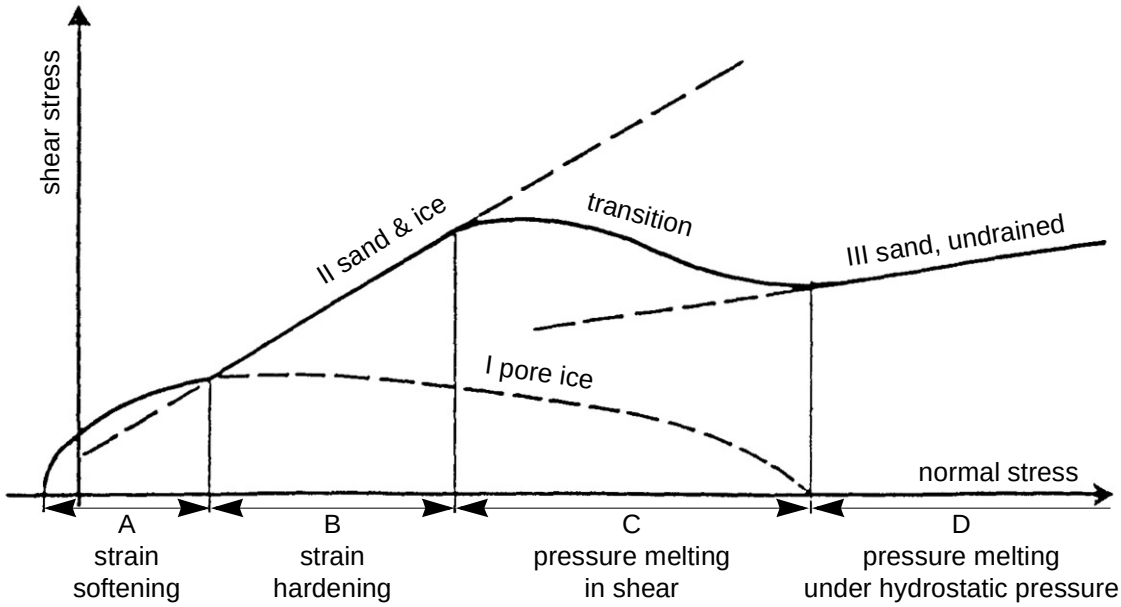

Figure 2-25: *Schematic representation of the whole failure envelope for frozen Ottawa sand (after Ladanyi, 1981).*

Based on earlier findings, such as those from Alkire and Andersland (1973), Sayles (1973) or Ting (1981), Ladanyi (1985) presents stress transfer mechanisms in frozen soils. He concluded that stress will be transferred mainly through the pore ice due to increasing hydrostatic pressure, if the soil is ice-rich. However, within a soil that also contains unfrozen water, the ice will carry more load initially than the water, which may enhance the pressure melting considerably.

Adachi *et al.* (1990) have developed a constitutive model for triaxial tests by introducing the stress history tensor that varies with respect to a generalised time: $dz = F(\text{strain rate})dt$, where dz is an increment of the time measurement z, t is the real time and the function F is called the *rate-dependency function* and has to be determined experimentally. The authors' approach is based on decomposition into an elastic and a plastic component. The latter uses a non-associated flow rule, which deals with strain hardening/softening effects. This model has been used for numerical modelling of triaxial tests on frozen sands (Oka *et al.*, 1994).

In addition, a summary of a number of uniaxial and triaxial compression tests on frozen, saturated sand that report Young's moduli, tangent, secant, shear, or cyclic moduli and stress-strain curves showing a distinct upper yield stress are shown in Andersen *et al.* (1995). There are also numerous studies, which confirm the high sensitivity of the strength of frozen soils to temperature (e.g. Haynes and Karalius, 1977; Zhu and Carbee, 1984). The decrease, which is more

significant for compression tests than for tensile tests, is primarily attributed to the increasing amount of water and decreasing strength of the ice matrix with increasing temperature. Sayles (1966) and Bourbonnais and Ladanyi (1985) presented unconfined compression strength for various materials, at temperatures from the melting point down to more than -100°C (Figure 2-26).

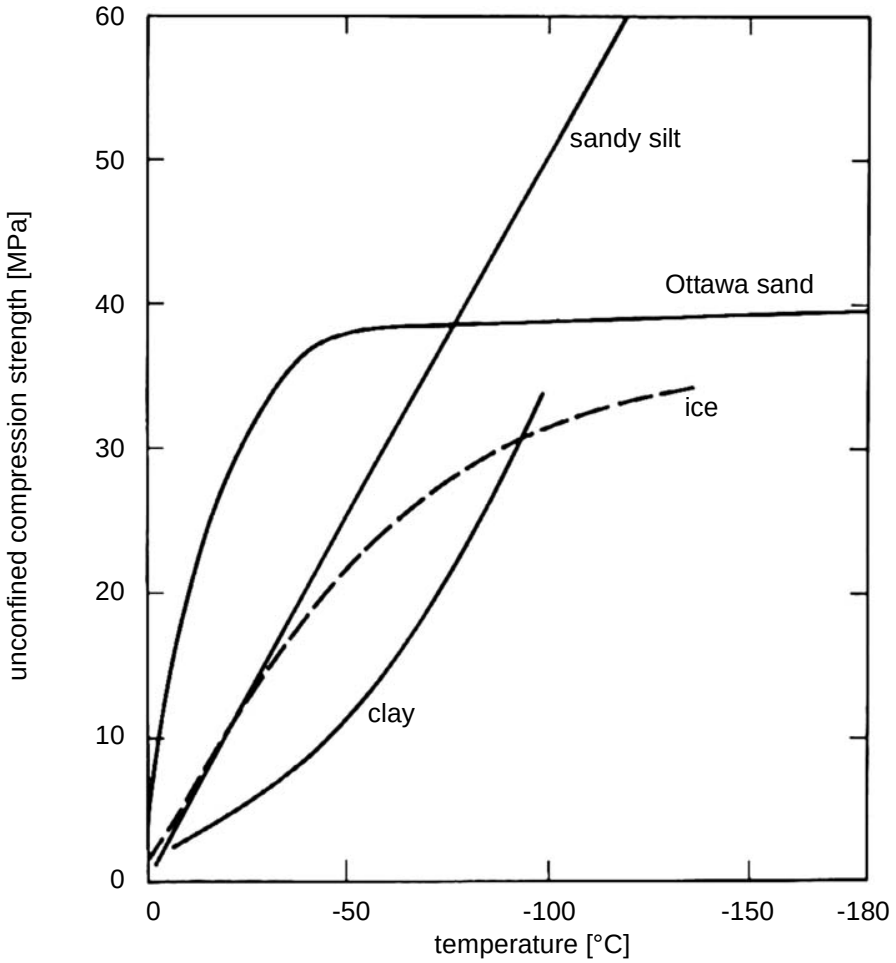

Figure 2-26: *Temperature dependency of unconfined (uniaxial) short term compression strength for various frozen materials (after Sayles, 1966).*

2.3.5 Creep

The effect of time on material behaviour has been noted from the earliest times of the development of engineering even though first tests on metals have only been carried out since the first decade of the twentieth century. In the middle of the same century, these phenomena had been recognised for other materials, such as concrete, clays, rocks or ice. Creep has then been defined as a deformation with time under a constant stress. A typical creep curve is shown in Figure 2-27. Three different stages can be distinguished: an initial strain ε_0 can be observed immediately after applying a load followed by the *primary creep* phase (AB), where the strain rate $\dot{\varepsilon}$ decreases. A phase exists from point B to C, in which nearly no change in strain rate occurs. This region is called the *secondary* or the *steady-state creep* phase and was already identified by Glen (1955) for

ice. The occurrence and length of the secondary creep phase, as well as the appearance of the third stage (CD), the *tertiary creep* phase depends on many different factors. The form of the creep curve is only stress dependent for a similar sample at the same temperature conditions (Figure 2-28). The strain rate accelerates during the tertiary creep phase, until a creep failure occurs (D). However, usually, the strain ε_f and the time t_f are defined as the failure criterion for creep.

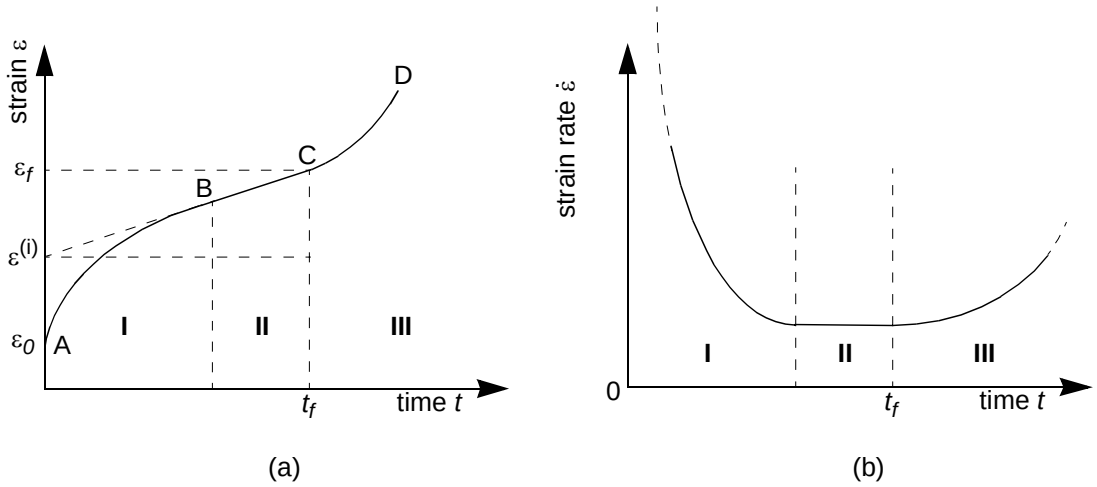

Figure 2-27: *Schematic creep curve for a material under constant load (after Andersland and Anderson, 1978).*
a) strain versus time (basic creep curve)
b) true strain rate versus time

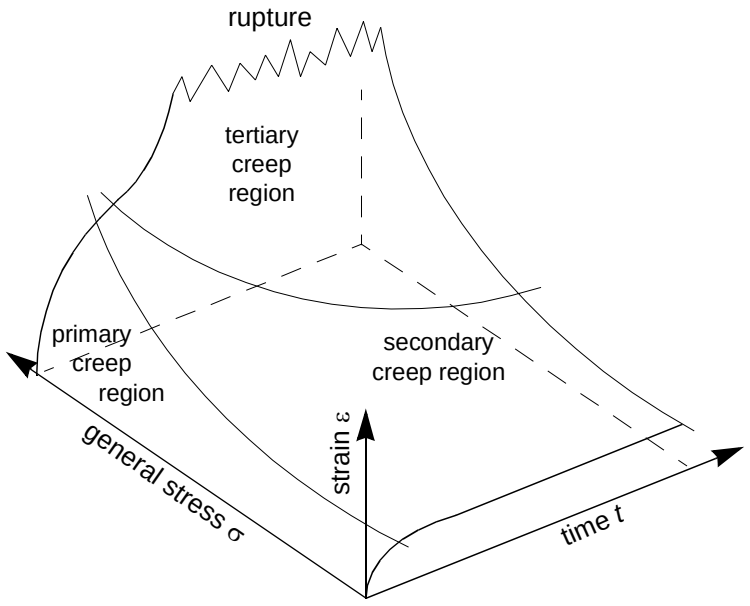

Figure 2-28: *Schematic stress dependency of creep curves (after Phukan, 1985).*

Creep of ice

Nye (1953) presented a flow law for ice based on a power law and analysed data from laboratory experiments as well as from a borehole experiment. Even though the ice conditions were not the same for the borehole contractions (relaxation) studied, the minimum strain rate was related to the overburden stress by a power of about 3. Glen (1955), whose early data were also used by Nye (1953), showed that laboratory made polycrystalline ice creeps in a similar fashion to metals at high temperatures corresponding to a power law between the stress σ and the strain rate $\dot{\varepsilon}$:

$$\dot{\varepsilon} = A \cdot \sigma^{n} \qquad [2\text{-}30]$$

The values for *n* in his studies are about 3.2. In contrast to the temperature dependency of *A*, Glen found none for *n* and therefore he proposes to use the Arrhenius approach (Equation [2-6]) in order to account for the temperature changes:

$$\dot{\varepsilon} = B \cdot exp\left(\frac{-Q}{RT}\right) \cdot \sigma^{n} \qquad [2\text{-}31]$$

If *n* is known, the activation *energy Q* can be derived from tests at various temperatures.

Many researchers investigated these type of creep laws and published different values for *n*. Some of the data are summarised in Table 2-3.

reference	year	*n*	type of ice	temperature [°C]
Glen	1955	3.2	polycrystalline	-0.02 – -12.7
Steinemann	1958	1.85 - 4.2 increase with σ	monocrystalline	-1.9 – -21.5
Mellor and Testa	1969	only activ. energy was published	polycrystalline monocrystalline	0 – -72.5 -20.3 – -61.5
Barnes *et al.*	1971	≈ 3; > 3 at $\sigma > 2000$ kPa	polycrystalline	0 – -45
Jones	1982	≈ 4 confined ≈ 5 unconfined	polycrystalline	-11
Mellor and Cole	1983	≈ 4	polycrystalline	-5
Cole	1987	2.8, $\dot{\varepsilon} = 10^{-7} - 10^{-6} s^{-1}$ 4.5, $\dot{\varepsilon} = 10^{-5} - 10^{-3} s^{-1}$	polycrystalline	-5
Rist and Murrell	1994	≈ 4.2, σ_c = 5 - 30 MPa	polycrystalline	-20 – -45
Arakawa and Maeno	1997	3.4, ductile region 6.5, brittle region	polycrystalline	-10 – -173
Meglis *et al.*	1999	4.0 - 4.6	granular ice	-5 – -8

Table 2-3: *Overview of different creep parameters for ice.*

The increase of *n* above a value of 3 is generally considered to be associated with the onset of microcracking. Cole (1987) observed an increase of *n* from 2.8 to 4.5 depending on the strain rate and grain size, which has an influence primarily on primary creep. Dynamic recrystallisation was assumed for low strain rates ($<10^{-6}$ s^{-1}). The formation of microcracking itself, however, depends on the confining pressure (e.g. Meglis *et al.*, 1999), in that dynamic recrystallisation is more likely to develop at high values. Nevertheless, Meglis *et al.* (1999) also conclude that several deformation mechanisms, including microcracking, pressure melting, melting caused by frictional heating and recrystallisation-enhanced creep are all active over a range of stresses. Their relative effect on the deformation mechanism, however, depends on the boundary conditions described above.

The role of grain-boundary sliding mechanisms on microcracking was studied among others extensively by Sinha (1979, 1984). Based on the well accepted assumption that grain boundary sliding is responsible for the delayed elastic (sometimes also called *anelastic*) strain, the first paper presents a nonlinear model that incorporates grain size effects. The second publication verifies the concept that polycrystalline materials may exhibit cracking activity on attaining a critical delayed elastic strain with experimental data on ice. Elvin and Shyam Sunder (1996) used finite element simulations of a unit cell made up of three hexagonal grains to demonstrate grain boundary sliding and showed that sliding is necessary to generate stresses that can nucleate and propagate a grain boundary microcrack.

Manley and Schulson (1997) have produced evidence suggesting that *n* is correlated with the ratio of the climb to the glide forces acting on the dislocation (see Figure 2-8).

The temperature dependency of deformation processes has been discussed by many authors (e.g. Mellor and Testa, 1969; Barnes *et al.*, 1971). Barnes *et al.* (1971) distinguished between processes at temperatures below and above -8°C. The liquid phase at temperatures close to zero centigrade allows dislocation climb and extensive grain-boundary gliding. Mellor and Testa (1969) also studied the effect of creep under uniaxial compression close to 0°C, and suggested an exponential relationship between axial strain rate $\dot{\varepsilon}$ and applied axial stress σ of the form:

$$\dot{\varepsilon} = \dot{\varepsilon}_0 \cdot e^{\sigma/\sigma_0}, \qquad [2\text{-}32]$$

with $\dot{\varepsilon}_0$ as the strain rate at zero stress, which is a theoretical value that can be determined as the intercept of a linear regression in a σ-$\dot{\varepsilon}$-diagram, and σ_0 as a constant value. Similar observations were described by Morgan (1991) who tested the uniaxial creep of polycrystalline ice at temperatures between -5°C and -0.01°C. The values of secondary strain rate were found to increase rapidly but smoothly at temperatures close to the melting point of the ice and could not be described by an Arrhenius equation. He concluded that the increasing amount of water between the grains facilitates sliding along the grain boundaries and enhances grain movement as well as recrystallisation. And therefore, Budd and Jacka (1989) concluded that close to the melting point, the creep is associated with internal melt water, particularly near stress concentrations. As a consequence, the temperature dependency of the minimum creep rate cannot be

explained any more using a constant activation energy. Table 2-4 summarises apparent activation energies for minimum creep rates at various temperatures determined by the power law relationship presented in equation [2-31].

temperature T_1 [°C]	-0.05	-1	-2	-5	-10	-20	-30	-40
temperature T_2 [°C]	-1.0	-2	-5	-10	-20	-30	-40	-50
temperature interval ΔT [°C]	0.95	1	3	5	10	10	10	10
strain rate ratio $\varepsilon(T_1)/\varepsilon(T_2)$	2.06	1.66	2.73	2.88	4.00	3.61	4.50	5.33
ratio $[\varepsilon(T_1)/\varepsilon(T_2)]/\Delta T$ [°C^{-1}]	2.16	1.66	0.91	0.58	0.40	0.36	0.45	0.53
activation energy [kJ/mole]	500	300	200	124	77	66	71	73

Table 2-4: *Apparent activation energy for minimum creep rate at σ = 1 bar (oct.) from -0.05° to -50°C (Budd and Jacka, 1989).*

Derradji-Aouat and Evign (2001) propose that up to the point where microcracks start to damage the ice, the strain can be divided into three parts: an instantaneous elastic strain $(\varepsilon_{ij})^{ie}$, induced by lattice deformation, a viscoelastic strain, $(\varepsilon_{ij})^{ve}$, induced by grain boundary sliding and a viscoplastic strain, $(\varepsilon_{ij})^{vp}$, induced mainly by the movement of dislocations. The microscopic processes that control the plasticity in polycrystalline ice are reviewed in Duval *et al.* (1983), who used other extensive reviews for polycrystalline ice (Goodman *et al.,* 1981; Frost and Ashby, 1982) to develop a diagram (Figure 2-29) that summarises the microscopic response of isotropic polycrystalline ice to stress. The axes are the equivalent stress, σ:

$$\sigma^2 = \frac{1}{2}[(\sigma_1 - \sigma_2)^2 + (\sigma_2 - \sigma_3)^2 + (\sigma_3 - \sigma_1)^2],$$

normalised by the Young's modulus E, and the temperature T normalised by the melting temperature T_M. The heavy lines divide the diagram into fields within which a single mechanism of deformation is dominant: rate-insensitive plasticity (top), power law (or Glen law) creep (right), and diffusional flow (bottom). Superimposed on the fields are contours of constant equivalent strain rates, $\dot{\varepsilon}$. They show the rate of deformation produced by a given combination of stress and temperature.

The diagram is intersected about halfway up by the onset of cleavage fracture. Unlike plasticity, fracturing processes depend on all three invariants of the stress tensor. Because of this the fracture stresses in tension and compression differ; and a sufficiently large confining pressure can suppress them entirely. Only then does the upper part of the diagram (with contours shown as broken lines) become accessible.

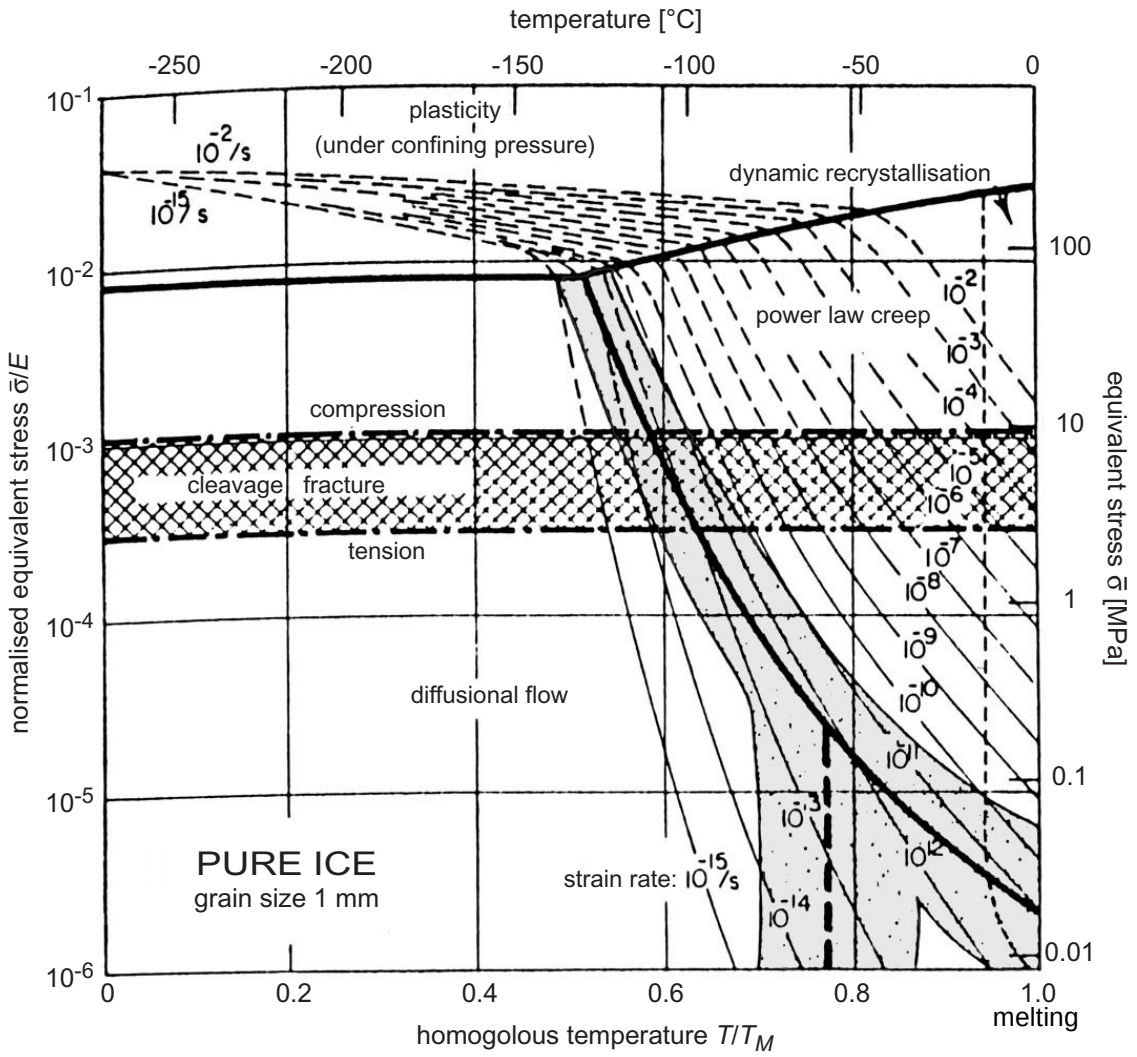

Figure 2-29: *A deformation mechanism diagram for ice with a grain size of 1 mm. It shows regimes of power-law (Glen, 1955) creep and diffusional flow, and the onset of cleavage fracture (Duval et al., 1983).*

The time to accelerated creep, at the beginning of the tertiary creep phase has been reckoned by Meglis *et al.* (1999) to be strongly dependent on the deviatoric stress.

Other attempts were made in order to model the entire creep behaviour of ice (primary, secondary and tertiary), not only focusing on the steady state creep phase. One such rheological model, accounting for microcracking during creep was presented by Sinha (1988; 1989b).

A review of further constitutive equations for ice is given in Mellor (1980) and Ashby and Duval (1985). However, there is general agreement on the form of the secondary, steady state creep. Glen's law is valid in simple compression. How to model the entire time dependent deformation, including primary, secondary and tertiary creep, on the other hand, is still under debate. Some authors propose laws with a phenomenological background (e.g. Sinha, 1978) and others start from physical models, involving state variables and develop differential

equations for their evolution with time (e.g. Michel, 1978; Ashby and Duval, 1985). Michel (1980) then extended his model to the case of crack formation and could explain why the yield point during ductile deformation can be as much as 40% higher than for brittle fracture. The model developed by Ashby and Duval (1985), which incorporates the mutual interaction between the grains under loading and relaxation, is based on creep data from dense isotropic polycrystalline ice (Jacka, 1983), tested at temperatures between -33°C and -5°C, under uniaxial compressive stresses ranging from 0.1 to 1.5 MPa. The rheological model consists of two parallel Maxwell elements (Figure 2-9). Another model, which is based on Burger's model (Figure 2-12), was proposed by Szyszkowski and Glockner (1985) and is able to model all three creep stages under constant stress conditions with eight parameters that have to determined experimentally from creep tests.

The mechanisms at failure from a constant strain-rate test under uniaxial compression were compared with tertiary creep failure from a constant load test by Cole (1983) and Mellor and Cole (1982; 1983). Thanks to special test equipment used in the first case, the author found that the internal structure of a material is roughly the same whether failure was reached by straining under a specific constant load or under a specific constant deformation rate. Therefore he concluded that the post-failure creep seems not to be affected by the prior loading history. For high strain rates, however, where brittle failure occurs, the findings are questionable.

A different analytical approach to model the deformation rate of hexagonal ice-crystal aggregates was presented by Thorsteinsson (2001) that includes the crystal orientation of the ice.

Despite the presented results on apparent activation energy (Table 2-4), Budd and Jacka (1989) displayed an extensive review of the rheology of polycrystalline ice. The tertiary creep phase is separated into an accelerating phase and a phase with increased, but constant strain rate. In contrast to Figure 2-27 and Figure 2-28, no creep failure occurs.

Creep of frozen soils

The rate process theory has also been applied to model the creep of frozen soils by assuming a thermally activated process (Andersland and Akili, 1967). Many other studies on different materials have revealed a number of activation energies, which are summarised in Table 2-5.

Most of the creep tests performed at the beginning of frozen soil research were conducted on uniaxial compression tests (see also Table 2-8), i.e. without confining pressure. Triaxial creep tests were carried out later when modern testing equipment was available. Probably the first triaxial creep tests on frozen sands have been reported by Goughner and Andersland (1968) or Sayles (1973; 1974). Alkire and Andersland (1973) showed that an increase in confining pressure results in an exponential decrease in the axial creep rates and increase in creep strength, which may by attributed to a change in mechanism. Between 0 and 1 MPa the dependency on the confining pressure is more pronounced than for higher pressures. However, this influence might be of secondary importance for the creep strain rates at the shallow depths under investigation, i.e. < ~30 m.

A certain depth or stress condition can be simulated in a triaxial test apparatus as well as observing volumetric changes of the sample indirectly via the change of the cell (confining pressure) liquid. The volumetric strain was often found not to be zero, even though the tests were conducted under undrained conditions (e.g. Ma *et al.*, 1997). Such behaviour is typical for unsaturated soils (e.g. Fredlund and Rahardjo, 1993), where the compressibility of the gas phase results in volumetric changes in the tested sample. In frozen soil mechanics, additional volumetric changes due to pressure melting, i.e. phase change, have to be expected. Since the shear strain is controlled by the shear strength and the average normal stress, it is not appropriate to calculate creep parameters under triaxial stress conditions directly from uniaxial creep equations.

author	**year**	**material**	**act. energy Q [kJ/mole]**	**temperature T [°C]**
Landauer	1955	snow	59	-5, -10, -20
Glen	1958	ice	133	-0.02 – -12.8
Dillon and Andersland	1967	polycrystalline ice	48	-1.5 – -10
Andersland and Akili	1967	frozen clay	392	-12 – -18
Mellor	1972	various rocks	1.6 – 2.1	+23 – -195
Haynes and Karalius	1977	frozen silt	174	0 – -56.7

Table 2-5: *Activation energies from the literature.*

A number of uniaxial compressive creep tests were conducted by Wijeweera and Joshi (1991) on saturated samples of fine-grained frozen soils. They reviewed a number of existing creep models first (which are also included in Table 2-6), and then introduced a new secondary creep model, concentrating on soils with no ice lenses. A different approach has been used by Domaschuk *et al.* (1991), whose model treats the frozen sand as an elastic medium with time-dependent deformation parameters.

Uniaxial creep tests:

author(s)	model
Vyalov *et al.*, 1962	$\varepsilon = \frac{\sigma \cdot t^{\lambda}}{\varpi (T+1)^{\kappa}}^{\frac{1}{m}}$ [2-33] ε axial creep strain σ axial stress T temperature in °C t time λ, m, ω, κ creep parameters
e.g. Fish, 1976; 1983 (Figure 2-30)	$\dot{\varepsilon} = \tilde{C}\frac{kT}{h} \cdot e^{\left(-\frac{Q}{RT}\right)} \cdot e^{\left(\frac{\Delta S}{k}\right)} \cdot \left(\frac{\sigma}{\sigma_0}\right)^{n+m}$ [2-34] $\dot{\varepsilon}$ axial creep strain rate $\tilde{C}$, $n \geq 0$, $m \geq 0$: temperature independent material parameters k Boltzmann's constant T absolute temperature in °K h Planck's constant Q activation energy R universal gas constant σ_0 temperature-dependent, ultimate instantaneous strength ΔS change in entropy
Fish, 1984 (Figure 2-30)	with the assumption of $n = 0$, a thermodynamic equation of creep was derived from [2-34]. $\dot{\varepsilon} = \tilde{C}\frac{kT}{h} \cdot e^{-\frac{Q}{RT}} \cdot e^{\left(\frac{\Delta S - \Delta S^*}{k}\right)}$ [2-35] $\frac{\Delta S^*}{k} = m \cdot ln\left(\frac{\sigma_0}{\sigma_{max}}\right)$, for ε = const. [2-36] ΔS change in entropy as a function of normalised time ΔS^* change in entropy as a function of stress ratios ΔS and ΔS^* are experimentally determined parameters and $\Delta S = 0$ during secondary creep σ_{max} peak value of stress in constant strain rate test

Table 2-6: *Summary of selected creep models for frozen soils under uniaxial compression (1/3).*

author(s)	model
Zhu and Carbee, 1983	$\varepsilon(t) = \varepsilon_0 + \frac{\varepsilon_f}{exp\,\beta \cdot t_m^{n-1}} \left(\frac{t}{t_m}\right)^{1-\beta} exp\left(\frac{\beta t}{t_m}\right) \cdot$ [2-37] $\cdot \left[\frac{1}{1-\beta} - \frac{\beta(t/t_m)}{(1-\beta)(2-\beta)} + \frac{(\beta(t/t_m))^2}{(1-\beta)(2-\beta)(3-\beta)} - \ldots\right]$ short-term creep: $t_m = t^* exp\left[k_1\left(\frac{1}{\sigma} - \frac{1}{\sigma^*}\right)\right]$ long-term creep: $t_m = t_c exp\left[k_1'\left(\frac{1}{\sigma} - \frac{1}{\sigma_c}\right)\right]$ σ^*, t^* and t_c material constants, independent of temperature k_1, k_1' temperature functions σ_c critical creep strength
Ting, 1983a	$\dot{\varepsilon} = A \cdot e^{\beta t} \cdot t^{-m}$ [2-38] A, m, β: experimentally determined soil constants Model can only be applied for loading conditions, which are sufficient to cause creep rupture. Secondary creep is considered as an inflection point in the strain-time diagram.
Gardner *et al.*, 1984	$\dot{\varepsilon} = (\varepsilon_m - \varepsilon_0)\left(\frac{t}{t_m}\right)^c exp[(c^{1/2} - c)(t/t_m - 1)]$ [2-39] $\cdot \left(\frac{1}{t}\right)(c + (c^{1/2} - c)t/t_m)$ c experimental parameter, describing the shape of the curve t_m time to inflection point m (see also Figure 2-30) ε_m - ε_o strain at inflection point m The model also assumes that secondary creep is just a point.

Table 2-6: *Summary of selected creep models for frozen soils under uniaxial compression (2/3).*

author(s)	model
Wijeweera and Joshi, 1991	$\dot{\varepsilon} = c_1 t^{S_i}$ for $t_0 \le t \le t_i$ [2-40] $\dot{\varepsilon} = c_2 t^{S_s}$ for $t_i \le t \le t_s$ [2-41] $\dot{\varepsilon} = \dot{\varepsilon}_s$ for $t_s \le t$ [2-42] $c_2 = \dot{\varepsilon}_s / (t_s^{S_s})$ *and* $c_1 = c_2^{m_1} c_i^{m_2}$, where [2-43] $m_1 = \frac{S_i - n_i}{S_s - n_i}$ *and* $m_2 = \frac{S_s - S_i}{S_s - n_i}$ t_0 time after initial loading t_i time at end of primary creep t_s time at end of secondary creep $\dot{\varepsilon}_s$ strain rate at end of secondary creep c_i, S_i, S_s, n_s, n_i constants to be determined from creep-test data This models assumes a logarithmic decrease of the strain rate during primary and secondary creep.

Table 2-6: *Summary of selected creep models for frozen soils under uniaxial compression (3/3).*

Triaxial creep tests:

authors	model
Goughner and Andersland, 1968	$\dot{\varepsilon} = constant \cdot \frac{1}{\lvert T \rvert^n}$, and [2-44] $\dot{\varepsilon} = \frac{K_1}{\sqrt{t}} \cdot e^{-n_1\sqrt{t}} + K_2 \cdot e^{n_2 t}$ [2-45] ε axial creep strain rate T temperature in °C n experimentally determined, stress-dependent parameter $K_{1,2}$, $n_{1,2}$ parameters that are constant for given T and σ
Andersland and AlNouri, 1970	$\dot{\varepsilon} = A \cdot e^{\left(-\frac{L}{T}\right)} \cdot e^{Nq} \cdot e^{-m\sigma_m}$ [2-46] ε secondary axial creep strain rate T absolute temperature in °K q $(\sigma_1 - \sigma_3)$; $\sigma_m = 1/3\ (\sigma_1 + \sigma_2 + \sigma_3)$ N $m + n$ A, L, n, m experimentally determined parameters

Table 2-7: *Summary of selected creep models for frozen soils under triaxial compression (1/2).*

authors	model
Domaschuk *et al.*, 1991	$\varepsilon_{ii} = \frac{1}{2G_c}\left(\sigma_{ii} - K_c \cdot \varepsilon_v + \frac{2}{3}G_c \cdot \varepsilon_v\right)$ [2-47] ε_{ii} axial strain σ_{ii} axial stress $K_c(t,T) = \sigma_m / \varepsilon_v(t,T)$ $G_c(t,T) = S_d \cdot \varepsilon_d(t,T)$ $\sigma_m = \frac{1}{3}(\sigma_1 + \sigma_2 + \sigma_3)$, mean normal stress ε_v volumetric strain $S_d = \sqrt{(\sigma_1 - \sigma_m)^2 + (\sigma_2 - \sigma_m)^2 + (\sigma_3 - \sigma_m)^2}$ resultant deviatoric stress $\varepsilon_d = \sqrt{(\varepsilon_1 - \varepsilon_m)^2 + (\varepsilon_2 - \varepsilon_m)^2 + (\varepsilon_3 - \varepsilon_m)^2}$ resultant deviatoric strain

Table 2-7: *Summary of selected creep models for frozen soils under triaxial compression (2/2).*

The models presented within Table 2-6 and Table 2-7 have been developed in order to satisfy specific problems and therefore it is difficult to apply them for other soils. The validity of the model presented by Domaschuk *et al.* (1991), for example, is limited to problems with similar soils, i.e. sand at temperatures of about -3°C, and Wijeweera and Joshi (1991) say that their model is only valid for fine-grained frozen soils having a massive texture with no ice lenses, and so the applicability for ice-rich soils is questionable.

Most of the models presented tend to model the entire creep process, including primary, secondary and tertiary creep: Goughner and Andersland (1968), Fish (1976; 1983; 1984), Ting (1983a), Zhu and Carbee (1983) or Gardner *et al*. (1984). In order to be able to model the behaviour with a single equation, the assumption had to be made that the secondary (steady state) creep phase can be reduced to an inflection point, i.e. the decrease of the strain rate with time is directly followed by an acceleration, without an interval of a constant strain rate. Except for Andersland and AlNouri (1970), who modelled secondary creep alone, the other models assume constant decrease in strain rate, and hence primary creep will be modelled (Vyalov *et al.*, 1962; Domaschuk *et al.*, 1991; Wijeweera and Joshi, 1991).

The unified constitutive equation and unified failure criterion that describe the entire creep process for constant stress tests and constant strain rate tests, which have been presented by Fish (1984), can be drawn as shown in Figure 2-30. The main advantage is the principle of superposition: creep curves at constant stresses and stress-strain curves at constant strain rates can be superimposed if the test data are presented as functions of the change of entropy, which is, in simple terms, a measure for the amount of disorder or 'chaos' in a system, over normalised time. Gardner *et al*. (1984), for example, have also used similar

creep and strain rate test curves as shown in Figure 2-30 for their creep model (Equation [2-39]). Experimental investigations led to the recommendation of a power law in order to calculate the time for the inflection t_m, where n and K are material and temperature dependent constants and σ the uniaxial stress:

$$t_m = K / \sigma^n$$

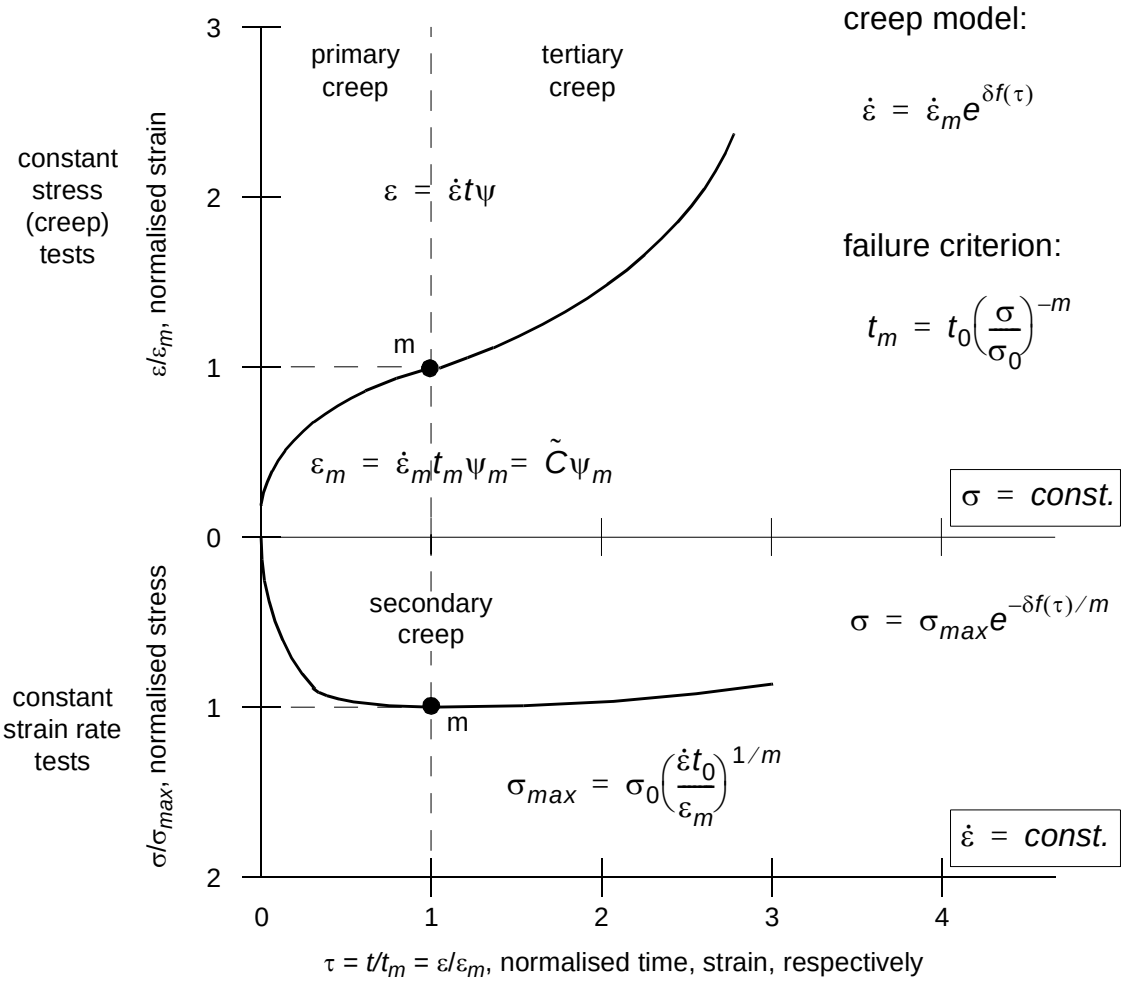

ψ integration factor for creep strain ε

ψ_m integration constant for creep strain at failure ε_m

δ time hardening parameter

Figure 2-30: *Creep model of Fish, 1984 (see also Table 2-7, Eqn. [2-35]) for a constant temperature.*

The linear relationship between the logarithm of the minimum creep rate $\dot{\varepsilon}_m$ and the logarithm of the time to reach this point t_m has been observed by numerous authors and discussed by Ting (1983b). This correlation cannot be used by itself to predict failure but, if one can predict either $\dot{\varepsilon}_m$ or t_m independently, the other value may be obtained.

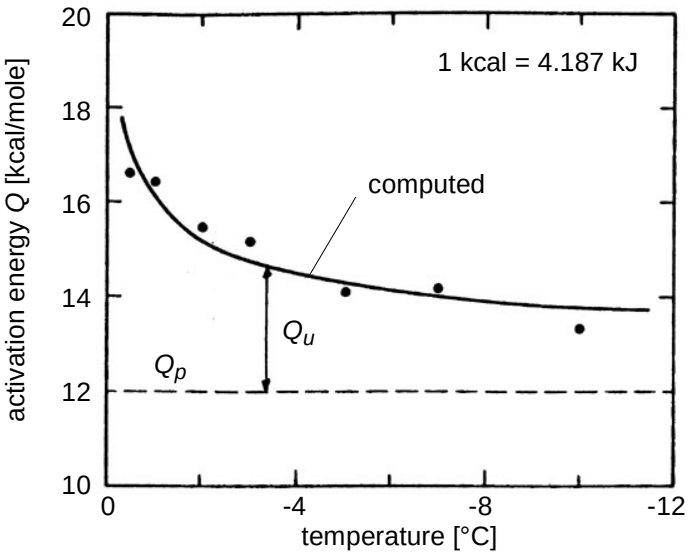

Figure 2-31: *Temperature variation of the activation energy of Fairbanks silt (Fish, 1985).*

The activation energy of a frozen soil Q, after Fish (1985), is the sum of the activation energy of the soil skeleton Q_p, which was found to be strain rate or temperature independent, and the activation energy of the unfrozen water Q_u. Figure 2-31 shows the decrease of the activation energy of the unfrozen water with decreasing temperature while the activation energy of the soil remains constant.

Ladanyi and Benyamina (1995) showed that relaxation tests in the post-failure range are a powerful alternative to creep tests, since the response of a frozen geomaterial is very similar in both cases. In contrast to a creep test, a relaxation test can be performed much quicker. Very similar creep parameters were determined using a power law type creep equation.

Dynamic properties of frozen soils have also been studied extensively, but will not be of any importance herein. Vinson (1978) summarised several field and laboratory studies and considered the parameters that had been found to affect the dynamic properties. A more recent investigation on dynamic creep was published by Zhu *et al.* (1997).

A very complicated constitutive model based on viscoelastoplasticity and the damage of ice was presented by He *et al.* (2000). Their model successfully predicts the whole process of creep, including the failure stage. However, it uses 19 parameters, which have to be determined experimentally with uniaxial and triaxial compression tests and have only been verified for a frozen silt (dry density of 1600 kg/m^3) at a temperature of about -5°C.

Table 2-8 summarises some selected experimental work on creep of frozen soils. From that compilation, it can be shown that uniaxial creep tests are still the most common test in frozen soil mechanics, since they are easier to carry out, even though tests at triaxial stress conditions would result in more appropriate results. However, since most of the design recommendations are very restrictive, uniaxial creep tests are a helpful tool in engineering practice, but should be replaced by triaxial tests in research.

author	year	material	test	temperature [°C]
Sayles and Haines	1974	frozen Suffield clay and Hanover silt	uniaxial	-9.44 – -0.55
Rein *et al.*	1975	sand-ice mixtures	uniaxial	-8.5
Haynes and Karalius	1977	frozen Fairbanks silts	uniaxial	0 – -56.7
Gardner *et al.*	1982	unsaturated Brussels sand	uniaxial	-10
Zhu and Carbee	1983, 1984	remoulded frozen Fair-banks silt	uniaxial	-10 – -0.5
Wijeweera and Joshi	1991	fine-grained frozen soils	uniaxial	-5 – -17
Goughner and Andersland	1968	frozen sand with 0 – 61% sand by volume	triaxial	-3.8 – -12.2
Andersland and AlNouri	1970	Sault Ste. Marie clay saturated Ottawa sand	triaxial	-10 – -18.1
Alkire and Andersland	1973	silica sand with 97% & 55% volumetric ice content	triaxial	-12
Sayles	1973	frozen Ottawa sand	triaxial	-3.9
Parameswaran and Jones	1981	frozen Ottawa sand	triaxial	-10
Jones and Parameswaran	1983	frozen sand with 0.1 – 0.6 weight fraction of sand	triaxial	-11
Ouvry	1985	frozen stiff clay	triaxial	-5 – -60
Savigny and Morgenstern	1986b	undisturbed ice-rich glaciol-acustrine clay	triaxial	-1.5 – -1.0
Hampton *et al*.	1988	LAF sand, very silty sand	triaxial	-10
Ladanyi and Morel Ladanyi and Benyamina	1989 1995	frozen Ottawa sand	triaxial	-5
Andersen *et al.*	1995	Manchester fine sand	triaxial	-10 – -25
Da Re & Da Re *et al*.	2000 2001	Manchester fine sand	triaxial	-2 – -10

Table 2-8: *Selected creep tests on frozen soils.*

2.3.6 Fracturing

Aspects of fracture mechanics have to be discussed when dealing with frozen materials and in particular with ice that demonstrates a peak strength under compression at the transition from creep to brittle failure. While ice is ductile at lower rates of deformation, it exhibits a brittle response under fast loading conditions, which may lead to localised high pressure zones and induce failure when

reaching a critical dimension (Dempsey *et al.*, 2001). In addition, the failure mode will almost certainly change during a loading event (Palmer, 1991a) influencing the fragment size of the crushed ice.

Rapid crack formation and propagation can result in destruction of the matrix and in a sudden loss of strength. Brittle compressive failure can be addressed in terms of frictional crack sliding, wing cracking and comb cracking (e.g. Schulson, 2001). The two latter processes will be discussed in more detail within the following sections.

Wing cracking

Wings initiate in response to localised tensile stresses, which develop through uniform sliding across parent cracks, inclined to the maximum principal stress of the applied compressive field (Figure 2-32). Cracks nucleate on grain boundaries and shear stress causes sliding across the crack faces, generating tension T at their tips (a). The wings begin from near the tips of the parent crack in a direction perpendicular to the maximum local tensile stress and then turning towards the direction of the most compressive stress (b), lengthening whenever displacement along the parent crack is sufficient to raise the mode-I stress intensity factor to the critical level K_{Ic}. Crack tip creep is expected within a region of 2r.

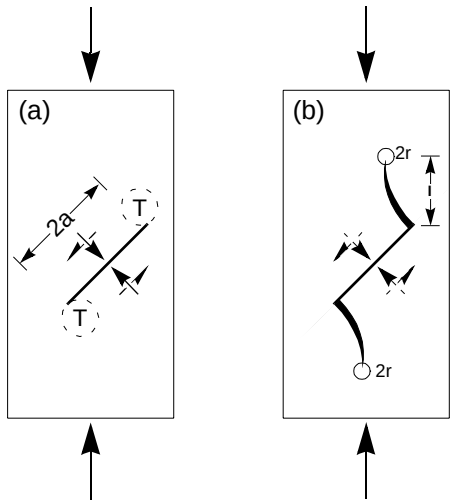

Figure 2-32: *Schematic sketch of a wing crack under compression (after Schulson, 1990).*

Shear faults and comb cracks

Longitudinal splitting is suppressed under confinement and an instability develops that is manifested by compressive shear faults. It is suggested that the key elements in triggering the instability are secondary cracks that might involve nonlinear sliding. The idea is that a gradient of displacement along a parent crack creates normal stresses that act across planes perpendicular to both the sliding plane and the sliding direction. Compressive stresses then develop on one side, while tensile stresses develop on the other (Figure 2-33). In this figure the upper-side material experiences a compressive stress while the under-side material experiences tension. The secondary cracks are imagined to form sequentially, starting near one tip of the parent crack and releasing proportionately more strain energy to the distance from the tip of the parent crack to the initiation site of the secondary crack.

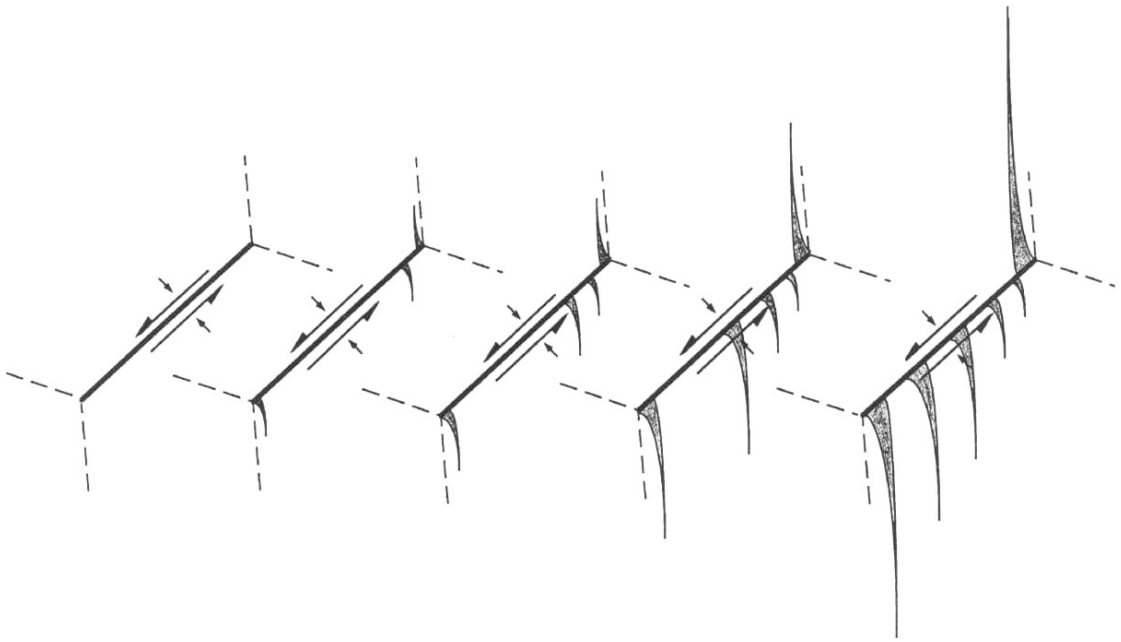

Figure 2-33: *Sketch showing creation of secondary cracks under compression through non-uniform sliding across an inclined, crack grain boundary (Schulson, 1990).*

Either external or internal secondary crack concentration may now trigger the instability since the nucleus grows under action of localised stress intensification along a band of reduced shear strength, ending in terminal failure (Figure 2-34).

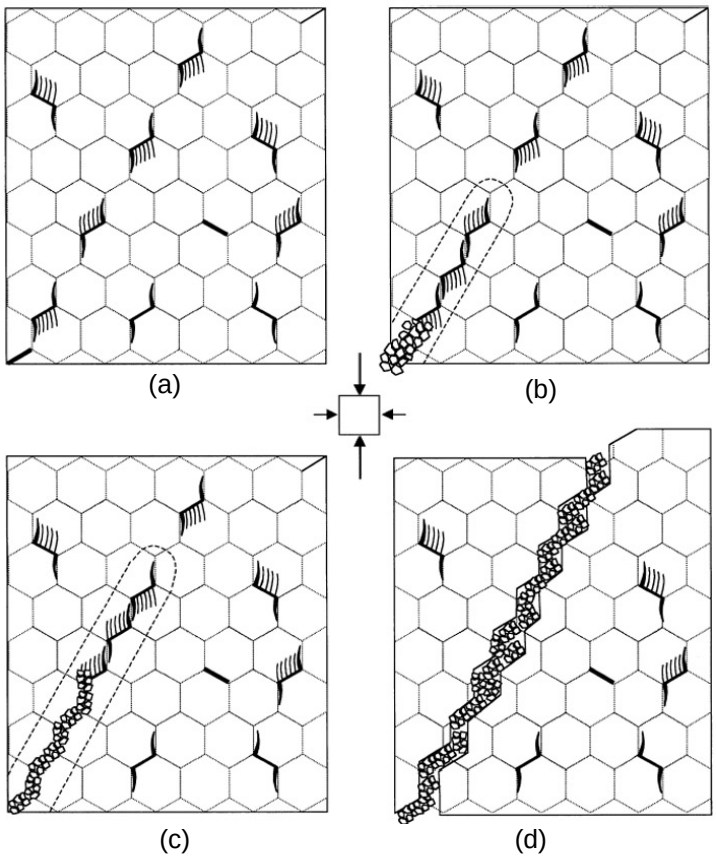

Figure 2-34: *Sketch of the initiation and growth of a microscopic compressive shear fault, from the onset of terminal failure (Schulson, 2001).*

a) before initiating.
b) near-surface comb crack fails, redistributing stress to adjacent material.
c) more comb cracks fail and localised damage spreads in a band across the section.
d) a microscopic shear fault has been developed.

The stress to trigger the fault σ_f, is assumed to be the applied stress that causes a near-surface microcolumn to break under confined loading and can roughly be approximated by:

$$\sigma_f = \frac{2K_{Ic}}{(3\beta h)^{0.5}[(1-\mu)(1-R)-2R\mu]} \text{ (Schulson } et\ al.\text{, 1991),} \qquad [2\text{-}48]$$

where R is the appropriate confining ratio ($R \cdot \sigma_1 = \sigma_2 = \sigma_3$), K_{Ic} is the fracture toughness or stress intensity factor mode I, μ is an experimentally determined friction coefficient, β is a slenderness ratio of the microcolumns ($\beta = h/w$), with $h = d/2$ and d as the grain diameter, and w is the width between secondary cracks. Since microcracking in ice appears to form suddenly and the cracks grow to their full size in very short time, the dissipation of energy due to local plasticity or creep at the crack tip may not be significant. As a consequence, Schulson *et al.* (1991) conclude from Sinha (1984) that the effective fracture surface energies for the formation of the cracks may not be different from the surface energy, which marks also the lowest possible value:

$$K_c = \sqrt{\frac{2\gamma E}{1-\nu^2}} \qquad [2\text{-}49]$$

E denotes the Young's modulus, ν the Poisson's ratio and γ the surface free energy, which can be expressed further as the difference between the surface free energy with respect to vapour γ_{vs}, and half of the grain-boundary free energy γ_{gb}.

Goodman (1980) measured the stress intensity factor K_{Ic} for polycrystalline ice at temperatures between -4 and -24°C and showed that the mean value of 115 $kNm^{-3/2}$ is very consistent over the chosen temperature range. On the other hand, Dempsey (1991) presented several effects that influence the fracture toughness of freshwater ice. The scattering of the data (e.g. for glacier ice and randomly oriented equiaxed freshwater ice, a fracture toughness between 31 and 180 $kNm^{-3/2}$ can be found in literature) are caused by different ice types, crack length, loading rate, specimen size, test temperature, specimen geometry, crack orientation, specimen preparation, and crack-tip radius. In general, most specimen sizes used had been sub-size in terms of the small yielding required by linear elastic fracture mechanics and therefore an upgrade of the specimen size was recommended.

Ductile-to-brittle transition

The ductile-to-brittle transition marks the point where the compressive strength reaches a maximum and is in Schulson's view the point where cracks begin to propagate, albeit in a stable manner. The transition strain rate under biaxial compression may be expressed as (Schulson and Nickolayev, 1995):

$$\dot{\varepsilon}_t = \frac{BK_{Ic}^3}{fd^{1.5}\left\{(1+\mu^2)^{0.5}-\mu-R[\mu+(1+\mu^2)^{0.5}]\right\}}, \qquad [2\text{-}50]$$

where B is a creep constant and d is the crack length. The factor f must be calculated from the Riedel-Rice (1980) model.

Additional remarks on fracturing of ice

An approach using fractal mechanics has been presented by Palmer and Sanderson (1991), who have demonstrated the link between the mechanics of fracture of a single fragment and the observed fractal size distribution of broken brittle materials, such as ice.

Palmer (1991) also presents a critical assessment of the application of fracture mechanics, since it can be made to explain too much. He concludes that new ideas, such as chaos theory, have to be integrated into traditional fracture mechanics.

Schulson (2001) summarised in his explanatory statement why critical crack density, which is often used as a failure criterion, is not a good model for ice. The following observations, might also be important for the interpretation of the laboratory tests of the current work:

- ice exhibits relatively minor mismatches in material properties,
- ice is far more damaged at failure on the ductile side of the brittle-ductile transition, than it is on the brittle side, yet does not split, and
- longitudinal splitting is often accompanied by very little global damage.

However, it must be noted that rock glacier deformations usually involve slow processes where creep dominates and brittle behaviour may not be a controlling mechanism.

2.3.7 Thermal Properties

Since the volume fraction of the different elements within a frozen soil is temperature dependent, the thermal properties of the mixture might change significantly with only a small change in temperature. Only the thermal conductivity needs to be considered for steady state conditions, whereas the thermal diffusivity becomes important in transient problems. The latent heat of fusion is significant when phase change occurs.

Although, the thermal properties of frozen soils are not directly used for the calculations within this research, it is nevertheless worthwhile to summarise the important thermal properties of frozen soils for future investigations. The thermal properties are important as soon as time dependent temperatures are calculated. Within the presented laboratory tests, temperatures were kept constant and only time dependent mechanical sample responses were recorded.

Thermal conductivity

The thermal conductivity of a frozen soil is the amount of heat flowing through a unit area of soil in a unit time under a unit temperature gradient and is called K (W/mK):

$$q = -K \cdot \frac{dT}{dx} \qquad [2\text{-}51]$$

Where q is the heat flow per unit area of soil and time (W/m^2), T is the temperature (°K), and x is the distance in the direction of heat flow (m).

Heat capacity

The volumetric heat capacity C (J/m^{3}K) is the amount of heat required to raise the temperature of a unit volume of soil by 1°K:

$$C = \rho \cdot c, \qquad [2\text{-}52]$$

ρ (kg/m^3) is the density of the soil and c (J/kg K) is the specific heat capacity.

Thermal diffusivity

The thermal diffusivity α is equal to K/C, which forms the relationship between the thermal conductivity and the volumetric heat capacity of a particular soil. It is important for analysing transient heat flow problems, and is described for a one dimensional case by the diffusion equation according to:

$$\frac{\partial T}{\partial t} = \alpha \cdot \frac{\partial^2 T}{\partial x^2} \qquad [2\text{-}53]$$

Some important thermal properties of soils are given in Table 2-9.

Material	**thermal conductivity *K* [W/m K]**	**heat capacity *c* [J/kg K]**	**thermal diffusivity α [10^{-6} m^2/s]**
Quartz	9.9	800	4.4
Dry Sand	0.58	800	0.48
Dry Clay	1.0	880	0.58
Water (0°C)	0.562	4217	0.13
Ice (0°C)	2.33	2090	1.22
Ice (-40°C)	2.66	2090	1.41
Air (0°C)	0.025	1006	19.49
Air (-20°C)	0.023	1006	16.60

Table 2-9: *Thermal properties of some materials (after Gieck, 1989).*

Thermodynamics

Even though no explicit thermodynamic calculations were conducted within this study, it is worth pointing to some literature that deals with it, since a major goal in permafrost research should be the formulation of a coupled mechanical and thermodynamical model. Formulations based on the classical continuum mixture theory (Truesdell and Toupin, 1960; overview in Bedford and Drumheller, 1983), have been proposed from numerous authors for the temperature modelling of large ice sheets, glaciers, polythermal ice or soils (e.g. Blatter and Hutter, 1991; Funk *et al.*, 1994; Greve *et al.*, 1998; Hutter *et al.,* 1999; Hutter and Svendsen, 2000). The thermodynamics of frost heave has been reviewed by Henry (2000).

Such models may be used in connection with the mechanical solution presented herein to allow for dynamic temperature variations that influence the mechanical response.

2.4 Numerical Modelling

Numerical modelling in permafrost research is dominated by climate and distribution modelling (e.g. Riseborough and Smith, 1993; Zhang and Stamnes, 1998). There are only very few attempts in transferring the material behaviour into a numerical model of a whole system of frozen soil (e.g. Puswewala and Rajapakse, 1993; Oka *et al.*, 1994), which might be the result of the large number of recommendations for modelling the constitutive behaviour and because various mechanisms, especially close to the melting point of ice, are still under investigation. Neaupane and Yamabe (2001), for example, use a Mohr-Coulomb failure criterion in their nonlinear elasto-plastic simulation of freezing and thawing of rock, which might not work for ice-rich soils, such as rock glaciers. Even though there is often not a unique answer available, numerical solutions have been proposed and applied successfully (e.g. Fowler, 1997) for practical problems and processes that are less under debate, such as thaw settlements or frost heave.

Aspects of numerical modelling of heat transfer are extensively reviewed in Goldstein *et al*. (2002) and will not be further discussed.

Leysinger Vieli and Gudmundsson (2001) investigated the flow mechanism of rock glaciers using numerical simulations of a gravity driven creeping viscous medium. Their model, however, homogenises the whole mass of the rock glacier and therefore its applicability to natural objects is questionable. An approach in modelling a rock glacier similar to glaciers, using Glen's flow law, was presented by Wagner (1996b) for the Murtèl-Corvatsch rock glacier and Konrad *et al*. (1999) for the Galena Creek rock glacier. Even though the models showed reasonable agreement for these particular rock glaciers and were able to replicate the *in situ* response, the author doubts that such a simple model, which does not account for the differences in soil properties over depth, can be generalised for other rock glaciers with different origins.

Up to date, not only sophisticated rock glacier modelling is lacking, but according to Matsuoka (2001), the slightly less complex processes of solifluction, cannot be modelled accurately either.

2.5 Permafrost Engineering

Due to the many phenomena explained within this chapter, special attention has to be paid to engineered structures. Many papers and guidelines have been written on this subject, focusing on a range of problems including foundations, dam and pipeline constructions or shafts, in particular in the former USSR and North America. A brief overview is given in Table 2-10.

author	title	year	country
Muller	Permafrost or permanently frozen ground and related engineering problems	1947	USA
Vyalov *et al.*	The strength and creep of frozen soils and calculations for ice-soil retaining structures	1962	USSR
Andersland and Anderson	Geotechnical Engineering for Cold Regions	1978	North America
Johnston	Permafrost Engineering Design and Construction	1981	Canada
Fish	Comparison of U.S.S.R. Codes and US. Army Manual for Design of Foundation on Permafrost	1983	USA / USSR
Phukan	Frozen Ground Engineering	1985	North America
Haeberli	Construction, environmental problems and natural hazards in periglacial mountain belts	1992	Switzerland
Andersland and Ladanyi	An Introduction to Frozen Ground Engineering	1994	North America
Stoffel	Bautechnische Grundlagen für das Erstellen von Lawinenverbauungen in alpinem Permafrost	1995	Switzerland
Oswell and Hanna	Aspects of Geotechnical Engineering in Permafrost Regions	1997	North America
Freitag and McFadden	Introduction to Cold Regions Engineering	1997	North America
Thalparpan	Lawinenverbauungen im Permafrost: Schlussbericht und Erläuterungen zu den Kapiteln IV und V der Richtlinien für den Lawinenverbau im Anbruchgebiet.	2000	Switzerland
Davies *et al.*	The effect of rise in mean annual temperature on the stability of rock slopes containing ice-filled discontinuities	2001	UK

Table 2-10: *Some literature on permafrost engineering.*

2.6 Conclusions from the Literature Review

A vast range of literature has been presented within this chapter, that deals with all sorts of aspects that might be related to rock glacier mechanics. The major challenge is the combination of the crucial discoveries from the geomorphological research on periglacial environments, from investigations on the mechanical behaviour of ice, soils and frozen geomaterials, as well as from numerical modelling of related phenomena. The definitions and the applicability of the various models presented herein have to be considered when attempting to describe the behaviour observed within the current project. Ladanyi (2002) presents such an approach, in which he extends findings and methods from the field of mud flow mechanics, rock mechanics and the mixture theory in order to describe frozen slopes and frozen debris at the bottom of glaciers.

Special conclusions from creep literature

The extensive review on literature about creep processes in ice as well as of frozen soils indicate that there seems to be no unique solution for the modelling of the creep behaviour of frozen geomaterials. Individual solutions were presented for most of the problems, that use various constitutive models, which are able to model the creep phase under investigation, i.e. primary, secondary or tertiary creep, including long term creep failure. However, the primary concern is the modelling of the whole creep phase and therefore, a crucial assumption is necessary: secondary creep is reduced to an inflection point. On the other hand, most of the authors agree that steady state creep (secondary creep) can be modelled fairly well with Glen's flow law (Equation [2-30]).

From experimental investigations, it is not clear if secondary creep really exists. In the author's view two main problems occur: *test duration* and *stress condition*.

- Often, a test does not last long enough to reach steady state creep. On the other hand, larger stresses will result in the development of tertiary creep within a very short period of time, and for such tests, linear strain for some minutes can be neglected.
- During a creep test, the volume of a frozen sample may change its geometry, i.e. the area changes and consequently, the stress decreases for a constant load. Even though some of the researchers are aware of that change and try to consider it in dealing with the tests presented, only computer controlled load application combined with on-sample deformation measurements may solve that particular problem. The strain rate will also decrease due to the stress decrease and therefore, no secondary creep stage will be obtained.

Not only are there problems concerning material behaviour due to test conditions, but also due to the soil conditions. Most of the triaxial tests have been performed on relatively fine sands, silts or clays and therefore the sample diameter could be maintained relatively small (<40 mm) without creating conflicts concerning the grain size. Several triaxial creep investigations presented dependencies on confining pressures, which are much too high to occur within an Alpine rock glacier and therefore such results might not be applicable.

Most of the tests were conducted on artificially frozen soils since the sampling of undisturbed frozen soils is extremely difficult. These samples might not show similar responses because of a possibly different crystalline structure of the ice matrix.

One of the few available sets of creep tests on undisturbed samples was reported by Savigny and Morgenstern (1986b), who tested undisturbed ice-rich glaciolacustrine clays at a temperature of about -1°C to obtain the steady state creep rate. Even though a large scatter was present in their data, the authors presented a best-fit power law for all tests in the form:

$$\dot{\varepsilon} = 1.9 \cdot 10^{-5} \sigma^{1.7} . \qquad [2\text{-}54]$$

The axial creep strain rate per year can be calculated as a function of the deviatoric stress σ in kPa. Unfortunately, the accuracy of the presented solution was not given.

Chapter 3

Field Observations

The core of the project has been the field investigations. Not only because cored drillings have been necessary to obtain original permafrost samples for the laboratory investigations, which will be presented in the next chapter, but also because field investigations and subsequent monitoring add crucial information to the understanding of rock glacier behaviour. Direct and indirect penetration into the rock glacier during the challenging drilling and the geophysical investigations revealed many new findings, such as water flow and high volumetric air contents, which are of importance when modelling rock glacier behaviour. In addition, a comparison between the two sites under investigation showed that rock glaciers can be very different.

Various instruments have been installed within the six boreholes for the monitoring of the temperatures and deformations. A deformation measurement system that is based on time domain reflectometry was installed for the first time within Alpine permafrost. Additional pressuremeter tests allowed the determination of creep properties in situ.

3.1 Introduction

It is important to understand the thermo-mechanical behaviour of perennially frozen ground, in particular of rock glaciers, for the calculation of future instabilities in Alpine regions, which might be induced by a scenario of global warming. Reproducible laboratory tests are very efficient because special features can be studied individually. However, such tests have to be related to field measurements since this is the only way of gaining knowledge of the general behaviour under natural conditions. Consequently, expensive field investigations should not be avoided and in addition, they offer the possibility of monitoring endangered

environments. It is, however, important that the laboratory is always considered when performing field investigations and *vice versa*. The advantages of both type of tests have to be evaluated in planning the work to be undertaken.

Within this project, field investigations were performed in order to achieve the following goals:

- to develop an understanding of the stratigraphy from boreholes,
- to use boreholes for cross-hole geophysical investigations,
- to obtain cores for testing in the laboratory,
- to carry out *in situ* testing to obtain mechanical properties *in situ* (pressuremeter test),
- to inspect the borehole walls using a down-hole camera,
- to measure vertical and horizontal borehole deformations in the boreholes,
- to measure temperatures in the borehole and surficially, and
- to investigate the hydrology within the rock glaciers.

Some of these investigations are only temporary, however, the borehole temperature and deformations are part of an ongoing Swiss permafrost observation network (PERMOS[1]: Vonder Mühll *et al.*, 2001b).

Originally, it was intended to investigate only one rock glacier (Muragl), however, there were unexpected difficulties with the borehole wall stability as well as an insufficient quantity of good quality core samples. In consequence, it was necessary to focus on a second location in the Swiss Alps (Murtèl-Corvatsch), where cored boreholes had already been drilled in 1987. This stratigraphy was expected to be favourable for successful extraction of undisturbed samples and the result also added new perspectives to the understanding of the phenomenon *rock glacier*.

3.1.1 Sites of Investigation

Two rock glaciers, located in the Upper Engadin, Swiss Alps (Figure 3-1), were chosen for the investigation into the thermo-mechanical behaviour of Alpine permafrost. Further details of these rock glaciers are given in the following sections (Chapter 3.2 and 3.3).

1. PERMOS was founded in 1999 and is a permafrost monitoring network, which collects data from Swiss permafrost sites. It is sponsored by the Swiss Academy of Sciences, the Swiss Federal Office for Water and Geology, and the Swiss Agency for the Environment, Forests and Landscape.

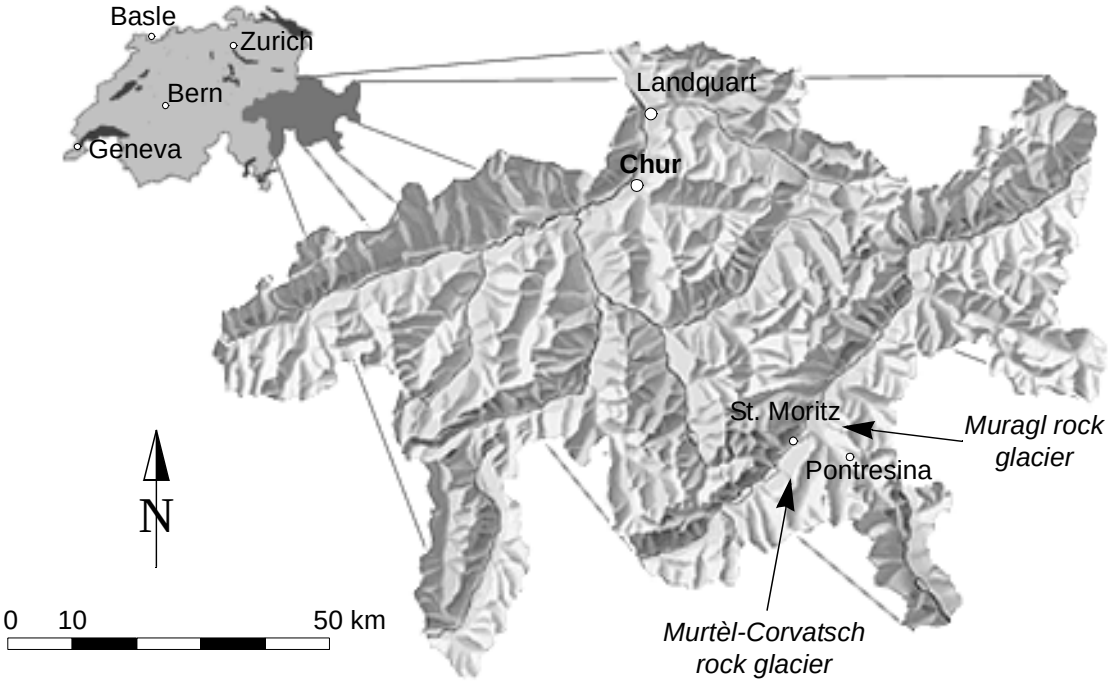

Figure 3-1: *Location of the two rock glaciers.*

An overview of the six new boreholes and the original borehole at Murtèl-Corvatsch is given in Table 3-1 and Table 3-2.

	Muragl rock glacier			
borehole	*1/1999*	*2/1999*	*3/1999*	*4/1999*
coordinates x/y [m]	791 025 / 153 726	790 989 / 153 687	791 038 / 153 679	791 017 / 153 688
elevation [m asl]	2536.1	2538.5	2558.2	2549.2
borehole depth [m]	70.2	64.0	72.0	71.0
drilling type	percussion	partially cored	partially cored	partially cored
geophysical logging	in all boreholes			
temperature monitoring	Oct.99 – Apr.00 Sep.02 –	Nov.00 –	Oct.99 – Apr.00 Nov.00 –	Oct.99 – Apr.00 Nov.00 –
deformation monitoring	–	–	Oct.99 – Jun.00	Oct.99 – Jan.00
crosshole georadar (Musil, 2002)	in all boreholes			

Table 3-1: *Boreholes at the Muragl rock glacier.*

	Murtèl-Corvatsch rock glacier		
borehole	*2/1987*	*1/2000*	*2/2000*
coordinates x/y	783 160 / 144 720	783 168 / 144 703	783 175 / 144 692
elevation [m asl]	2670.2	2672.9	2672.3
borehole depth [m]	62.0	51.9	63.2
drilling type	partially cored	partially cored	partially cored
temperature monitoring	1987 –	Nov. 00 –	–
deformation monitoring	inclinometer 1987 – 1995	TDR Dec. 00 –	TDR Dec. 00 –
pressuremeter test	–	7	–

Table 3-2: *Boreholes at the Murtèl-Corvatsch rock glacier.*

3.1.2 Drilling Techniques

Drilling in such an environment was a challenge, since the experience in coring through inhomogeneous media, containing a range of materials including large boulders and pure ice, is rather limited. Many boreholes have been drilled in the arctic regions with many successful core recoveries in permafrost (e.g. Lange, 1968; Lange and Smith, 1972; Lange, 1973a; Kudryashov and Yakovlev, 1991) and in ice (Lange, 1973b; Holdsworth *et al.*, 1984). However, most of the successful core recoveries originate from frozen soils of a fine-grained nature (frozen clay, silt or fine sand), where the interstitial ice was either hardly visible, or a high ice content or even massive ice was found.

Hvorslev and Goode (1963) mention that it is impossible to formulate definite and detailed recommendations for core drilling in frozen soils under all conditions. And Mellor and Sellmann (1975) show that the basic elements of all drilling systems have to take three functions into account: i) penetration through the soil, ii) removal of the surplus material and iii) stabilisation of the borehole wall. Special systems may have to be chosen depending on the conditions, e.g. the drilling rig (Dickinson *et al.*, 1999) or the drill bits (Sellmann and Mellor, 1986).

The first deep scientific borehole was drilled in an Alpine rock glacier in 1987 (Haeberli *et al.*, 1988; Vonder Mühll, 1996). In addition to this borehole, only a few other boreholes exist in rock glaciers:

- Murtèl-Corvatsch rock glacier (10 m deep: Barsch, 1977),
- RG II, Yukon, Canada (21 m deep: Johnson and Nickling, 1979),
- Gruben, Switzerland (7 m deep: Barsch *et al.*, 1979),
- Schafberg, Switzerland (65 m and 37 m deep: Vonder Mühll and Holub, 1992; Vonder Mühll, 1993), and

- Galena Creek rock glacier (9.8 m deep: Clark *et al.*, 1996; Steig *et al.*, 1998).

The technique used for the new vertical boreholes was slightly adapted from that used already for the drillings at Murtèl-Corvatsch in 1987 (Haeberli *et al.*, 1990b). In contrast to constructing a tent covered drill tower, a MENZI Ghelmina drilling rig was placed on a crawler type vehicle, which was transported to (and partially around) the site by a helicopter. The total weight of the rig was about 4 t (Figure 3-2).

(a)

(b)

Figure 3-2: *Pictures of the drilling rig.*
a) on site (Photo: L. Arenson).
b) during set up with a helicopter (Photo: D. Vonder Mühll).

The whole rig was then assembled on site with the main focus being on the collection of good quality undisturbed samples. Two possible sources of core disturbance had to be considered, in particular, with the drill system: mechanical and thermal perturbations. The former was taken into account by using a triple tube drilling rig and the latter by cold air flushing. The various components of the drill system on site are schematically displayed in Figure 3-3 and pictures of the various components of the drilling system are shown in Figure 3-4. At first, air from the environment is compressed up to about 10 bars in an Atlas Copco diesel engine compressor, type XAHS (1). The compressed air was cooled down within a hose of 200 m length (2) that had been buried under the snow and then was dried in a 2 m^3 air tank (3), which had been placed in the shade and doused with cold water. Additional cooling was achieved by using a heat exchanger (4). An additional coupling (5) allowed other hoses to be added for the use of the compressed air directly near the drilling rig (6). The compressed air was expressed from the drill bit (7) at the drill tip (8), and due to the expansion, it cooled down

some additional degrees centigrade. Antecedent measurements of temperatures at the drill bit outside the borehole showed that a temperature of about -5°C to -10°C could be expected at the bottom by the borehole.

Depending on the amount of solid particles, the soil remained frozen. The air left the hole by rising around the drilling rods, cooling it and on the other hand, carrying fine drill dust to the surface (9). These borehole cuttings also gave very important information about the stratigraphy at the drill tip. In addition, information about the drilling process, such as the axial force, which has to be applied, the rotation speed or water in the borehole add to the knowledge of the structure of the ground. It was therefore very important to note every remark of the drill crew and to be on site all the time.

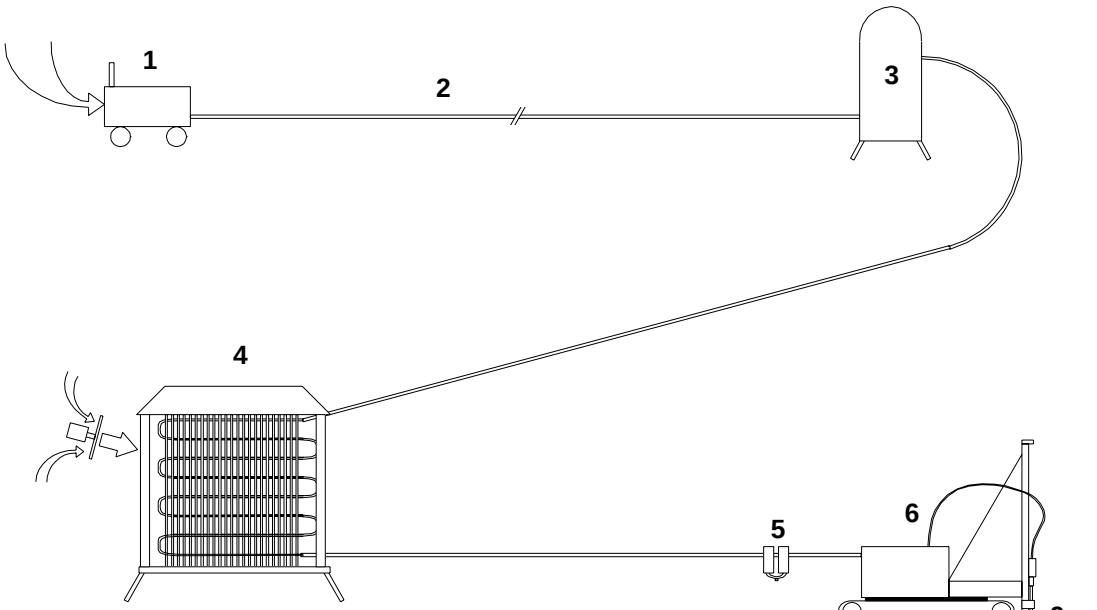

1 compressor
2 air hose (covered under the snow)
3 air tank
4 heat exchanger
5 coupling
6 drill rig
7 drill bit
8 drill tip
9 drill dust

Figure 3-3: *Schematic set up of the drilling system.*

compressor, generator and fuel tank (1)

air tank and hoses (2,3)

heat exchanger (4)

coupling (5)

folded drill rig (6)

drill bit with holes for air flushing (7)

Figure 3-4: *Pictures of the components of the drill system (Photos: L. Arenson/ M. Sperl).*

The triple tube drilling system used is shown in Figure 3-5. The outer metal tube, which was directly connected to the drill bit, rotated while the inner metal tube remained stationary. As a consequence, a length of nominally undisturbed core (max. 1.5 m) slid slowly into the plastic liner within the inner steel tube, remaining in the original orientation while the sample was extracted. Therefore, a minimum of disturbance was guaranteed. On site, the plastic liners were cut into two halves with a handsaw for transport, preferentially at an already broken section, and stored in a freezer at about -18°C.

The different stiffnesses of the rocky blocks and the ice required different drill bits. Diamante drill bits were used for rocks whereas ice had to be scraped with hard metal drill bits, which produced good quality cores. The whole drill string had to be raised and the bit removed and replaced by a diamante drill bit for sections with large boulders. Such changes of the bits were necessary on a regular basis owing to the large variability of the rock glacier materials. Therefore the maximum possible length of the plastic liner (1.5 m) could rarely be filled.

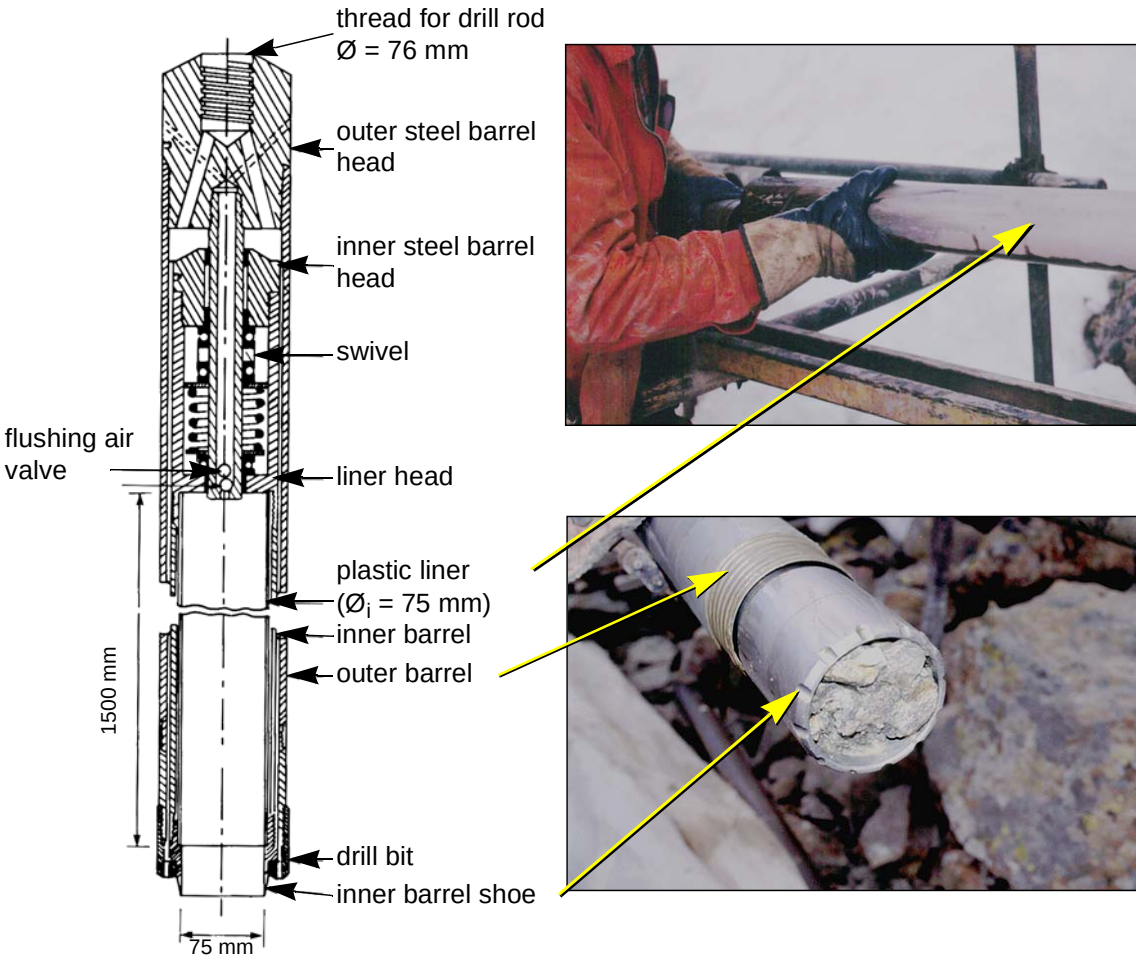

Figure 3-5: *Triple tube drilling system (Photos: L. Arenson).*

a) diamond drill bit: Seyferle: Type XUPER W2: $Ø_i$ = 75 mm, $Ø_o$ = 106 mm

b) hard metal drill bit T-6-101: Seyferle: Type R35: $Ø_i$ = 75 mm, $Ø_o$ = 106 mm

c) hard metal drill bit for ice: $Ø_i$ = 75 mm, $Ø_o$ = 106 mm

d) percussion drill bit for cased drilling: Type ODEX: $Ø_o$ = 140 mm

e) drill bit for percussion drilling: $Ø_o$ = 90 mm/115 mm

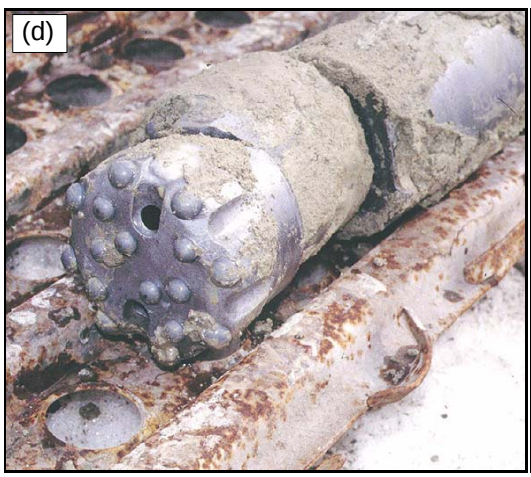

Figure 3-6: *Drill bits used for drilling and coring in permafrost (Photos: L. Arenson).*

3.2 Muragl

3.2.1 Site

The first site under investigation was the Muragl rock glacier (Figure 3-7). This rock glacier has quite a long history of research and it has been investigated already in the first half of the twentieth century in terms of geomorphology (Salomon, 1929; Domaradzki, 1951). Further investigations concentrated on the geophysical properties of Alpine permafrost (Barsch, 1973; 1978; Vonder Mühll, 1993; Vonder Mühll and Schmid, 1993) or BTS measurements (Haeberli, 1992). However, no boreholes have been drilled up to 1999 and therefore no detailed information about the subsurface conditions had been available other than surface geophysical measurements performed in conjunction with this project. The georadar profiles showed strong scattering from the highly heterogeneous rock-ice mélange, in such a way that no useful subsurface information could be extracted. However, additional subsurface and cross-hole refraction and reflection seismic revealed very useful results, such as stratification planes, icy layers and the depth of the bedrock (Musil *et al.*, submitted, a; b), which are used for the spatial determination of the stratigraphy.

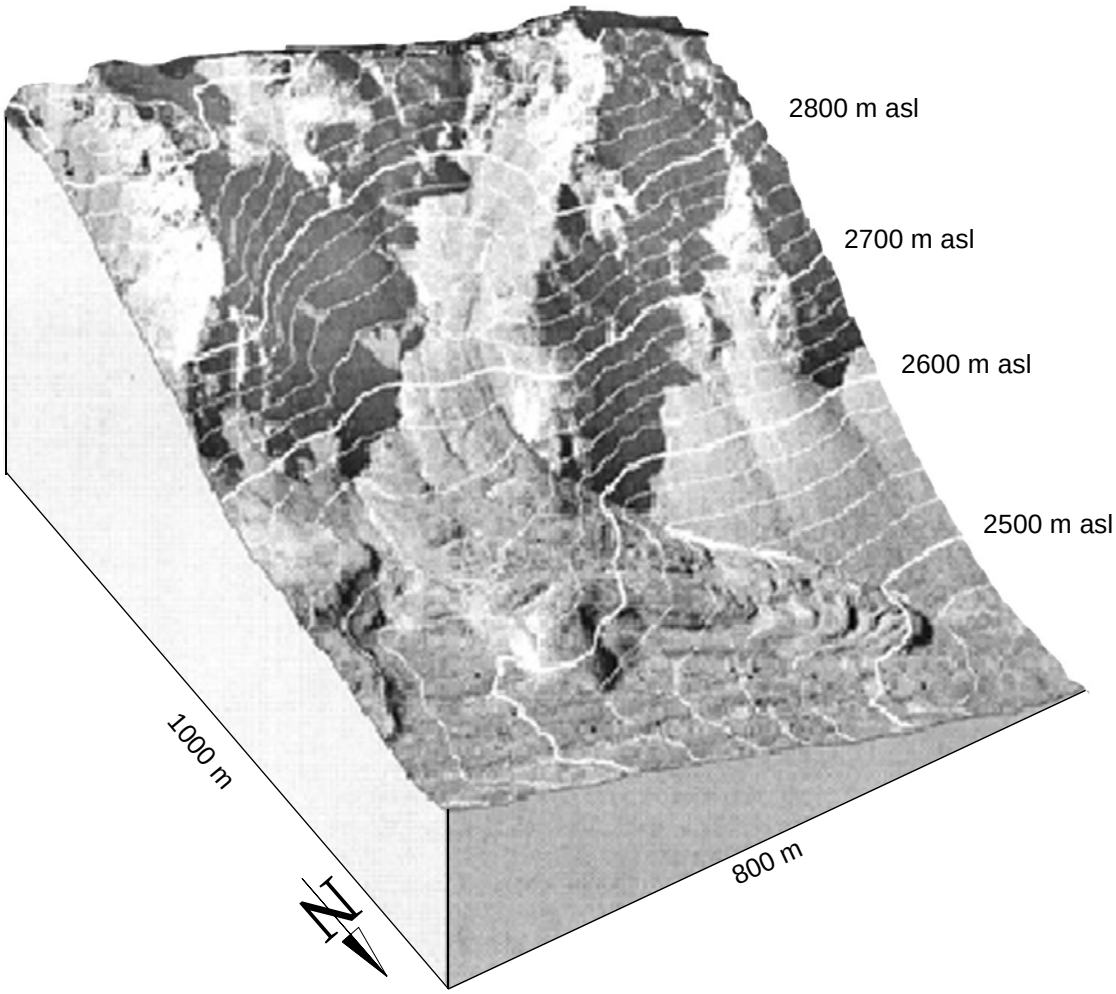

Figure 3-7: *Muragl rock glacier: Synthetic oblique view with a 1994 orthophoto and 20 m contour lines (Kääb and Vollmer, 2000).*

The location of the boreholes had been chosen with respect to the following critical points:

- compressive flow region with a maximum annual horizontal component of surface deformation of about 0.2 m (Figure 3-8),
- possible degrading or degraded permafrost, i.e. one borehole should be in an area, which was formerly permafrost,
- distances between the boreholes must allow effective cross-hole geophysical investigations to be carried out,
- the supposition that different generations of rock glacier existed at this location should be possible to be proven.

The surface flow fields were already known from average annual surface velocities and average annual changes in surface elevation between 1981 and 1994 (Kääb, 1998: Figure 3-8). These were calculated from digital image analyses of high-precision aerial photography (image scale approx. 1:6'000) that are able to determine the surface deformations with an accuracy of about 1.5 centimetres per year (cm/a). The low velocities at the edges of the rock glacier were accounted for as indicators of an area of degrading or former permafrost.

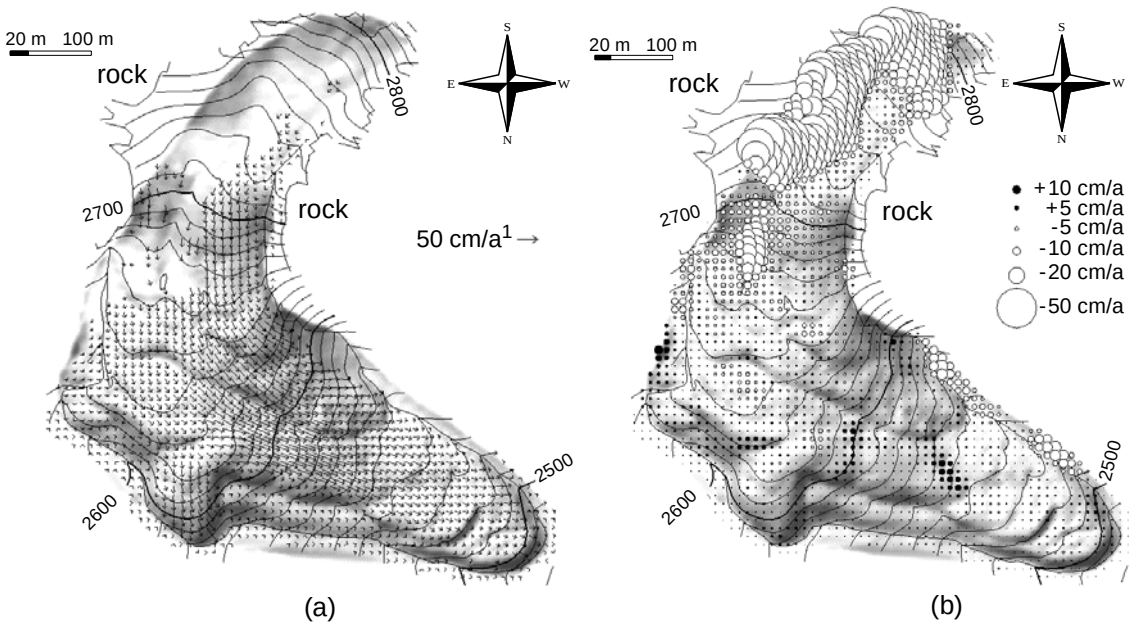

[1] centimetres per year

Figure 3-8: *a) Average annual surface velocity 1981 – 1994 (Kääb, 1998).*
b) Average annual changes in elevation 1981 – 1994 (Kääb, 1998).

As a result of these pre-investigations, four boreholes were drilled with locations shown in Figure 3-9 and given in Table 3-1. Borehole 1/1999 was located on the flank of the rock glacier in the hope that this would help to expose the lateral extension of the permafrost.

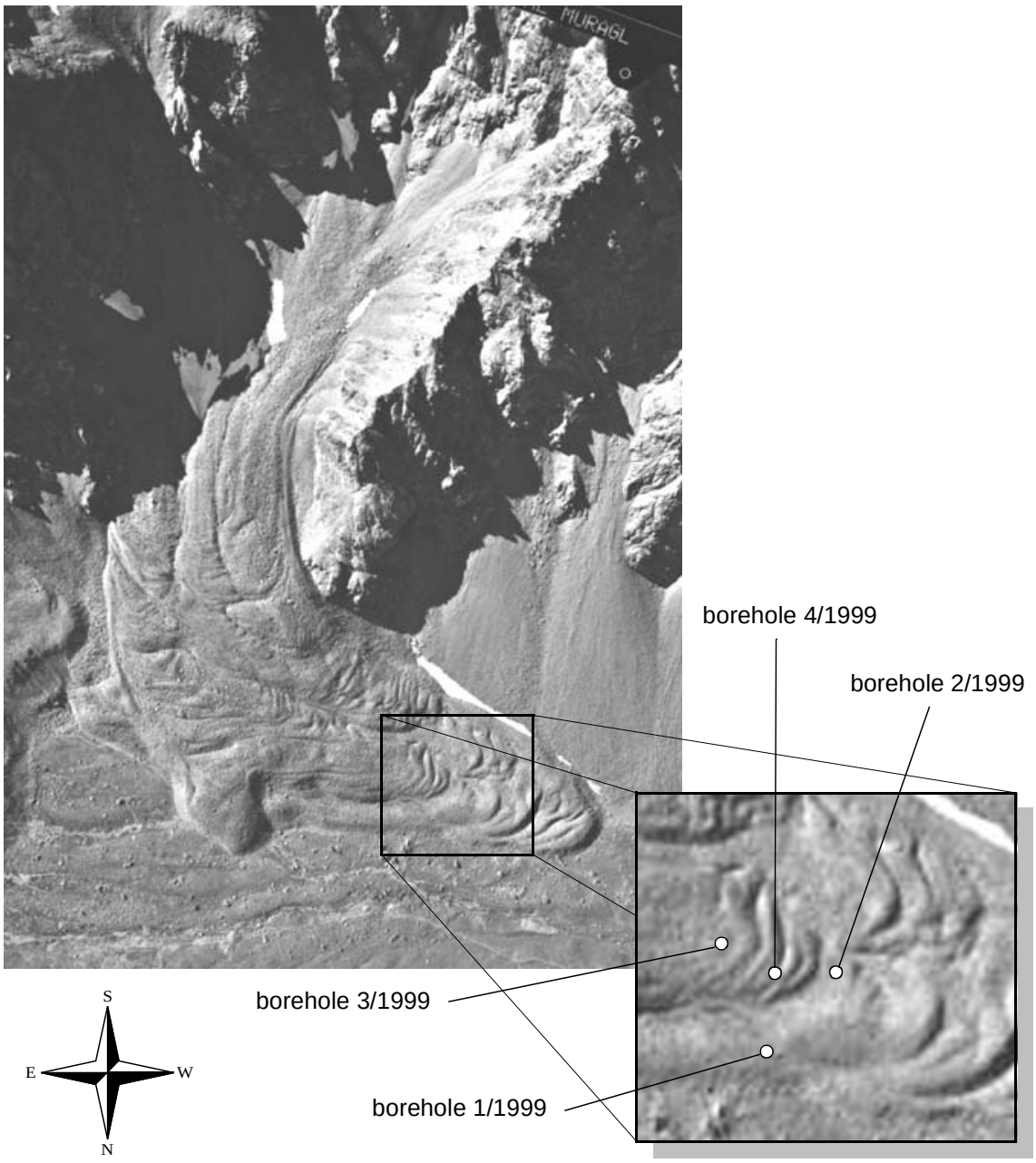

Figure 3-9: *Borehole location at Muragl rock glacier (Photo: Federal Office of Cadastral Surveys).*

3.2.2 Boreholes

Drilling the boreholes at these locations in this particular rock glacier was much more difficult than expected. In contrast to the experiences at Murtèl-Corvatsch rock glacier (see Section 3.3), the percentage of solid particles was much higher and these were coarser, too: gravel, stone and block size material. The drill bits used for coring often had to be changed, sometimes every 5 to 10 cm, resulting in very poor sample quality or even loss of the sample. Borehole 1/1999 was a percussion drilled borehole with a casing, using the ODEX drilling system with a borehole diameter of 140 mm, down to 21.45 m, and a standard down-hole drill bit, which produced a borehole diameter of 115 mm, down to a total depth of 70.2 m. As expected, no ice was encountered during the drilling. A casing was necessary to cope with the borehole instability of the upper part of the borehole, which was not required in the denser layers and the bedrock at larger depth. The groundwater table was reached at 18.0 m but then levelled at a depth of about 15.0 m (Figure 3-15).

It was intended to core samples from the next borehole (2/1999), which was situated in the middle of the rock glacier, where permafrost with ice was expected. After a 6.5 m thick layer of large boulders, some layers with gravel and sand within an icy matrix were found. However, the volumetric amount of ice was relatively small and was at temperatures close to zero centigrade, which, together with the coarse deposits, led to poor sample quality and instability of the borehole wall. The heat, which was generated during the cutting of the solid particles, could not be dissipated and the sample melted. As a result, gravels could rotate with the drill bit, causing additional damage to the sample. Many cores were therefore destroyed during the drilling process and a metal casing was necessary to stabilise the wall. As a consequence, the ODEX system was used as soon as a cored sample had been brought out of the borehole. At the end, the diameter of the cored borehole was 140 mm, instead of the 106 m of the triple tube drill bit. Ice was encountered in the cored samples and also within the drill chips between a depth of 6.5 and 17.0 m. Bedrock was reached at 35.5 m depth.

The third borehole, which was located at the highest elevation, yielded even fewer cores, since the amount of stones and rocks was higher even than in the other boreholes. The top, unfrozen layer was 5.5 m deep, probably due to the ridge on which the borehole was drilled. The soil consisted of a mixture of blocks, gravel, cobbles and sand, with decreasing ice content between 5.5 m and 20.0 m. One boulder, with a thickness of more than 1.2 m, had to be penetrated at a depth of 10 m. No more ice was found at depths greater than 20.0 m and a dry, very porous layer had to be drilled through between 23.0 m and 29.0 m. The air from the flushing system vanished completely into the ground and the borehole wall was very unstable.

The fourth borehole was drilled in the middle of the triangle formed by the first boreholes. Fewer large boulders were encountered within the permafrost, and therefore more undisturbed samples were obtained. The layer between 4.7 m and 9.7 m, where the percentage of small sized materials, i.e. sand and silt, was higher than within the subsequent layers, was particularly fruitful. The thickness of the active layer was only about 2.7 m, since the borehole was drilled

in a furrow between two ridges. The ice free layers started at a depth of 15.75 m and were dense at the beginning, but had large air voids between 20.25 m and 23.25 m, where all the air disappeared into the ground.

The stones and boulders, which are mainly gneiss or gneissic granite (Figure 3-10), have a uniaxial compression strength of up to 35 MPa with a Young's modulus of up to 6 GPa.

Figure 3-10: *Gneissic granite from the Muragl rock glacier at borehole 4/1999, 11.5 m depth, diameter: 75 mm (Photo: L. Arenson).*

borehole:	**1/1999**	**2/1999**	**3/1999**	**4/1999**
depth [m]	70.2	64.0	72.0	71.0
start coring at [m]	–	6.3	8.0	4.75
end coring at [m]	–	17.40	23.0	15.3
total length cored [m]	–	11.1	15.0	7.75
undisturbed cores [m/%]	–	2.8 / 25	3.6 / 24	4.75 / 61
disturbed cores [m/%]	–	6.2 / 56	–	1.3 / 17
bedrock at [m]	49.50	35.5	36.5	32.0
water encountered at [m]	18.0	34.4	32.0	30.3
ice in cores or chips down to [m]	–	17.0	20.0	15.75

Table 3-3: *Borehole characteristics: Muragl rock glacier.*

Only 7.5 m from a total of 11.1 m of undisturbed cores that were extracted were sufficient for triaxial testing because the cores had to be 16 cm long without any fault. In addition, cores with larger diameters were extracted during the drilling of borehole 2/1999. The rest of the extracted material was used for soil classification and for the determination of the volumetric ice content.

Various drilling velocities could be achieved depending on the drill system (coring, percussion, ODEX: Figure 3-11), with average drilling velocities as follows:

- percussion drilling (diameter = 115 mm): 5.1 m/h
- cored drilling (diameter = 106 mm): 0.7 m/h
- cased percussion drilling (ODEX; diameter = 140 mm): 4.2 m/h
  This system was usually used after the cored drilling, therefore, it was mostly achieving an expansion of the borehole.

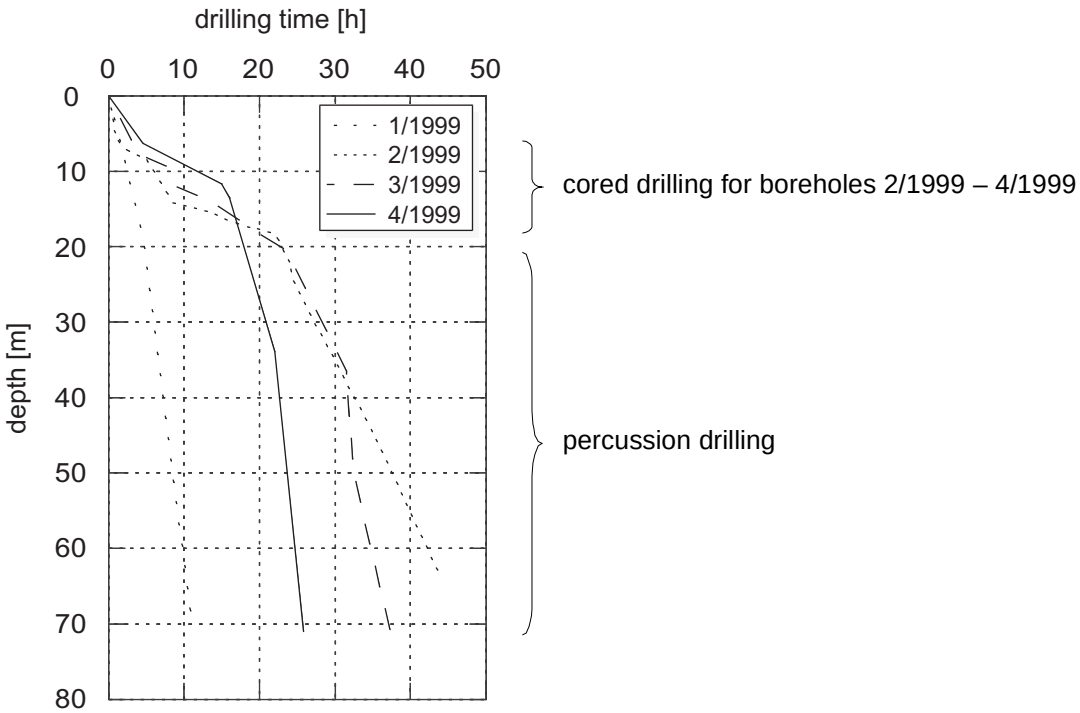

Figure 3-11: *Drilling progress, Muragl rock glacier.*

3.2.3 Installation of Casing

Plastic casings had to be put in all four boreholes due to the instability of the walls, in order to have access down the hole for further investigations. Four plastic casings were selected from a range of diameters, depending on their eventual purpose, were placed within the steel casing of the ODEX drill system. Injection tubes were fixed at three different depths to the outer side of the casing for the two boreholes 3/1999 and 4/1999 that were later used for deformation measurements. The steel casing was then pulled out of the ground and injection was carried out with a mixture of WILMIX®400 grout and Opalit (about 2%). The grout had a water/cement value of 0.5 and the maximum grain size was 0.5 mm.

The two boreholes, 1/1999 and 2/1999 were cased with a 3'' and a 4'' plastic casing, respectively, down to the bedrock. The purpose of these two casings was purely to prevent collapse of the borehole, so that geophysical measurements could be performed and temperature chains could be lowered.

Figure 3-12: *Settlement hook system coupling.*

Vertical and horizontal deformation measurement systems, which are explained in more detail in a later chapter (Chapter 3.2.7), were installed in the other two boreholes. A USBR-type settlement hook system (Slopeindicator, 2002) was used in order to be able to measure vertical movements above the bedrock. Below this, where only minor deformations were expected, inclinometer tubes were put into the borehole. The latter, which had a length of 3 m, were glued and bolted together, while the 95 cm long inclinometer tubes for the settlement measurements had a telescoping coupling (Figure 3-12) that allowed for a vertical compression of 1.7 cm.

Problems during installation

Several problems occurred during the injection of these two boreholes. The relatively stiff mixture, which was necessary in order to prevent significant loss into the surrounding ground, plugged up the injection tube at the bottom of borehole 4/1999. In addition, the plastic casing of borehole 3/1999 filled with grout, since the tube had not been precharged with water before the injection started. As a consequence, the pressure head at the bottom of the casing was so high that the lowest coupling between the plastic tubes collapsed and the grout leaked into the tube. Even though the casing was flushed immediately for several hours, and the grooving, which is necessary for the guidance of the deformation measurement probes, as well as the telescopic couplings of the vertical deformation system were brushed intensively, it was impossible to remove all of the grout, so that the vertical deformation measurements could not be performed as desired. The amount of grout used for the installation of the tubes was much higher than expected. This indicates that even more grout disappeared into the voids within the ground underneath the permafrost base than previously thought. However, the tubes bedded in well enough via the combination of grouting, wall instability and rock glacier movement to obtain reasonable data for the vertical borehole deformation.

Further details of the installation process are given in Arenson (2000).

3.2.4 Geophysical Borehole Logging

Even though the boreholes were cased down to the bedrock, geophysical downhole logging was conducted in order to locate inhomogeneities and to detect changes in the properties of different layers. Detailed descriptions of the various geophysical logging methods can be found in Vonder Mühll (1996).

It was not possible to fill borehole 2/1999, 3/1999 and 4/1999 with water for the current project, due to voids between the lowest casing and the bedrock and joints in the bedrock and therefore, the results are of limited quality. The calibre log reveals information of the borehole diameter and was neither influenced by water nor the casing. Measurements of the natural radioactivity (gamma ray log) can be used for the qualitative determination of ice, since ice is nearly inactive. With the gamma-gamma log it is possible to determine the density of the adjacent ground. Cavities behind the casing may influence the measurements. Neutrons that are sent into the ground will be slowed down, in particular due to hydrogen in the water or ice. The quality of this measurement decreases for empty boreholes. Fast neutrons will penetrate less than slow neutrons. Joints can be detected within the resistivity log, since they influence the natural dispersion of an applied current. This technique, however, is only applicable within a water filled borehole. Acoustic high frequency signals will be sent into the ground for the sonic logs, and with the measured transit times, P-wave velocities can be calculated from the difference between the arrival times of two receivers. This measurement technique is also only suitable within a water filled borehole.

log	measures	1/1999	2/1999	3/1999	4/1999
Casing		22 m steel	37 m PVC	38 m steel	34 m steel
Calibre	diameter	x	x	x	x
Gamma ray log	ice content	x	x	x	x
Gamma - gamma log	density	x	x	x	x
Neutron - neutron log long & short	hydrogen -> water and ice	x	x	x	x
Sonic	P-wave velocity		x	x	x
Resistivity	joints	x	x	x	x

Table 3-4: *Geophysical borehole logging at the Muragl rock glacier.*

Comparisons between the different methods, (e.g. borehole 1/1999: Figure 3-13) show variations in density and ice content. The data, however, do not provide exact information but may help during the determination of the stratigraphy. Borehole 1/1999 shows large variabilities of the density in the uppermost 16 m, which is an indicator of a high porosity. Similar layers were found within the other three boreholes under the permafrost base. The neutron – neutron logs also clearly showed the ice within the boreholes 2/1999, 3/1999 and 4/1999. However, since groundwater and ice results in a similar response, additional observations are necessary (e.g. temperatures, drilling chips). The resistivity logs revealed that there are some joints in the bedrock, in borehole 1/1999 in particular down to about 53 m.

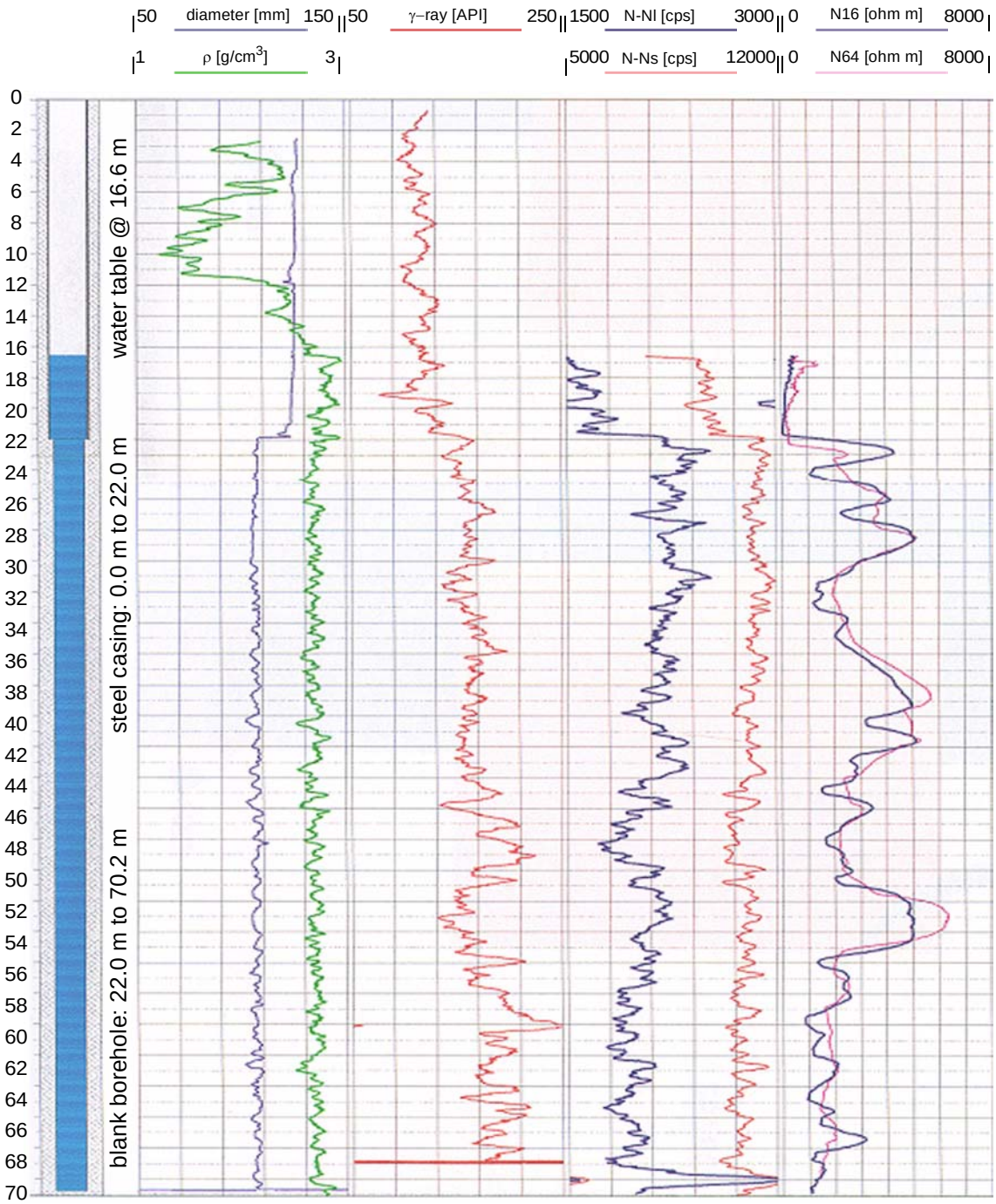

Figure 3-13: *Borehole logging at the Muragl rock glacier, borehole 1/1999 (EGS, 1999).*

Detailed information from the different logs can be found in the documentation of the two companies that performed these tests (EGS, 1999; GEOTEST, 2000).

3.2.5 Stratigraphy

Analysing the cores together with data from a combination of sources, such as, geophysical borehole loggings, drill chips and remains (e.g. Figure 3-14), observation from the drilling crew, *etc*., allowed a 3D-model of the subsurface to be set up.

Figure 3-14: *Drilled remains from borehole 3/1999: 12.2 - 13.1 m (Photos: L. Arenson).*

Additional information from the geophysical investigations performed by the Institute of Geophysics (Musil *et al.*, submitted, a; b) helped with the spatial distribution of the various layers determined from the boreholes and therefore with the refinement and adaptations of the model. The main features of the subsurface are:

- No ice within borehole 1/1999.
- On top of the permafrost table, there is a 2.0 m to 6.0 m thick seasonally unfrozen active layer with large, interlocking and loose boulders. The diameter of these boulders may be of several metres. The thickness of this layer depends on the surface undulations, since the permafrost table itself has a much smoother profile, which follows the average slope of the rock glacier.
- The volumetric ice content is very heterogeneous and was determined to be in the range of 40 to 80%. Clear ice lenses of several centimetres can be found in-between two larger stones or blocks.
- The maximum depth of the layer in which ice was encountered varies from 15.8 m (4/1999) to 20.0 m (3/1999).
- A loose, uncompacted, silty, sandy gravel layer with a very high air void ratio is present underneath the ice containing layers (~25 m depth). This layer disappears towards the side of the rock glacier.
- Bedrock was found at depths between 36.5 m and 32.0 m, on top of which lies a compact layer of gravel, sand, silts with an increasing number of boulders closer to the bedrock. The thickness of this layer is about 9 m, within which the groundwater table may be observed. It was more or less constant throughout the observed time period (Figure 3-15).

- The surface of the bedrock seems to be parallel to the mean surface of the rock glacier in the downhill direction, but in the transverse direction (NNE – SSW) the bedrock dives to a slightly larger depth.

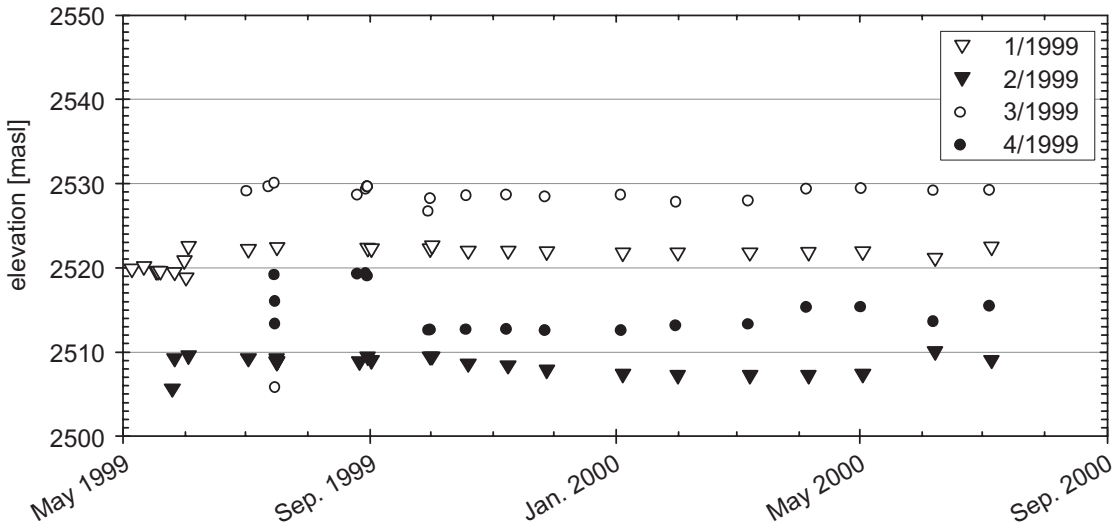

Figure 3-15: *Groundwater tables at all boreholes at Muragl rock glacier.*

In summary, a profile of the subsurface ground can be drawn as shown in Figure 3-16.

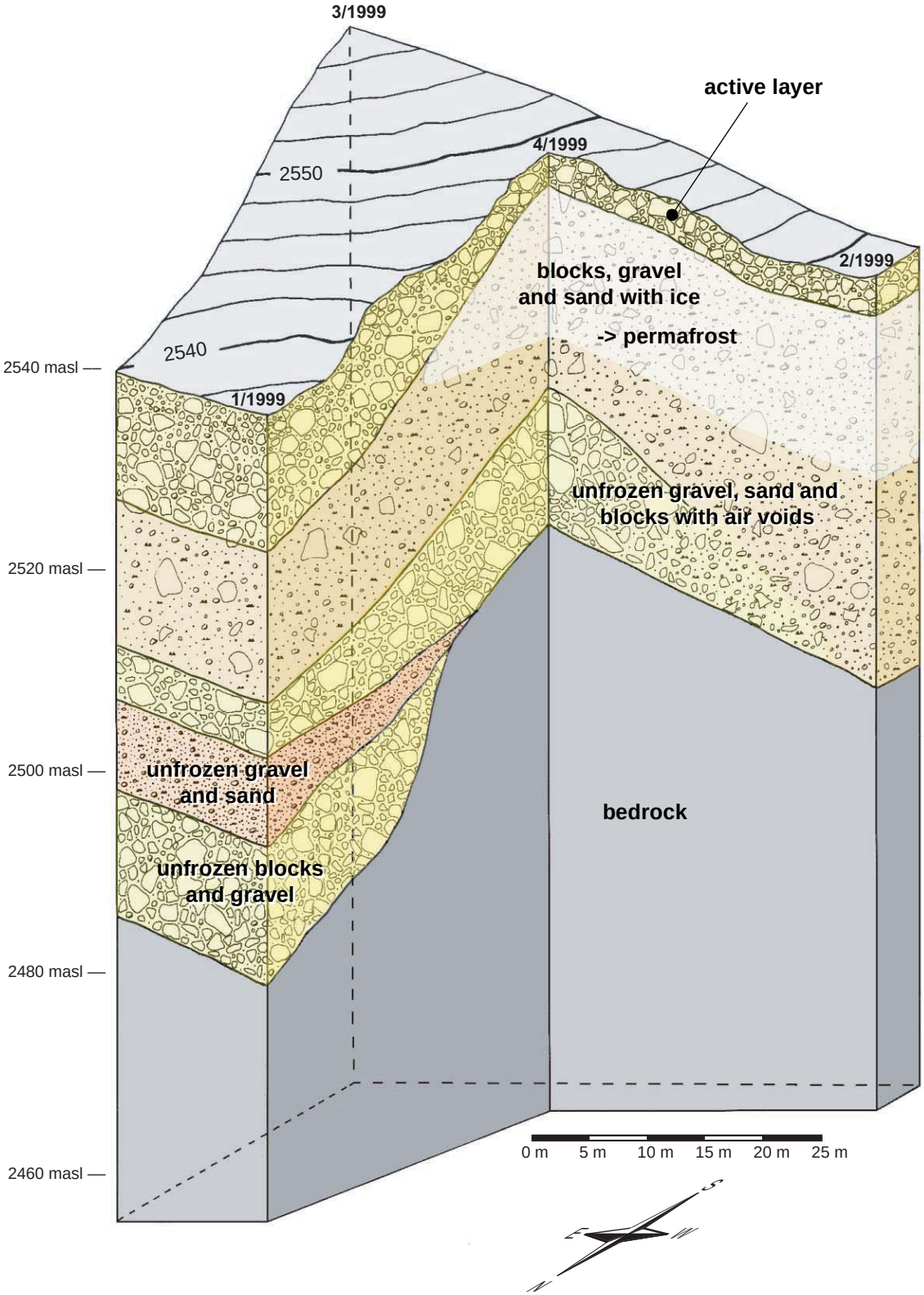

Figure 3-16: *Stratigraphy of the Muragl rock glacier.*

Analyses of the cored samples revealed a volumetric ice content of 40-70% with a volumetric content of solids between 20 and 56% (see also Figure 4-15). The ice content decreases with increasing depth within the permafrost layer. The true grain size distribution, however, cannot be determined easily from the cores, since many of the stones and blocks within the ground are larger than the diameter of the samples, which was 74 mm. A large sample of about 100 kg was taken from the surface of a side slope of the rock glacier with grain diameters smaller than 125 mm. The particle size distribution curve indicates a typical Fuller-distribution, which was similar in shape to that obtained from a drilled core at a depth of 15 m (Figure 3-17).

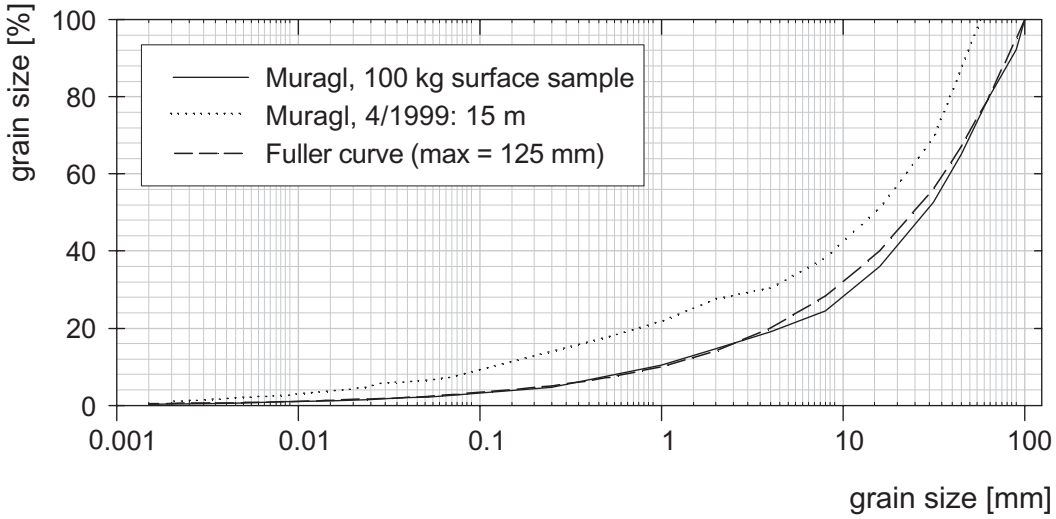

Figure 3-17: *Grain size distribution curves for different samples from the Muragl rock glacier.*

The solid particles within the Muragl rock glacier do not seem to have a predominant grain size. The entire range of grains from blocks of some metres in diameter to silt size particles is present, in such a way that minimum air voids could be achieved. However, the randomness of the distribution prevents this from occurring throughout the whole rock glacier. A classification after the USCS system (SN 670 008a, 1997) based on collected samples would result in sandy, well graded gravels with silt and stones (GW-GM). However, if the maximum particle size in the sample is not representative, the classification is likely to change.

3.2.6 Temperatures

Temperature chains with up to 25 thermistors of the type YSI 44006 and spacing increasing with depth were ordered from Stump Bohr AG. The accuracy of the thermistors is ±0.1°C within a temperature range of about -5°C – +5°C. The connecting cable was of the type Isocol CY 30 x 0.34 mm^2, with a diameter of 13.4 mm. Calibration was carried out in an ice bath by the Laboratory of Hydraulics, Hydrology and Glaciology at ETH. Three chains were installed in three of the boreholes in 1999, and data were logged at one logger tower, which was powered by a solar panel (Figure 3-18).

1) snow height measurement
2) solar panel
3) air temperature sensor

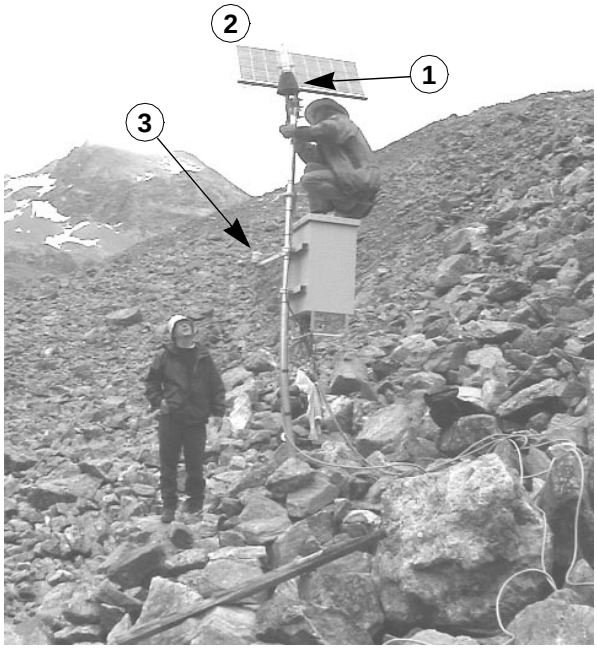

Figure 3-18: *Logger tower at Muragl rock glacier (Photo: L. Arenson).*

Automatic reading of the temperatures within three boreholes was started in January 2000. The temperatures at all depths are recorded every six hours. The data are then stored on an SRAM card. Since the boreholes had to be empty for the parallel deformation measurements (see section 3.2.7), the chains hung in the air for most of the time. With ongoing shearing of the borehole and also of the tubes, the deformation measurements were no longer possible and since the tube cracked, water filled the holes. It is assumed that the temperature chains within the three boreholes 2/1999, 3/1999 and 4/1999 are grouted into the soil by ice and debris after summer 2001.

Some additional manual temperature readings were performed in 1999 before the automatic reading started, although some disturbance had to be considered due to the drilling.

Some data was lost in summer 2000 due to problems with the power supply at the logging station. Following one year of monitoring borehole 1/1999, the thermistor string TK 015 was moved to borehole 2/1999. Fortunately, it has been possible to manufacture an additional thermistor string, which was placed into borehole 1/1999 in September 2002 and since then all four boreholes are monitored within the framework of PERMOS.

Air temperatures (Figure 3-19) and snow heights (Figure 3-20) were measured at the tower in addition to the borehole temperatures. Due to movements of the rock glacier, the tower tilted from about January 2001 until August 2001 and as a consequence, the snow height is not accurate and the smooth air temperatures indicate that the temperature sensor was covered under the snow. It is assumed that more accurate measurements have been available since summer 2001, even though the mast was still moving with the surface. However, the

measurements show, that during the winter 2000/2001 more snow was present, in particular at the beginning of the season (December), compared with the subsequent winter 2001/2002, where the snow started to accumulate only in January. As a consequence, the soil temperatures were much colder at greater depths during winter 2001/2002.

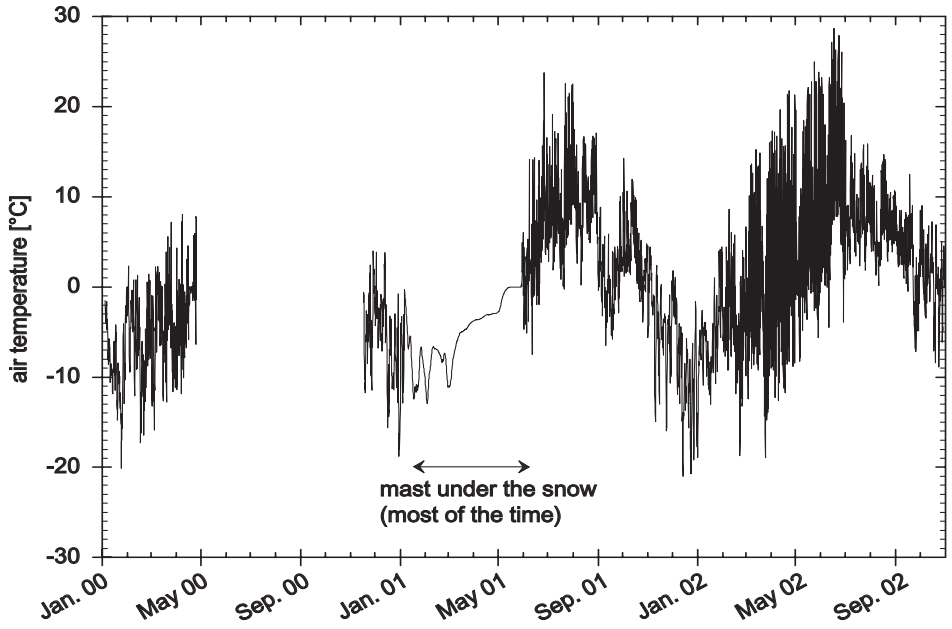

Figure 3-19: *Air temperatures at the Muragl rock glacier.*

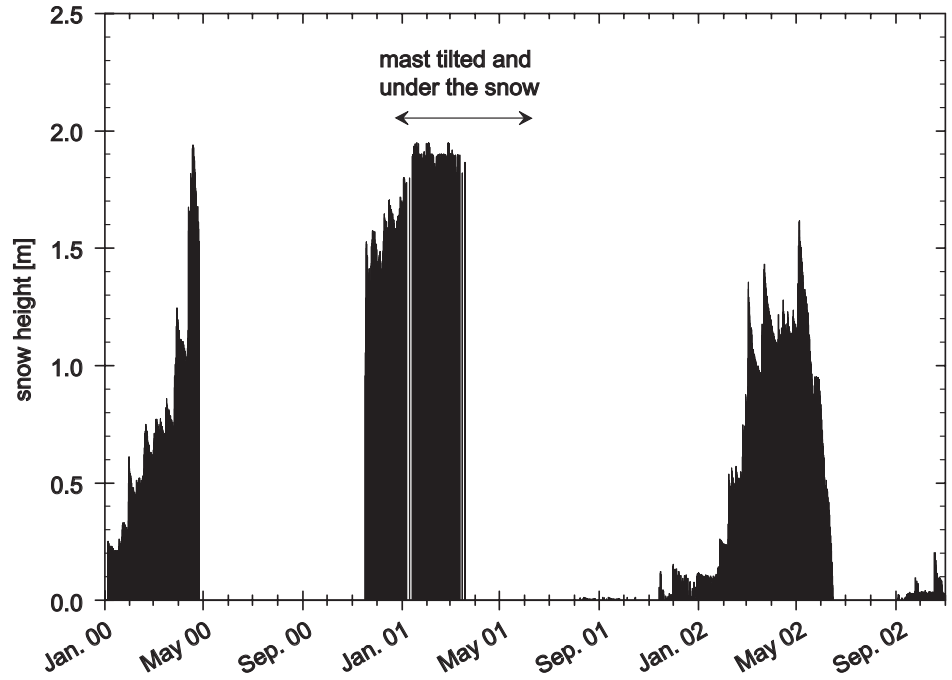

Figure 3-20: *Snow height measurements at the Muragl rock glacier.*

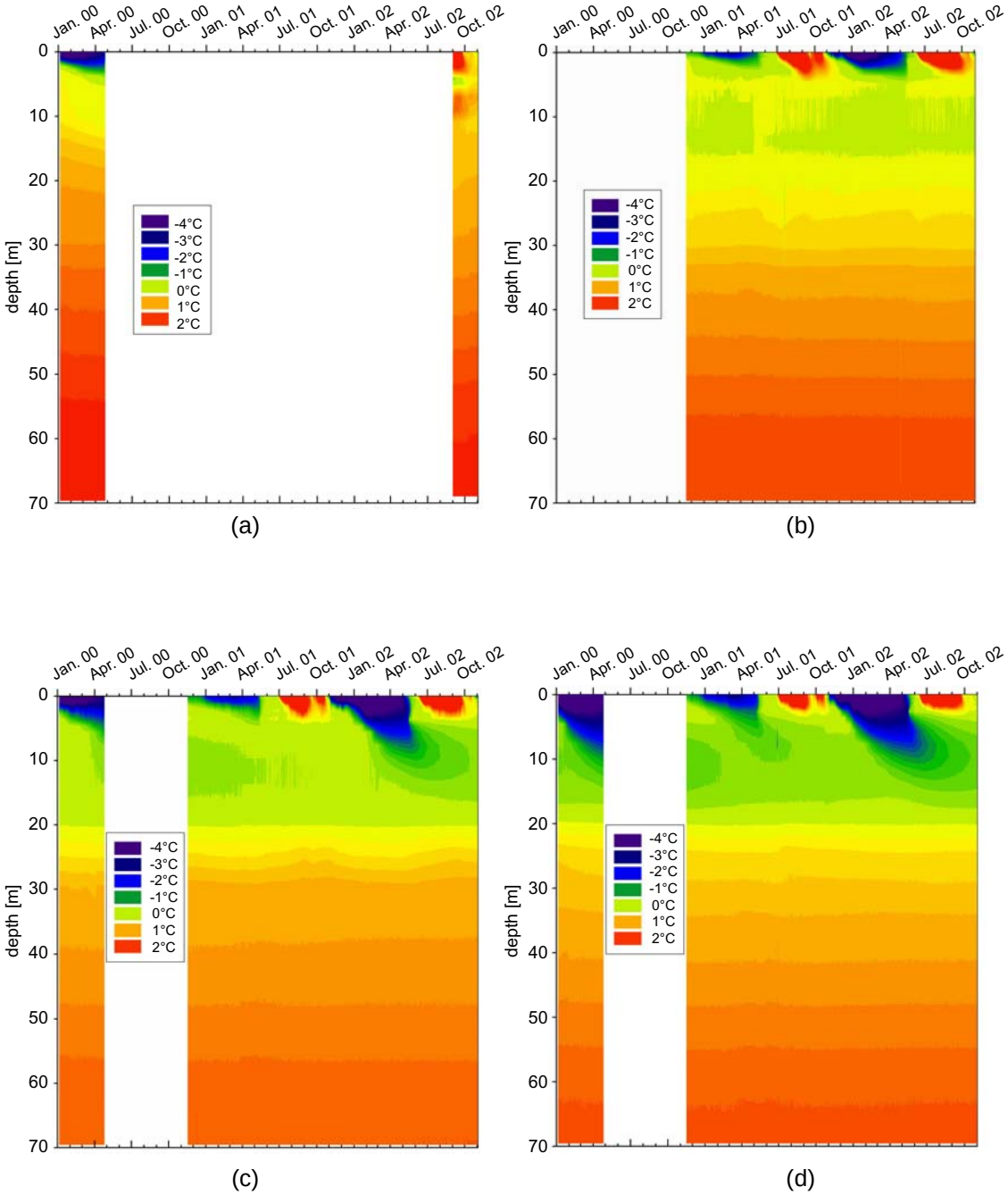

Figure 3-21: *Temperature data from the Muragl rock glacier.*
a) borehole 1/1999 (January – May 2000 & since September 2002).
b) borehole 2/1999 (since November 2000).
c) borehole 3/1999 (data loss: 26.4. – 15.11.2000).
d) borehole 4/1999 (data loss: 26.4. – 15.11.2000).

A summary of the temperature data are given in Figure 3-21. The temperatures are shown with depth for distinct data in Figure 3-22. The depth of the permafrost base can be determined from these figures as the point of zero centigrade. Comparing these plots with the drill logs, a difference can be found between the depth of the permafrost base and the occurrence of ice. The temperature reaches zero centigrade at a depth of 20 m for both boreholes whereas, ice was encountered until a depth of 20.0 m and 15.8 m within borehole 3/1999 and 4/1999, respectively. The material beneath the permafrost is sufficiently permeable, that as the ice melts, the water is released and cannot accumulate there and be re-frozen at a later time. It is unlikely that, once melted, the permafrost can be regenerated within the current climate environment.

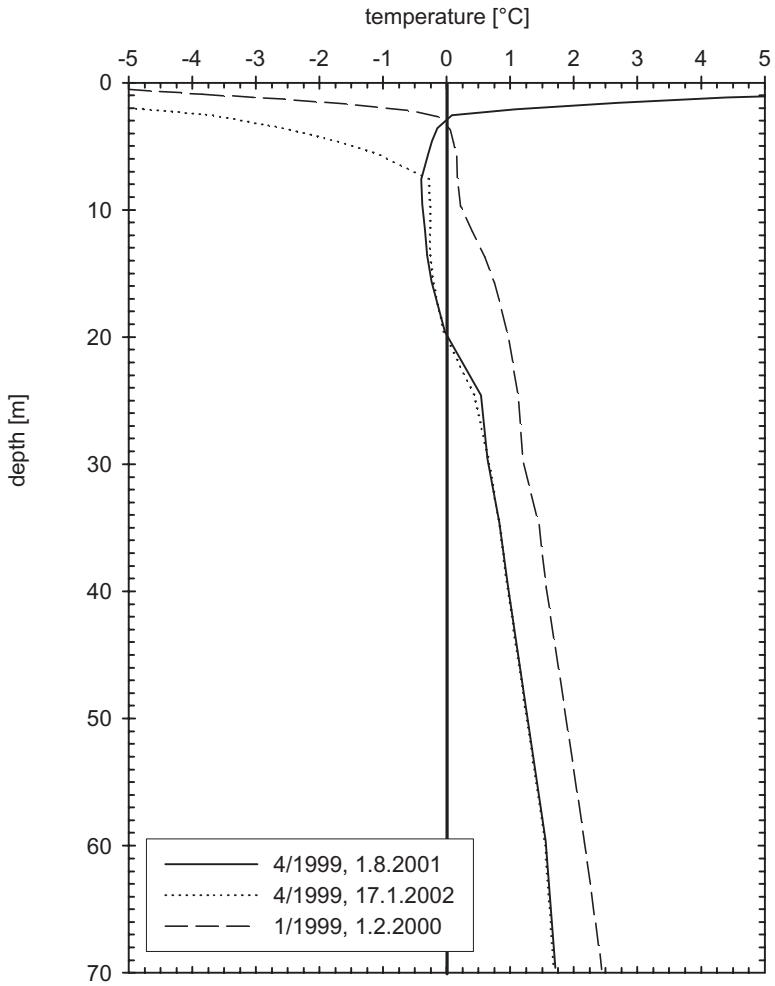

Figure 3-22: *Temperature profile for borehole 1/1999 and 4/1999 of the Muragl rock glacier.*

The influence of the snow cover on the ground temperatures can also be shown at the Muragl rock glacier, even though no data are available during summer 2000. There was, however, more snow during the winter of 2000/2001 than during the year before (Figure 3-20). As a consequence, the temperatures within the layers close to the surface were colder during the first year of measurement (see Figure 3-21) for a depth of 10 m. If the snow falls early in the winter, it acts as an insulator, and the cold air temperature cannot penetrate into the ground, whereas a thick snow cover during spring preserves the cold soil temperatures for a longer period.

3.2.7 Borehole Deformation

Different systems were installed in some of the boreholes in order to measure the internal horizontal and nominally vertical movements. Good results were obtained from slope inclinometer measurements using the SINCO Digitilt system for determining the horizontal movements, which has, for example, also been used in the Arctic for the determination of *in situ* creep properties in ice-rich permafrost (Savigny and Morgenstern, 1986a). A USBR-type settlement hook system, which is not in very widespread use, was used for the measurements of the vertical deformations. Both of the vertical and horizontal measurement systems use the same PVC-tube for guiding the measurement probes. Due to problems, which occurred during the installation of the tubes (see Chapter 3.2.3), the first readings have to be used with caution, since some bedding in was still possible within the borehole due to the grouting process. A zero reading was take on 1. October 1999 that serves for the determination, subsequently, of relative movements.

Horizontal deformations

A well established slope inclinometer measurement system for internal horizontal borehole deformations was chosen for the investigations at the Muragl rock glacier. The inclinations in two orthogonal directions were measured every 2 feet (0.61 m) along the tube (Figure 3-23c) with a SINCO Digitilt probe (Figure 3-23a), which uses null-balance accelerometers as sensing elements. A special PVC-tube of 71 mm internal diameter, with two sets of diametrically opposed internal channels (Figure 3-23b), guides the probe. The wheels of the probe are usually guided in the A-direction, which results in a slightly better accuracy. The tubes are oriented in a way that the A-direction represents the direction of the expected main deformation. A set of two readings is taken from the bottom to the top in both the A0/B0 and A180/B180 direction with the aim of eliminating the zero offset of the instrument. The accuracy of the inclination of one set of reading, as quoted by the manufacturer, is ±0.02°. Since three sets of readings were always performed for one value, the accuracy could be reduced substantially to about ±0.005°, which was determined by comparing the sets of readings.

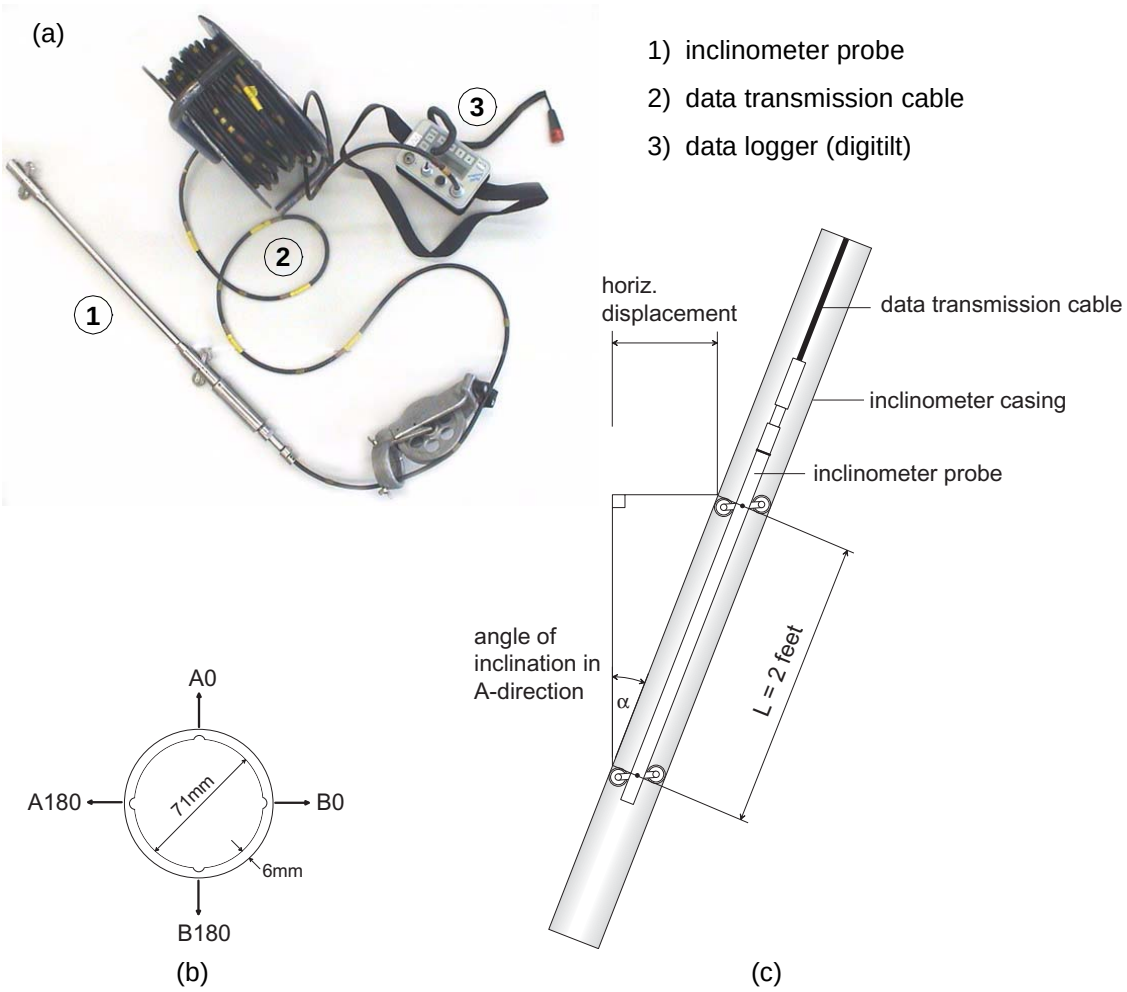

Figure 3-23: *Principle of SINCO Digitilt slope inclinometer measuring system.*
a) Picture of the system (Photo: L. Arenson).
b) Cross section through PVC tube, showing the four channels.
c) Longitudinal section through inclinometer casing and probe.

The resultant horizontal deformation can be determined by adding the displacements in the A and B-directions, starting from the bottom as shown in Figure 3-24 for the boreholes 3/1999 and 4/1999.

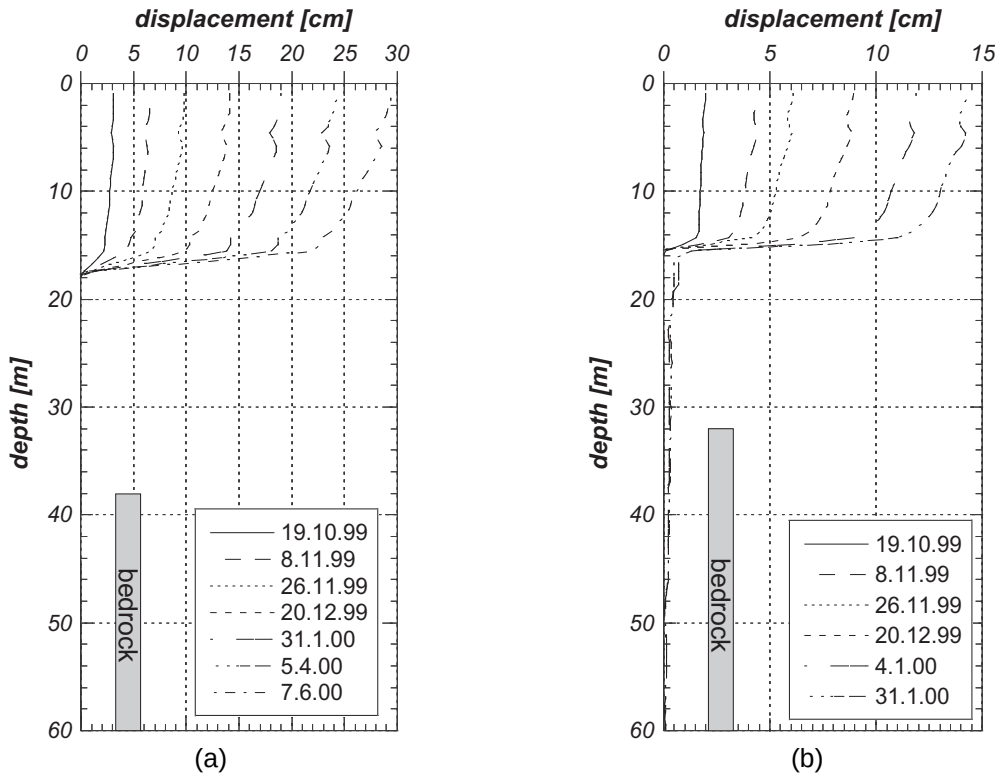

Figure 3-24: *Horizontal down-slope borehole deformation (relative to zero reading 1. October 1999).*
a) borehole 3/1999.
b) borehole 4/1999.

The deformation profiles indicate a clear shear zone at the bottom of the icy layers within both boreholes. About 80% of the total deformation measured at the surface was observed within this shear zone, that was determined to lie between 15.6 and 17.9 m for borehole 3/1999 and 13.7 and 16.0 m for borehole 4/1999, respectively. Underneath the active layer at depths of about 5 m, extrusion flow can be observed, which may be attributed to the interlocking within the boulders of the active layer and slightly faster movements of the icy layers underneath.

Horizontal shear strains, that are calculated from Equation 3-1 for each reading interval, and after the definition shown in Figure 3-25, are given in Figure 3-26 for both boreholes.

$$\dot{\varepsilon}_h = \frac{du}{dt \cdot dh} \qquad [3\text{-}1]$$

$\dot{\varepsilon}_h$ horizontal strain rate

du relative horizontal deformation in-between two readings (Figure 3-25)

dt time between the two readings in seconds

dh probe length (61 cm)

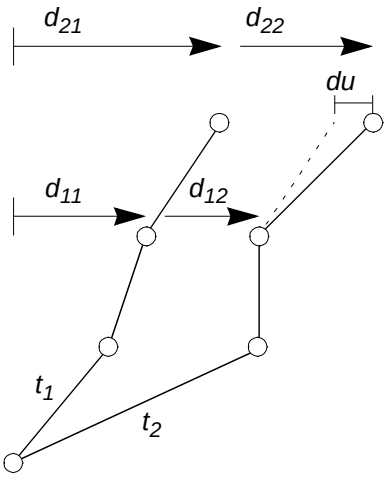

$$du = (d_{22} - d_{12}) - (d_{21} - d_{11})$$

Figure 3-25: *Definition of relative horizontal deformation du.*

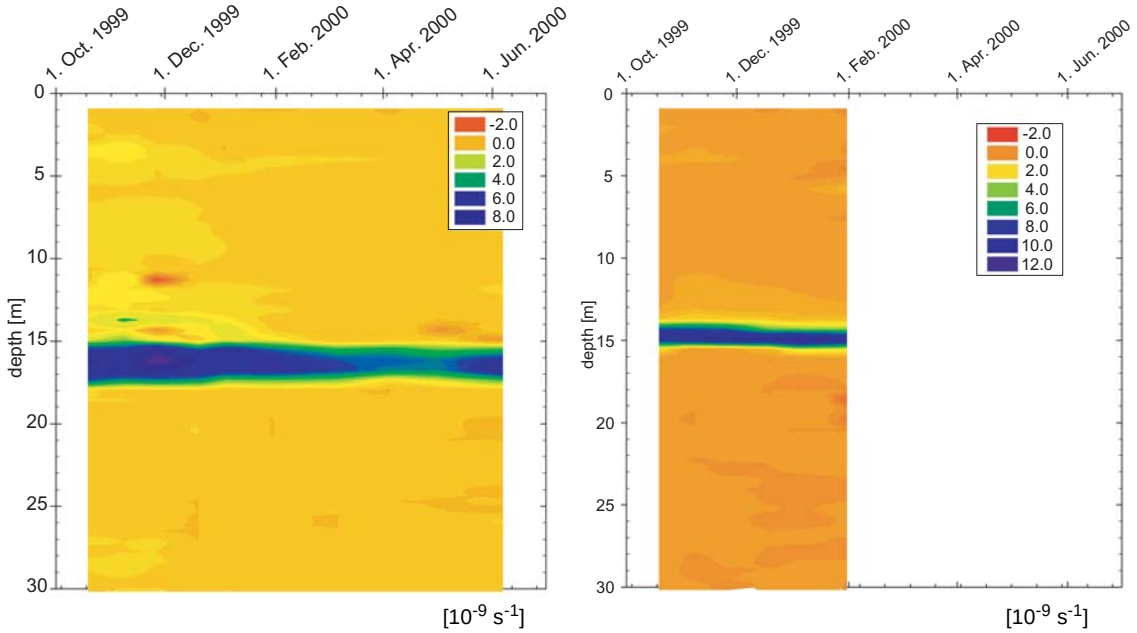

(a) borehole 3/1999 (b) borehole 4/1999

Figure 3-26: *Horizontal strain rate for the Muragl rock glacier.*

A seasonal change in the strain rates during the observation period can be seen for borehole 3/1999. A maximum of about $10 \cdot 10^{-9}$ s^{-1} was calculated following the summer season 1999, which was delayed to November/December because of the phase lag of 3–4 months between peak temperature at the surface and the temperature of the main shear zone. The shear zone deformation is about 12 times faster than of the overlying layer for both boreholes. The minimum strain rate occurred in May, again a phase lag of 3–4 months from the lowest winter surface temperature.

The surface deformation can be calculated by plotting the accumulated deformation from the bottom to the top of the borehole (Figure 3-27a). In contrast to earlier observations on other rock glaciers in the Swiss Alps (Wagner, 1992; Arenson *et al*., 2002), the Muragl rock glacier shows seasonal changes in the velocity, whereby the total velocity is smaller during the winter months than during the summer months (Figure 3-27b). Unfortunately, the deformations within the shear zone were so large after 4 and 9 months, respectively, that the radius of the inclinometer tubes reached a value smaller than the minimum permissible radius of curvature of 5.3 m, which is necessary in order to lower the inclinometer probe. It was only possible to observe a decrease in the surface velocity for borehole 4/1999 (4 months) whereas borehole 3/1999 lasted nine months, covering one maximum and one minimum of the surface velocity in December and May, respectively. A sinusoidal curve fit was calculated for the surface velocity $v_{surface}$ (in mm/d), as a function of the time t (in d) after Equation 3-2.

$$v_{surface} = v_0 + C_0 \cdot sin(\varpi_0 \cdot (t + t_v)) \text{, with} \qquad [3\text{-}2]$$

v_0 = 1.2 mm/d

C_0 = 0.6 mm/d

ω_0 = 1.263 d^{-1}

t_v = 14 d

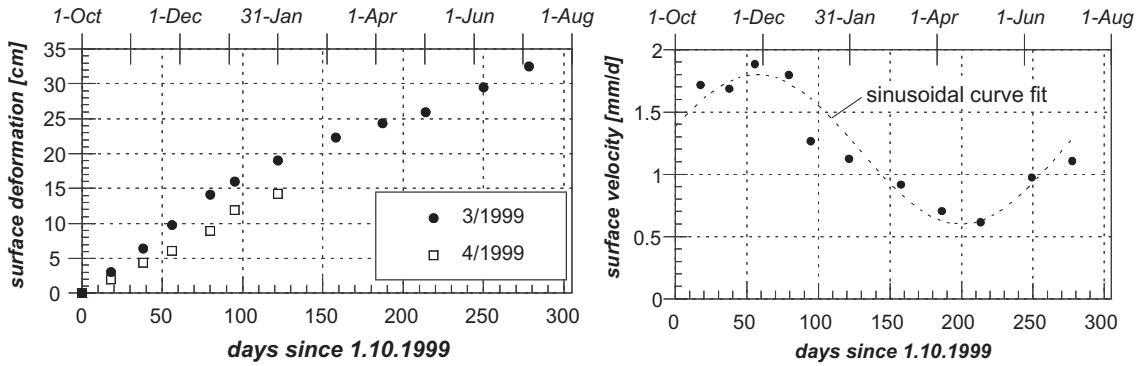

Figure 3-27: *a) Surface deformation since 1. October for borehole 3/1999 and 4/1999.*
b) Surface velocity since 1. October for borehole 3/1999.

The velocity at the surface, which is about 46 cm and 43 cm per year for borehole 3/1999 and 4/1999, respectively, is mainly a function of integration of movements in the shear zone. Retarded temperature changes within this layer result in the observed phase lag of the deformation response. The temperatures development within the shear zone is therefore the crucial factor for future change in deformation.

Vertical Deformations

Vertical deformations were measured using the SINCO settlement USBR-type probe for the Muragl rock glacier, which uses telescoping coupling between the inclinometer casings (Figure 3-28). The USBR-type probe has two spring-loaded arms that catch on the bottom edge of the casing section near the coupling (• in Figure 3-28) when the operator pulls the probe up on the survey tape. A special mounting device is fixed above the inclinometer casing to guarantee that the tensile stress within the tape is always the same. In contrast to the magnet extensometers, which were used for example at the Murtèl-Corvatsch rock glacier in 1987, the casing has been well grouted into the ground and can move with it.

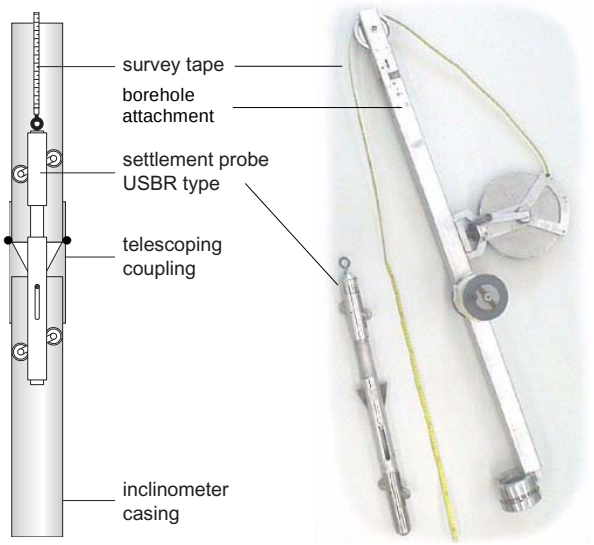

Figure 3-28: *Vertical deformation measurements with the SINCO settlement USBR-type probe (Photo: L. Arenson).*

However, the problems during the installation of the inclinometer casings and the grouting of the boreholes reduces the accuracy of the results and several markers could not been measured anymore. In order to measure the vertical displacements more accurately (5-10 times), different systems, such as Increx or rod extensometers are recommended. Due to the horizontal deformations of the inclinometer tubes, the data do not represent the vertical deformation of the rock glaciers but the extension or compression of the tubes. This can be done if 3D deformation profiles are required. The distributions of these deformations are, nevertheless, helpful in revealing the flow mechanisms.

The basic conclusion that can be drawn from this data is that the majority of the differential settlement occurs around the shear zone for both boreholes (Figure 3-29). The differential settlements are calculated as the difference of the distance of a marker point from the top between two subsequent readings. The

actual deformation of the ground between two points can be determined by subtracting the differential settlement of two depths. Very minor changes can be observed above and below the shear zones.

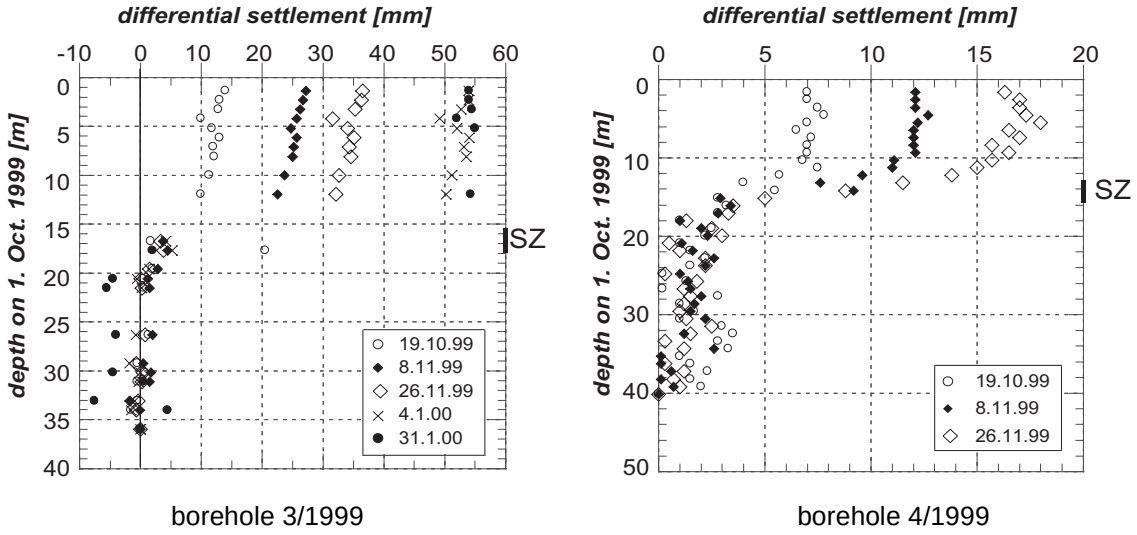

Figure 3-29: *Vertical deformations with time. Net differential settlement measured from the top of the borehole means compression, which results in a decrease of the rock glacier thickness (SZ: shear zone).*

3.3 Murtèl-Corvatsch

Originally there had been no intention to add a second test site to the project. However, the poor quality of the samples obtained from the Muragl rock glacier, and the borehole instabilities, which made *in situ* testing impossible, threatened any chance of achieving the objectives within the geotechnical part of the project. In consequence, two additional boreholes were drilled at the well known Murtèl-Corvatsch rock glacier, where two boreholes had been completed successfully in 1987, of which the second borehole was more than 60 m deep. The stratigraphy, the temperature distribution and the internal rock glacier deformation was already available from that borehole (e.g. Haeberli *et al.*, 1998). Therefore it was known that the volumetric ice content is much higher, and that a better sample quality might be achieved.

3.3.1 Site

The Murtèl-Corvatsch rock glacier is probably the best investigated rock glacier within the Alpine environment. This rock glacier has attracted researchers for many decades due to its easy accessibility and its distinct *classical rock glacier* appearance (see also Chapter 2.2). Long-term velocity measurements, using aerial photographs dating as far back as 1932, have been published by Barsch and Hell (1975). New techniques, such as digital image analysis, allowed more precise surface deformation measurements to be made (e.g. Kääb, 1998; Kääb *et al.*, 1998). Extensive geophysical investigations have also been performed on the Murtèl-Corvatsch rock glacier. Barsch (1973), Fisch *et al.* (1977), Vonder Mühll (1993), Lehmann and Green (2000) and Hauck (2001), among others, have carried out seismic, geoelectric and/or georadar measurements.

A significant milestone in Alpine permafrost research was reached by the successful drilling of the deep borehole at Murtèl-Corvatsch in 1987 (Haeberli *et al.*, 1990b). Several publications emerged from that borehole, discussing many aspects of rock glaciers, such as dynamics (Wagner, 1992; Kääb *et al.*, 1998), morphology (Haeberli *et al.*, 1998), internal structure (Vonder Mühll and Holub, 1992), temperatures (Vonder Mühll *et al.*, 1998), taliks and hydrology (Vonder Mühll, 1992), climate change, just to name the most important.

Based on that knowledge, two additional deep boreholes were drilled through the permafrost at the beginning of May 2000, 19 m and 32 m upslope from borehole 2/1987, respectively. Georadar measurements from Lehmann and Green (2000) revealed excellent data of the subsurface (Figure 3-30). From internal deformation measurements and the drilling logs it was then assumed that the first distinct reflection (black arrow) marked the shear surface and the second reflection marked the bedrock. Today, however, it must be assumed that these interpretations might need to be adjusted. Reflections revealed by data from ground penetrating radar are induced by a change in the dielectric properties of the ground, in particular from a dry to a wet state. Therefore, it must be asked whether these reflections actually indicate zones of preferential groundwater flow through the permafrost. The new campaign showed that water entered the borehole during the drilling in the middle of the permafrost, leading to the conclusion, that water flows through voids within the permafrost. Naturally this will be most prevalent in zones with a high voids ratio, which also appears to correlate with the previous designated shear zone determined from borehole 2/1987.

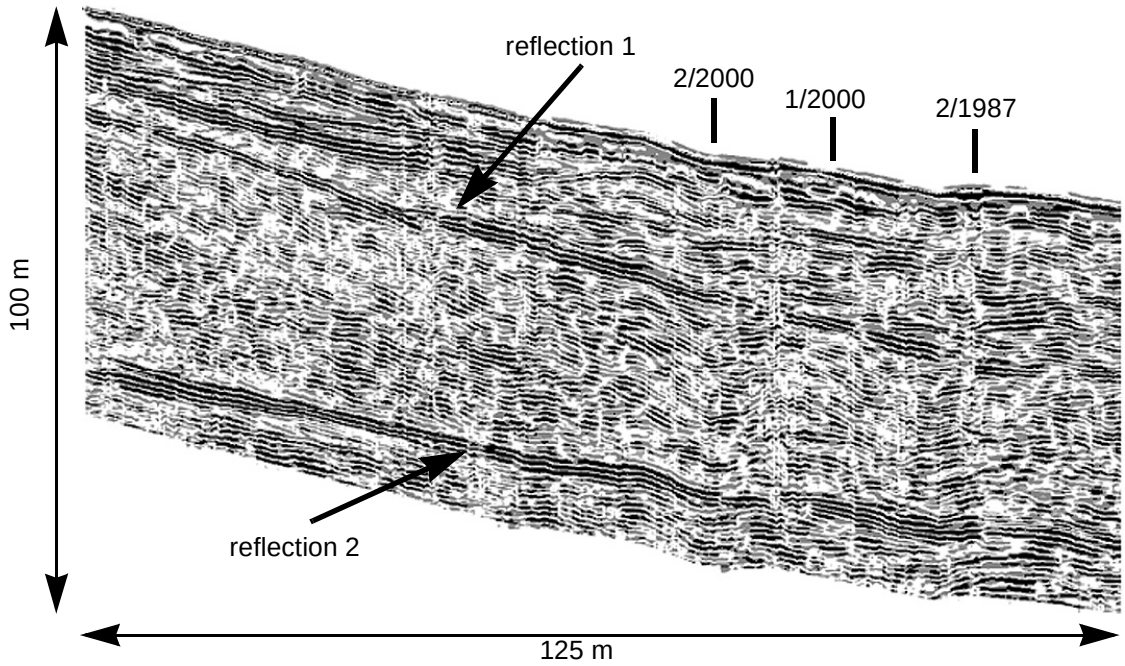

Figure 3-30: *Georadar measurements from the Murtèl-Corvatsch rock glacier (after Lehmann and Green, 2000).*

Average annual surface velocities and average annual changes in the surface elevation were calculated from aerial photographs for the period between 1987 and 1996 by Kääb (1998) (Figure 3-31).

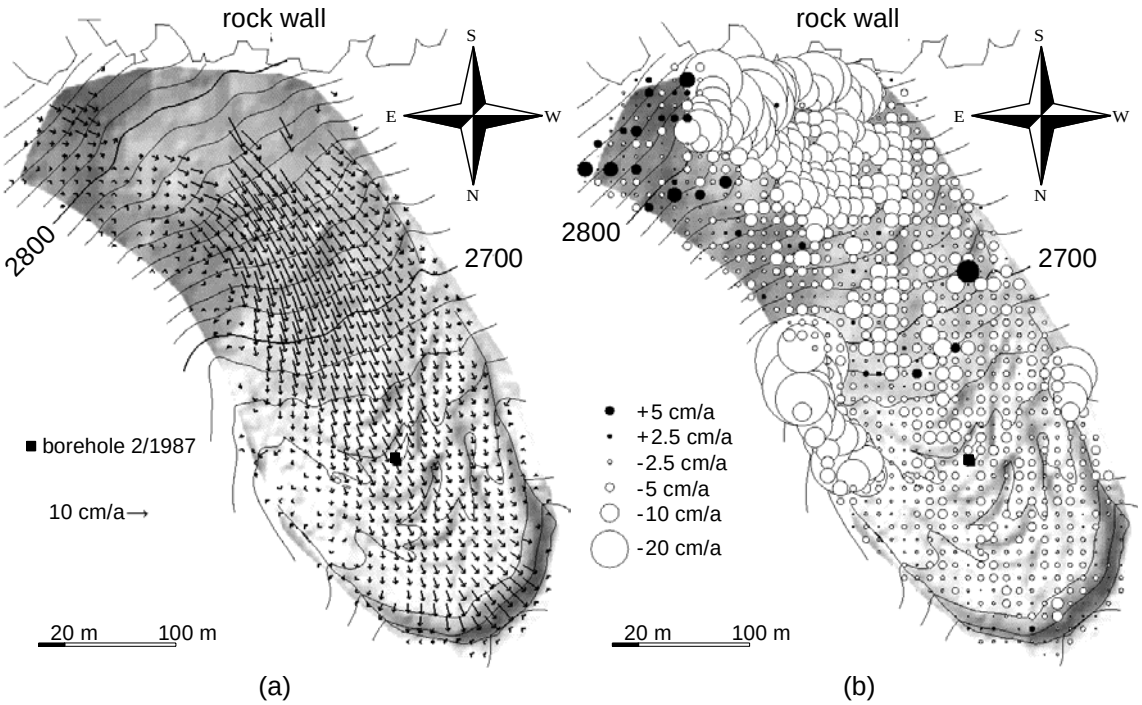

Figure 3-31: *a) Average annual surface velocity 1987 – 1996 (Kääb, 1998).*
b) Average annual changes in elevation 1987 – 1996 (Kääb, 1998).

It can be seen from Figure 3-31 that the annual surface velocity was less than about 7 cm/a at borehole 2/1987 and was expected to be only slightly greater at the location of the planned boreholes. There is also a general trend of settlements of the whole rock glacier, i.e. the rock glacier gets thinner with time. The annual change in elevation within the area of the boreholes is in-between 2 and 7 cm per year. The locations of all boreholes are shown in Figure 3-32. The main objective during the second drilling campaign was the recovery of undisturbed rock glacier samples. Furthermore, pressuremeter tests were planned in borehole 1/2000 for an *in situ* determination of creep parameters and therefore, the boreholes had to be drilled without a casing. Some additional geophysical investigations were also planned, that required a borehole without casing. Deformation measurements with time domain reflectometry should reveal more detailed information about the deformation behaviour. The coaxial cables, that are necessary for such a measurement, were planned to be grouted into both boreholes and an additional thermistor string was to be grouted into the borehole 2/2000 to measure soil temperatures.

Figure 3-32: *Aerial photograph of the Murtèl-Corvatsch rock glacier taken by Federal Office of Cadastral Surveys in September 1996.*

3.3.2 Boreholes

Less difficulties occurred during the drilling process since the ice content was much higher than within the Muragl rock glacier. Higher penetration rates were achieved and a casing was only necessary in the top metres within the active layer. High pressure dilatometer tests were conducted at different depths (see also Chapter 3.3.7) in borehole 1/2000. The drill rig was in action during the day and pressuremeter creep tests were performed during the night. The progression of the borehole was monitored visually by lowering a borehole camera, with illumination for inspection purposes. The percentage of solid particles and air voids increased with increasing depth, resulting in instabilities of the borehole wall. At depths larger than 40 m, the boreholes collapsed several times due to large blocks and free water, which was encountered within the ice. Large air voids were found at a depth of 50.0 m in borehole 1/2000 and 57.6 m in borehole 2/2000, respectively, which led to a complete loss of the flushing air. Despite the air voids, boulders with diameters of more than a metre were also encountered. Even at a depth of 63.2 m within borehole 2/2000, the bedrock was not reached.

Further drilling without a casing, similar to the Muragl rock glacier, was not possible due to the high possibility of losing the drill bit. Even with the steel casing (ODEX system) that was used for borehole 2/2000, further drilling below 63.2 m was not successful. Hence, there is no proof of the depth of the bedrock from these two additional boreholes, which led to the conclusion that a large boulder was at the bottom of the borehole 2/1987, which was taken erroneously to be the bedrock.

The penetration velocity depended strongly on the material. Progress of up to 1 m/h was achieved with full core recovery within the ice-rich layers. The percussion drilling was nearly twice as fast within the stable sections with higher percentage of soil particles. However, this reduced to a few metres per day in the lowest and most unstable part of the boreholes where there was a much higher percentage of air voids and larger particles.

Almost full recovery was achieved when the nominally undisturbed cores were being drilled using the triple tube system (as for Muragl, Section 3.2.2) (Table 3-5). However, due to the mechanical stress of the drilling processes and the release of stress following extraction, some parts of the sample were occasionally heavily disturbed with obvious cracking. In addition, some of the ice seems to be of a granular nature (Figure 3-33) and is therefore not very ideal for triaxial testing because some of the samples broke apart before they could be placed into the testing device. In the end, about 30% of the lengths of cored samples were of good enough quality to be able to perform triaxial creep tests, such as the sample shown in Figure 3-34.

	1/2000	**2/2000**
depth [m]	51.9	63.2
start coring at depth [m]	10.3	6.7
end coring at depth [m]	27.65	22.35
total length cored [m]	17.35	15.65
nominally undisturbed cores [m/% recovery]	16.85 / 97	15.05 / 96
disturbed cores [m/% recovery]	0.5 / 3	0.6 / 4
water encountered at depths of [m]	3.4 27.0	4.0 45.0
ice in cores or chips down to [m]	50.0	57.0

Table 3-5: *Borehole characteristics: Murtèl-Corvatsch rock glacier.*

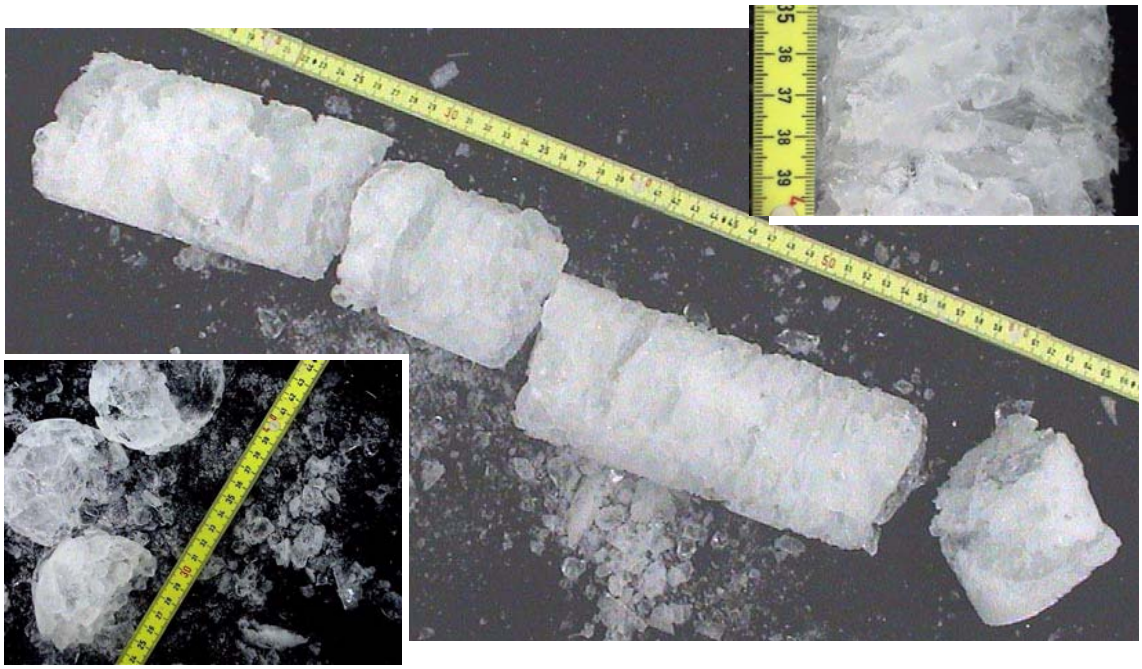

Figure 3-33: *Granular ice at 12.33-12.90 m from borehole 2/2000, Murtèl-Corvatsch rock glacier (Photos: L. Arenson).*

Figure 3-34: *Core from borehole 1/2000: 21.00 - 21.30 m (Photo: L. Arenson).*

Four main layers can be distinguished from inspection of the cores and the borehole records (Figure 3-35):

- **Top layer with large boulders:** The top metres are covered with boulders that can have diameters of several metres. All fine particles have been washed away by melt– and rain water. The thickness of this layer is more or less equal to the thickness of the active layer. However, boulders were found within the first metres below the permafrost table indicating that the active layer might once have been thicker. Finer particles can also be found frozen into the top of the permafrost table, where they have been transported by the water run-off.

- **Ice-rich layer:** An ice-rich layer was found underneath the boulders with a thickness of about 20 m. This layer consists of pure ice with some solid inclusions. The inclusions are mainly of silt or sand sized grains, even though a block of several centimetres was found in borehole 1/2000 at a depth of 9.8 m.
- **Frozen gravel:** Even though the ice content decreases steadily with depth, a distinct line can be drawn underneath which larger particles were found. The pores between the disperse distributed cobbles are filled with gravel, sand and silt, and the volumetric ice content decreased from nearly 100% down to 50–70% (see also Figure 4-16). The line between the two layers corresponds very well with the measured shear zone (see Chapter 3.3.5).
- **Unfrozen, blocky layer:** A zone containing large boulders with diameters up to several metres and large air voids was found underneath the ice-containing layer. Based on the geomorphological evolution (Haeberli *et al.*, 1998), it is assumed that these boulders have accumulated just above the bedrock, even though it was not reached by the boreholes. It is thought that they were transported on top of the rock glacier to the front face, where they have fallen down the steep slope and then have been rolled over by the creeping rock glacier. This layer is a free-draining layer, very highly permeable to both water and air, which can circulate beneath the permafrost and induce thermal anomalies. This layer can also be seen as a talik (Vonder Mühll, 1992).

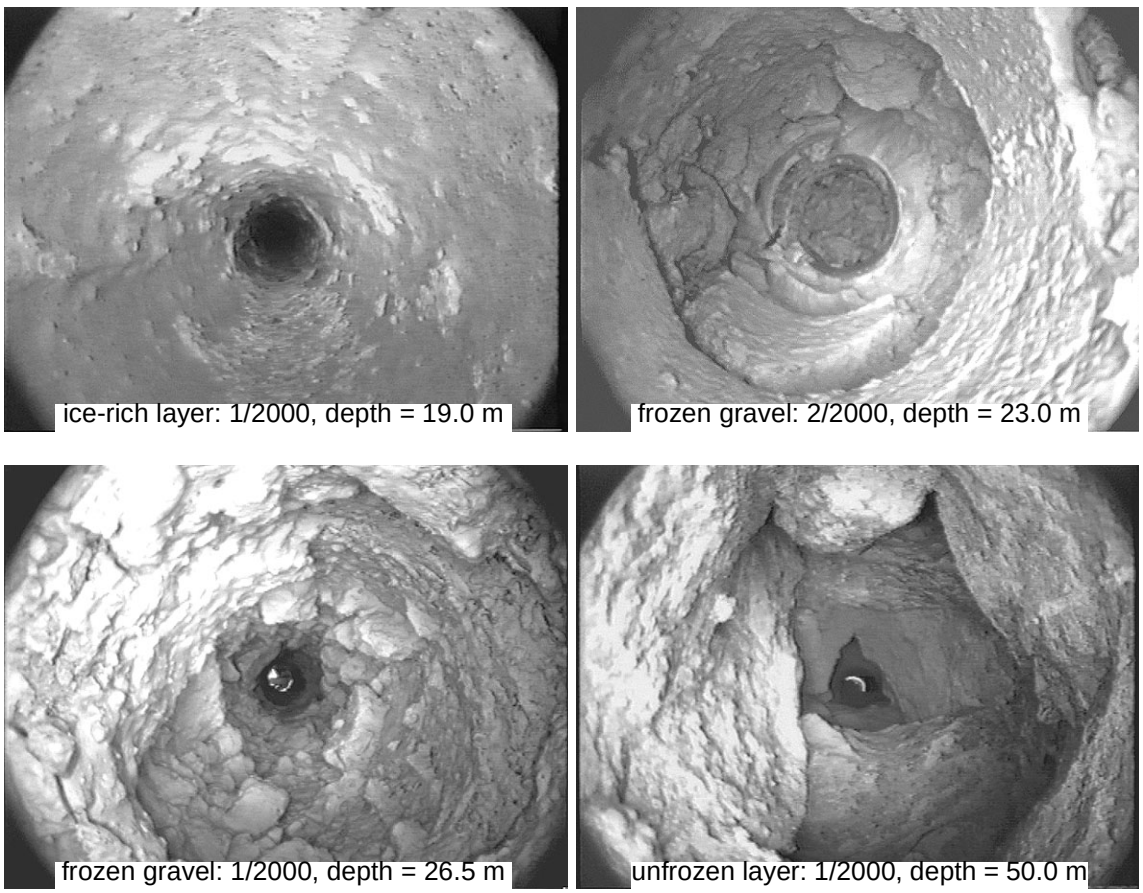

Figure 3-35: *Pictures from a borehole camera at different depths.*

A model of the subsurface can be compiled based on the three boreholes (Figure 3-36).

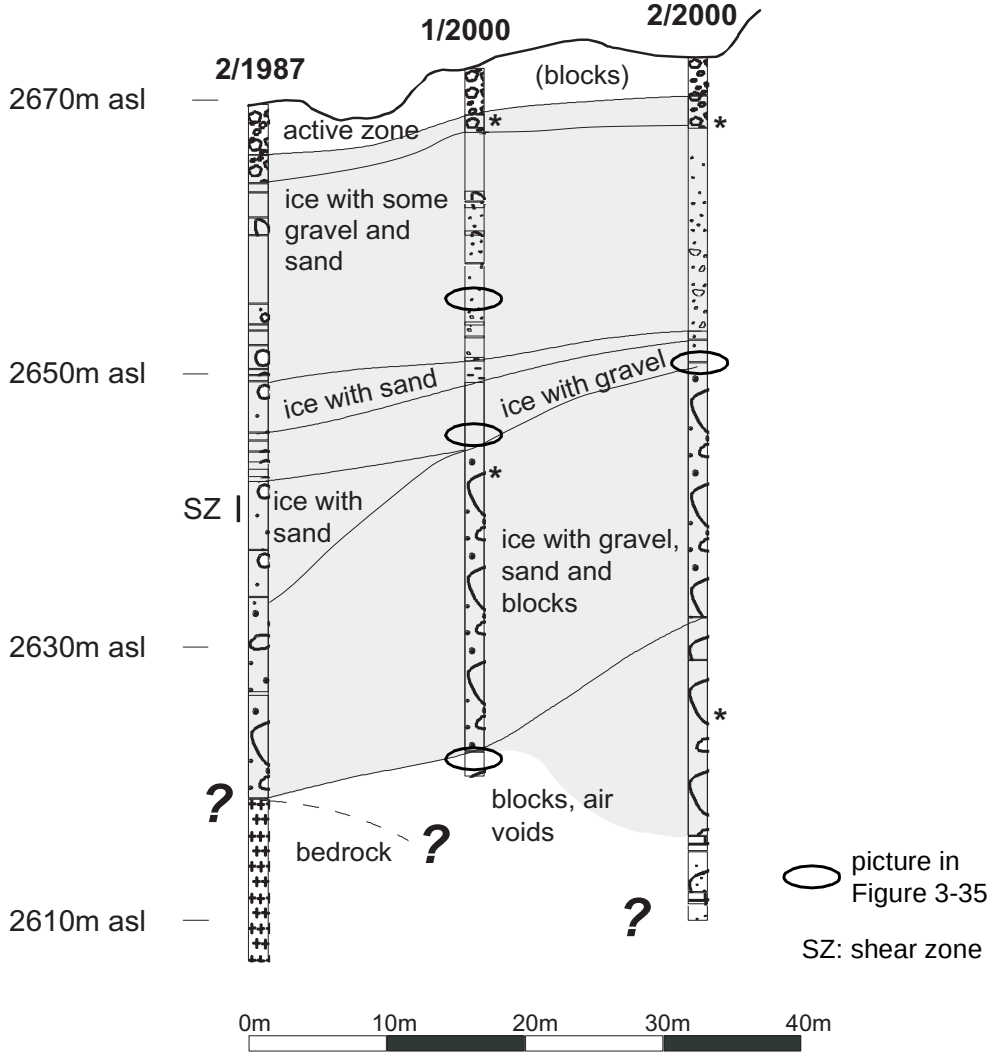

Figure 3-36: *Internal structure of a section through the Murtèl-Corvatsch rock glacier. Water leakage into the borehole (*) was observed during drilling.*

3.3.3 Monitoring Measurements in Boreholes

It was planned that borehole 1/2000 should be drilled without a steel casing and that it should only be protected for the top five metres with a PVC tube. After installing the coaxial cable for the time domain reflectometry (see Section 3.3.6), the borehole should be filled with water so that the cable would then be frozen perfectly into the ground. However, the borehole collapsed at a depth of about 18 m and an attempt to re-open it using a steam drilling rig failed. As a consequence, deformations could only be recorded for the upper 18 m.

Additional measurements with borehole-to-surface seismics were planned in borehole 2/2000 and therefore, a 3'' PVC casing was necessary over the entire depth. It was placed together with a 1'' hose outside the PVC casing prior to removing the steel casing. Following the measurements in the PVC tube, a second coaxial cable and a chain of thermistors were installed down to a depth of

61.4 m. The voids at the bottom of borehole 2/2000 made the grouting of the tube very difficult. The level of the grout (cement/Opalite = 4:1) dropped several times to a depth of 37 m during the first day. However, it was possible to fill the rest of the borehole with a slightly coarser mixture containing a maximum grain size of 8 mm on the second day.

3.3.4 Temperatures

The temperature data from borehole 2/1987 (Figure 3-37) are unique for the Alpine region, and are therefore very important for analysing long-term trends in thermal interaction between the perennially frozen ground, the snow cover and the air temperature (e.g. Vonder Mühll *et al.*, 1998; Vonder Mühll *et al.*, 2001b).

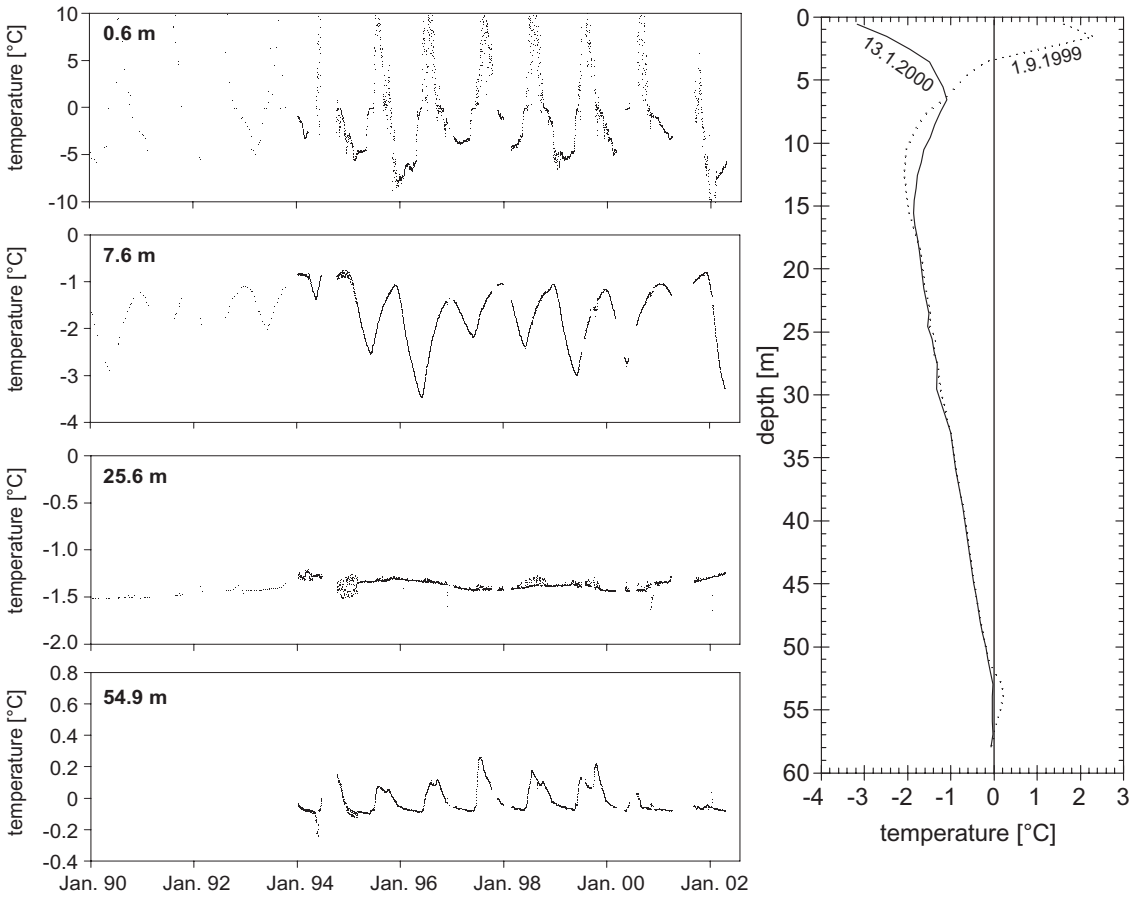

Figure 3-37: *Temperatures of the Murtèl-Corvatsch rock glacier borehole 2/1987 for various depths with time and two points of time (after Vonder Mühll, 2002).*

A new thermistor string of the same type as the one used for the Muragl rock glacier, was put into the PVC tube of borehole 2/2000. Compared with the records shown in Figure 3-37 for borehole 2/1987, the new temperature data show rather unexpected behaviour (Figure 3-38a) that is explained in detail in Vonder Mühll *et al.* (submitted). However, in focusing on the depth between 10 and 20 m, it is suggested that the effect of the infiltration of water at 0°C on the temperature can be observed between March and May (Figure 3-38b), which is then able to drain away again, resulting in a sharp increase of those temperatures up to zero centigrade, followed by an approximately exponential decay. Given that temperatures

do not seem to change much with time below 20 m (Figure 3-38a), it is possible that there is a hole in the casing and that the tube was filled with melt– or runoff water, resulting in temperatures of zero centigrade between 20 and 25 m. When the supply of water did not exceed the rate of flow out of the borehole, the level of the water in the borehole dropped, which is confirmed by the decrease in temperature occurring first at shallower depths (7.5 m followed by 10 m, then by 15 m and by 20 m depth). The negative temperatures at a shallower depth indicate that the water cannot have flowed from the top. Only when the water froze (by November 2001), did the ground temperatures dip below zero centigrade once more, but increased again in summer 2002. Ongoing monitoring of the temperatures is necessary in order to find a clear answer for this temperature behaviour within borehole 2/2000.

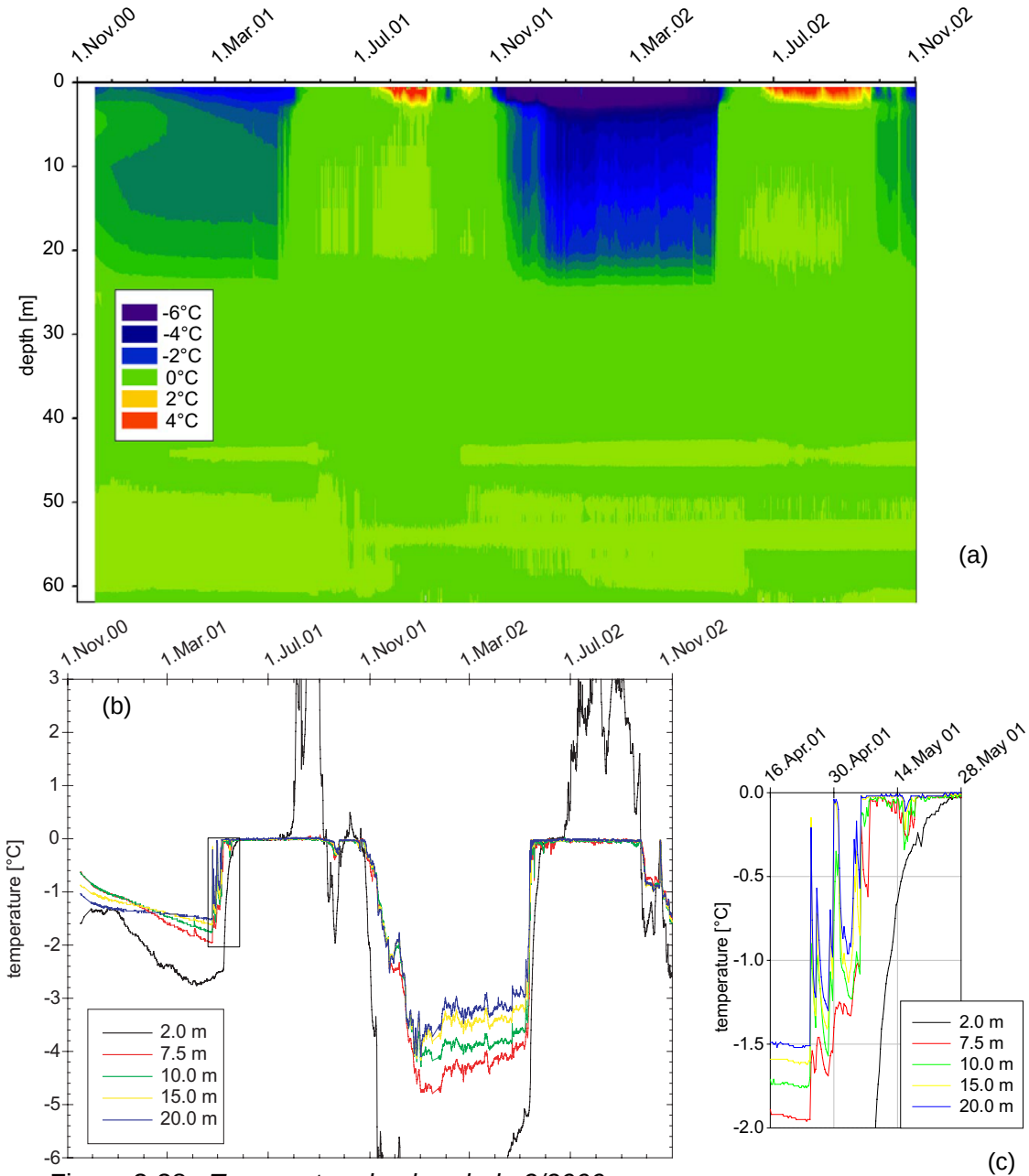

Figure 3-38: *Temperature log borehole 2/2000.*
a) time-temperature-depth plot.
b) time-temperature plot for various depths.
c) blow up of b) from 16. April to 28. May 2001.

3.3.5 Borehole Deformation of Borehole 2/1987

Vertical and horizontal deformation measurement systems were installed in 1987 in the second borehole (Wagner, 1992; 1996b; Haeberli *et al.*, 1998; Arenson *et al.*, 2002). These data revealed highly significant information concerning the internal flow regime of the Murtèl-Corvatsch rock glacier. They have been added and are also briefly described during the next sections. Therefore, absolute deformation data were already available from the slope inclinometer and magnetic extensometer measurements and it was decided to install a new deformation measurement system that is used intensively in the mining industry for ongoing monitoring of joint deformations: time domain reflectometry, TDR (O'Connor and Dowding, 1999).

Horizontal deformation

Horizontal deformations have been measured over a period of eight years from 1987 – 1995 (Figure 3-39). The shear deformations at a depth of about 30 m were so large in 1995 that the radius of the tube did not allow further lowering of the inclinometer probe and it is quite likely that the casing was severely damaged. The discontinuity of the vertical measurements in the shear zone with time for the years 1995 and 1996 confirms this (Figure 3-40). In addition, the horizontal deformation measurements show that the layers within the rock glacier have different creep susceptibilities. Extrusion beneath the active layer (~3.4 m depth) and faster shearing rates at depths of about 18 m, 22 m and 28 m were observed, which might be induced by different equivalent shear stiffnesses of adjacent layers, which is probably caused by the percentage of solid particles.

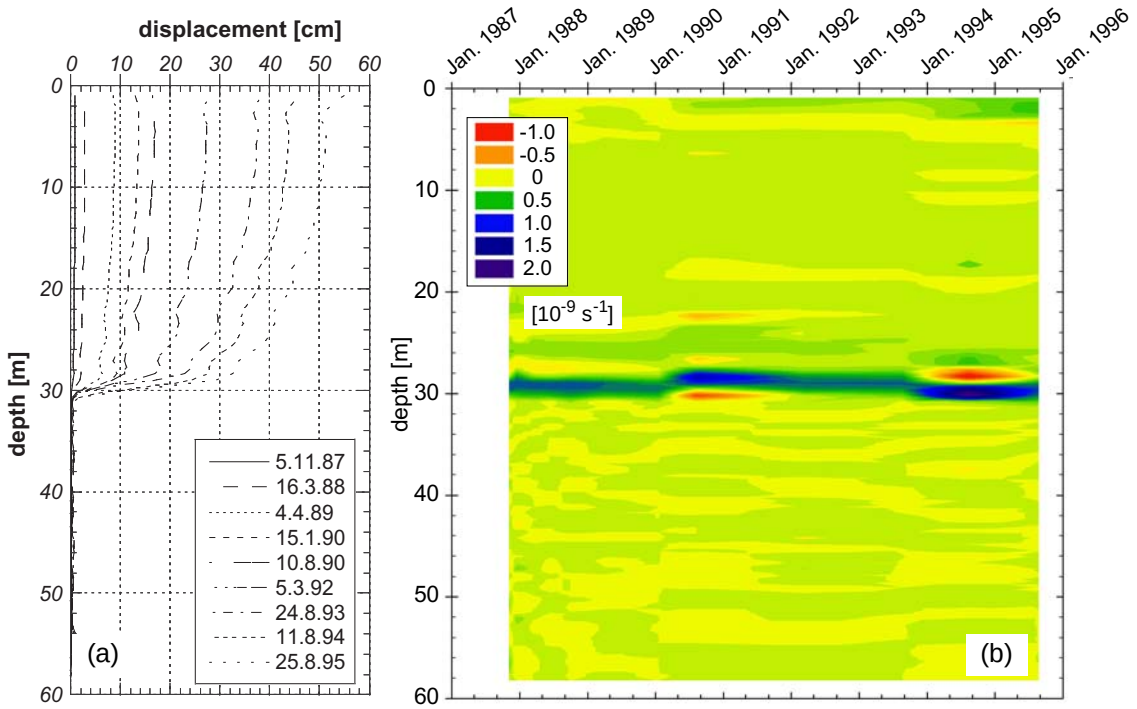

Figure 3-39: *Horizontal movements, borehole 2/1987 Murtèl-Corvatsch rock glacier (some data after Wagner, 1996b).*
a) Horizontal displacement.
b) Horizontal strain rates [10^{-9} s^{-1}] (Definitions: Equation 3-1 and Figure 3-25).

Vertical deformation

Magnetic rings were fixed with an adhesive tape outside the inclinometer casing, and were separated by intervals of between 3 and 5 metres. They were used for the measurement of vertical deformation within the rock glacier. The position of the magnets can be detected easily using a magnetic sounding lead. The magnet rings can be located to within an accuracy of ±1 mm. The main problem is, however, that the inclinometer plastic casing might not follow the vertical movements of the soil mass and, therefore, the magnetic rings do not represent absolute values.

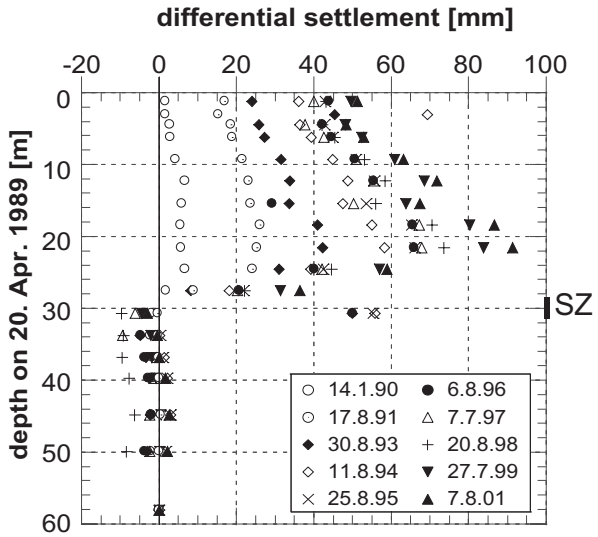

Figure 3-40: *Vertical deformations with time. Net settlement measured from the top of the borehole means compression, which results in a decrease of the rock glacier thickness (SZ: shear zone; some data from S. Wagner, 1996b).*

However, similar to the measurements at Muragl, distinct movements can be observed within the shear zone at a depth of about 30 m (Figure 3-40). Additional settlements occur at around 20 m depth, inducing a slight expansion between 10 m and 20 m. The data show that an extension of the borehole of about 4 cm occurred from 1995 to 1996, which would indicate a thickening of the rock glacier. Since a rise in the thickness would be completely against the ongoing trend of the settlement measurements, this effect must have been induced by the shearing of the casing at the depth of the shear zone.

3.3.6 Time Domain Reflectometry (TDR)

Time domain reflectometry (TDR) might prove to be a useful tool for deformation measurement in rock glaciers in the future, since the relatively flexible cable is grouted (or frozen) directly into the ground (O'Connor and Dowding, 1999). The system has been successfully used in jointed rock masses and recently also for soft soils (Dowding *et al.*, 2001) and to monitor landslides (Kane *et al.*, 2001). In order to judge whether a measuring device follows the soil deformation profile accurately, a flexibility ratio *K* can be defined, similar to that used for determining the pile – soil stiffness (Randolph, 1983):

$$K = \frac{\pi d l^2 \tau_s}{(EA)_p \Delta w_{res}} \qquad [3\text{-}3]$$

d pile diameter

l embedded length of pile

$(EA)_p$ cross-sectional rigidity of the pile:
E = Young's modulus
A = cross sectional area of the hollow tube

τ_s peak skin friction

Δw_{res} relative movement needed between pile and soil for the value of skin friction to reduce from peak to residual in a strain-softening soil.

The flexibility ratio of a TDR cable is about ten or more times larger than that of a standard inclinometer tube. In this case the cable should follow the soil deformation more closely (Figure 3-41), and the resolution in terms of the depth of the shear zone should be improved. In addition, continuous monitoring is possible without having to make manual measurements. Such a system was installed in the new boreholes at the Murtèl-Corvatsch rock glacier. In the future it should then be possible to identify i) fine shear bands, ii) change in depth of the shear zones and eventually iii) seasonal changes. The latter will only be measurable if the velocity increases, and the shear zone is above the zero annual amplitude, so that seasonal temperature changes can affect the creep.

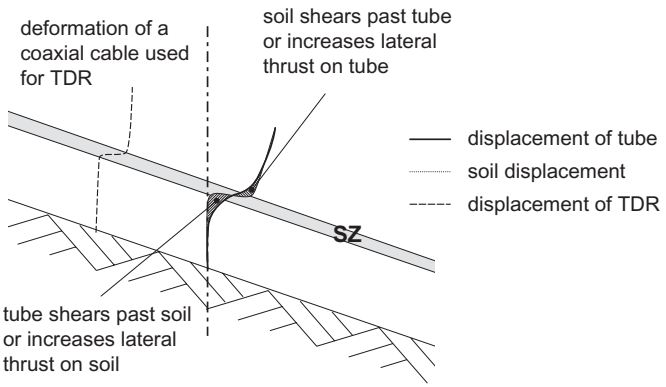

Figure 3-41: *Sketch of a deformed stiff tube in a shear zone (SZ).*

Material and method

A cable tester sends a voltage pulse waveform down a coaxial cable, which has been grouted into a borehole (Figure 3-42). Any fault or crimp in the cable results in a change of the characteristic impedance. The pulse is transmitted along the cable every 200 μs and when it encounters such a change, the pulse reflects and returns to the cable tester (Figure 3-43). Further details of the principles and possibilities of time domain reflectometry are explained in O'Connor and Dowding (1999).

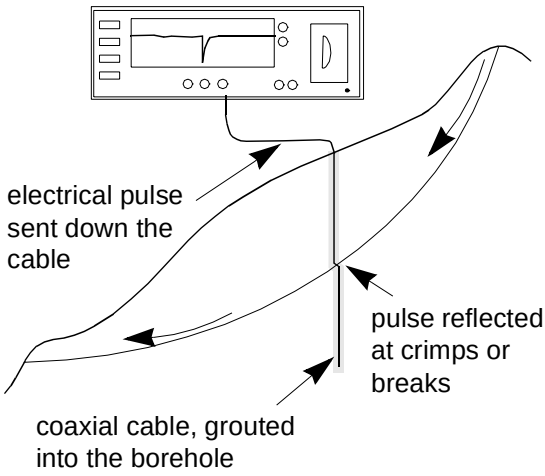

Figure 3-42: *Cable tester attached to TDR cable undergoing deformation due to slope failure (after Kane, 2000).*

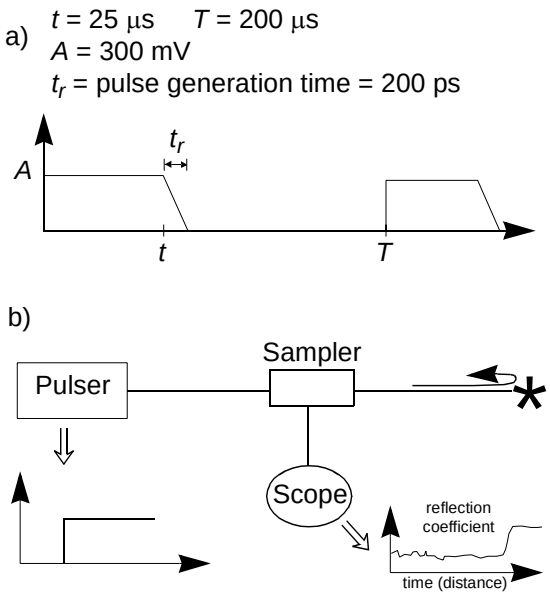

Figure 3-43: *Basic components of TDR cable tester (after Tektronix, 1992).*
a) nominal pulse waveform.
b) operating principle and system components.

Table 3-6 summarises the main specification of the TDR-deformation monitoring system used for the two new boreholes drilled in 2000. However, the programme for the data acquisition changed several times during the project and therefore the values in the table are not necessarily up to date.

	1/2000	**2/2000**
grouted cable		
Manufacturer	Cablewave	
type	FXA12-50, RG/231	
inner conductor	copper-clad aluminium, $Ø_0$=4.09 mm	
outer conductor	smooth aluminium, $Ø_0$=12.7 mm, t=1.27 mm	
dielectric	foam	
characteristic impedance	50 ohms	
propagation velocity	81%	
length [m]	56.1	62.2

Table 3-6: *TDR specification for the Murtèl-Corvatsch rock glacier.*

	1/2000	2/2000
transmission cable		
Manufacturer	Suhner Switzerland	
type	RG/213	
inner conductor	bare copper braid, $Ø_0$=2.25 mm	
outer conductor	copper wire netting, $Ø_0$=8.10 mm	
dielectric	PE	
Jacket	PVC	
characteristic impedance	50 ohms	
propagation velocity	66%	
length [m]	0	51.5
cable tester	Tektronix MTDR 1502B	
data storage	Campell CR10X	
reading cycle	10 days	10 days
start at [m]	35.0	51.5
end at [m]	62.5	112.5
average of readings	8	8
cable length per reading [m]	2.5	2.5
data points per reading	250	250
bits per reading (13bit/cm)	35.75kb	79.3kb

Table 3-6: *TDR specification for the Murtèl-Corvatsch rock glacier.*

Calibration

In order to compare the TDR wave-forms with absolute deformation of the cable, crimps at different spacings were tested on a similar cable in the laboratory (Figure 3-44). The result showed that obtaining a relationship between the amplitude of the wave-form and the deformation is nearly impossible. The signal flattens off with increasing distance from the origin and two crimps, which had been visible as two peaks for a short distance (x = 6 m, Figure 3-45a) merge into one weaker signal (x = 71.5 m, Figure 3-45b). However, the calibration might help in the interpretation of the curves.

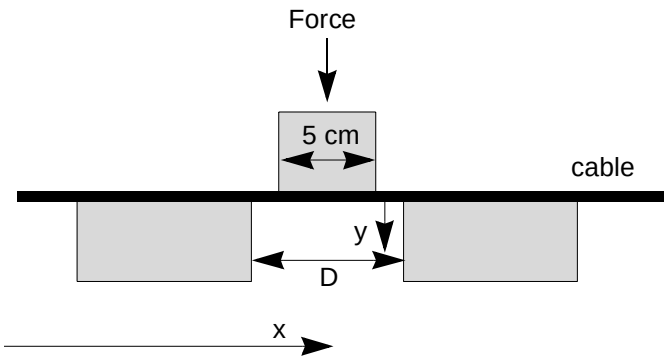

Figure 3-44: *Calibration set-up.*

cursor: 6.605 m
distance/division: 0.025 m/div
vertical scale: 1.45 mρ/div
v_p: 0.81
noise filter: 16 avg

A_{max} = 7.21 mρ
B = 0.16 m

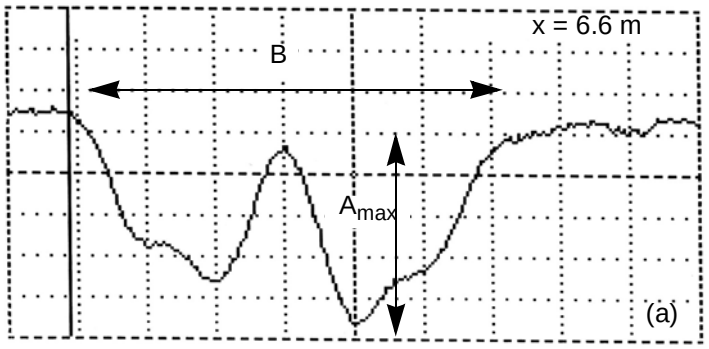

cursor: 71.468 m
distance/division: 0.05 m/div
vertical scale: 1.93 mρ/div
v_p: 0.81
noise filter: 16 avg

A_{max} = 10.63 mρ
B ≅ 0.165 m

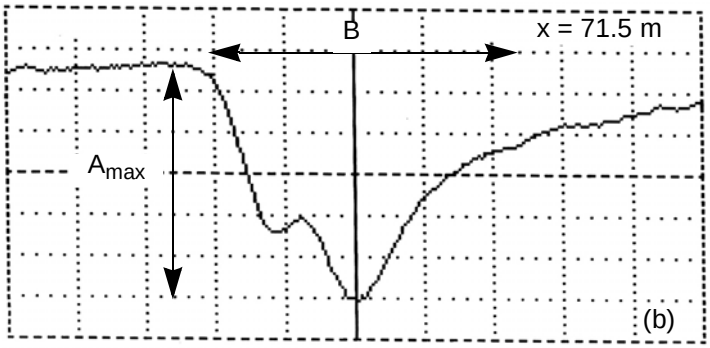

Figure 3-45: *Wave-form of a similar crimp at two different distances. D = 8 cm, y ≅ 14 mm.*

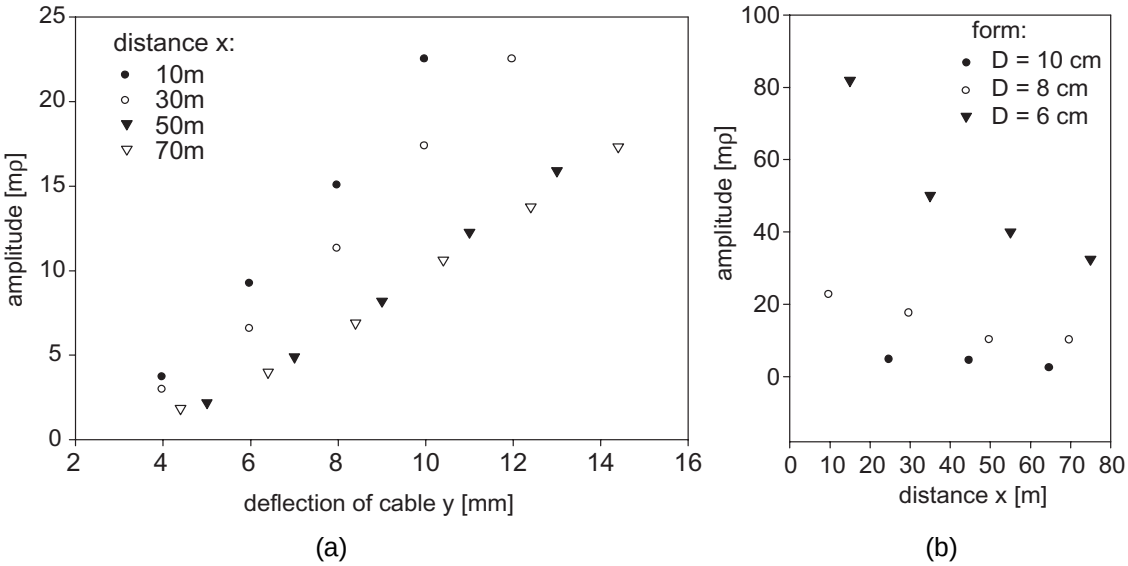

Figure 3-46: *Calibration of TDR cable: D = 8 cm.*
a) Amplitude of wave versus cable deformation.
b) Amplitude of wave versus distance from cable origin.

The result of the calibration clearly showed that the amplitude of the wave increases with the size of the crimp, although the relationship is slightly curved (Figure 3-46a). However, the signal depends exponentially on the distance between the origin of the cable and the crimp when this is severe enough (Figure 3-46b). The form of the deflection in the cable also has a major influence on the

amplitude. With reducing distance *D* between the two base blocks (Figure 3-44), the form of the cable became more distinctly bent, which increases the amplitude of the reflection wave. A larger distance led to a smoother bending profile and therefore a smaller amplitude of the wave.

The conclusions reached from the cable calibration are that determination of the magnitude of the movement cannot be easily made, even though the spike of the TDR wave reveals information about the depth of the shearing, and of the temporal occurrence. The amount of the movement cannot be determined, even with a calibration (e.g. Francke *et al.*, 1994). In addition, the TDR is not able to provide information about the direction of the movement. Nevertheless, it is a cheaper and more efficient means of determining depth of the shear zone and could be used at other sites in conjunction with slope inclinometers.

First Results

The TDR cable in borehole 2/2000 was grouted in July 2000 down to a depth of 61.2 m. The installation of the second cable was done in September 2000, after the borehole had collapsed at 18 m. The monitoring, however, started in December 2000. Further adaptation to the programme had to be made, and therefore some data were lost. The temperature records indicated that the cables have not been perfectly frozen in place and therefore, these data have to be treated with caution.

However, some major differences in the deformation behaviour between the two locations can be recognised, even after this relatively short observation period. There has been virtually no movement within the upper 18 m of borehole 1/2000. The main peak that can be seen in Figure 3-48, originates from a crimp (Figure 3-47) at 5.5 m depth that had been created prior to insertion in the borehole for a better orientation of the depth. More scattering of the data (Figure 3-48a) occurred in March 2001 than in November 2001. This was because fewer readings have been averaged during the initial monitoring period.

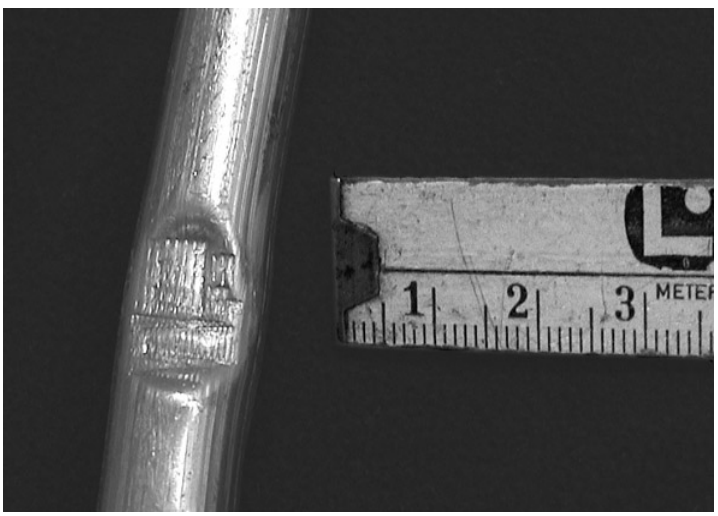

Figure 3-47: *TDR-cable with orientation crimp.*

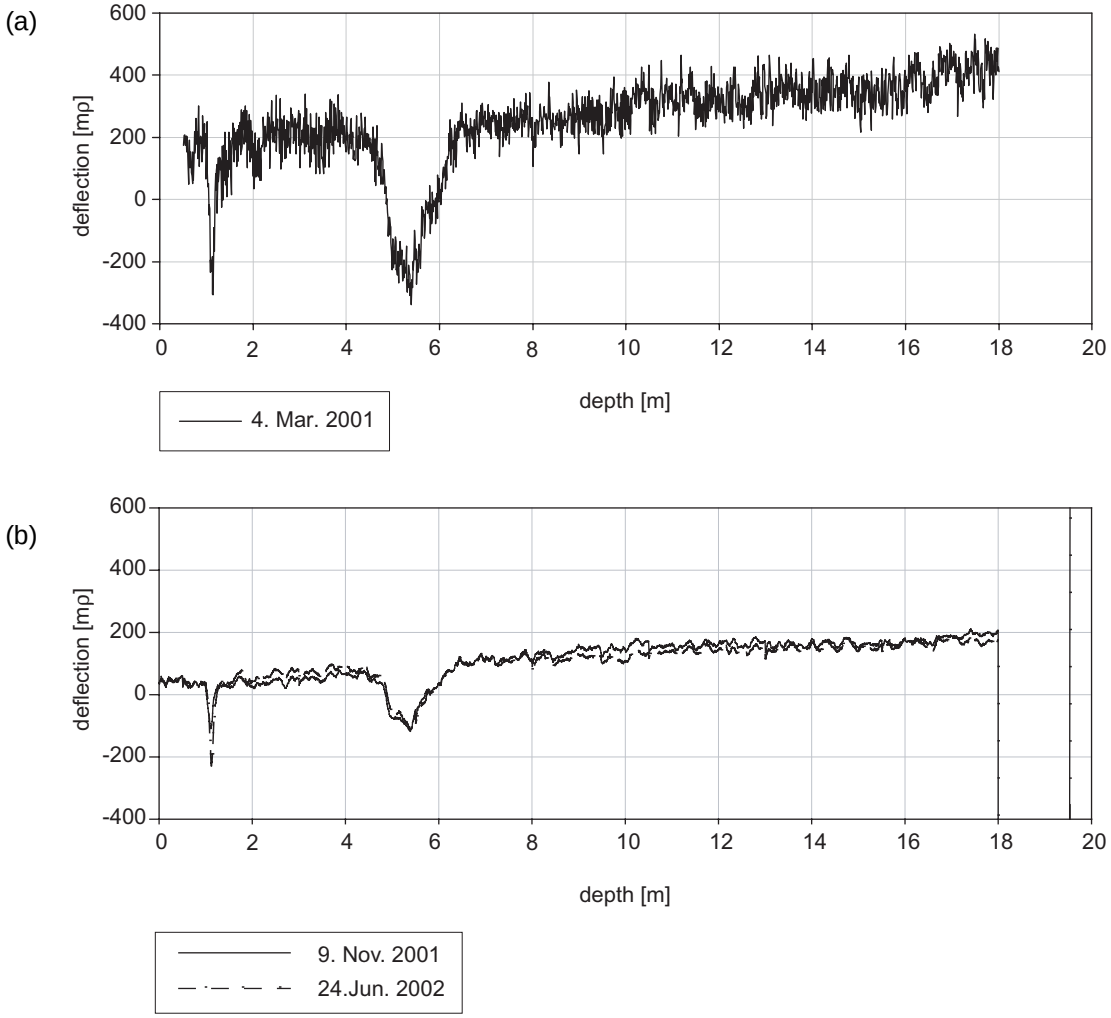

Figure 3-48: *TDR amplitude curve for borehole 1/2000.*
a) 4. March 2001
b) 9. November 2001 & 24. June 2002

Borehole 2/2000 shows a slightly different behaviour. The original curve shows many more peaks and irregularities than the first cable. These features originate from different crimps that had been applied prior to insertion for subsequent in-hole orientation and are also due to some bending during installation. However, in comparing the curve from March 2001 with the curve from December 2001, it can be observed that the cable sheared completely at a depth of 17.7 m. The shearing event happened within the ten day reading interval between 19. August and 29. August 2001. No further indication of any acceleration of creep velocity was noted before that date despite a small peak that started to develop at a depth of 19.9 m. It was found during the calibration that severe deflections were necessary in order to shear the cable. It is now assumed that a lateral deformation of at least 2.5 cm happened at this depth within these 10 days.

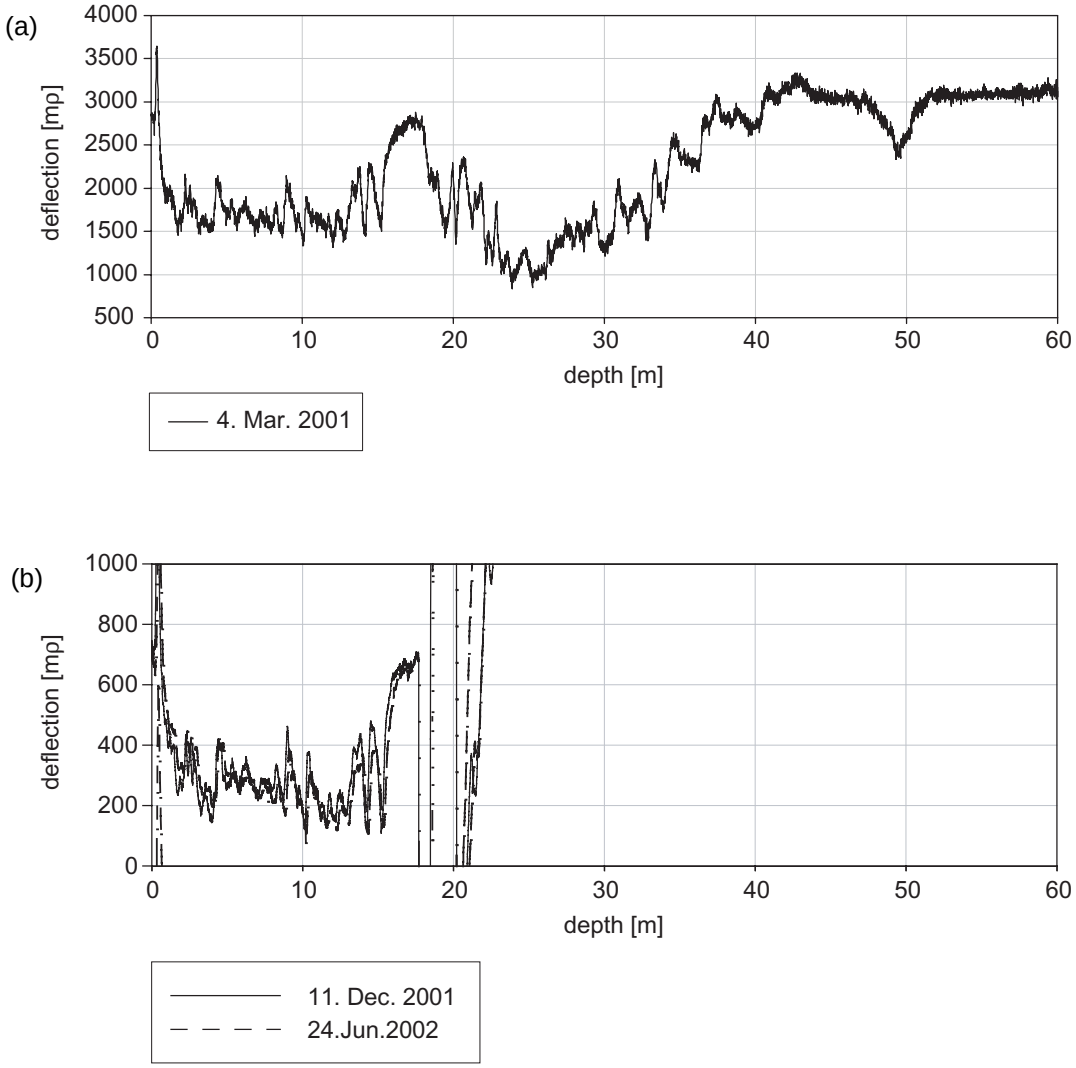

Figure 3-49: *TDR amplitude curve for borehole 2/2000.*
a) 4. March 2001
b) 11. December 2001 & 24. June 2002

3.3.7 High Pressure Dilatometer (HPD)

Introduction

In situ tests were conducted in addition to the samples tested in the laboratory, to determine *in situ* soil parameters. The accurate determination of mechanical parameters *in situ*, however, is complicated by disturbance and size effects. Either a testing device has to be brought into the ground without causing excessive thermo-mechanical disturbance, which might change the properties measured significantly, or samples have to be cored and tested afterwards in a laboratory.

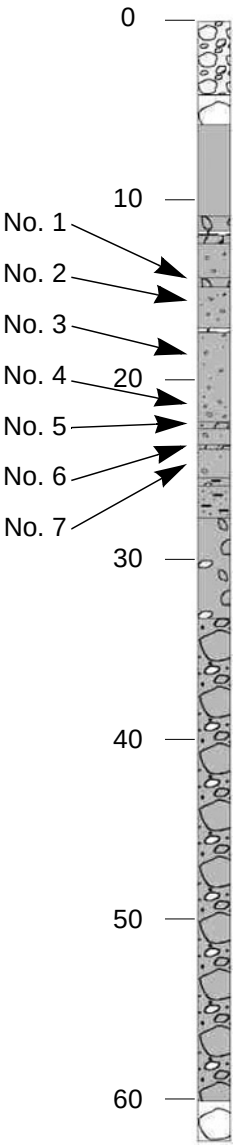

Figure 3-50: *Location of Pressuremeter tests in borehole 1/2000.*

In any case, a very useful device for measuring the creep parameters of frozen materials *in situ* is the pressuremeter (e.g. Ladanyi and Johnston, 1973; Ladanyi, 1980; Kjartanson *et al.*, 1988; Murat *et al.*, 1989; Ladanyi and Melouki, 1993). Due to the large grain size and the high strength of the rock glacier material, a self-boring pressuremeter (e.g Yu and Collins, 1998), could not be used. Pre-boring is necessary in frozen material, so relaxation and hence both thermal and mechanical disturbance of the wall will occur, which must be taken into account while analysing the results. In addition, potential size effects have to be considered. Briaud (1992) recommends a maximum grain size of 63.5 mm for proper pressuremeter testing, which could not be guaranteed within the Murtèl-Corvatsch rock glacier. This may result in an uneven expansion of the pressuremeter probe and in slightly higher creep strain rates since softer sections will be more compressed.

Pre-bored pressuremeter tests were performed over a depth between 14.7 m and 24.5 m in borehole 1/2000 (Figure 3-50) with the Cambridge Insitu HPD 95 pressuremeter (Figure 3-51). The instrument is 95 mm in diameter and has a length of about 2 m. The central third of the probe is covered by a tough nitril rubber membrane with a thickness of about 6 mm. Pressure is applied to the inside of the instrument and the membrane expands, pressing against the borehole wall. The radial displacement of the inside boundary of the membrane is measured at six points equally distributed around the centre of the expanding section. The entire length of the membrane is covered with a sheath of eighteen stainless steel strips, which are stiff in an axial direction but free to expand radially. This sheet protects the membrane from sharp edges and is known as the ‘Chinese Lantern’. The individual strips do not overlap in the closed position.

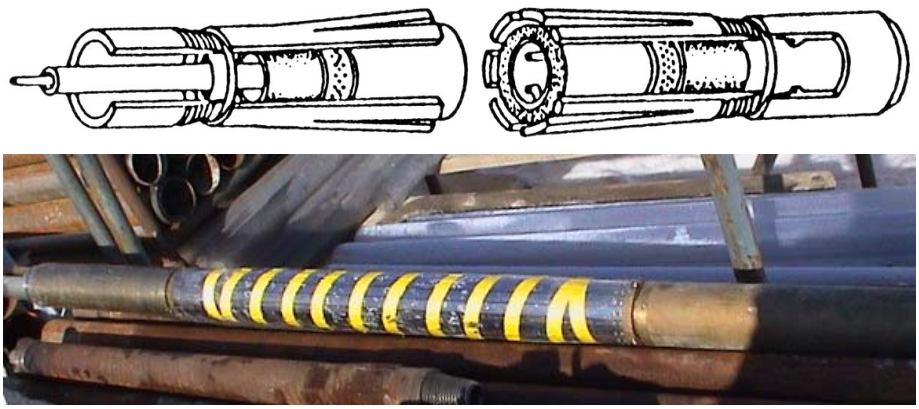

Figure 3-51: *High pressure pressuremeter (HPD) (Briaud, 1992; Photo: L.Arenson).*

Since the time dependent behaviour of the frozen material was of interest, creep tests were conducted in ice-rich material at several depths in a relatively smooth section of the borehole (Figure 3-35), at varying cavity pressures. The assumed compositions of the ice-soil material were derived from core analyses at the locations of the tests, and are given in Figure 3-50 and Table 3-7, respectively, together with the type and duration of the test.

The thermal and the mechanical disturbances of the drilling had to be considered during the analyses of the test results. Since a direct evaluation of the effect of these errors on the determination of creep strain rates is not possible, they have to be minimised with a suitable test methodology, including that

- the tests were carried out shortly after the corresponding depth had been reached, and
- the probe must be pre-cooled and permitted to equilibrate to the local temperature prior to conducting the expansion.

test No.	depth [m]	test description	test duration [min]	soil description (ice content in vol.-%)
1	**14.7**	shear test	65	ice with some sand and silt (~90%)
2	**16.0**	3 creep stages 2 unload-reload loops	210	ice with some sand and silt (~90%) many air voids
3	**18.5**	5 creep stages 3 unload-reload loops	1650	ice with gravel, sand and air voids (~80%)
4	**21.2**	4 creep stages 3 unload-reload loops	810	ice with silt and sand (~80%)
5	**22.5**	4 creep stages 3 unload-reload loops	1360	ice with gravel and sand (some larger stones ?) (~77%)
6	**23.4**	shear test	25	ice with stones, gravel and sand (~80%)
7	**24.5**	5 creep stages 4 unload-reload loops 2 relaxations	1450	ice with stones, gravel and sand (~86%)

Table 3-7: *Overview of pressuremeter tests in borehole 1/2000.*

The calibration of the pressuremeter is very important (Kjartanson *et al.*, 1990). The six arms, the load cells and the temperature sensor were tested in the laboratory before and after the campaign. The influence of the membrane was tested in the laboratory, but in addition at the cold temperatures on site. Since creep tests were planned, an additional creep calibration was performed in a steel cylinder before the *in situ* testing.

Pressuremeter Theory

The pressuremeter test can be considered theoretically to be represented by the expansion of an infinitely long cylinder in an infinite mass of soil. The effect of the first assumption is only minor, even though the probe has a finite length (e.g. Briaud, 1992). The principal stresses are the radial stress σ_{rr}, the circumferential stress $\sigma_{\theta\theta}$, and the vertical stress σ_{zz} (Figure 3-52), which can be expressed as:

$$\sigma_{rr} = \sigma_{OH} + \Delta\sigma_{rr} \quad [3\text{-}4]$$

$$\sigma_{\theta\theta} = \sigma_{OH} + \Delta\sigma_{\theta\theta} \quad [3\text{-}5]$$

$$\sigma_{zz} = \sigma_{OV} + \Delta\sigma_{zz} \quad [3\text{-}6]$$

with σ_{OH} and σ_{OV} as the horizontal and vertical total stress at rest, respectively, and $\Delta\sigma_{rr}$, $\Delta\sigma_{\theta\theta}$ and $\Delta\sigma_{zz}$ as the increase or decrease of total stress in the radial, circumferential and vertical directions, respectively. The determination of the horizontal and vertical stress at rest is very trivial. However, Palmer (1972) showed that the calculated stress-extension relation for a Ménard pressuremeter test in overconsolidated London clay is not strongly sensitive to errors in estimates of the *in situ* stress condition.

The displacement in the radial, circumferential and vertical directions are *u*, *v* and *w*. Because the cylinder is of infinite length, the displacements in circumferential and vertical directions are zero. An initial point in the undeformed soil prior to loading is given by the radial distance *r*, the radial position during loading is then given by $\rho = r + u$.

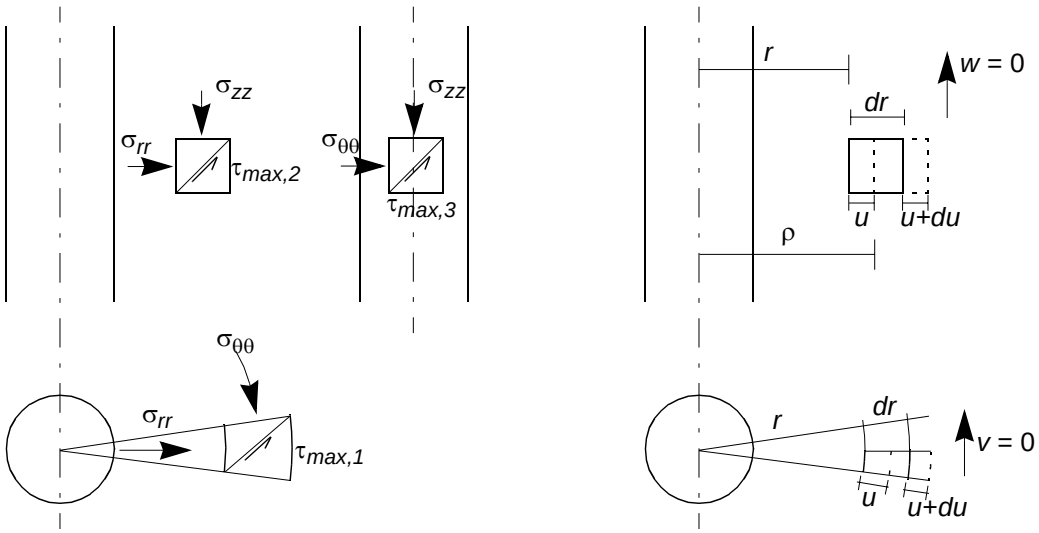

Figure 3-52: *Definition of stresses and displacements (Briaud, 1992).*

The principal strains are the radial strain ε_{rr}, the circumferential strain $\varepsilon_{\theta\theta}$, and the vertical strain ε_{zz}. By definition, the relationship between strains and displacements (Figure 3-52) for small strain theories and for these geometrically constrained problems are:

$$\varepsilon_{rr} = \frac{du}{dr} \qquad [3\text{-}7]$$

$$\varepsilon_{\theta\theta} = \frac{u}{r} \qquad [3\text{-}8]$$

$$\varepsilon_{zz} = 0 \qquad [3\text{-}9]$$

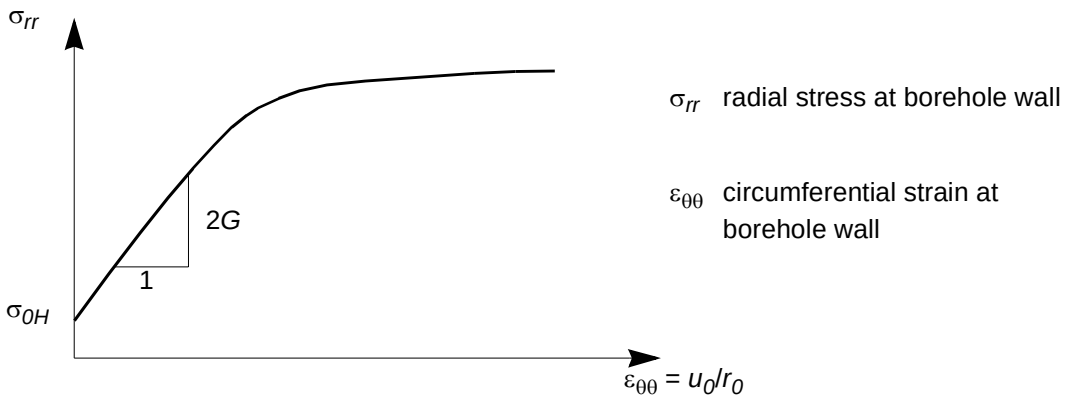

Figure 3-53: *In situ stress-strain curve from pressuremeter test curve.*

The equation of equilibrium is $\frac{d\Delta\sigma_{rr}}{d\rho} + \frac{\Delta\sigma_{rr} - \Delta\sigma_{\theta\theta}}{\rho} = 0$ [3-10]

A constitutive model is needed to link the compatibility and equilibrium conditions: linear elasticity may be adopted, provided yielding does not occur, and Hookes law is quoted here for isotropic conditions (E and ν, same in rr, $\theta\theta$ and zz directions), in terms of normal principal strains:

$$\varepsilon_{rr} = \frac{1}{E} \cdot (\Delta\sigma_{rr} - \nu(\Delta\sigma_{\theta\theta} + \Delta\sigma_{zz})) \qquad [3\text{-}11]$$

$$\varepsilon_{\theta\theta} = \frac{1}{E} \cdot (\Delta\sigma_{\theta\theta} - \nu(\Delta\sigma_{zz} + \Delta\sigma_{rr})) \qquad [3\text{-}12]$$

$$\varepsilon_{zz} = \frac{1}{E} \cdot (\Delta\sigma_{zz} - \nu(\Delta\sigma_{rr} + \Delta\sigma_{\theta\theta})) \qquad [3\text{-}13]$$

Solving the differential equation for equilibrium [3-10] with the boundary conditions $u = 0$ for $r = \infty$ and $u = u_0$ for $r = r_0$ (at the borehole wall), the stresses and the strains can be expressed anywhere in the soil by:

$$u = \frac{u_0 r_0}{r} \qquad \varepsilon_{rr} = \frac{u_0 r_0}{r^2} \qquad \varepsilon_{\theta\theta} = -\frac{u_0 r_0}{r^2} \qquad [3\text{-}14]$$

$$\sigma_{rr} = \sigma_{OH} + 2G\frac{u_0 r_0}{r^2} \qquad \sigma_{\theta\theta} = \sigma_{OH} - 2G\frac{u_0 r_0}{r^2} \qquad [3\text{-}15]$$

G: shear modulus

The increment of radial compressive strain is equal to the magnitude of the increment of circumferential strain but is opposite in sign (tensile) due to the constant volume assumption. The increase in radial stress (compression) is equal to the decrease in circumferential stress (Equation 3-15).

If p is the pressure acting on the borehole wall (Figure 3-53),

$$\sigma_{rr} = \sigma_{OH} + (p - \sigma_{OH})\frac{r_0^2}{r^2}. \qquad [3\text{-}16]$$

In reality, however, ice and frozen soils, do not behave elastically and at constant volume. These materials show distinct time and load dependent deformation behaviour. The total strain is the sum of an elastic portion ε_e and a time dependent, viscoplastic portion ε_{vp}. For short term creep tests, i.e. steady state creep has not yet been reached, the time dependent primary creep strain, can be defined after Hult (1966) and Ladanyi (1972) as:

$$\varepsilon_{vp} = \left(\frac{\dot{\varepsilon}_c}{b}\right)^b \left(\frac{\sigma_e}{\sigma_c}\right)^{n_1} t^b \quad \text{or in terms of strain rate, as:} \qquad [3\text{-}17]$$

$$\dot{\varepsilon}_{vp} = \left(\frac{\dot{\varepsilon}_c}{b}\right)^b \left(\frac{\sigma_e}{\sigma_c}\right)^{n_1} \qquad [3\text{-}18]$$

b and n_1 are the creep exponents, $\dot{\varepsilon}_c$ is an arbitrary reference strain rate and σ_c the reference stress corresponding to the reference strain rate $\dot{\varepsilon}_c$ and σ_e denotes the value of the *Von Mises* equivalent stress

$$\sigma_e = \frac{1}{2}\sqrt{(\sigma_{rr} - \sigma_{\theta\theta})^2 + (\sigma_{\theta\theta} - \sigma_{zz})^2 + (\sigma_{zz} - \sigma_{rr})^2} \quad \text{at} \quad \dot{\varepsilon}_{vp} = \left(\frac{\dot{\varepsilon}_c}{b}\right)^b.$$

Equation [3-17] can also be written as $\varepsilon_{vp} = A\left(\frac{\sigma_e}{\sigma_c}\right)^{n_1} t^b$. [3-19]

A different approach using Glen's flow law for the determination of the radial creep strain rate for a constant internal pressure p applied in the borehole was proposed by Kjartanson *et al.* (1988). It is assumed that steady-state creep is reached. The minimum value of the radial strain rate $(\dot{r}/r)_{min}$ is calculated as:

$$\left(\frac{\dot{r}}{r}\right)_{min} = ap^{n_2} \qquad [3\text{-}20]$$

where a and n_2 are the creep parameters that have to be determined experimentally, and $(\dot{r}/r)_{min}$ is equal to $\dot{\varepsilon}_{vp,\,min}$ of Equation [3-18].

Parameter determination

At least three creep stages are necessary in order to determine the creep parameters at different depths. Comparable pseudo-elastic secant shear moduli may be calculated from the slope of unload-reload loops in the pressuremeter pressure – radial strain space at specific time intervals. The determination of creep parameters from Equation [3-19] is described in Ladanyi and Johnston

(1973) for general cases. Both approaches, i.e. Equation [3-19] and Equation [3-20] were used for the data of the Murtèl-Corvatsch rock glacier and are presented explicitly in Arenson *et al*. (submitted, a).

In addition, stress relaxation tests can offer a very helpful alternative since the problem of transient creep effects during the loading stage, which cannot be applied instantaneously, are eliminated (e.g. Ladanyi, 1982; Ladanyi and Huneault, 1987; Ladanyi and Melouki, 1993). The mean of all six radial deformation transducers should be maintained at a constant value during a stress relaxation test as the cell pressure is regulated manually and recorded. This is not a simple task and therefore no suitable test data can be presented.

Test results

A set of typical pressuremeter creep test results is shown in Figure 3-54 for two depths. Different magnitudes of cavity pressure as well as the duration of the creep stages were chosen depending on the test. The influence of composition can be seen by comparing the radial creep strain rates of these two depths (Figure 3-55). A warm probe on one hand and borehole wall disturbances on the other hand, resulted in slightly higher values for low cavity pressures during the test at a depth of 18.5 m.

The test at a depth of 18.5 m, where the volumetric ice content is only slightly higher, but air voids were present, shows a less pronounced reaction to an increase in the cavity pressure. On the other hand, the strain rate at low stresses is higher. The first effect is reflected in a lower value of n_1/n_2 and the latter in a higher value of A/a. Summaries of all values determined by both approaches are given in Table 3-8 and Table 3-9. One of the major problems in determining the creep parameters with the primary creep approach is that the expansion at 1 minute of creep is usually taken as a reference point. For the first loading steps at low cavity pressure, large strains were observed, which are thought to originate from borehole wall disturbances. For the depth, where only three or four loading steps were performed, a later reference point was chosen (e.g. 10 minutes) in order to eliminate large strains at the beginning, which are not creep induced.

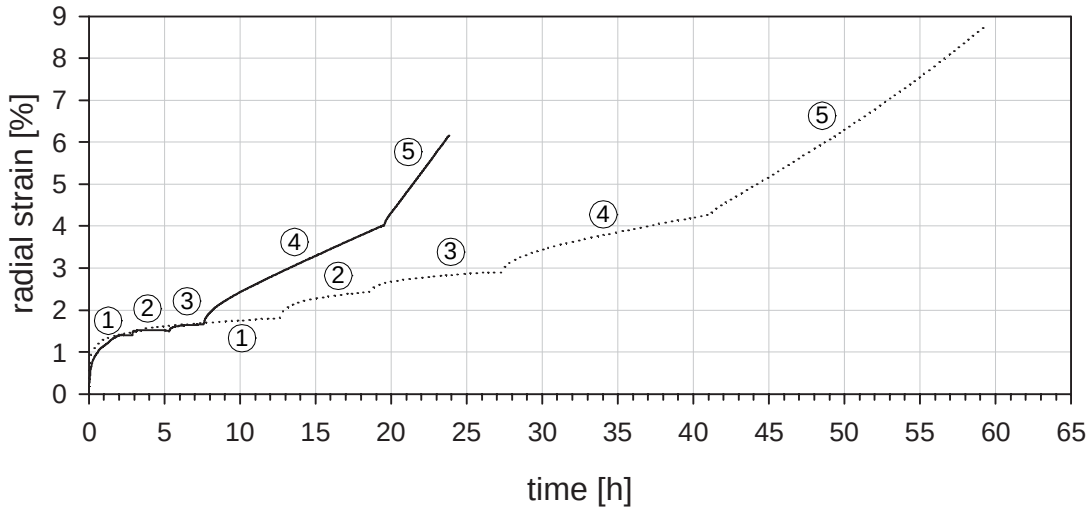

	depth	*step 1*	*step 2*	*step 3*	*step 4*	*step 5*
·····	18.5 m	206 kPa	692 kPa	1166 kPa	2335 kPa	3292 kPa
——	24.5 m	34 kPa	394 kPa	1138 kPa	2282 kPa	3025 kPa

von Mises equivalent stress σ_e at creep stages

Figure 3-54: *High pressure dilatometer test at 18.5 and 24.5 m depth within borehole 1/2000, Murtèl-Corvatsch rock glacier.*

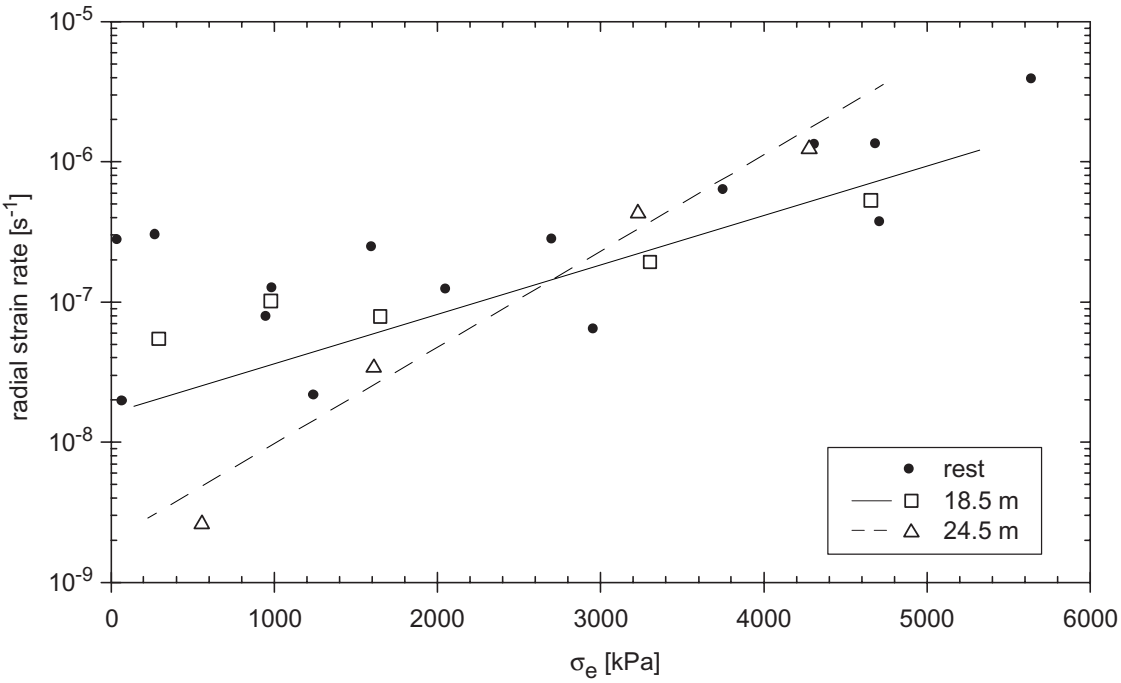

Figure 3-55: *Radial creep strain rate against von Mises equivalent stress σ_e for all pressuremeter tests. The tests shown in Figure 3-54 are shown individually.*

test No.	depth [m]	ice content [Vol..%]	creep parameters (Equation [3-19]) $\varepsilon_{vp} = A\left(\frac{\sigma_e}{\sigma_c}\right)^{n_1} t^b$		
			n_1	b	A [min^{-b}]
2	16.0	90	0.60	0.66	$8.5 \cdot 10^{-7}$
3	18.5	80	1.08	0.61	$6.1 \cdot 10^{-8}$
4	21.2	80	0.61	0.69	$1.1 \cdot 10^{-6}$
5	22.5	77	1.41	0.82	$1.6 \cdot 10^{-9}$
7	24.5	86	1.46	0.80	$1.8 \cdot 10^{-9}$

Table 3-8: *Creep parameters after Equation [3-19] for pressuremeter tests at borehole 1/2000, Murtèl-Corvatsch rock glacier.*

test No.	depth [m]	ice content [Vol..%]	creep parameters (Equation [3-20]) $\dot{\varepsilon}_{vp,\,min} = a\sigma_e^{n_2}$	
			n_2	a
1	16.0	90	2.03	$9.1 \cdot 10^{-15}$
2	18.5	80	0.71	$7.7 \cdot 10^{-10}$
3	21.2	80	0.90	$2.7 \cdot 10^{-10}$
4	22.5	77	1.43	$5.5 \cdot 10^{-12}$
5	24.5	86	3.02	$1.1 \cdot 10^{-17}$

Table 3-9: *Creep parameters after Equation [3-20] for pressuremeter tests at borehole 1/2000, Murtèl-Corvatsch rock glacier.*

Unload-reload loops were performed between the creep stages with a reduction of radial strain $\Delta\varepsilon_r$ of up to 0.04%. Shear moduli G could be calculated using

$$G = \frac{1}{2}\frac{\Delta p}{\Delta\varepsilon_r} \qquad [3\text{-}21]$$

Even though the material seems to creep unequally, the moduli are quite consistent at each unloading stage over the chosen depths. Rather than varying as a function of the depth, the shear modulus depends on the applied cavity pressure. However, this influence wears off with increasing mean pressure in the borehole (Figure 3-56). The low shear moduli at the low cavity pressure may result from disturbances induced by the drilling or due to the high air content (e.g. Figure 3-33). The soil is compacted and not deformed during the first loading steps. Therefore a shear modulus G of about 1.5 ± 0.3 GPa seems to be reasonable. For comparison, Sinha (1984) uses a shear modulus of 3.8 GPa for ice

in his considerations and Hobbs (1974) gives a summary of several studies that show shear modulus between 3.45 GPa and 3.80 GPa for polycrystalline ice at a temperature of -5°C.

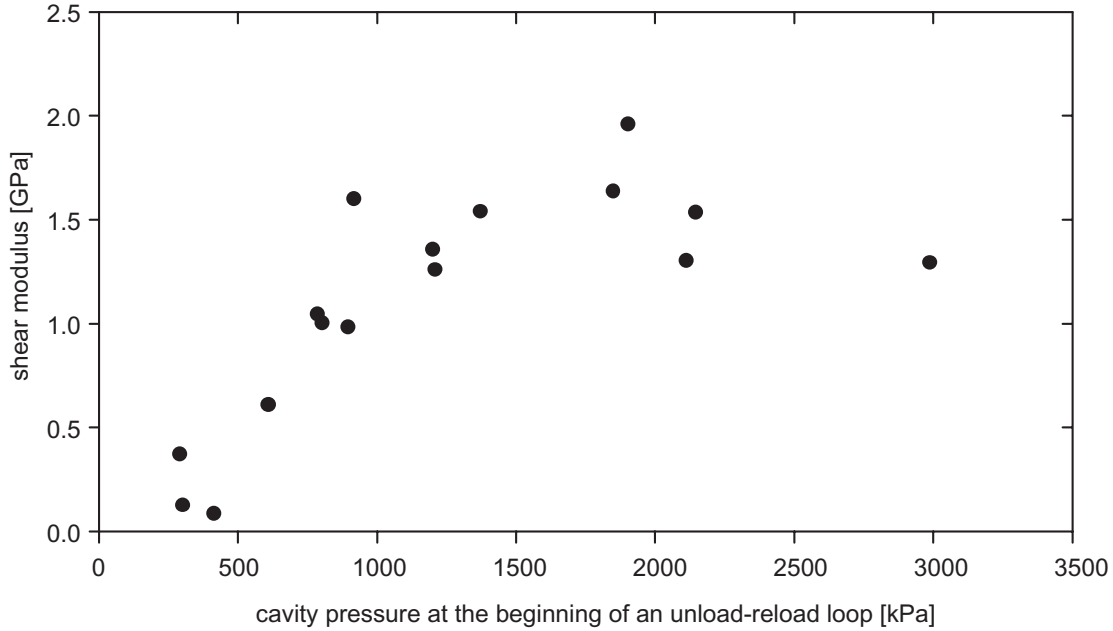

Figure 3-56: *Shear moduli as a function of the cavity pressure at the beginning of the unload-reload loop.*

A yield stress of between 2 and 3 MPa could be determined for the depths tested (Figure 3-57).

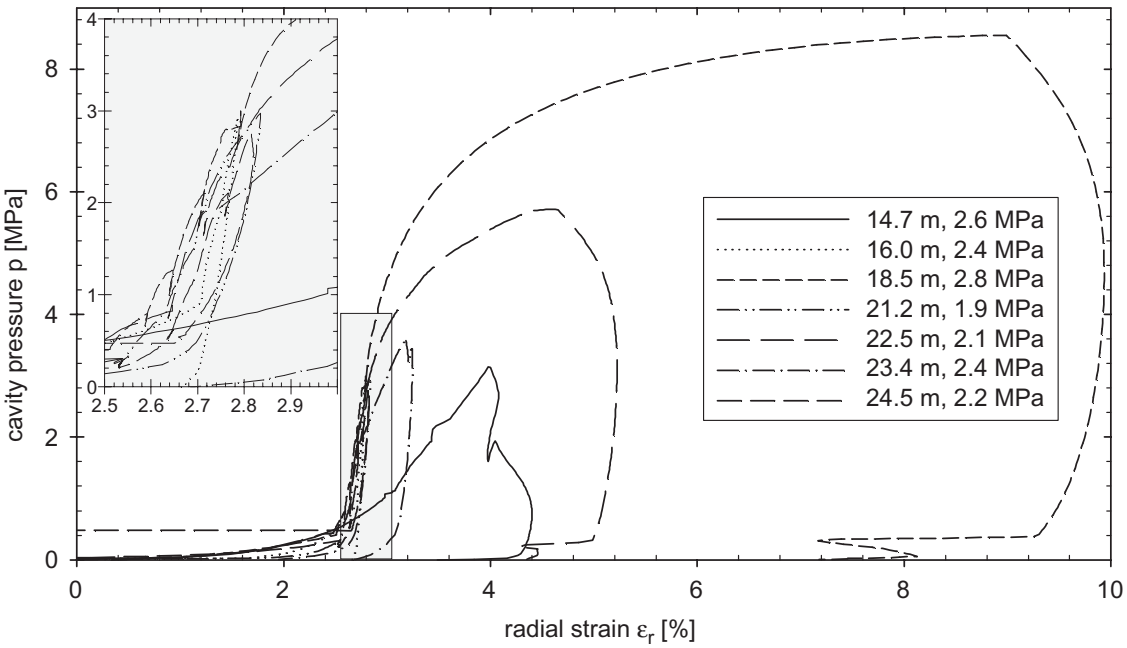

Figure 3-57: *Shearing phase: maximum cavity pressure and lower yield stress.*

A detail within Figure 3-57 has to be explored in more detail. The test at a depth of 24.5 m shows a residual pressure of about 450 kPa at the end of the test rather than a value of zero, as expected. A possible explanation for this behaviour is porewater pressure. The origin of this pressure might be water that froze at the test location during the test, inducing a pressure due to the volume expansion during freezing (Figure 3-58). Free water within the borehole is very unlikely, since this would imply about 45 m head of water.

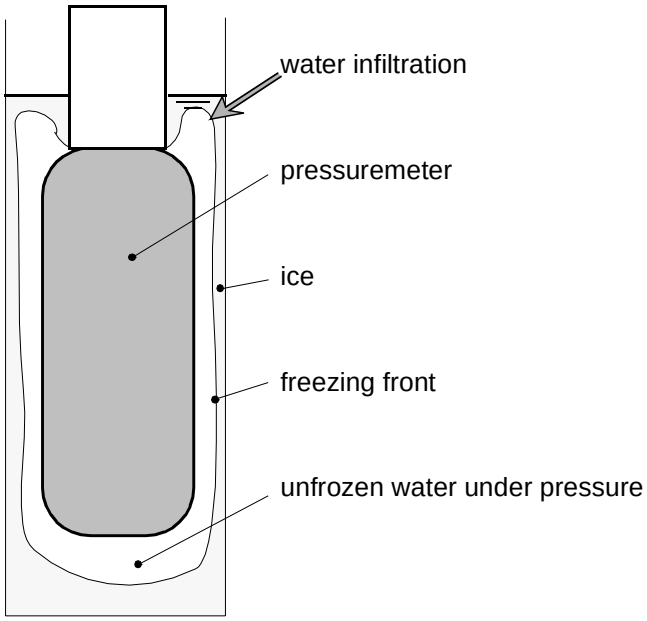

Figure 3-58: *Water pressure at the end of pressuremeter test at a depth of 24.5 m.*

Summary of pressuremeter tests

Several pressuremeter tests were conducted within borehole 1/2000 at the Murtèl-Corvatsch rock glacier in order to determine *in situ* creep parameters. Two different methods had been used for the analyses of the test results, one adopted a primary creep approach, while the other assumed steady state conditions (secondary creep). The data analysis has to be carried out carefully, since both methods are very sensitive to small changes in the creep parameters. Due to the relatively short time the soil is maintained under a constant stress, it is reasonable to use a primary creep approach that includes the change in the strain rate with time, such as proposed by Ladanyi and Johnston (1973). In contrast, steady state conditions should be modelled and therefore the second approach is more appropriate. Both methods indicate similar trends in terms of stress dependency (creep factor n) and general creep susceptibility (creep factor A/a). For this particular case, the secondary creep approach is probably more appropriate, also because the tests have been carried out long enough in order to achieve constant strain rates. The whole primary creep response, however, could be modelled very effectively by the first approach recommended.

A comparison between the pressuremeter data and the laboratory creep tests will be given in Section 6.2.

Laboratory Testing

Various samples of frozen soil were tested under a range of boundary conditions in order to study the thermo-mechanical behaviour of rock glacier materials. All tests were performed in a triaxial apparatus to simulate in situ stress conditions. The sample composition and the particle size distribution of the solids were determined following each test. In addition, some thin sections were analysed to determine the grain sizes of the ice crystals.

The triaxial test equipment will be described within this chapter, including some calibration tests. Then test results of artificially frozen samples as well as of cored samples from the various boreholes at Muragl rock glacier and Murtèl-Corvatsch rock glacier, including the sample preparation, handling and storage, will be presented and discussed briefly. The main outcome of the laboratory tests will be summarised at the end of this chapter, which form the basis of the analyses given in Chapter 5.

4.1 Triaxial Testing Equipment

Three new triaxial testing apparatuses were designed and constructed at the Institute for Geotechnical Engineering in 1999/2000 for the triaxial tests presented within this study. This new equipment is capable of performing fully automated stress and strain controlled tests. The predecessor of these triaxial apparatuses had been designed for triaxial tests on snow (Bartelt and von Moos, 2000; von Moos, 2002). The original design had then been adopted to suit tests on frozen soils as well as on soft clays (Trausch-Giudici, in prep). The air controlled cell pressure acting on the snow triaxial sample had to be replaced by a standard system using a cell fluid. All three triaxial testing apparatuses were placed within a temperature-controlled cold chamber.

4.1.1 IGT Cold Chamber

The cold chamber (ETH HIF Kli 11, Type CELLTHERM) has internal dimensions of 2.45 m x 1.75 m x 2.25 m and is insulated by a PU foam of 120 mm thickness (Figure 4-1). The Technoblock ACM 120 refrigeration device is specified for a room volume of up to 90 m^3 and a temperature range of between -5°C and +5°C. In addition to the ventilator within the cooling unit, three additional ventilators (fans) were placed in the cold chamber for better air circulation, and hence the temperature was more constant throughout the whole room.

The arrangement of the testing units is also shown in Figure 4-1. When three tests are running simultaneously, it is assumed that the temperature regime is common to all three samples, although temperature is measured within each cell. However, the mean temperature within the chamber may differ up to 0.5°C, depending on the location within the chamber and the given temperature. The temperature variation of the cold chamber itself is about ±1°C, which is rather large. However, within the triaxial pressure cells, the temperature variations are more than a magnitude smaller due to the large volume of the cell liquid that acts as a damper on temperature variations. The three tests were started simultaneously most of the time, since the sample preparation for the tests had to be performed within the IGT cold chamber.

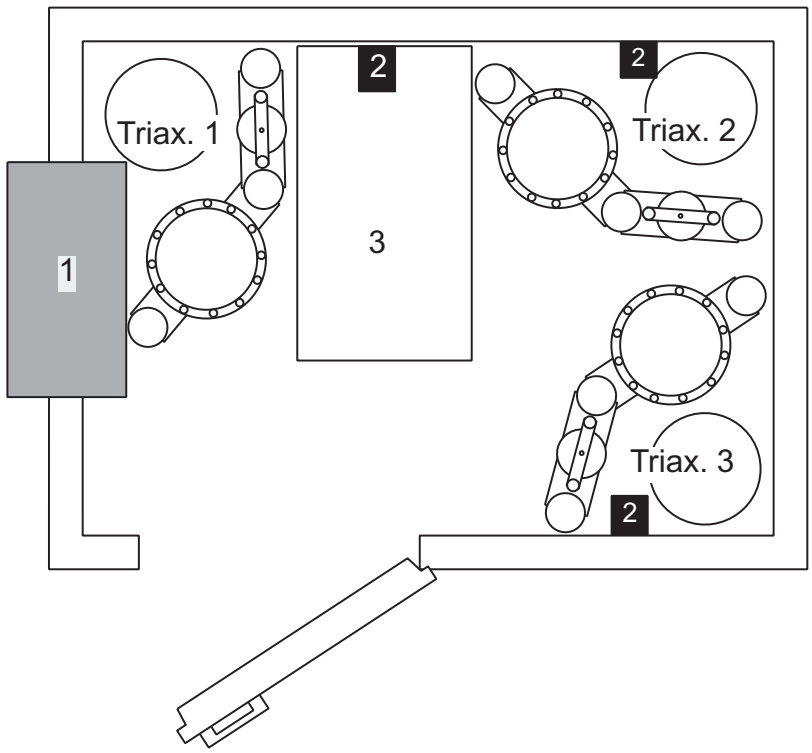

1) refrigeration unit
2) ventilators (fans)
3) working table for test set-up

Cold chamber:

wall thickness: 120 mm

inner dimension:
245 cm x 175 cm
height: 225 cm

outer dimension:
269 cm x 199 cm
height: 253 cm

Figure 4-1: *Characteristics of the IGT cold chamber with the location of the three triaxial test apparatuses.*

4.1.2 Mechanical Set Up

The triaxial test equipment had been adapted from the snow triaxial device so that cell pressures up to 1 MPa and axial forces up to 20 kN were possible. The plattens were set up for sample diameters of 74 mm. This dimension

corresponded to the diameter of the samples cored with the triple tube drill system described in the previous chapter and allowed an axial stress of up to 4650 kPa to be applied. A back-pressure unit was also added, since the devices should also be capable of testing unfrozen soils, even though that unit was not used for the tests presented herein. Sketches of the triaxial apparatus are given in Figure 4-2 and Figure 4-3, ignoring the back-pressure unit. In the following text, the numbers in brackets refer to these figures.

The device is computer controlled, with software developed at the Institute for Geotechnical Engineering, based on National Instrument's LabView, Version 5.1. A pressure piston (1) regulates the cell pressure and is driven by a stepper motor (2) of the type Phytron ZSH 57/2.200.4.2. An additional gear box, with a reduction gear ratio of 1:16, regulates the advancement of the lead screw (3), and the shaft coupling (4) between the gear box and the screw reduces stresses in the system. The lead screw, which has a 1 mm pitch, attaches to the loading frame (5) by rotation in a satellite roller nut. With this combination of reduction gear ratio and pitch of the satellite roller screw, the motor needs 6400 steps to run 1 mm (400 steps per rotation), which corresponds to 0.15 μm per step. The axial force and displacement is controlled similarly to the cell pressure piston.

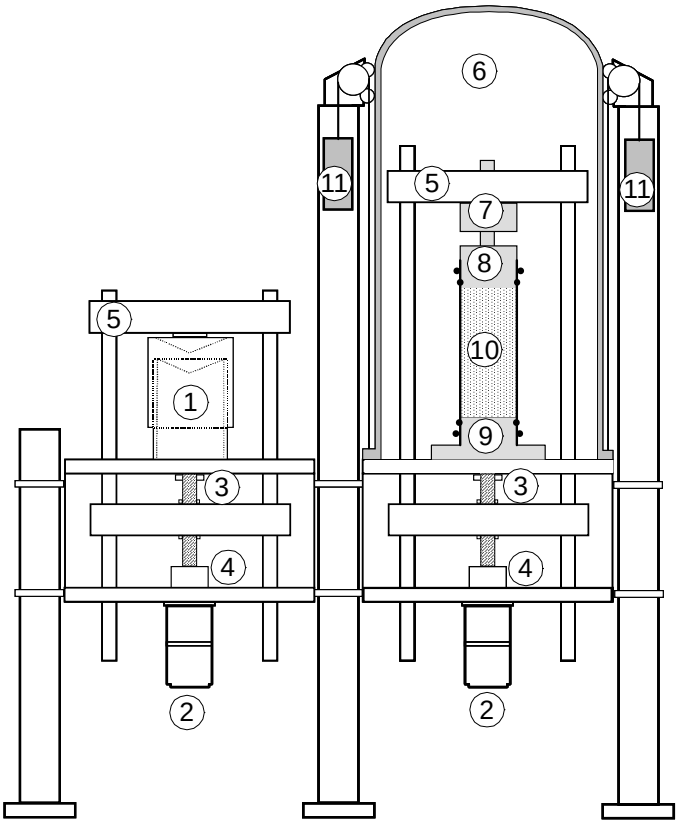

1) Cell pressure cylinder
2) Stepper motor
3) Lead screw
4) Shaft coupling
5) Loading frame
6) Pressure cell
7) Load cell
8) Top load platten
9) Bottom load platten
10) Sample with rubber membrane and sealing rings
11) Counterweight

Figure 4-2: *Triaxial test apparatus: mechanical set up.*

The tie bars of the loading frame (5) for the axial force system pass through the base plate of the pressure cell (6) through an air-tight interface. The load cell (7) is fixed to the upper cross beam of the loading frame, i.e. the friction between tie bars and base plate does not affect the axial force readings of the load cell. However, since the load cell is fixed to the loading frame, the cell pressure that acts on the area, on which the load cell is mounted to the frame is guided out of the cell and therefore, compensation is necessary. The following correction values

were determined for the three triaxial cells by calibration as:

- Triax. No. 1: 1.070 N/kPa$_{\text{cell pressure}}$
- Triax. No. 2: 1.051 N/kPa$_{\text{cell pressure}}$
- Triax. No. 3: 1.054 N/kPa$_{\text{cell pressure}}$

The top load platten (8) is connected beneath the load cell with the displacement transducer (16) mounted on a bracket fixed in-between the platten and the load cell. Only the compliance of the load plattens can affect the measurement of the displacement transducer. The bottom load platten (9) is fixed to the base plate of the cell. Drainage from the top and bottom plattens is assured by 2.9 mm thick brass filters (12) with pore diameters of 0.8 mm and by PVC porewater tubes, which lead through the base plate of the cell into two pore pressure transducers (13/14). Pores within a frozen soil sample contain air and unfrozen water, which do not have to be interconnected. Therefore, only total stresses can be measured. However, the pore system, such as transducers, tubes and plattens, are filled with antifreeze, and therefore air pressures acting at the top and the bottom of the sample can be measured during a test. The values measured by the pore pressure transducers are smaller than the pressures originally acting in the sample due to the compressibility of air. Nevertheless, the measurements of these pressures reveal interesting results, which help to understand the different processes developing within the sample during a test. In particular, effective stresses might vary for different soil compositions, even though the total stresses are similar. The brass filters (12) have to be dry, and the voids ratio has to be large enough not to induce suction due to capillary forces, in order not to affect the sample by allowing the antifreeze to enter the pore system.

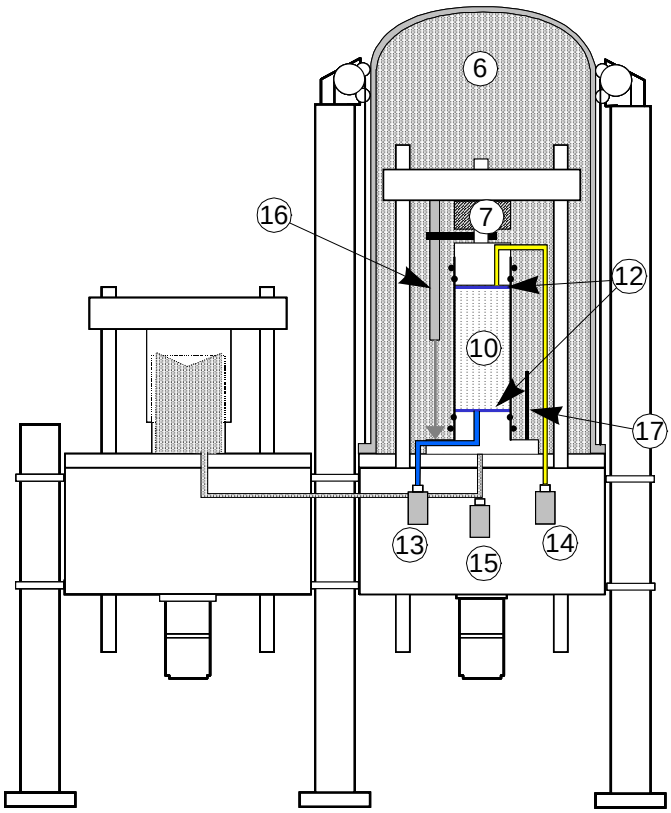

6) Pressure cell, filled with antifreeze
7) Load cell (20 kN)
10) Sample with rubber membrane and sealing rings
12) Brass filter
13) Pore pressure transducer bottom
14) Pore pressure transducer top
15) Cell pressure transducer
16) Displacement transducer (LVDT)
17) Temperature sensor (PT 100)

Figure 4-3: *Triaxial test apparatus: test control set up.*

All stepper motors can be controlled manually with a joystick within the cold chamber for the placement of the sample, since the computers for the test control are placed outside the cold chamber. A special mount (Figure 4-4) holds the sample centrally in a horizontal position allowing the positioning of the top platten and the O-rings for the correct sealing of the sample.

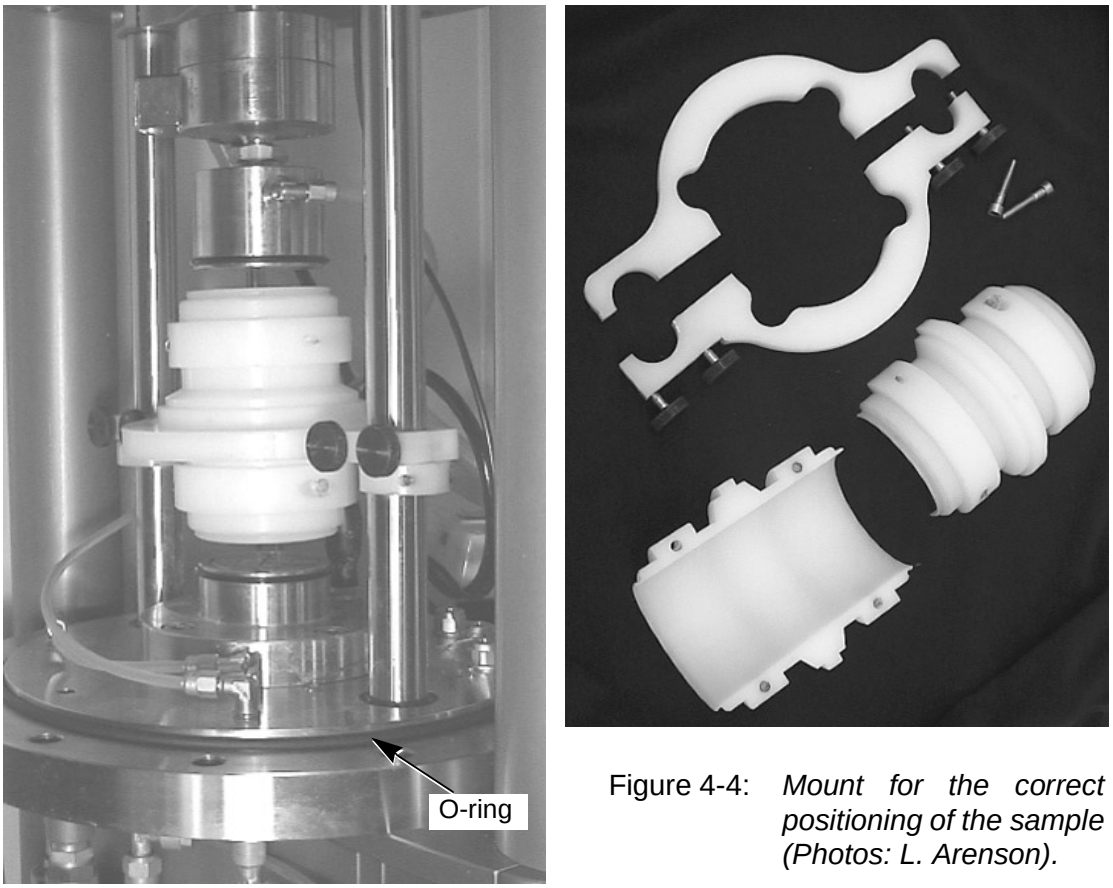

Figure 4-4: *Mount for the correct positioning of the sample (Photos: L. Arenson).*

The cell is closed and filled with deaired antifreeze after the specimen has been positioned and carefully sealed. The change of the cell fluid volume will be measured in order to obtain the change in the sample volume, and therefore no air can be allowed in the cell. The filling process has to be carried out slowly and carefully.

Counterweights (11) are placed within the legs of the apparatus in order to assist the opening and closing of the 20 kg pressure cell, which is sealed to the base plate with a prestrained O-ring (as seen in Figure 4-4 left). The cell is then screwed down to the base plate with 12 M14 screws, allowing a cell pressure of up to 1 MPa.

A conical piston has been used for the volume measurement device within the cell pressure cylinder. The open cone faces upwards to prevent air bubbles from entering the cell. A channel leads to the cell water system with the pressure transducer (15) under the base of the cell. A valve is mounted at the top of the piston to allow the cell liquid to be de-aired. One step of the stepper motor corresponds to a volume change of 1.227 mm^3. A correction of the cell volume has to be considered when moving the loading frame of the axial pressure within the cell. This correction is a function of the frame diameter and for the system used herein, the cell volume changes exactly 1.41 cm^3 per millimetre axial deformation.

One to three temperature sensors (17) measure the temperature of the cell liquid close to the sample. It is assumed that this temperature corresponds to the temperature within the frozen sample.

Electronic set up

Each transducer signal is amplified in a junction box located outside the cold chamber. A 16 bit AD board with 8 channels digitises the signals prior to storage in the computer. The stepper motors are controlled by a motion controller and a motor interface, which has a switcher that limits the maximum allowed load and displacement of the stepper motors.

Software set up

Different control modes are possible for each control unit (cell pressure, porewater pressure, axial pressure):

- *Panel Mode*: The control of the unit is possible with the joystick.
- *Regulating Mode*: Within this mode, a pressure (e.g. cell pressure) or a force (e.g. axial load) will be held constant. The regulating speed can also be given (e.g. kPa/s, N/s) and therefore, loading ramps are possible. This mode will be used with the maximum possible axial loading speed of 10 N/s for creep tests, where the axial stress is held constant.
- *Move Velocity Mode*: The displacement velocity of the loading frame can be controlled. This is the standard mode for a triaxial shear test with a constant strain rate.
- *Move Position Mode*: A relative or absolute position of the loading frame can be given. However, this mode is usually only used during the setting up of a test.

Since these triaxial test apparatuses can be also used for standard triaxial testing, it is possible to run stress path tests that couple axial stress and cell pressure.

The software controls the progression of the test with a PID-control (Proportional, Integral, Differential). It is possible for the user to specify the regulating parameters, which controls how the system corrects errors between a nominal and the actual value of the measurement concerned. The controlling parameters are as follows:

- *The proportional parameter*, which multiplied by the error (nominal – actual) in digits, results in the rate at which the stepper motor attempts to eliminate the error (the bigger the error, the faster the rate).
- *The integral parameter*, which multiplied by the time integral of the error, results also in a rate of correction so that the error will not increase with time.
- *The differential parameter*, which, multiplied by the time differential of the error, results in a rate of correction so that the instantaneous error is not too large.

- *The deadband*, which is the minimum accepted nominal error minus the actual error in digits.
- *The integral limit*, which limits the results of the integral parameter to increase the stability of the control system.

During a test, the software is able to display the data in different types of graphs or in a value table. Both table and graphics are updated on-line with the same frequency as the storage rate. In addition to the measured values, variables can be defined, which are then calculated from measured data and geometrical data, such as those based on the specimen dimensions at the start of a test. These calculated values can be evaluated also in the on-line graphics and will be stored together with the measured data.

Table 4-1 and 4-2 give an overview of the technical details of the various measurements:

transducer	range calibration	precision	resolution	temperature range	sensor
displace-ment	100 mm 10 mm/V	± 0.1% of end value	0.003 mm	-20 – 85°C	HBM WA100
load cell	20 kN 4 kN/V	± 0.1% of end value	1 N	-10 – 70°C	HBM U2B
PWP top	1 MPa 200 kPa/V	± 0.1% of end value	0.03 kPa	-15 – 85°C	SENSTEC 8267
PWP bot-tom	1 MPa 200 kPa/V	± 0.1% of end value	0.03 kPa	-15 – 85°C	SENSTEC 8267
cell pres-sure	1 MPa 200 kPa/V	± 0.1% of end value	0.03 kPa	-15 – 85°C	SENSTEC 8267
cell temper-ature	-45 – 100°C 10°C/V	< 0.1°C	0.003°C		PHILIPS PT100

Table 4-1: *Triaxial test apparatus: instrumentation.*

transducer	range calibration	resolution	velocity	move-ment rate	pressure or force
cell volume	720 cm^3 1.227 mm^3/ step	0.02 cm^3 < 0.5 kPa	0.00001 – 10 kPa/s	0.0024 – 2.1 mm/s	0.5 – 1000 kPa
axial force	92 mm 0.15625 μm/ step	< 0.01 kN	0.00001 – 100 N/s	0.05 mm/d – 1 mm/s	0.02 – 20 kN
PW volume back pres-sure[a]	720 cm^3 1.227 mm^3/ step	0.02 cm^3 < 0.5 kPa	0.00001 – 10 kPa/s	0.0024 – 2.1 mm/s	0.5 – 1000 kPa

Table 4-2: *Details of the stepper motors, type DCX-AT200.*

a. not used for the undrained tests within this study.

4.1.3 Calibration

Initially, changes in the sample volume due to pressure melting and compression were planned to be measured with the change of the cell volume. However, calibration tests of the cell volume showed that there are numerous effects that influence the volume within the cell and these effects depend on factors that varied strongly. The applied pressure, the temperature, the time for the filling of the cell, as well as the time between two tests, just to name a few, seem to affect this value. As a consequence, the change in volume was only taken as a trend indicator and not as an absolute value. Brittle failure, for example, resulted in a rapid increase of the sample volume, which could clearly be measured. The value of this increase, however, cannot be determined exactly.

Temperature changes also have to be considered due to the large volume of the cell liquid (about 52 litres), which is aggravated by the fact that different parts of the cell volume undergo differential temperature changes. The cell pressure unit and the tubes connecting the piston to the cell show larger changes in temperature, and as a consequence in volume, than the cell liquid within the cap. Calibration tests showed that the coefficient of volume change due to temperature γ is about $2 \cdot 10^{-4}$ K^{-1}, for the cell liquid used within the current study.

4.1.4 Deformations

Vertical deformation

The deformation is measured between the top cap and the base of the sample, as shown in Figure 4-3, in contrast to Rist *et al*. (1991), where the strains are measured directly on the specimen. The plattens are stiff enough, not to deform under the applied loads and therefore, the signal of the LVDT (Linear Variable Differential Transformer) gives directly the vertical deformation of the sample. In addition, the deformation measurement device is not affected by the distortion of the sample, and therefore the measured value is always vertical. Bedding errors can by minimised by carefully moving the loading frame on the sample until a small axial force is recorded.

Horizontal deformation

Measurement of horizontal deformations of a sample during a test would allow for a more accurate determination of the sample area during creep and shearing, and hence a more precise establishment of the axial stresses acting vertically on the sample would be possible.

The main focus of the tests performed during this study lay on the axial creep strain rate under constant load, and therefore, the vertical deformations were in the range of some percentage strain implying that a deformation measurement device on the sample had not been suitable. As a consequence, volume changes of the cell liquid were measured during the test. The problem, however, is the large amount of cell liquid in contrast to the sample volume, and in particular in the change of volume. Furthermore, even small temperature changes of the cell liquid have to be taken into account (see Chapter 4.1.3).

The sample geometry was measured before and after every test and compared with the axial deformation and the values of the volume change measurement. Even though the tests were undrained, volume change of several percentage volume strain occurred, due to various effects that will be discussed later. Therefore, the change in the area was much smaller than standard assumptions using constant volume would suggest. This was the main reason why the axial load was applied manually using a force control instead of automatically calculating the sample area and controlling the axial stresses over the test time, which would be the correct approach for unfrozen and saturated soils.

4.1.5 Notation for Stresses and Strains

The notation used for the analysis of the data is the following:

p hydrostatic pressure $= \frac{J_1}{3} = \frac{1}{3}(\sigma_1 + \sigma_2 + \sigma_3)$, where J_1 is the first invariant of the stress tensor

q equivalent stress $= \sqrt{3J_{2D}} = \frac{3}{\sqrt{2}}\tau_{oct}$

where J_{2D} and τ_{oct} are the second invariant of the deviatoric stress tensor and the octahedral shear stress, respectively. In terms of principal stresses, *q* becomes to

$$\sqrt{\frac{1}{2}[(\sigma_1 - \sigma_2)^2 + (\sigma_2 - \sigma_3)^2 + (\sigma_3 - \sigma_1)^2]}.$$

For triaxial test conditions, where $\sigma_2 = \sigma_3$ is called the confining pressure (Figure 4-5), the deviatoric stress *q* turns into $\sigma_1 - \sigma_3$.

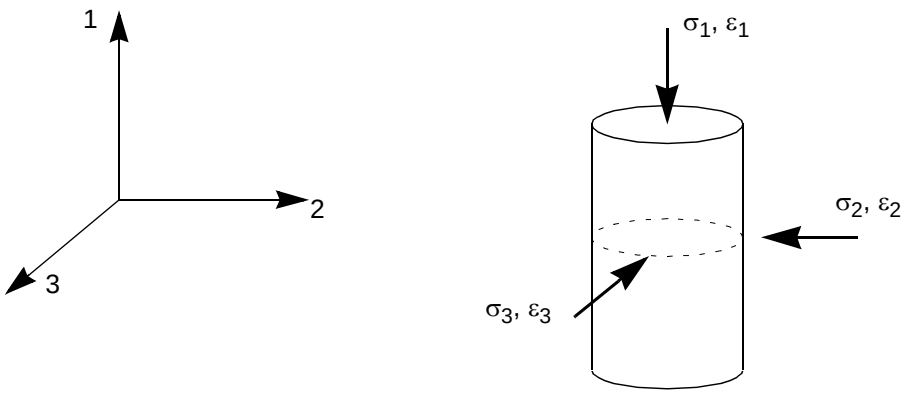

Figure 4-5: *Schematic diagram showing direction of principal stresses and strains for triaxial loading. Direction 1 is axial, and directions 2 and 3 are lateral.*

ε_v volumetric strain $= I_1 = (\varepsilon_1 + \varepsilon_2 + \varepsilon_3)$, where I_1 is the first invariant of strain tensor

ε equivalent strain = $\sqrt{3I_{2D}} = \frac{3}{\sqrt{2}}\gamma_{oct}$, where I_{2D} and γ_{oct} are the second invariant of the deviatoric strain tensor and the octahedral shear strain, respectively:

$$\varepsilon = \sqrt{\frac{1}{2}[(\varepsilon_1 - \varepsilon_2)^2 + (\varepsilon_2 - \varepsilon_3)^2 + (\varepsilon_3 - \varepsilon_1)^2]}$$

For the comparison with pressuremeter tests (see Chapter 3.3.7), the von Mises Equivalent was also used:

$$\sigma_e = \frac{1}{2}\sqrt{(\sigma_1 - \sigma_2)^2 + (\sigma_2 - \sigma_3)^2 + (\sigma_3 - \sigma_1)^2} \quad [4\text{-}1]$$

For triaxial testing conditions, where $\sigma_2 = \sigma_3$ and $q = \sigma_1 - \sigma_3$, σ_e can be calculated as

$$\sigma_e = \frac{\sqrt{2}}{2}q\,. \quad [4\text{-}2]$$

4.2 Test Procedures

It is important that the sample is brought to a correct stress level before the actual creep test starts, in order to produce a test result that mirrors natural stress conditions as closely as possible. This is true for the artificially frozen samples as well as for the cored samples. Testing the latter case, sample disturbances due to mechanical and thermal stress during transport and storage have to be minimised. Therefore, the samples were stored for at least one week in the cold chamber at the temperature at which the tests were intended to be performed. In addition, the sample was 'consolidated' almost isotropically for at least 24 hours, under undrained conditions with the cell pressure equal to the confining pressure of the test, and a minimal deviatoric stress q of about $3 \cdot 10^{-4}$ kPa was applied. The deviatoric stress q was applied to guarantee that the top platten is always in contact with the sample. The temperature of the cell liquid, which was slightly warmed during the filling process, stabilised during the consolidation period, so that the temperatures and the stresses applied approximated those formed *in situ*.

As mentioned above, the stress and temperature history of the sample is important. Some authors showed that the creep of ice is relatively insensitive to how the level of strain had been attained. However, Cole (1983) and Meglis *et al*. (1999) state that the total strain accumulated during the prior loading history of a sample is a strong factor in determining the creep rate.

Thin sections of different samples after the test and of untested samples were cut in order to study the microstructure of the samples. However, they might not perfectly represent the structure during the test since the release of the stress at the end of a test, the time break between the test and the thin-sectioning, the section preparation, and the differences in temperature (thin sections were performed at -18°C), may cause some additional microstructural changes. These might include the quenching of melted regions, stress-release cracking,

static recrystallisation, grain growth or crack healing. Nevertheless, differences in the grain sizes or deformation of grains could be observed and are summarised later within this chapter.

4.3 Testing of Artificially Frozen Samples

Even though guidelines exist for the classification and index testing of artificially frozen soils, based on the Unified Soil Classification System (USCS) (Sayles *et al*., 1987), they cannot be adopted easily for the type of problem studied in this work. However, reporting of test information has been conducted in the way it has been proposed by these authors.

4.3.1 Sample Preparation

The samples were prepared in a rather similar way to those described by Jones and Parameswaran (1983) and Singh and Jordaan (1996), who have used artificially frozen samples for testing crushed ice. The main problem is the volume expansion arising during freezing. Ideally, a horizontal freezing front has to be guaranteed by allowing any excess water to drain away from the base of the sample. Figure 4-6 shows a sketch of the sample preparation mould used herein. The base (4), the drainage system (5) and the expansion bottle are heated up to about 5°C. In addition, a spinning screw within the expansion bottle guarantees that the zero centigrade water is not freezing.

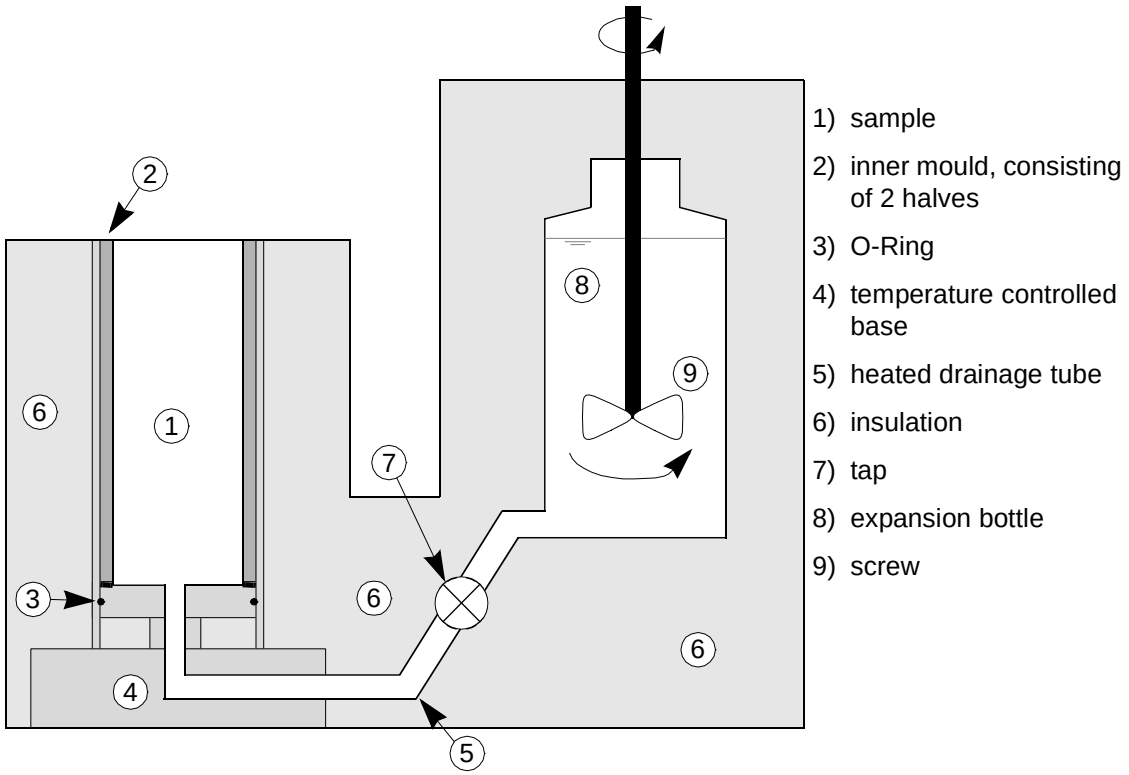

Figure 4-6: *Mould for the preparation of artificially frozen samples.*

The material used for the preparation of the artificially frozen samples should be as close as possible to that in the original samples. However, since the drilling was performed later than expected, not all factors could be taken into consideration at this stage. A very important point was the volumetric air content, which was up to twenty percent under natural conditions, but lower for the artificial samples. The solid composites that were mixed with the crushed ice, had been collected from a side slope of the Muragl rock glacier. The crushed ice is made from de-ionised water with a crushed-ice machine (Type: Frigidyn, Kibernetik AG).

The preparation of a sample was performed following the subsequent steps:

1. Mixing of crushed-ice – solid particle mixture. The dry soil has been pre-cooled to the same temperature as the ice.
2. The mixture is placed in the mould (2 in Figure 4-6) and compacted if necessary.
3. The expansion bottle is filled with de-aired water at a temperature of zero degrees centigrade.
4. The whole preparation system is put into an open freezer.
5. A vacuum is put on the mould (2) and the tap (7) is opened carefully. The crushed-ice – soil mixture is saturated from the bottom to the top. Filling the 16 cm high mould lasts about 30 minutes.
6. The open mould stays in the freezer for about 72 hours. The temperature at the base (4) and within the drainage tube (5) is held constant at about 5°C, allowing the excess water to be pushed back into the expansion bottle. The level of the water within the mould and the expansion bottle have to be equal at the beginning of the freezing process.
7. After the whole sample is frozen, the inner mould (2) can be dismantled, bisected and the sample is ready to be cut into the length needed.

It is important that samples are always prepared in a similar way in order to be able to compare the results. The effect of sample preparation on strength has been discussed, among others, by Baker and Konrad (1985). They found that a relatively homogenous density distribution could be achieved with the multiple sieve pluviation (MSP) method, whereas the wet rodding (WR) method resulted in heterogeneous samples. However, in order to achieve high volumetric ice contents, i.e. the particles are not in contact with each other, the MSP method cannot be applied.

4.3.2 Test Overview

The tests carried out on these artificial samples served two purposes. Firstly, the test methodology was improved in terms of the test equipment and adaptation to the software. It was also possible to study specific parameters, which affect the response of frozen soil samples, since the composition of the sample could be

prepared as desired. Two type of tests were carried out: constant strain rate (CSR) and constant stress, creep (CSC) tests. Several creep stages were applied for some tests until a total axial strain of 10 – 16% was reached. Thereafter, a relaxation was applied in order to reduce the axial stress and then the samples were sheared under a constant strain rate to determine shear strength. The author is aware that the sample may already have been damaged due to the creep stages, and that boundary conditions may play a role since the height is no longer twice the sample diameter. However, these values of shear strength are useful when comparing the creep results. The following parameters were studied for tests at a temperature of about -3.7°C:

- type of ice: samples with crushed polycrystalline ice and samples of columnar-grained ice,
- grain size of the solid particles,
- ice content, and
- confining pressure.

Table 4-3 gives an overview of the tests in terms of sample composition and type of test. Problems occurred with the sealing at times and therefore several tests had to be stopped or could not even be started. As a consequence, only a limited number of tests can be compared.

test No.	composition [Vol.%]			grain size [mm]	type of ice	temperature [°C]	cell pressure [kPa]	type of test
	ice	solids	air					
1	100	-	-	-	cg	-2.76 / -3.21	201.0	CSC/CSR
2	100	-	-	-	cg	-3.11 / -3.15	204.2	CSC/CSR
4	100	-	-	-	cr	-3.23 / -3.21	200.0	CSC/CSR
6	100	-	-	-	cg	-3.22	199.8	CSR
7	100	-	-	-	cr	-3.20	200.0	CSR
9	61	20	19	8 – 16	cr	-3.28	200.1	CSC
10	67	17	16	8 – 16	cr	-3.44	200.0	CSR
11	98	-	2	-	cr	-3.58	200.5	CSC
12	92	8	0	8 – 16	cr	-3.42	199.7	CSR
13	85	12	3	8 – 16	cr	-3.51	100.1	CSC
14	90	7	3	0 – 16	cr	-3.51 / -3.48	100.1	CSC/CSR
15	93	5	2	0 – 16	cr	-3.36	100.1	CSC/CSR
18	65	31	4	0 – 16	cr	-3.35 / -3.37	100.7	CSC/CSR
19	82	14	4	4 – 8	cr	-3.66 / -3.70	100.1	CSC/CSR
20	88	8	4	8 – 16	cr	-3.38 / -3.33	100.1	CSC/CSR
21	86	8	6	2 – 4	cr	-3.41 / -3.44	100.7	CSC/CSR
24	97	1	2	< 0.5	cr	-3.44 / -3.42	100.1	CSC/CSR

cr crushed ice: sample preparation as described in 4.3.1
cg columnar-grained ice

Table 4-3: *Triaxial laboratory tests on artificially frozen samples.*

The tests were focused on the original artificially frozen samples, and therefore no further parameter studies were carried out after cores from the first drillings at Muragl were available and the triaxial test devices were running as expected.

Four typical samples are shown in Figure 4-7 after a test. All samples are prepared using the method described above. In contrast to test No. 11 (Figure 4-7b), where pure ice was tested, test Nos. 9, 15 and 19 had 20.2%, 4.6% and 13.5% solids, respectively, more or less homogeneously distributed within the sample.

(a) (b) (c) (d)

Figure 4-7: *Four artificially frozen samples after a creep test.*
a) test No. 9 (w_i = 20%) *b) test No. 11 (w_i = 98%)*
c) test No. 15 (w_i = 5%) *d) test No. 19 (w_i = 14%)*

Constant stress creep tests (CSC)

The creep tests were carried out with several creep stages in order to determine the stress-dependency of the minimum creep rate for various samples. A creep stage lasted until the axial creep strain rate was more or less constant, so that a minimum creep rate could be established. This is shown in the various diagrams and was used for subsequent analysis. Further interpretation of the creep tests are given in Chapter 5.

After some time when the creep rate was thought to be nearly constant or an increase could be observed, either a new creep stage was applied or the creep phase of the test was stopped. An overview of the different creep stages and if an increase in creep rate (tertiary creep) was reached, is given in Table 4-4.

test No.	stage I		stage II		stage III		stage IV		stage V		stage VI		stage VII	
	kPa	d	kPa	d	kPa	d	kPa	d	kPa	d	kPa	d	kPa	d
1	220	2.9	-	-	-	-	-	-	-	-	-	-	-	-
2	207	2.8	-	-	-	-	-	-	-	-	-	-	-	-
4	208	3.7	-	-	-	-	-	-	-	-	-	-	-	-
9	97	28	186	24	169	8.9	-	-	-	-	-	-	-	-
11	100	28	197	24	294	28	268	12*	714	5.9*	-	-	-	-
13	94	4.6	199	4.1	397	3.3	789	3.4*	-	-	-	-	-	-
14	100	3.2	199	4.1	194	22	768	5.3*	-	-	-	-	-	-
15	198	2.8	396	6.9	767	4.1*	-	-	-	-	-	-	-	-
18^{+}	198	4.1	396	4.0	592	5.9	783	4.2*	960	2.9*	1112	0.5*	970	0.6*
19^{+}	201	4	420	4.2	496	3.8	589	3.4*	529	6.6*	491	3.0*	735	0.5*
20	199	4.0	393	4.2	483	3.8	567	3.4*	464	6.6	428	3.0	-	-
21	99	2.5	199	3.0	394	14	580	4.4*	472	4.0	739	1.0*	-	-
24	198	2.1	298	2.5	396	4.0	586	10*	768	1.3*	-	-	-	-

d duration of creep stage in days
* tertiary creep reached
$^{+}$ one additional creep stage

Table 4-4: *Total deviator stress and duration of the different creep stages on artificially frozen samples.*

Calculation of stresses

A change in cell volume was considered while deducing the axial stress from the axial load, even though the values might not be absolutely correct. However, this assumption is better than assuming that the sample remains at constant volume. The area $F(t)$ of the sample at a time t was calculated as follows:

$$F(t) = \frac{F_0 H_0 - \Delta V(t)}{H_0 - \Delta H(t)} \qquad [4\text{-}3]$$

F_0 area of the sample at the beginning of the test

H_0 height of the sample at the beginning of the test

$\Delta V(t)$ volume change at time t

$\Delta H(t)$ axial change of height at time t

Where the change of volume is not considered, [4-3] is reduced as follows and the area can be calculated as

$$F(t) = F_0 \cdot \frac{H_0}{H_0 - \Delta H(t)}. \qquad [4\text{-}4]$$

The influence for different values of net total volumetric strain, which are assumed to be reached at 17% axial strain on the area, and therefore on the deviatoric stress, can be seen in Figure 4-8. The volumetric strain ε_v remains equal to the axial strain ε_a for a constant area throughout the test. Because strains up to 20% could be reached during a creep tests, it is important to check the volume changes and to measure the volume at the end of a test in order to estimate the volumetric strain of the sample during a test. The results showed that stresses could be underestimated by more than 10%!

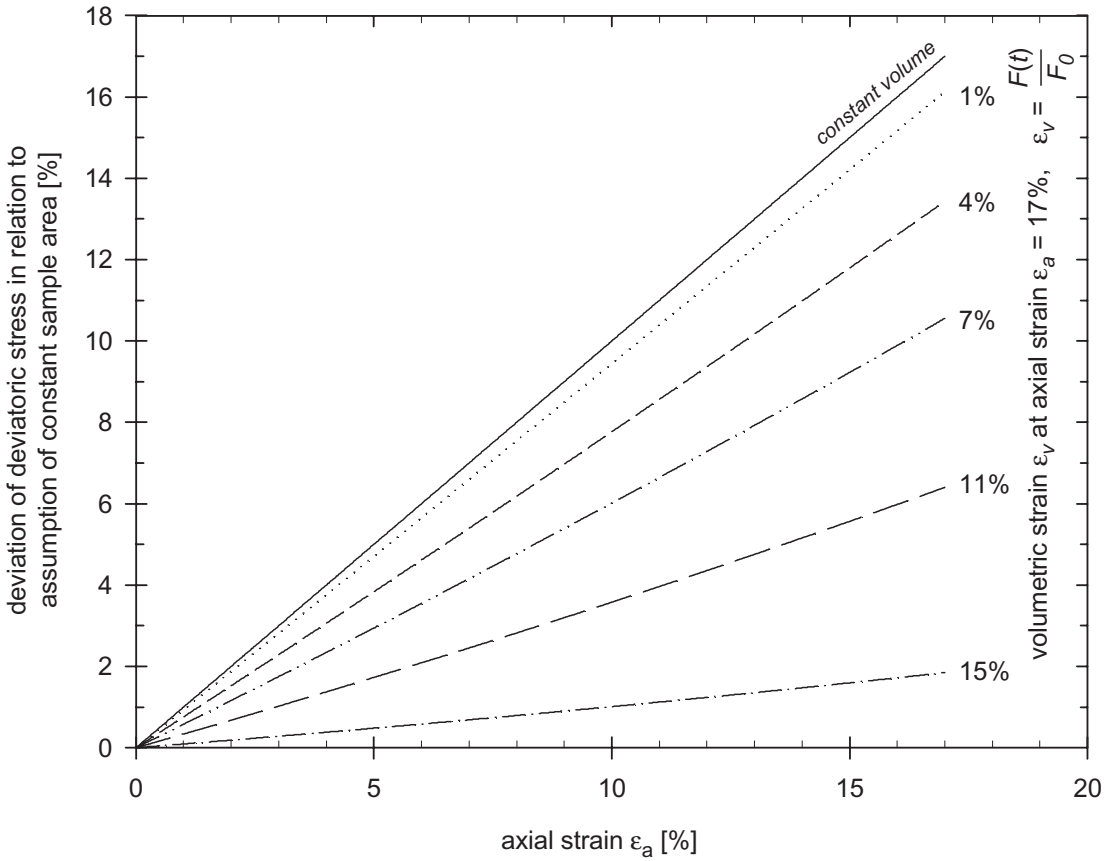

Figure 4-8: *Influence of volume change on the area for a triaxial sample: H_0 = 150 mm, D_0 = 75 mm for different volumetric strains at the end of axial deformation.*

Effect of sample composition

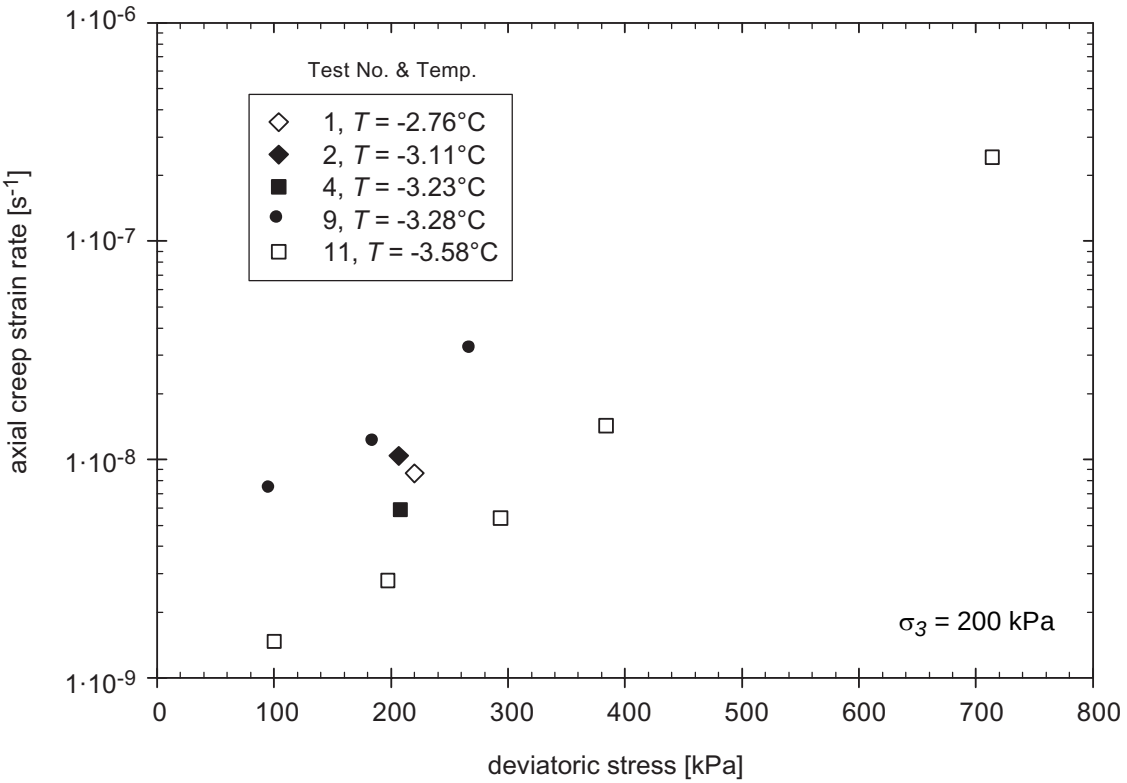

Figure 4-9: *Triaxial creep tests at a confining pressure of 200 kPa for different ice and soil mixtures.*

Only trends can be interpreted from the tests presented in Figure 4-9, since the amount of data is rather limited and the test quality was rather poor. In addition, there had not been a significant difference in temperature and composition between the tests. Nevertheless, the tests performed on a sample without any solid particles, test No. 11, which was carried out at the coldest temperature, shows the lowest minimum axial creep strain rates. The creep susceptibility of test No. 9, which had a volumetric ice content of 61% and a significant volumetric air content of about 20%, is the highest within this series. This test, however, has to be interpreted with caution, since the pore pressures measured at the top and the bottom of the sample have been close to the cell pressure, indicating that a leakage might have been present, even though the sample had not shown damages from the antifreeze at the end of the test.

Further effects of the sample composition are shown in Figure 4-10 for a confining pressure of 100 kPa.

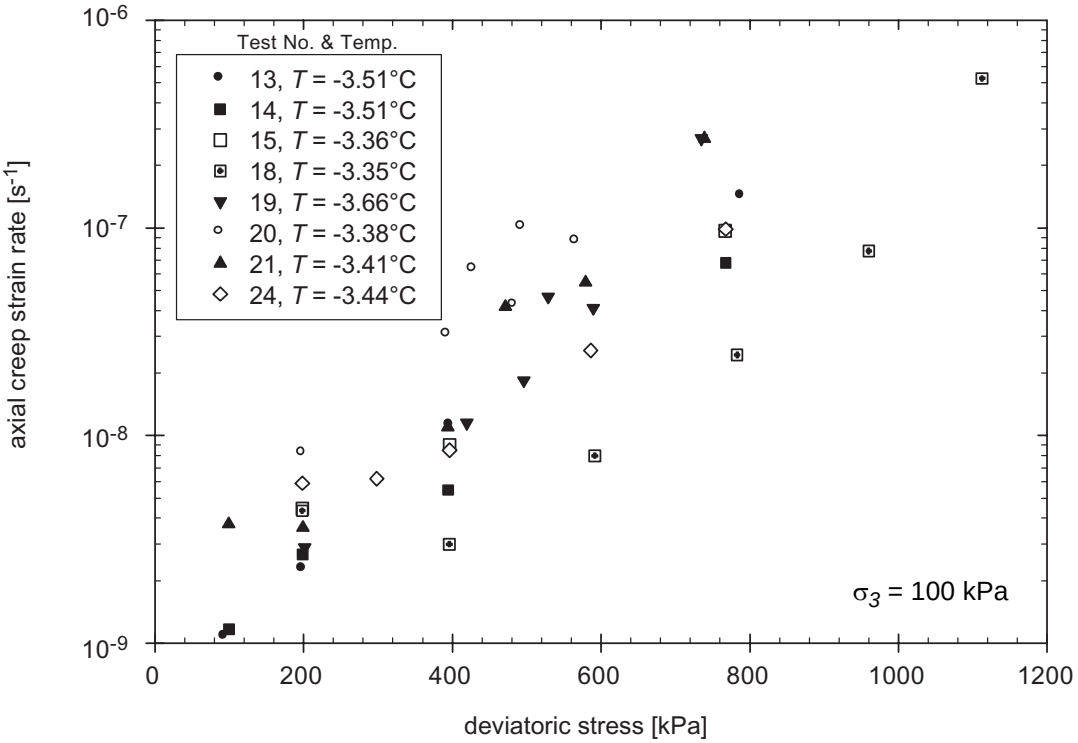

Figure 4-10: *Triaxial creep tests at a confining pressure of 100 kPa and temperature T = -3.5 ± 0.16°C for different soil mixtures.*

Test No. 18, which had the lowest volumetric ice content of these samples, showed the lowest axial creep strain rates. Slightly colder temperatures lead to lower creep strain rates, as can be shown by comparing test No. 14 (T = -3.51°C) with test No. 15 (T = -3.36°C). Both samples contained grain sizes between 0 and 16 mm and a volumetric ice content of about 90%. The influence of the grain sizes cannot be demonstrated using tests Nos. 15, 20, 21 and 24, since the differences are not noteworthy enough.

Tertiary creep

Most of the artificially prepared samples were brought to tertiary creep during at least one of the creep stages (see Table 4-4).

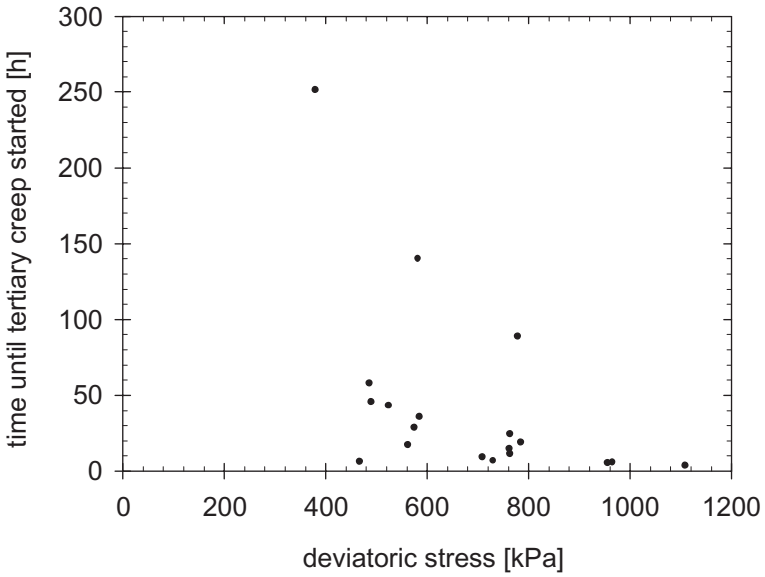

Figure 4-11: *Tertiary creep for artificially frozen samples.*

The time until tertiary creep occurred during each creep stage varied, depending on the composition of the samples and the temperature. Tertiary creep was only observed for deviatoric stresses higher than about 400 kPa (Figure 4-11), with test No. 11 providing the only exception. Several tests, that were loaded even for several weeks at deviatoric stresses up to 400 kPa, have not shown any sign of tertiary creep (Table 4-5).

test No.	deviatoric stress	time	test No.	deviatoric stress	time
9	97.1 kPa	27.7 d	**11**	100.0 kPa	27.7 d
9	185.6 kPa	23.7 d	**11**	197.4 kPa	23.7 d
9	268.6 kPa	8.8 d	**11**	293.6 kPa	28.2 d
14	394.4 kPa	21.5 d	**15**	393.2 kPa	6.9 d
18	591.6 kPa	5.9 d	**21**	394.3 kPa	13.8 d

Table 4-5: *Long term creep tests for artificial samples that failed to demonstrate tertiary creep during these stages.*

Effect of confining pressure

Two different confining pressures were chosen, which are in the range of the *in situ* stresses expected in the rock glaciers. No significant variations could be determined, implying that the small difference in confining pressure has nearly no influence on the sample response. In order to measure different behaviour much larger differences in the applied stress are necessary (e.g. Ladanyi, 1981). In addition, the number of tests that can be used was so limited that no further conclusions can be drawn at this point.

Summary of triaxial creep tests on artificial samples

Despite the limited number of tests that could be analysed, some major conclusions can be drawn:

- Increasing temperatures result in increasing axial creep strain rates.
- Both the volumetric ice content and the air content have a strong influence on the creep behaviour. Increasing volumetric ice content and air content result in increasing axial creep strain rates.
- The grain size distribution does not seem to have a major influence on the creep strains within the tested range.

These preliminary conclusions were considered when preparing the type of tests for the samples obtained from the two rock glaciers.

Constant strain rate tests (CSR)

As shown in Table 4-3, several tests were carried out with constant strain rates in order to determine maximum and residual shear strength as a function of the composition and axial strain rate. Some of the tests were conducted at the end of a creep test, so that the pre-shear test deformation was already significant. A relaxation step of more than 24 hours was applied before the samples were sheared in order to let the creep stresses disappear so that some self healing may occur. An overview of the relevant results is given in Table 4-6, and the dependency of the peak values and residual values on the axial strain rate are shown in Figures 4-12a and b, respectively.

test No.	creep	σ_3	$\dot{\varepsilon}$	ε_{start}	q_{max}	$\Delta\varepsilon_{qmax}$	q_{res}	temperature
		[kPa]	[$10^{-5}s^{-1}$]	[%]	[kPa]	[%]	[kPa]	[°C]
1	yes	201	4.80	2.5	2998.1	1.03	1584.9	-3.21 ± 0.02
2	yes	204	4.84	3.5	2809.7	0.72	1370.8	-3.15 ± 0.02
4	yes	200	4.78	2.2	3032.2	0.64	1441.3	-3.21 ± 0.04
6	-	200	4.71	0.0	2608.0	0.44	863.7	-3.22 ± 0.01
7	-	200	4.75	0.0	3172.0	0.42	1522.8	-3.20 ± 0.01
10	-	200	6.37	0.2	2899.9	0.82	1460.5	-3.44 ± 0.01
12	-	200	6.32	0.0	2142.9	0.96	1303.2	-3.42 ± 0.05
14	yes	100	0.98	7.7	1851.1	0.85	1516.7	-3.48 ± 0.01
15	yes	100	1.02	10.1	1748.0	0.85	1267.3	-3.36 ± 0.02
18	yes	100	1.23	13.0	2016.5	0.78	1497.0	-3.37 ± 0.02
19	yes	101	0.98	9.1	1625.0	0.77	1222.5	-3.70 ± 0.02
20	yes	101	1.04	15.1	1496.2	0.84	1205.8	-3.33 ± 0.02
21	yes	100	0.74	8.9	1668.9	0.75	1210.6	-3.44 ± 0.03
24	yes	100	0.07	4.6	1157.0	0.58	882.0	-3.42 ± 0.05

Table 4-6: *Triaxial shear tests on artificially frozen samples.*

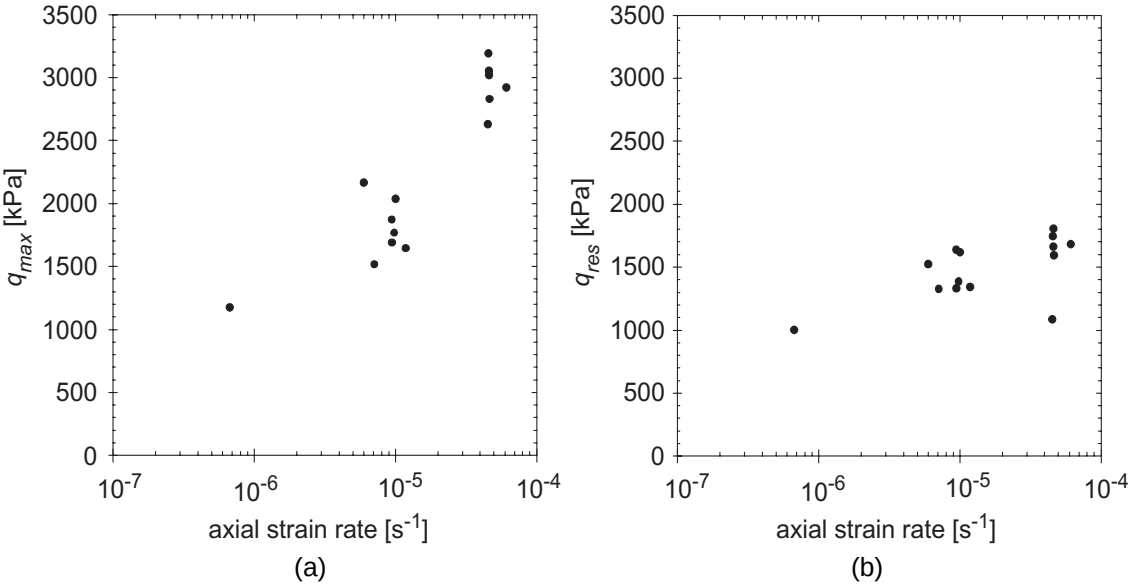

Figure 4-12: *Influence of the strain rate on peak values of shear stress (a) and residual values of shear stress (b) for triaxial shear tests on artificially frozen samples.*

As expected, higher peak values were recorded for higher strain rates. On the other hand, there is a smaller influence of the strain rate on the residual value. The influence of dilatancy, defined as the difference between the peak and the residual value of shear stress, reduces with decreasing strain rate. The value of q_{max}/q_{res} was about 1.8 ± 0.2 for the high shearing velocities, whereas this value was about 1.3 ± 0.1 for axial strain rates of around $1.0 \cdot 10^{-5}$ s^{-1}. The composition of the sample did not largely affect the strength of the material within the range of samples tested. However, the variation in the samples and test conditions had been too large to be able to make definite statements. Further investigations are necessary.

Comparing the ratio between the maximum and the residual shear strength with the volumetric ice content, a general trend showed a decrease of this ratio with increasing ice content (Figure 4-13). However, some samples with 100% ice showed rather high differences between the two shear strengths. This was due to the preparation of the samples. The samples that were made of columnar-grained ice showed a much stiffer response up to brittle failure and therefore produced much higher maximum shear strengths. As soon as some air was trapped between the crystals, as for the crushed ice samples, the response was much more ductile.

The effect of the air can also be shown in Figure 4-14, where the ratio between the maximum and the residual shear strength is compared with the volumetric air content. This ratio decreases with increasing volumetric ice content for similar volumetric ice contents, even though it had not been easy to determine the percentage of air in the frozen samples.

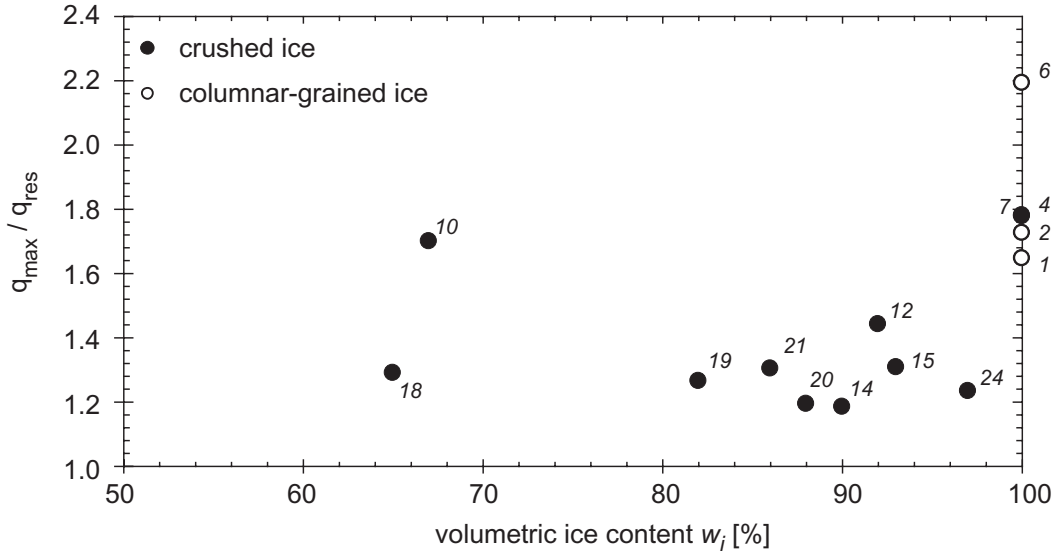

Figure 4-13: *Peak shear strength normalised by residual shear strength versus volumetric ice content for artificially frozen samples. The numbers close to the data points indicate the individual test number (see Table 4-6).*

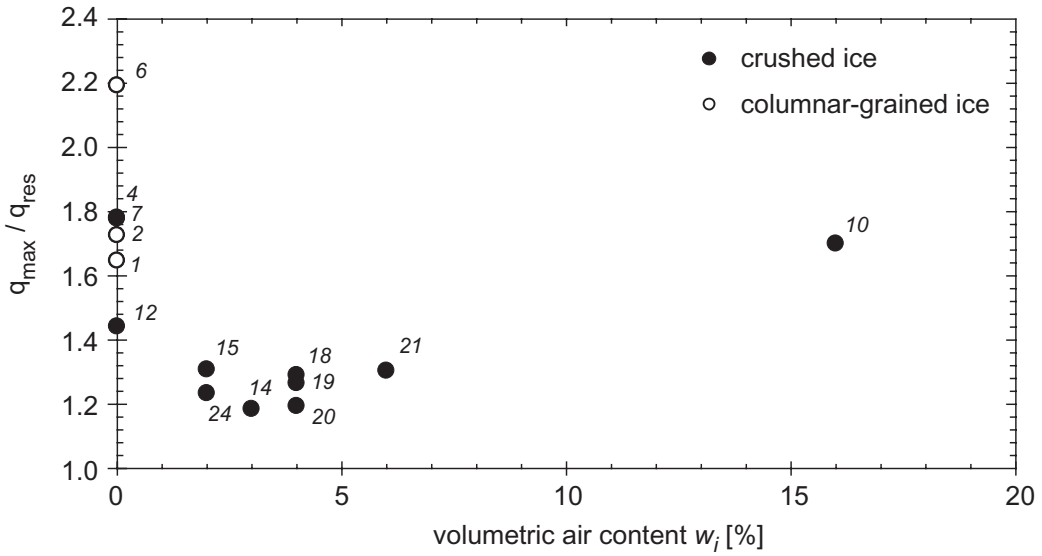

Figure 4-14: *Peak shear strength normalised by residual shear strength versus volumetric air content for artificially frozen samples. The numbers close to the data points indicate the individual test number (see Table 4-6).*

All tests showed a rather stiff response and the peak strength was reached within 0.4% to 1.0% axial strain, with a mean value of 0.75%, independent of the strain rate or on whether creep strains were allowed or not before the CSR-test started.

4.4 Testing of Cored Samples

Even though the results obtained from the artificially frozen samples are insufficient in themselves, the author decided to proceed with tests on the soil samples from the two rock glaciers once they were available. The main goal, which had been the testing and refinement of the triaxial testing devices as well as the preparation and installation of the samples, was achieved using the artificially frozen samples. In addition to the results obtained, recommendations have been made for future research by focusing on distinct problems arising during the tests from this test series on *in situ* samples.

4.4.1 Sample Characteristics

The permafrost samples tested herein originate from two rock glaciers, with quite different characteristics, as described in Chapter 3. Even though the volumetric ice content is rather different, in particular for the upper 20 m within the Murtèl-Corvatsch rock glacier, the structure and its formation are similar. The interstitial ice is granular, with grains of different sizes, varying with depth (cf. Chapter 4.5). A mean c-axis orientation with a value close to the slope angle of the surface was determined for a sample at a depth of 9.5 m from analyses of the cores drilled in 1987 (Haeberli *et al*., 1990b). However, the granular characteristics at a depth of about 12.6 m (e.g. Figure 3-33) leads to the assumption that the c-axis orientation was rather random.

The samples were stored in their plastic liner in a freezer at -18°C (on site, during transport and prior to testing) after taking them out of the inner steel liner of the drilling string. The samples were cut into a length of about 15 cm using a circular saw. A specially constructed guide system allowed a coplanar top and bottom surface to be manufactured. The friction generated when sawing samples with low volumetric ice content led to local melting of the ice, which was later replaced by refreezing. However, it was thought that the influence of the artificially refrozen edges on the end results of the tests was negligible, since tests of samples with refrozen edges showed similar responses to samples without repairs. Samples that were ready to be tested were stored within the plastic liner in the cold chamber at the temperature at which the tests were to be carried out. It could then be guaranteed that a uniform temperature existed within the sample. The plastic liner was removed just before the sample was put into the triaxial testing device, in a similar way to the artificially frozen samples.

Mechanical as well as thermal disturbances from transport, storage and preparation of the sample, have to accepted, but strenuous efforts have to be made to keep them to a minimum. Thin sections showed that melting and refreezing occurred at the edge of some samples. The main response of the sample should not be influenced, since only minor parts of them were affected directly. Nevertheless, these disturbances, which may influence up to 5% of the area, have to be kept in mind while analysing the test results.

4.4.2 Overview of the Samples

Numerous problems occurred at the beginning of the test series with the cored samples with the impermeability of the system, resulting in the loss of various samples during the first creep stage. The samples obtained from the Muragl rock glacier had been of very limited quality in any case, so that only a few results could be obtained. The sample had to be without obvious mechanical damage over a length of at least 16 cm, in order to be able to use it for triaxial testing. Samples of that quality were only available from borehole 4/1999. The composition of all of the samples are combined for presentation in Figure 4-15, even though only five of the samples could be analysed after a successful test.

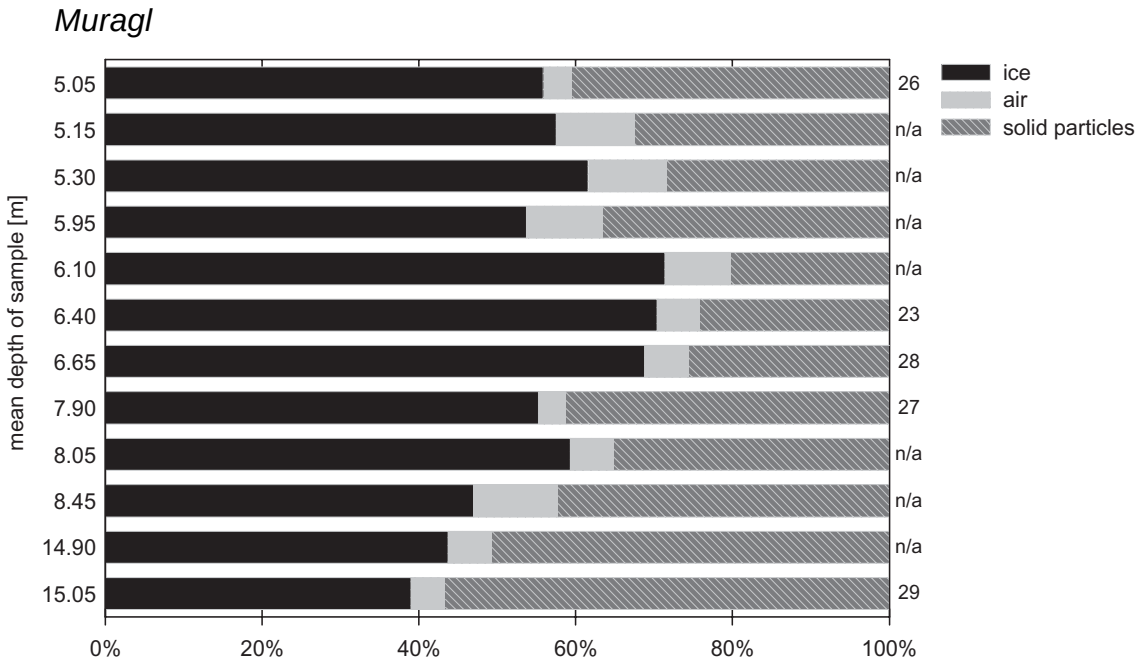

Figure 4-15: *Different phases of the samples tested from the Muragl rock glacier borehole 4/1999 (figure at right hand side refers to test number).*

The sample quality of the boreholes drilled in the Murtèl-Corvatsch rock glacier in 2000 were quite good and therefore several tests could be carried out. Problems that occurred due to the thin rubber membrane during the tests with the Muragl samples were solved by using a second membrane. The loss of tests could therefore be reduced significantly. As shown in Figure 4-16, borehole 2/2000 delivered many more samples than the other borehole although good samples were obtained at greater depths within borehole 1/2000.

Murtèl-Corvatsch

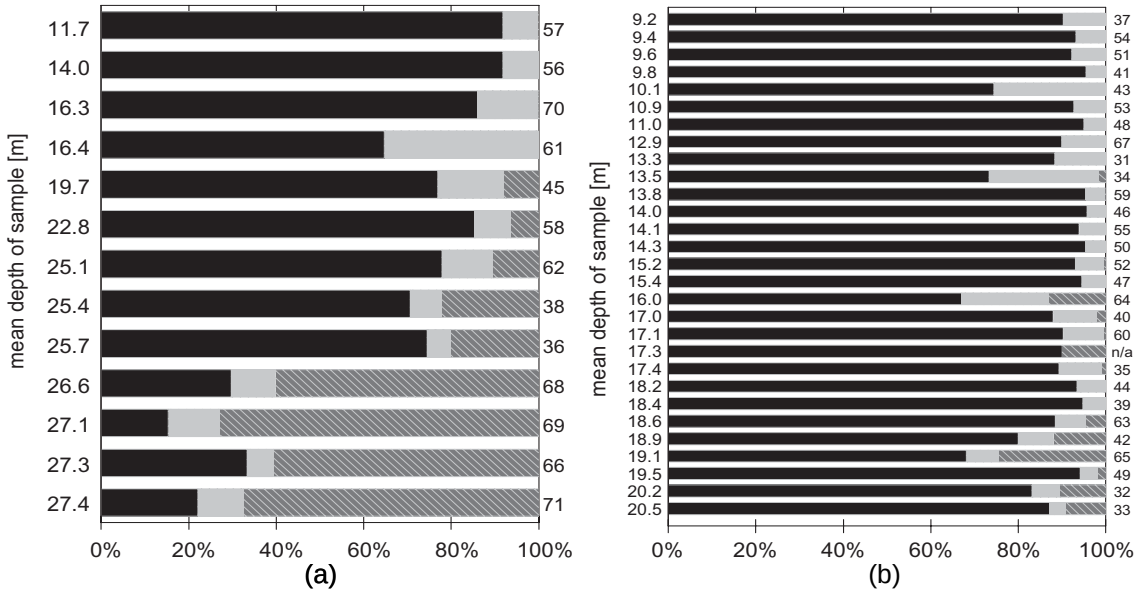

Figure 4-16: *Different phases of the samples tested from the Murtèl-Corvatsch rock glacier (figure at right hand side refers to test number).*
a) borehole 1/2000
b) borehole 2/2000

The determination of an accurate value of the volumetric ice content for samples with high percentage of solid particles had not been easy, since the shape of the samples was not always very smooth (Figure 4-17). The sample volume was determined using the height and the area at the top, the middle and the base and therefore, the rough surface of the sample could not be considered. Consequently, the calculated volumetric ice content for samples with high contents of solid particles may be too low and the volumetric air content too high. This fact has to be considered, when comparing test responses versus volumetric ice contents.

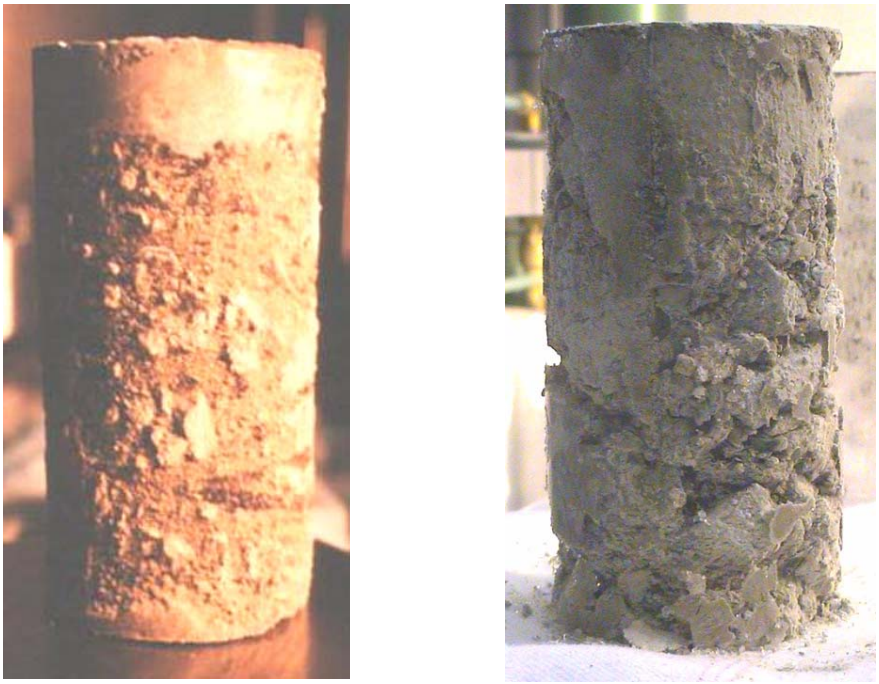

(a) (b)

Figure 4-17: *Samples No. 36 (a) and No. 69 (b). The volumetric ice content assuming a smooth sample surface was determined as being 74.5% and 15.4%, respectively.*

4.4.3 Creep Tests

Numerous creep tests were performed on samples from the Muragl and Murtèl-Corvatsch rock glaciers. In addition to the original composition and depth (see Figure 4-15 and Figure 4-16), the following parameters were varied:

- temperature: -1.1°C – -4.2°C
- sample composition: volumetric ice content between 15% and 100%
- confining pressure: 10 – 400 kPa
- number of creep stages 1 – 5
- tertiary creep: yes / no

Table 4-7 to Table 4-9 give an overview of the tests performed.

test No.	depth	σ_3	stage I		stage II		stage III		stage IV		stage V		temp.
	m	kPa	kPa	d	kPa	d	kPa	d	kPa	d	kPa	d	°C
26	5.00-5.15	151	202	4.0	304	4.9	397	3.0*	-	-	-	-	-3.43±0.02
23	6.40-6.55	200	152	11	302	7.0	402	9.0	598	5.0	789	1.3*	-3.72±0.05
28	6.65-6.80	300	200	3.5	397	6.6	585	4.0	-	-	-	-	-3.74±0.05
“	“	300	402	2.6	504	3.0*	-	-	-	-	-	-	-2.43±0.08
27	7.90-8.05	100	199	3.5	396	6.5	593	4.5*	-	-	-	-	-3.43±0.12
“	“	100	390	3.7	489	8.3	564	19	-	-	-	-	-2.08±0.04
29	15.05-15.20	100	488	19	-	-	-	-	-	-	-	-	-2.42±0.06

* tertiary creep reached

Table 4-7: *Triaxial creep tests on cored samples from borehole 4/1999, Muragl rock glacier.*

test No.	depth	σ_3	stage I		stage II		stage III		stage IV		stage V		temp.
	m	kPa	kPa	d	kPa	d	kPa	d	kPa	d	kPa	d	°C
56	13.90-14.05	200	392	0.7	487	4.0	576	2.2	-	-	-	-	-4.15±0.02
70	16.28-16.43	401	188	5.1	376	6.6	559	11	-	-	-	-	-3.89±0.09
61	19.60-19.75	201	175	15	-	-	-	-	-	-	-	-	-4.15±0.04
45	22.72-22.87	200	184	11	352	6.0	483	2.0	-	-	-	-	-1.15±0.05
58	25.00-25.15	200	355	0.7	434	4.0	537	3.4*	599	2.6	-	-	-4.45±0.04
62	25.32-25.47	201	194	4.6	383	3.4	565	6.9	-	-	-	-	-3.90±0.04
38	25.60-25.75	200	150	4.3	293	3.8	382	3.3	548	3.6*	658	2.2	-2.26±0.03
36	25.85-26.00	201	199	6.6	384	6.5	529	4.6	624	1.0	-	-	-2.02±0.02
68	26.57-26.72	200	199	3.9	397	11	593	8.8	801	7.0	-	-	-4.28±0.08
69	27.01-27.16	200	198	3.7	395	3.4	601	9.6	1006	14	-	-	-3.74±0.19
66	27.16-27.31	201	196	6.0	395	5.0	595	12	795	6.0	1181	4.7	-4.00±0.13
71	27.31-27.46	400	200	1.8	-	-	-	-	-	-	-	-	-4.42±0.05

* tertiary creep reached

Table 4-8: *Triaxial creep tests on cored samples from borehole 1/2000, Murtèl-Corvatsch rock glacier.*

test No.	depth	σ_3	stage I		stage II		stage III		stage IV		stage V		temp.
	m	kPa	kPa	d	kPa	d	kPa	d	kPa	d	kPa	d	°C
37	9.21-9.36	200	194	7.5	365	8.0	432	6.9	639	1.1*	-	-	-1.97±0.03
54	9.36-9.51	10.4	199	3.6	1185	1h$^+$	-	-	-	-	-	-	-1.08±0.04
51	9.51-9.66	200	200	4.2	386	3.8	534	5.0	-	-	-	-	-1.35±0.03
41	9.75-9.90	401	149	2.2	295	6.1	485	3.1*	555	4.5	-	-	-2.05±0.09
43	10.00-10.15	50.0	138	5.4	251	7.6	-	-	-	-	-	-	-2.09±0.11
53	10.80-10.95	300	196	3.6	1241	1h$^+$	-	-	-	-	-	-	-1.12±0.05
67	12.81-12.96	200	194	7.0	377	8.1	553	8.8	-	-	-	-	-4.06±0.09
31	13.25-13.40	150	64.6	13	191	6.8	377	7.0	511	4.3	-	-	-2.07±0.04
34	13.40-13.55	400	181	5.0	262	6.1	330	7.5	469	1.2	-	-	-2.05±0.03
59	13.77-13.92	200	197	4.0	398	7.2	570	11	592	6.2	-	-	-4.16±0.05
46	13.92-14.07	201	199	6.0	393	3.1	766	0.9	1082	0.4	-	-	-1.08±0.05
55	14.07-14.22	200	198	3.6	1312	2h$^+$	-	-	-	-	-	-	-1.33±0.03
50	14.22-14.37	201	199	4.2	391	3.8	555	5.0	-	-	-	-	-1.07±0.03
52	15.17-15.32	200	197	3.9	386	3.4	549	4.6	-	-	-	-	-1.14±0.02
47	15.32-15.47	200	196	11	379	6.0	535	3.1	643	3.5	-	-	-1.35±0.04
60	17.05-17.20	200	200	6.8	383	11	560	6.2	-	-	-	-	-4.41±0.06
35	17.35-17.50	200	198	4.3	292	6.1	370	7.5	518	9.3	903	0.2*	-2.26±0.03
44	18.10-18.25	50.0	150	2.0	296	3.4	471	3.1	523	4.5	-	-	-2.34±0.10
39	18.36-18.51	201	198	1.9	291	3.8	346	3.3	541	3.6	653	2.4	-2.00±0.02
63	18.51-18.66	200	196	4.6	394	3.4	572	9.4	762	1.5*	-	-	-3.94±0.05
65	19.05-19.20	200	200	3.6	401	3.4	589	9.6	817	1.5*	-	-	-4.23±0.04
32	20.16-20.31	150	149	13	292	6.8	478	7.0	613	4.3	-	-	-2.38±0.05
33	20.47-20.62	250	197	7.8	390	4.7	561	5.3	668	3.8	-	-	-2.06±0.03

* tertiary creep reached
$^+$ creep failure

Table 4-9: *Triaxial creep tests on cored samples from borehole 2/2000, Murtèl-Corvatsch rock glacier.*

Effect of sample composition and temperature

The tests presented in Figure 4-18 are all carried out at a confining pressure of about 200 kPa. The temperatures, and the volumetric ice content varied as shown in the table adjacent to the diagram.

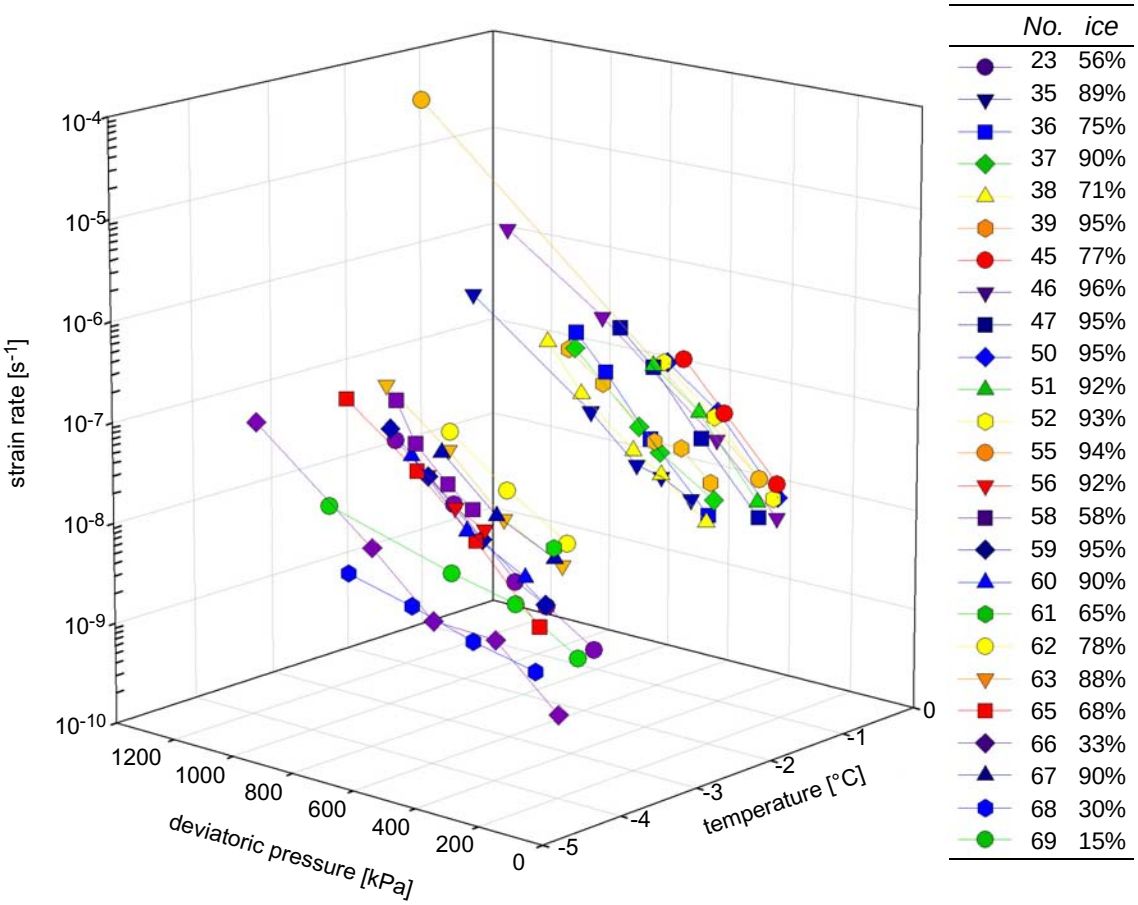

Figure 4-18: *Triaxial creep tests at σ_3 = 200 kPa for different volumetric ice contents and temperatures.*

The temperature and ice content are the major parameters influencing the creep strain rate. Test No. 23, which has a volumetric ice content of only 56%, shows the lowest axial strain rates, whereas test No. 56, that had a higher ice content (92%), was performed at a lower temperature, showed a much higher strain rate. The increase in ice content could not completely compensate for the decrease in temperature. On the other hand, the strain rate of the tests performed at warmer temperatures (-1.0 – -2.0°C), but similar ice content (e.g. Nos. 35, 37, 39, 46, 47, 50, 51, 52 & 55: w_i = 89 – 96%), is higher than for test No. 56.

Detailed analyses of the data will be made in the next main section (see Chapter 5). In the following, a simple power law was used to fit the axial creep rates against the applied stress in order to study the influence of the temperature and volumetric ice content (equation [2-30]):

$$\dot{\varepsilon} = A \cdot q^n$$

For every test, *A* and *n* values were determined (cf. Chapter 5.1) and the axial creep rates for representative deviatoric stresses *q* between 200 and 800 kPa were interpolated or extrapolated where necessary (Figure 4-19 and Figure 4-20).

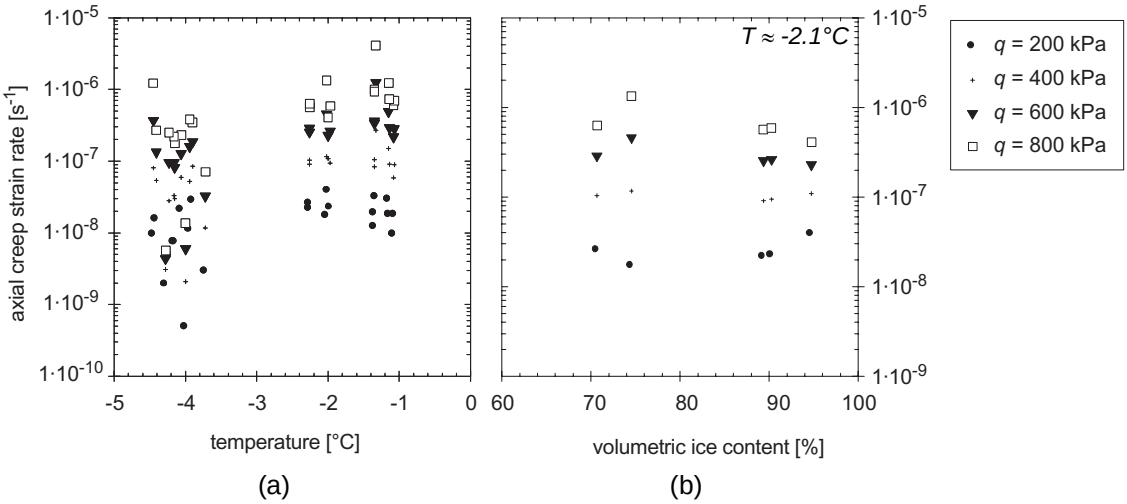

Figure 4-19: *Axial creep strain rate as a function of (a) the temperature and (b) the volumetric ice content for samples from both rock glaciers.*

In contrast to the volumetric ice content, a temperature dependency can be shown in relation to the strain rates. The creep rate increases with increasing temperature (Figure 4-19a), whereas nearly no influence of a volumetric ice content larger than 65% on the creep rate can be observed for the samples tested at -2.1°C and -1.2°C (Figure 4-19b & Figure 4-20a). The samples tested at a colder temperature (T ≈ -4.2°C) had lower ice contents and for these tests, a significant difference in the axial creep strain was measured (Figure 4-20b). There seems even to be a peak in the axial creep strain rate for a volumetric ice content between 85 and 95% at about -4.2°C.

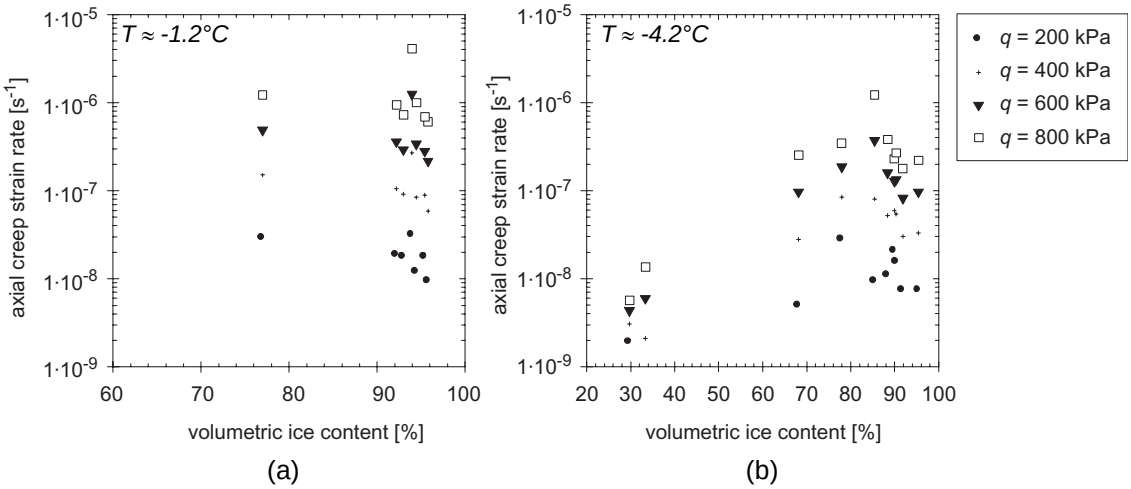

Figure 4-20: *Axial creep strain rate as a function of the volumetric ice content for two different temperatures: a) T ≈ -1.2°C, b) T ≈ -4.2°C.*

Effect of confining pressure

Several tests were carried out at various confining pressures σ_3 in order to study the effect of this variable on the axial creep strain rate (Figure 4-21).

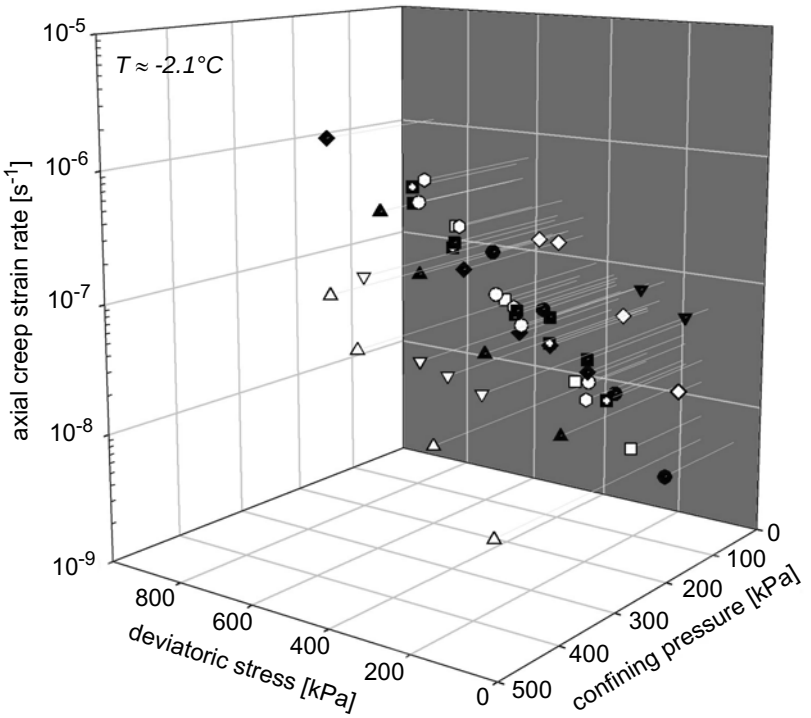

No.	ice	σ_3
31	88%	150kPa
32	83%	150kPa
33	87%	250kPa
34	73%	400kPa
35	89%	200kPa
36	75%	201kPa
38	71%	200kPa
37	90%	200kPa
39	95%	201kPa
41	96%	401kPa
43	74%	50kPa
44	93%	50kPa

Figure 4-21: *Effect of confining pressure and deviatoric stress at a temperature of -2.1°C.*

Similar to the previous analyses, equation [2-30] was used to show the dependency of creep rate on confining pressure for distinct deviatoric stress at a temperature of about -2.1°C (Figure 4-22). A slight decrease of the minimum creep rate was observed for low deviatoric stresses with increasing confining pressure. But the confining pressure does not appear to influence the creep velocity for higher deviatoric stresses.

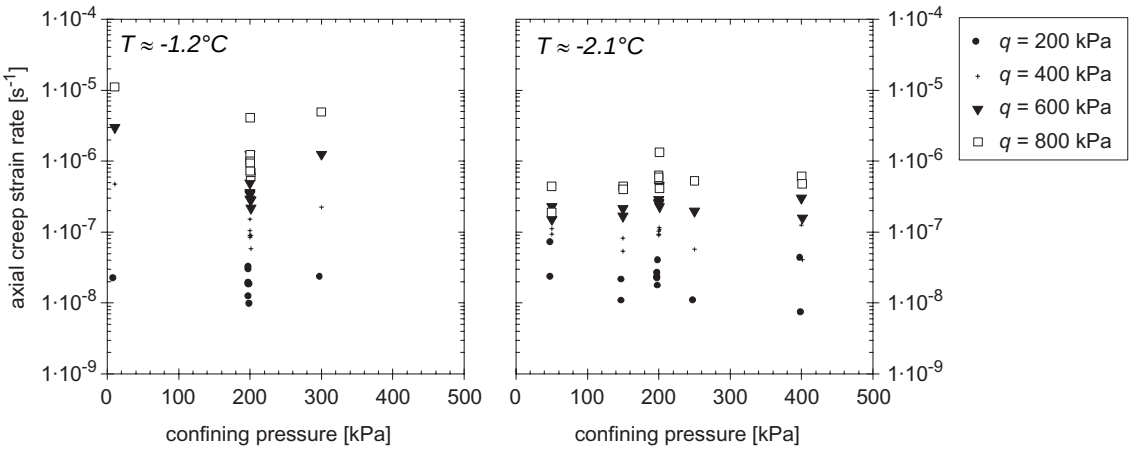

Figure 4-22: *Effect of confining pressure at a temperature of -1.2°C and -2.1°C.*

Creep stages

Up to five creep stages were applied to the same sample, since the number of cores was very limited and the differences between the cores could vary intensively. Some tests were carried out in order to study the effect of applying a new loading step on an already loaded sample. Therefore, two more or less identical samples were chosen, of which one was loaded directly with an axial load, while the other was brought to the same loading condition by smaller steps.

Test No. 29, that had a volumetric ice content of 39%, was loaded in one step to a deviatoric stress of about 490 kPa. A creep strain rate of $1.5 \cdot 10^{-8}$ s^{-1} was measured after more than 400 hours (Figure 4-23), which was thought to be the minimum. In comparison, test No. 27 was preloaded for more than 18 days with various creep stages at two different temperatures. After that time and an axial strain of 2.2%, a creep stage with a deviatoric stress of 490 kPa was applied. A minimum creep strain rate of $2.3 \cdot 10^{-8}$ s^{-1} was determined after about 90 hours of loading. The tests were carried out at temperatures of -2.42°C (No. 29) and -2.08°C (No. 27), respectively. The slightly higher creep rate for the second sample may be explained by the higher ice content of 55% and the warmer temperature. This comparison showed that similar minimum creep strain rates can be determined from single or multi-stage creep tests and that for the individual step, shorter times can be expected until this minimum is achieved.

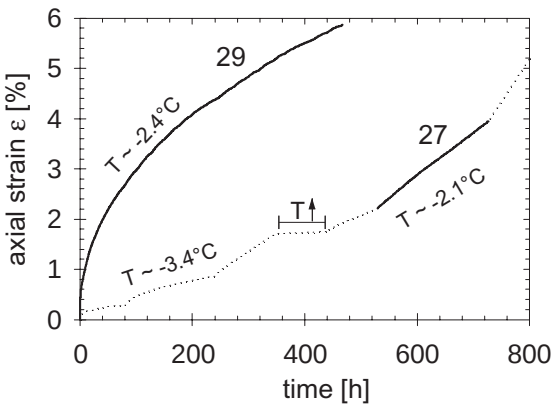

Figure 4-23: *Effect of the number of creep stages on the creep strain rate for two samples from the Muragl rock glacier.*
No. 27: T = -2.08°C, w_i = 55%
No. 29: T = -2.42°C, w_i = 39%

Volumetric creep strains were also analysed. Even though the volumetric measurements are not accurate for absolute values, they can reveal relative information, in particular since the strain rate is derived from the volumetric strain, and hence an increase in accuracy can be expected. For test No. 27, a volumetric strain rate of $2.6 \cdot 10^{-8}$ s^{-1} was determined and for test No. 29, $7.5 \cdot 10^{-9}$ s^{-1}, respectively for q = 490 kPa. Considering the measuring technique used, these values are more or less in the same range, also indicating that multiple stage creep tests are a good tool for the determination of stress dependent creep strain rates.

The difference in the total strain can be explained by the slightly higher air content of sample No. 29. Due to the high percentage of solid particles and a rough top of the sample, it is also possible that the top platten has not been perfectly seated on the sample and therefore the strains were recorded at the beginning, even though the sample was not compressed over the whole area.

Tertiary creep

Creep is usually divided into three stages: i) primary, ii) secondary or steady state and iii) tertiary creep (Figure 2-27). The latter is characterised by an increase in the strain rate up to creep failure. During the current research the main focus was on stress conditions that are present within a rock glacier at depths up to 70 m. No tertiary creep was reached under these stress conditions within the testing time (see Table 4-7 – Table 4-9). However, some tests were carried out in order to investigate when tertiary creep might play an important role.

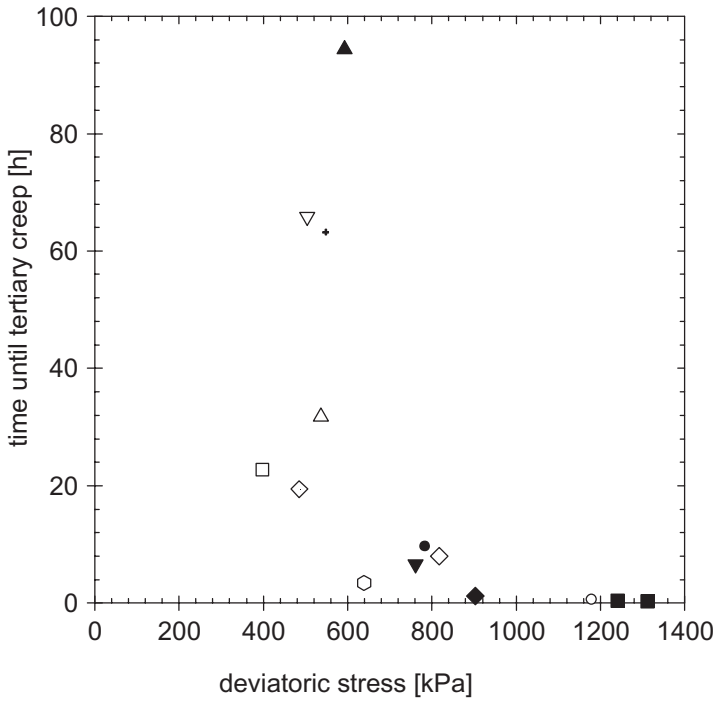

	No.	ice	σ_3	temp.
●	23	70%	200kPa	-3.72°C
□	26	56%	151kPa	-3.43°C
▲	27	55%	100kPa	-3.43°C
▽	28	69%	300kPa	-2.43°C
◆	35	89%	200kPa	-2.26°C
⬡	37	90%	200kPa	-1.97°C
+	38	71%	200kPa	-2.26°C
◇	41	96%	401kPa	-2.05°C
▪	53	93%	300kPa	-1.12°C
○	54	93%	10kPa	-1.08°C
■	55	94%	200kPa	-1.33°C
△	58	85%	200kPa	-4.45°C
▼	63	88%	200kPa	-3.94°C
◇	65	68%	200kPa	-4.23°C

Figure 4-24: *Tertiary creep for various tests on samples from both rock glaciers.*

The temperature influence is very important, when comparing the time until tertiary creep starts. In order to reach about the same time (4-6h) at a temperature of -2.0°C (No. 37), the deviatoric stress had to be increased from 640 kPa to 790 kPa at a temperature of -3.7°C (No. 63). The difference in ice content might have played an important role as well. Comparing the data for deviatoric stresses between 400 and 600 kPa, the ice content is the factor that influences tertiary creep. Test No. 27 had the lowest volumetric ice content and shows the longest resistance against an acceleration of the creep strain rate.

The confining pressure is observed to be of a secondary importance, which is similar to the findings relative to the axial creep strain rates. The tests Nos. 28 and 38 had different confining pressures but equivalent volumetric ice content and temperature and showed very similar behaviour.

In theory, tertiary creep occurs when an acceleration in the creep strain rate is measured. But the samples tested have not shown such text book behaviour, since the boundary conditions within the sample change due to an acceleration

in axial deformation. Figure 4-25 shows two typical curves for tertiary creep. After a minimum in axial creep strain rate was reached (1) an acceleration could be observed. However, this acceleration did not continue up to creep failure but decreased again and the axial creep strain rate levelled off at a new value (2). This effect might have two reasons:

1. Due to an increase in axial deformation, an increase in the area occurred and therefore the axial stress decreased since the test was controlled with the axial load.
2. Ongoing deformation of the sample resulted in a compaction of the material and therefore the sample may be stiffer and consequently only showed steady state creep under the current axial load.

An attempt was made to compensate for an increase in the area with an increase of the axial load by considering the change in the cell volume.

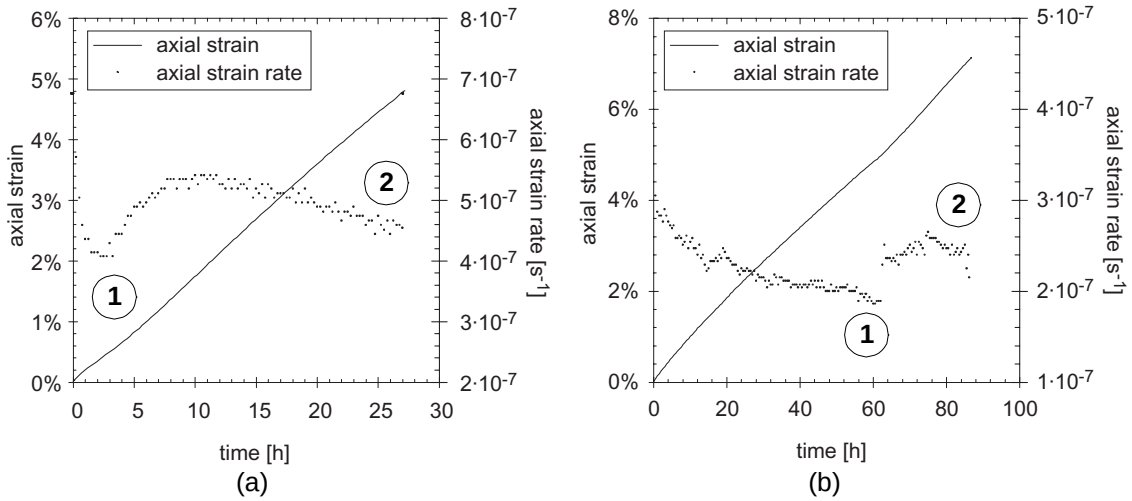

Figure 4-25: *Axial strain and axial strain rate versus time for two representative samples that showed tertiary creep during their fourth creep stage.*
a) Sample No. 37, q = 639 kPa
b) Sample No. 38, q = 548 kPa

The tests demonstrated that this four phase material is able to resist stress concentrations, accompanied by tertiary creep. This could be a kind of stick-slip mechanism, in which the stress built up, leading to an acceleration in the creep rate, until stress redistribution and structural changes occurred together with a reduction in the creep rate.

Similar to the observations made for artificially frozen samples, several tests never reached tertiary creep, even though deviatoric stresses of more than 350 kPa were applied for several days (Table 4-10).

test No.	deviatoric stress	time	test No.	deviatoric stress	time
27	563.9 kPa	18.5 d	**66**	595.3 kPa	12.2 d
29	487.6 kPa	19.5 d	**67**	552.8 kPa	8.8 d
35	518.2 kPa	9.3 d	**68**	396.6 kPa	11.2 d
59	570.3 kPa	11.0 d	**68**	593.2 kPa	8.8 d
60	383.4 kPa	11.0 d	**69**	1005.8 kPa	14.2 d
63	572.2 kPa	9.4 d	**70**	559.1 kPa	11.2 d
65	589.0 kPa	9.6 d			

Table 4-10: *Long term creep tests for rock glacier samples that did not reach tertiary creep within creep stage test duration of more than 8 days.*

4.4.4 Constant Strain Rate Tests

A strain rate controlled shear test was performed for most of the tests at the end of the multi-stage creep tests. A relaxation of at least 30 hours was imposed before starting the test, in order to allow stress release and self-healing of the sample. Characteristic values for the tests performed are given in Table 4-11 – Table 4-13.

test No.	σ_3	$\dot{\varepsilon}$	ε_{start}	q_{max}	$\Delta\varepsilon_{qmax}$	q_{res}	temp.
	[kPa]	[$10^{-5}s^{-1}$]	[%]	[kPa]	[%]	[kPa]	[°C]
23	200	0.07	4.3	1236.0	0.47	901.2	-3.70 ± 0.09
26	151	0.02	8.4	373.1	9.68	373.1	-3.43 ± 0.13
27	100	0.72	10.3	2147.6	0.35	1433.4	-2.08 ± 0.03
28	300	7.00	12.5	1425.6	0.63	799.2	-2.48 ± 0.01
29	100	0.67	5.9	1456.3	0.81	1253.9	-2.41 ± 0.04

Table 4-11: *Test characteristics for samples from borehole 4/1999, Muragl rock glacier.*

test No.	σ_3	$\dot{\varepsilon}$	ε_{start}	q_{max}	$\Delta\varepsilon_{qmax}$	q_{res}	temp.
	[kPa]	[$10^{-5}s^{-1}$]	[%]	[kPa]	[%]	[kPa]	[°C]
36	201	0.92	26.3	1136.8	1.00	1060.7	-2.10 ± 0.02
38	200	0.84	23.8	1267.8	0.94	1167.4	-2.31 ± 0.02
45	200	0.09	18.3	653.0	0.70	601.6	-1.13 ± 0.04

Table 4-12: *Test characteristics for samples from borehole 1/2000, Murtèl-Corvatsch rock glacier.*

test No.	σ_3 [kPa]	$\dot{\varepsilon}$ [$10^{-5}s^{-1}$]	ε_{start} [%]	q_{max} [kPa]	$\Delta\varepsilon_{qmax}$ [%]	q_{res} [kPa]	temp. [°C]
58	200	0.74	33.7	1479.8	1.17	1391.7	-4.42 ± 0.03
61	200	0.88	16.8	697.8	2.25	682.2	-3.98 ± 0.02
62	200	0.08	16.8	812.0	1.35	769.3	-3.84 ± 0.05
66	200	0.72	5.9	2556.3	0.77	2209.5	-3.94 ± 0.01
68	200	0.67	2.6	2534.2	1.00	1896.0	-4.37 ± 0.04
69	200	0.70	5.1	2477.7	0.75	2034.7	-3.61 ± 0.07
70	401	0.92	23.7	1678.7	1.15	1358.8	-3.90 ± 0.01

Table 4-12: *Test characteristics for samples from borehole 1/2000, Murtèl-Corvatsch rock glacier.*

test No.	σ_3 [kPa]	$\dot{\varepsilon}$ [$10^{-5}s^{-1}$]	ε_{start} [%]	q_{max} [kPa]	$\Delta\varepsilon_{qmax}$ [%]	q_{res} [kPa]	temp. [°C]
31	150	0.79	14.8	1307.4	0.51	1058.4	-2.07 ± 0.02
32	150	0.83	16.3	1432.1	0.92	1262.3	-2.39 ± 0.02
33	250	0.85	22.6	1374.1	0.80	1193.6	-2.06 ± 0.02
34	400	0.84	19.1	1226.1	0.88	1016.0	-2.03 ± 0.02
35	200	0.01	25.2	483.7	0.65	483.7	-2.20 ± 0.06
37	200	0.09	22.3	922.6	0.72	699.7	-1.99 ± 0.04
39	201	0.88	23.3	1664.7	0.68	1230.4	-2.04 ± 0.02
41	401	0.75	10.5	1609.1	0.55	1243.3	-1.97 ± 0.03
43	50.0	0.80	19.6	755.2	1.04	734.1	-2.02 ± 0.02
44	49.9	0.79	16.3	1484.1	0.69	1161.4	-2.27 ± 0.02
46	201	0.08	13.3	983.0	0.90	841.8	-1.05 ± 0.07
47	200	0.88	25.6	1922.9	0.92	1278.4	-1.36 ± 0.01
50	201	0.08	15.7	908.7	0.67	750.7	-1.06 ± 0.06
51	200	0.40	19.1	1243.7	0.75	965.8	-1.36 ± 0.04
52	200	4.07	16.1	1881.9	0.37	1464.9	-1.16 ± 0.01
67	200	0.79	19.8	1686.7	0.75	1391.5	-3.87 ± 0.08
59	200	0.79	22.5	1957.6	1.06	1784.7	-4.04 ± 0.01
60	200	0.76	17.0	1711.7	1.06	1512.0	-4.33 ± 0.01
63	200	0.84	19.5	1690.3	1.07	1424.0	-3.91 ± 0.02
65	200	0.76	13.4	1903.0	1.07	1599.9	-4.22 ± 0.03

Table 4-13: *Test characteristics for samples from borehole 2/2000, Murtèl-Corvatsch rock glacier.*

The creep stages lasted for various times, since the samples showed different creep behaviour, and therefore the strains until the samples were relaxed, and the constant strain rate test was started, were different (e.g. Table 4-13). Due to these large strains, most of the samples did not fulfil the requirement any more that the sample needs to be twice as high as the diameter for a triaxial shear test. Under these conditions, boundary effects such as friction at the plattens might influence the test results and the failure mechanisms might also be changed since radial spreading may be limited. However, the size effects entailed in representing the response of a rock glacier by a small sample under triaxial stress conditions were considered to be more critical. On one hand, most of the samples did not show a distinct shear zone within the sample and on the other hand, the sample could move with the filter plates since the friction between the plattens and the filter plates was very low.

As a consequence, the results of the tests presented should allow a reasonable characterisation of the response of frozen material to triaxial compression as a function of

- ice content and composition,
- temperature,
- confining pressure, and
- strain rate.

One of the major difficulties is the determination of the forces acting, and hence the stresses. The *total* stresses that are calculated from the axial load cell entail composition of stresses acting within the four phase system consisting of soil particles, ice, air and water. Responsible for the frictional shearing resistance, however, are the *effective* stresses acting between the solid components within this mixture (soil particles and ice). Positive pore pressures, i.e. the pressure within the unfrozen water and air, result in a decrease of the *effective* stresses and hence in a reduction of the shearing resistance. Consequently, *effective* stresses should be determined from triaxial tests in order to be able to formulate resistance.

It was possible to measure pressures acting in the pores at the top and bottom plattens with the triaxial testing equipment used for this study. But it was not possible to distinguish between air pressures and water pressures. Much smaller pore pressures were recorded for samples with high air contents due to the compressibility of air. Samples with interlocking pores also showed smaller pore pressures than samples with trapped voids. The pressure could not been distributed through the sample for such cases and local pore pressure concentrations reducing the effective stresses have to be accepted.

Sample behaviour

Typical examples of sample behaviour are shown in the subsequent figures for four representative tests. Since all of the shear tests were started after extensive axial creep deformation (Table 4-13), no small strain behaviour with an upper yield region (cf. Chapter 2.3.4) could be observed. Most of the test results showed a steep increase of the deviatoric response up to a maximum with subsequent strain softening (Figure 4-26). The porewater pressures and the cell volume indicated that dilatancy occurred in most of the cases (two examples shown in Figure 4-27), i.e. volume increase and porewater pressure decrease at the end of the test, after a short decrease and increase, respectively (Figure 4-27a, b). The differences in the response are mainly due to temperature, applied strain rate and composition. No dilatancy, i.e. sample compression and increase in porewater pressure, was encountered for slow tests (e.g. No. 37) despite the slight peak in the $q - \varepsilon$ diagram, whereas faster tests (e.g. No. 68 & 52) showed distinctly dilatant behaviour with the rate increasing with the axial strain rate despite more than 3°C difference in temperature. Test No. 60, which was exposed to about the same shear strain rate as No. 68 but a much higher volumetric air content (>10%), seems to reach a minimum value of compression followed by an extension with a possible, but very retarded trend to dilate, which may be an effect of the compressibility of air. The fastest test (No. 52) of the presented data in Figure 4-26 and Figure 4-27 shows a very pronounced dilatant response with a volume increase of more than 2% and a decrease in pore pressure of about 60 kPa at an axial strain of 8%. The trend in volume and pore pressure change has not at all levelled off, indicating that the sample has not reached a residual state and that changes are still going on.

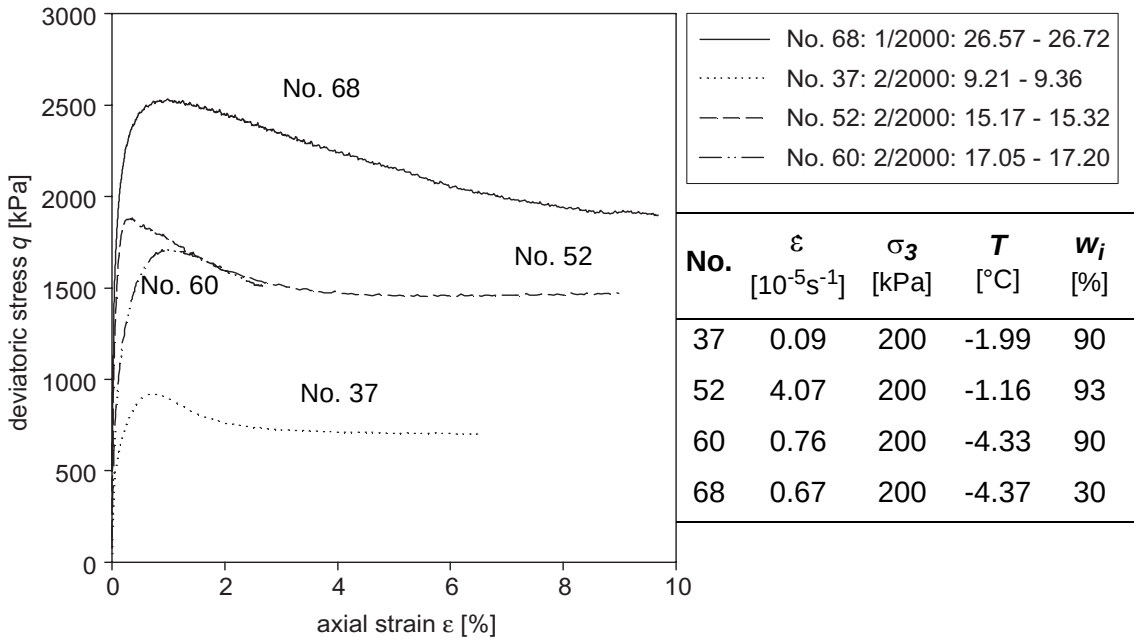

No.	$\dot{\varepsilon}$ [$10^{-5}s^{-1}$]	σ_3 [kPa]	T [°C]	w_i [%]
37	0.09	200	-1.99	90
52	4.07	200	-1.16	93
60	0.76	200	-4.33	90
68	0.67	200	-4.37	30

Figure 4-26: *Stress strain behaviour for four representative shear tests.*

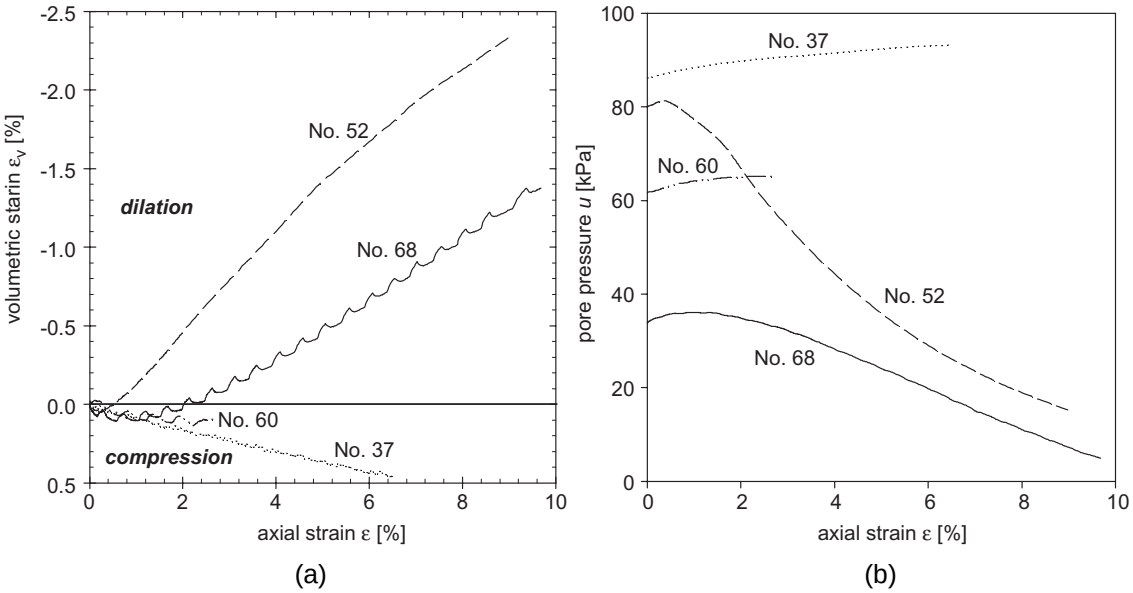

Figure 4-27: *Volume change (a) and pore pressure (b) for the tests shown in Figure 4-26.*

Ice content and composition

Figure 4-28 shows peak and residual shear strength values for samples with different compositions at the three temperatures under study, at an axial strain rate of about $8 \cdot 10^{-6}$ s^{-1}.

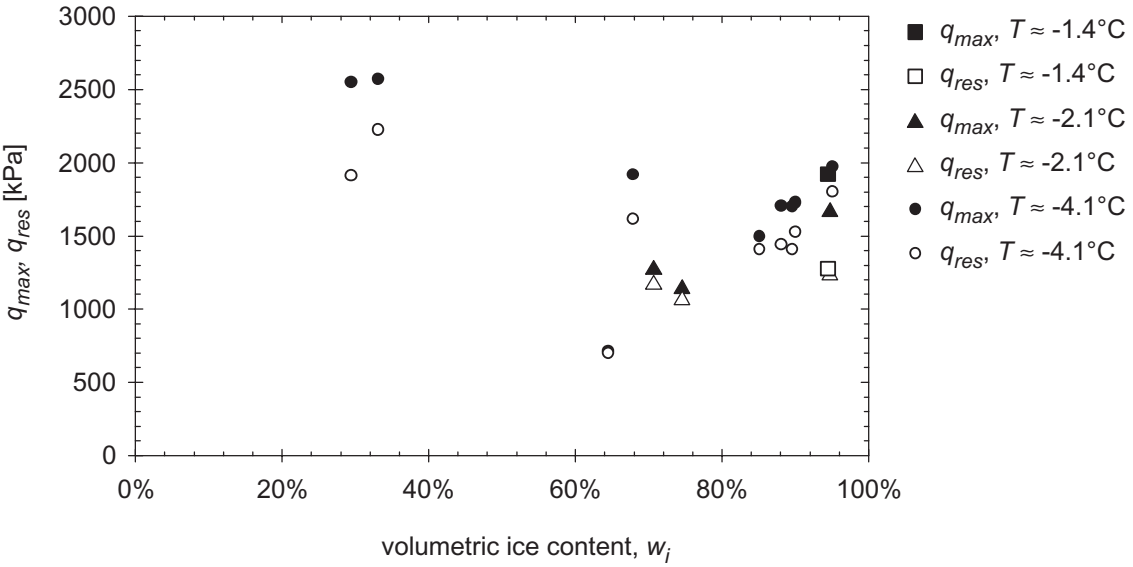

Figure 4-28: *Effect of volumetric ice content on shear strength.*

No obvious trend can be observed for volumetric ice contents larger than 70% indicating that the ice is the dominating phase. Nevertheless, a slight increase mainly of the peak shear strength can be noted at high volumetric ice contents (>90%), which might be the effect of a change in mechanism from ductile to brittle. Similar to the observations by Ting *et al*. (1983), the shear resistance,

peak and residual, increases for low ice contents. The particles are in contact with each other, mobilising friction and consequently the shear resistance increases.

Temperature

Despite the ice content, the temperature is the most important factor, which influences the shear strength that can be mobilised in a frozen soil. The peak and residual deviatoric stresses are displayed in Figure 4-29 for two different axial strain rates and various samples with ice contents larger than about 60%. The mobilised shear resistance increases with decreasing temperature, though this effect wears off with decreasing axial strain rate. A linear increase of the deviator *q* with decreasing temperature seems to be the best representation of the scattered data within the tested temperature range, even though the coefficient of correlation is very low.

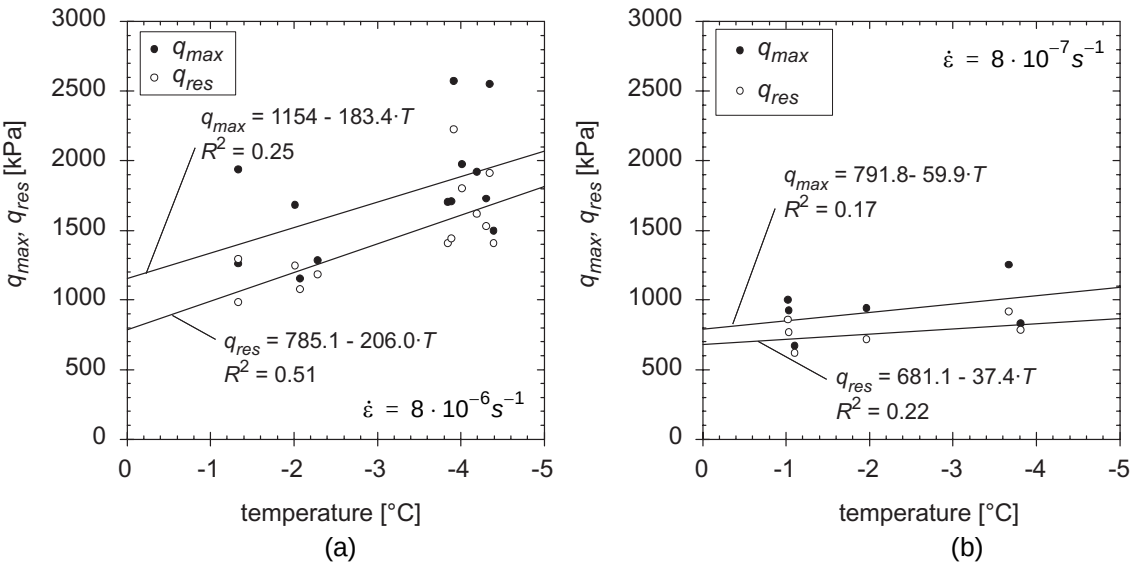

Figure 4-29: *Temperature dependency of maximum and residual shear strength as a function of test temperature and applied strain rate.*
a) axial strain rate = 8·10^{-6} s^{-1}
b) axial strain rate = 8·10^{-7} s^{-1}

Strain rate

The effect of the applied strain rate on shear resistance was already shown in Figure 4-29, where a decrease in the peak values as well as in the residual values could be observed for decreasing strain rates. In addition, the ratio between the maximum and residual value approaches 1.0 with decreasing strain rate. The material starts to creep at the lower strain rates and therefore, stress redistribution occurs, suppressing the tendency for dilation and no additional shear resistance of the frozen soil can be mobilised. The influence of the volumetric ice content is also demonstrated in Figure 4-30.

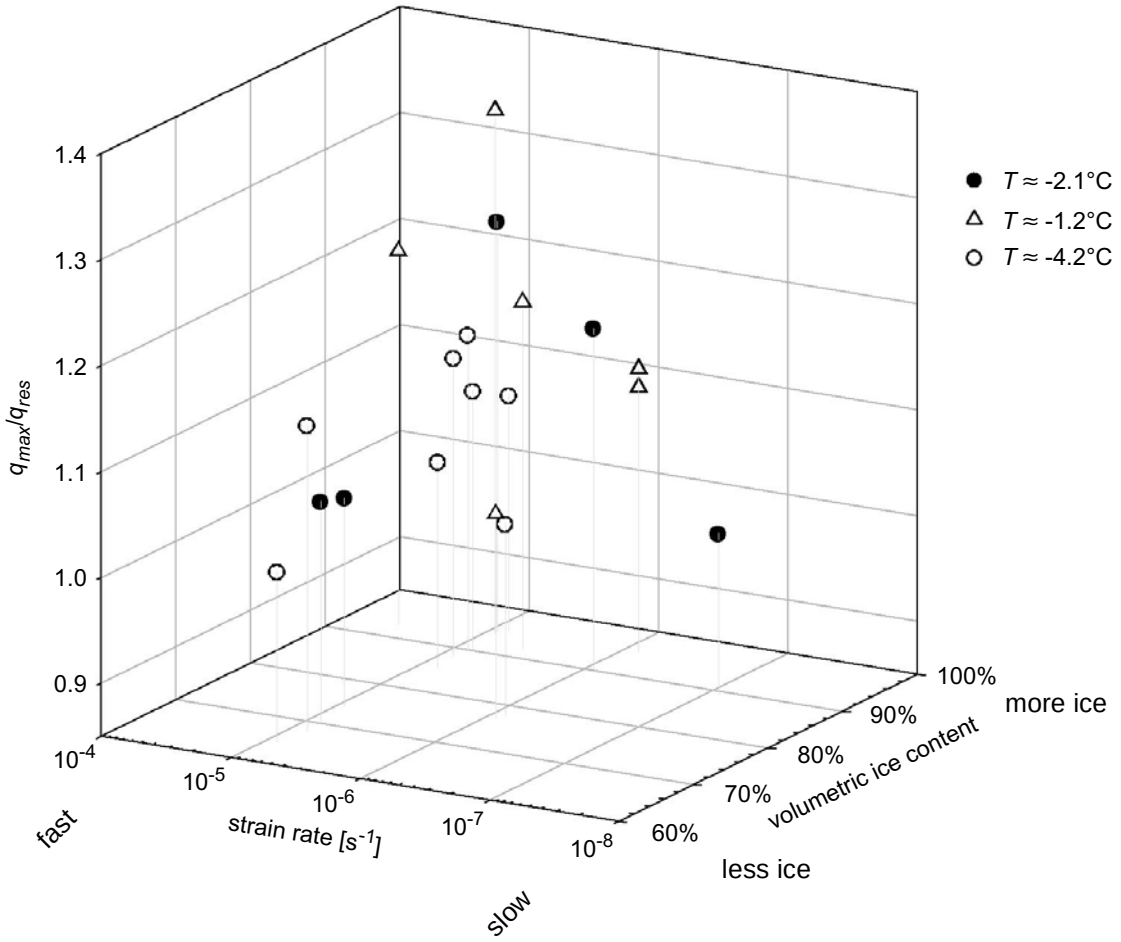

Figure 4-30: *Effect of strain rate on the ratio between peak and residual shear strength.*

Confining pressure

The artificially prepared samples showed no obvious influence of the confining pressure on the shear strength, and this was also confirmed by the tests performed on real permafrost samples. Samples with volumetric ice contents larger than 60%, in particular, seem not to be affected by a hydrostatic pressure. Figure 4-31 displays results for CSR tests at a temperature of about -2°C and an axial strain rate between 0.7 and $0.9 \cdot 10^{-5}$ s^{-1} (Nos. 27, 29, 31, 32, 33, 34, 36, 38, 39, 41, 43 & 44).

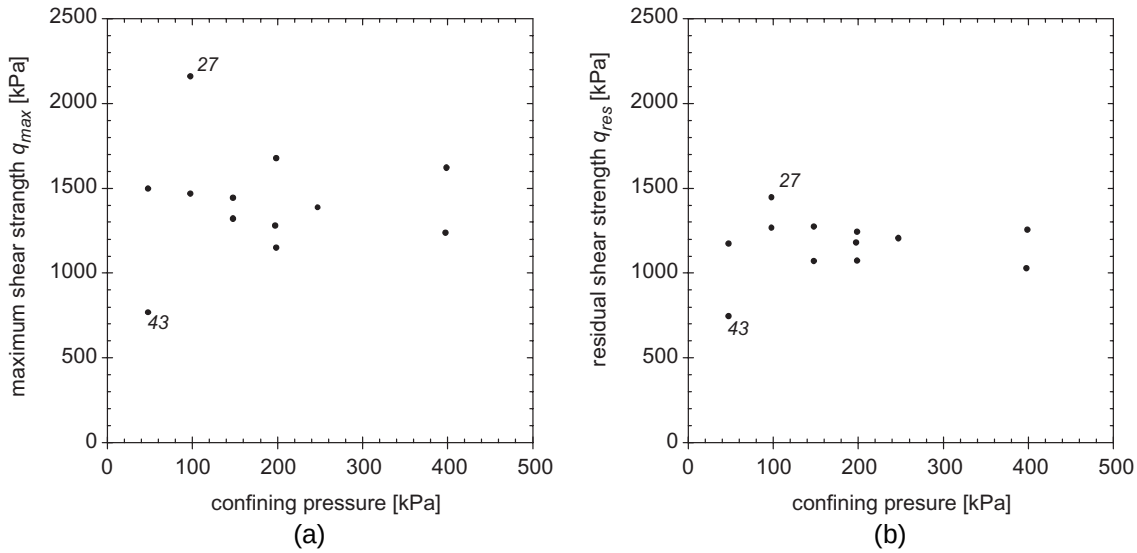

Figure 4-31: *Confining pressure versus peak (a) and residual (b) shear strength for samples at a temperature of about -2°C and an axial strain rate between 0.7 and $0.9 \cdot 10^{-5}$ s^{-1}.*

Sample No. 27 that had a volumetric ice content of only 55% delivered a high value for the peak deviatoric stress q_{max} of 2147.6 kPa (Figure 4-32a) and has probably developed a shear zone running at about 30° to the horizontal plane. For the residual value, however, the ice content seems to be much less important. On the other hand, a very low value of peak and residual deviatoric stress was obtained for sample No. 43 (10.00 – 10.15 m). This sample had an extremely high air content (25.6%) without a measurable component of soil. A picture of this sample is shown in Figure 4-32b and indicates general rearrangement of ice granules and bulging of the sample in the lower third.

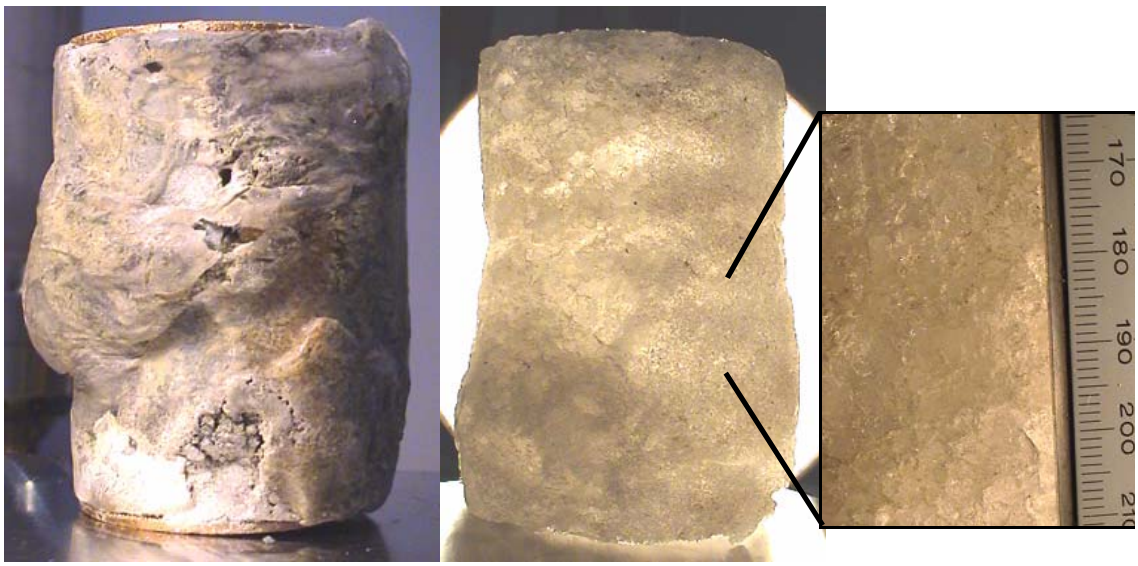

Figure 4-32: *Sample No. 27 (a) and No. 43 (b) after the test.*

During the creep and the shear test, the sample was compacted and the air was compressed. This compression could be recorded during the test with the upper, as well as the lower pore pressure transducer (Figure 4-33).

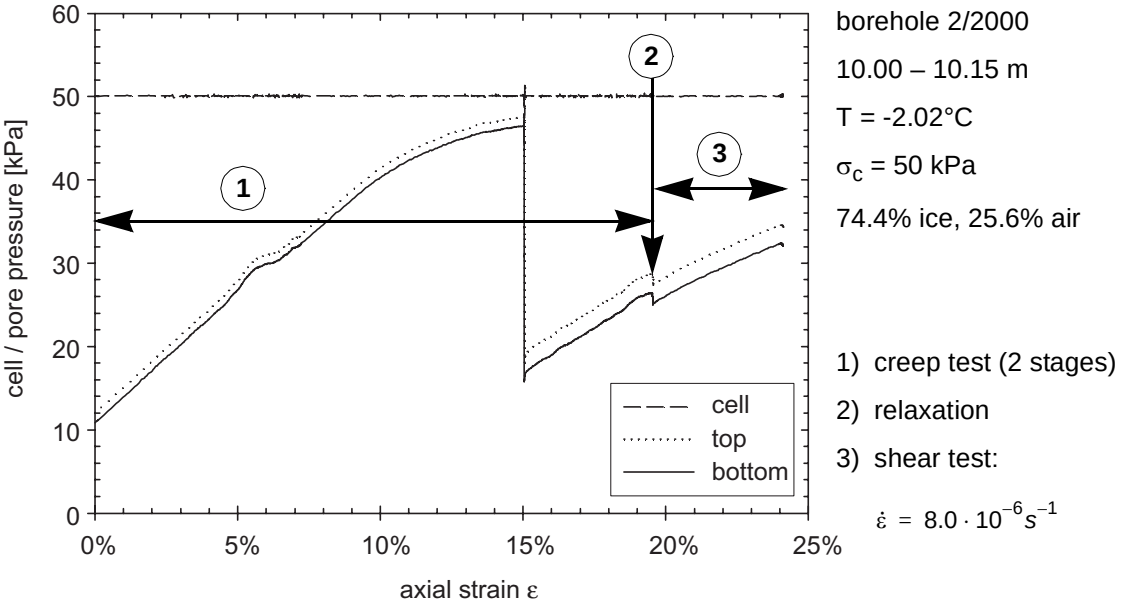

Figure 4-33: *Cell and pore pressures for test No. 43, during creep, relaxation and shear test.*

A sudden release of the pressure was observed during the second creep stage, accompanied by a sudden increase in the volumetric creep strain of about 0.5% (Figure 4-34), but not in the axial strain. The author assumes that some air voids, that had previously been closed, were opened to a larger volume, and therefore, the pressure could be released. This release was accompanied only by a change in the radial shape of the sample (Figure 4-32b). However, this volume of newly linked air cavities were pressurised again by the ongoing axial strain, resulting in a subsequent increase in the pore pressures.

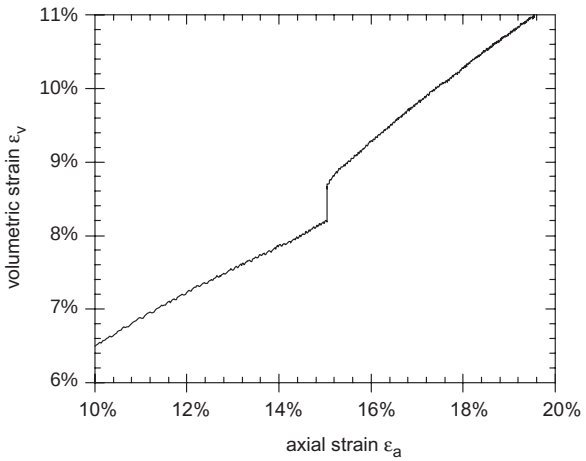

Figure 4-34: *Axial and volumetric creep strain for test No. 43.*

Self healing

Self healing during a shear test was also recorded for another test series (Almasi, 2001; Arenson *et al.*, submitted, b). Test No. 66, for example, had been stopped after the test was sheared up to an axial strain of 4.62% (Figure 4-35). A peak value could be determined prior to this at ε_a ~ 1%. After a relaxation period of 54.4 hours, the sample was reloaded at the same axial strain rate ($7.2 \cdot 10^{-6}$ s^{-1}). As shown in Figure 4-35, the second peak value at ε_a ~ 5.2% was

lower than the first peak. But the self healing appears to have been eliminated after an additional axial strain increment of $\Delta\varepsilon_a$ ~ 5% and about 2.5 J of extra work *W* was brought up between ε_a = 5 – 10% and appears to have rejoined the original curve, as if no relaxation would have happened. The extra work was calculated by summarising the additional force (stress x area) multiplied with the measured deformation for a finite time step. The high peak value demonstrates that the structure within the shear plane must have healed, and the newly formed bonds had to be rebroken before the shearing could proceed on the previously developed plane. A value closer to the first peak could probably be determined if the sample were relaxed much longer although this should be investigated.

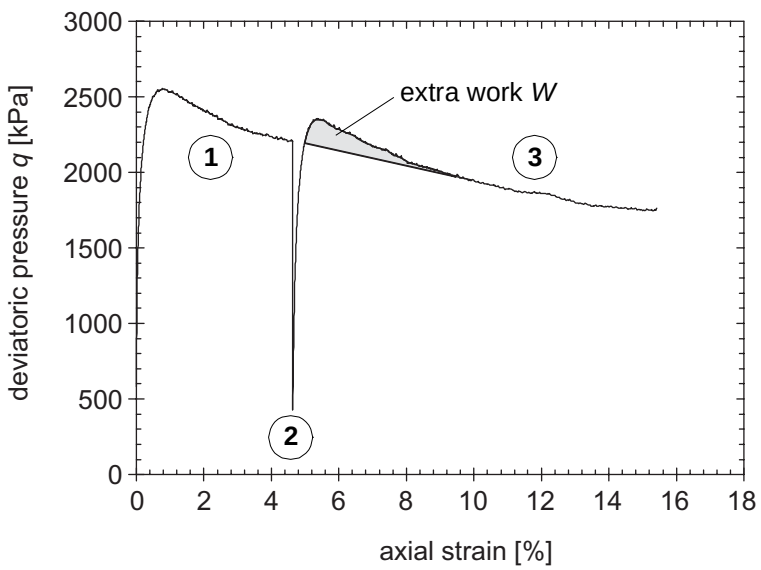

borehole 1/2000

27.16 – 27.31 m

T = -4.00°C

σ_c = 201 kPa

33.4% ice, 60.5% solids

5 creep stages

$\dot{\varepsilon} = 7.2 \cdot 10^{-6} s^{-1}$ (CSR)

1) first shear test
2) relaxation
3) second shear test

Figure 4-35: *Shear test of sample No. 66 with two shear phases.*

Peak strength versus residual strength

A comparison between the peak value q_{max} that was achieved at the beginning of the shearing process in triaxial compression and the residual value q_{res} for large strains for the shear tests performed on the Muragl and the Murtèl-Corvatsch rock glacier samples showed, that dependent of the strain rate, sample composition and temperature, a ratio between 1.0 (ice rich samples, low strain rate) and 1.5 (low ice contents, high strain rate) with a mean value of 1.21 can be determined (Figure 4-36). The correlation coefficient R^2 for the mean value is 0.94.

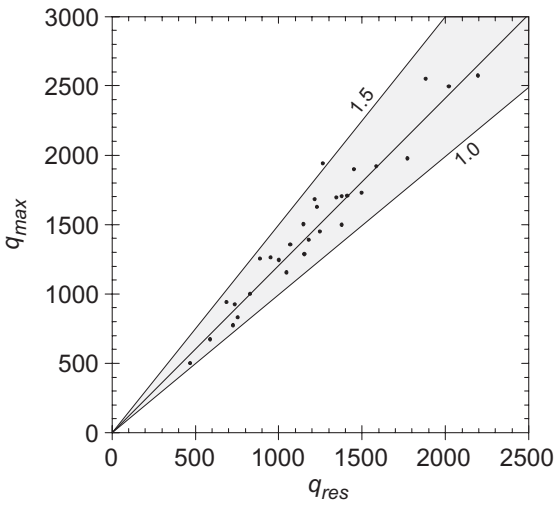

Figure 4-36: *Peak against residual shear strength (all tests: Muragl and Murtèl-Corvatsch).*

4.4.5 Creep (CSC) versus Shear (CSR) Tests

Comparisons between the triaxial constant stress (creep) tests and the constant strain rate tests showed that a relationship can be found that is independent of the applied temperature and confining pressure. Values of minimum axial creep strain rates derived from the creep stages were calculated similar to Chapter 4.4.3 using Glen's flow law, and were plotted versus peak shear strength and residual shear strength for two different strain rates (Figure 4-37). The minimum pre-shearing creep rate decreases with increasing deviatoric resistance. This decrease is more pronounced for samples with high shear resistance. Since creep response as well as shear strength are a function of temperature and sample composition it is reasonable that the two types of test can be linked as presented. Only CSR tests with similar strain rates should be compared, since the applied strain rate controls the microstructural mechanism and is therefore very important.

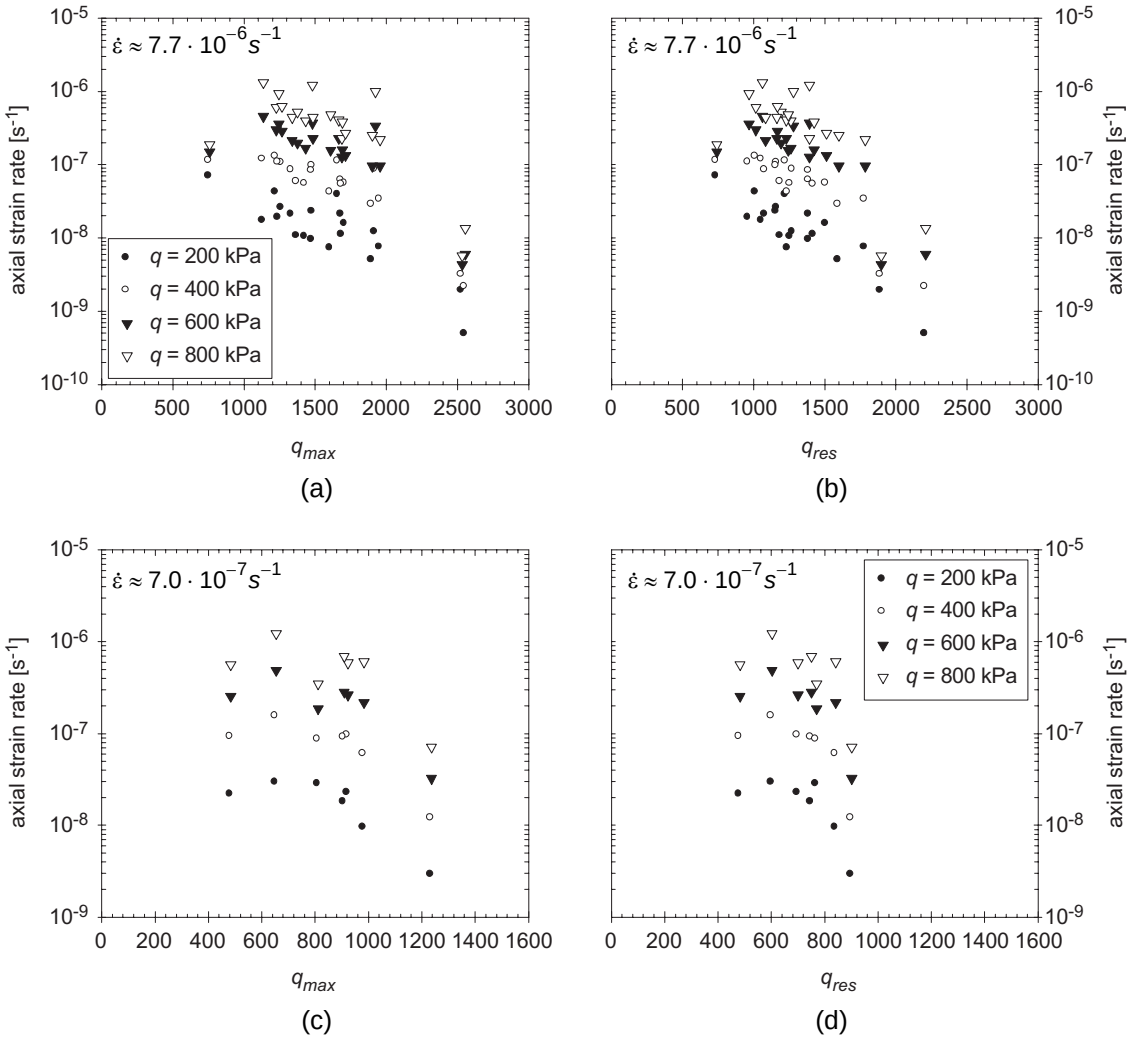

Figure 4-37: *Minimum values of axial creep strain rates versus shear strength for rock glacier samples from Muragl and Murtèl-Corvatsch.*
a) peak shear values for $\dot{\varepsilon} \approx 7.7 \cdot 10^{-6} s^{-1}$
b) residual shear values for $\dot{\varepsilon} \approx 7.7 \cdot 10^{-6} s^{-1}$
c) peak shear values for $\dot{\varepsilon} \approx 7.0 \cdot 10^{-7} s^{-1}$
d) residual shear values for $\dot{\varepsilon} \approx 7.0 \cdot 10^{-7} s^{-1}$

4.5 Thin Sections

Some thin sections were prepared in order to study the microscopic structure of the soil using a shine-through apparatus with polarisation filters and for comparison with samples from borehole 2/1987 (Wagner, 1990).

4.5.1 Sample Preparation and Setup

Different methods were used for the preparation of the thin sections, depending on whether solid particles were present or not. The samples were cut with a band or a circular saw to a thickness of a few millimetres (2 – 5 mm). The ice samples were then cut with a microtome to a thickness of some tenths of a millimetre (~0.6 mm). Samples containing solid particles had to be ground using emery paper of different roughnesses to the desired thickness. As expected, the quality was much worse than the samples prepared using the microtome and scratches of the emery paper were visible.

The pictures were taken using a digital camera with a digital zoom that was mounted on a shine-through apparatus, as shown in Figure 4-38. The aluminium box scatters the light so that the light source underneath the polarisation filter was homogeneous. The diameter of the filters was 80 mm allowing the whole sections of the samples to be analysed.

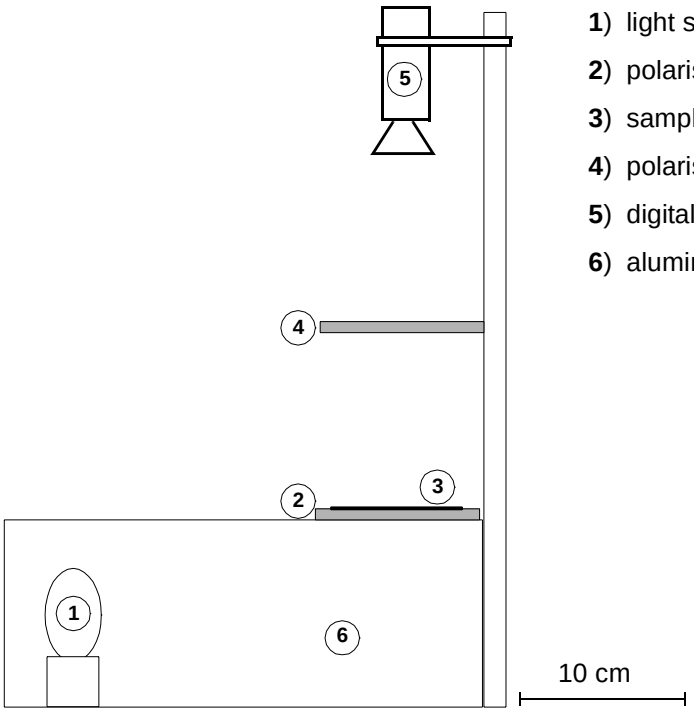

1) light source
2) polarisation filter (Polariser)
3) sample
4) polarisation filter (Antiliser)
5) digital camera (digital zoom: 40x)
6) aluminium box

Figure 4-38: *Shine-through apparatus for taking pictures of thin sections.*

4.5.2 Results

The quality of the pictures decreases dramatically as soon as soil particles are present (e.g. Figure 4-39d). The solid particles prevented the ice crystals from growing unhindered and therefore, the size of the crystals was smaller (cf. Figure

4-39c, d). In order to obtain good quality pictures, the thin section should be smaller than the grain size of the ice crystals, inferring that the more solid particles, the thinner a section had to be. On the other hand, it had been very difficult to make these sections smaller using an emery paper without either mechanical or thermal destruction of the very fragile ice matrix. And hence, only a few pictures were taken successfully. Nevertheless, some observations could be made, when analysing pictures such as those presented in Figure 4-39.

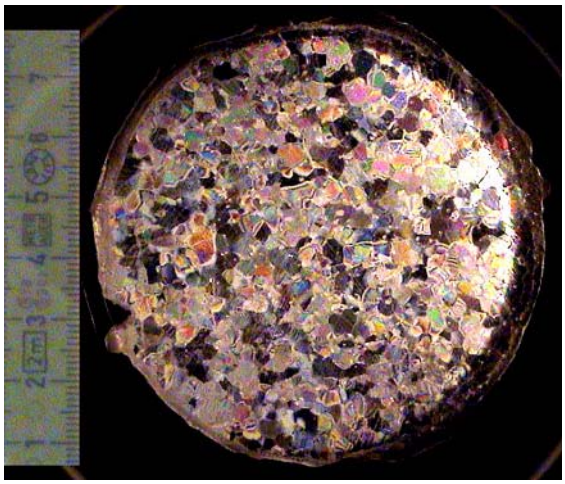

a) borehole 2/2000; 8.0 m

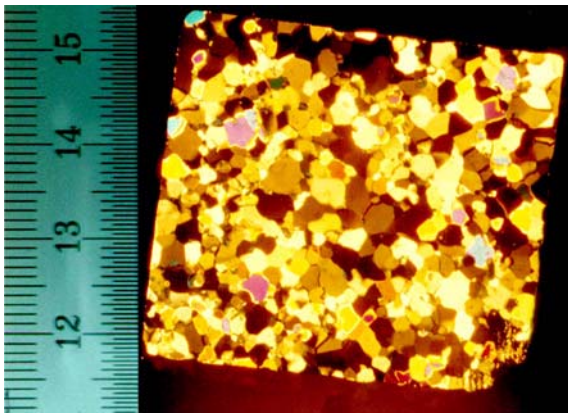

b) borehole 2/2000; 11.3 m

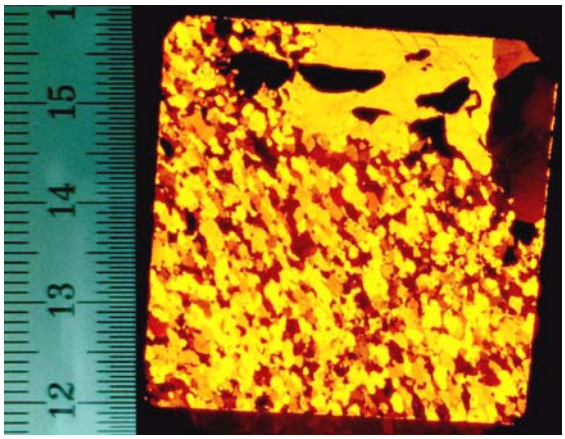

c) borehole 2/2000; 15.5 m

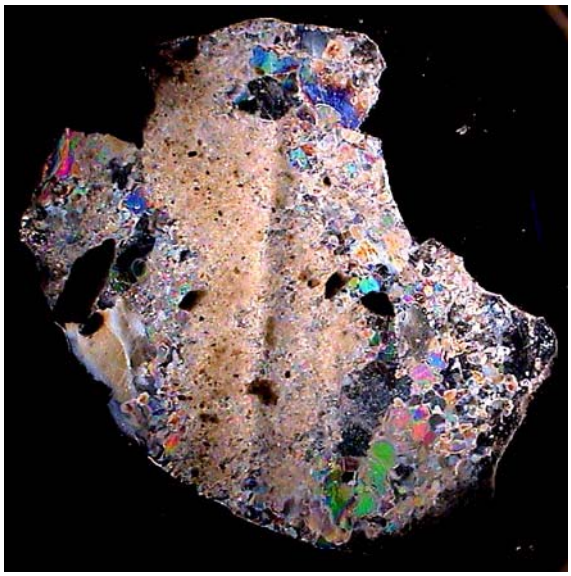

d) borehole 2/2000; 20.1 m
with solid particles (brown/black)

depth	crystal grain size	air voids
8.0 m	< 5 mm	some, small
11.3 m	< 5 mm	none
15.5 m	< 3.3 mm	none
20.1 m	< 3 mm	some, very small

Figure 4-39: *Thin sections from different depths of the Murtèl-Corvatsch rock glacier.*

- The grain size of the ice crystals decreases with increasing depth.
- Solid particles, such as silt and sand grains result in smaller ice crystals.
- Air voids were observed between the ice crystals at different depths, even though no distinct deformation or concentration was noted for the samples analysed.
- The crystals at a depth of 15.5 m show an elongation in a distinct direction perpendicular to the direction of the borehole, i.e. horizontally. However, this was the only sample where such a phenomenon was noted.

These observations show that the crystal diameters were slightly smaller for the 2000 series than within borehole 2/1987, where equivalent diameters of ice crystals of about 1 cm at a depth of 7.5 m or 0.5 cm at 9.5 m and 11 m were recorded (Wagner, 1990). A possible explanation might be the larger depth of the samples presented compared to the relatively shallow depth of the samples from borehole 2/1987.

4.6 Summary of Laboratory Tests

Several types of samples were tested under various conditions in a triaxial test device. Creep properties, as well as the shear resistance were investigated successfully on 55 (CSC) and 49 (CSR) tests, respectively, as a function of the sample preparation, sample composition, i.e. volumetric ice and air content, pressure/stress conditions, loading conditions, i.e. strain rates, and temperature (Figure 4-40). Artificially frozen samples were tested at the beginning in order to improve the triaxial testing equipment, the sample preparation techniques, and to be able to define the sample composition. Subsequently, tests were carried out on samples from the Muragl and Murtèl-Corvatsch rock glaciers. Since the creep tests lasted up to ten weeks and due to the very limited quality and quantity of available samples, only a restricted number of tests could be carried out. It was therefore difficult to find clear relationships for one distinct parameter, since the other parameters could not easily be held constant. However, trends could be determined, forming the basis for further analyses in the subsequent chapters.

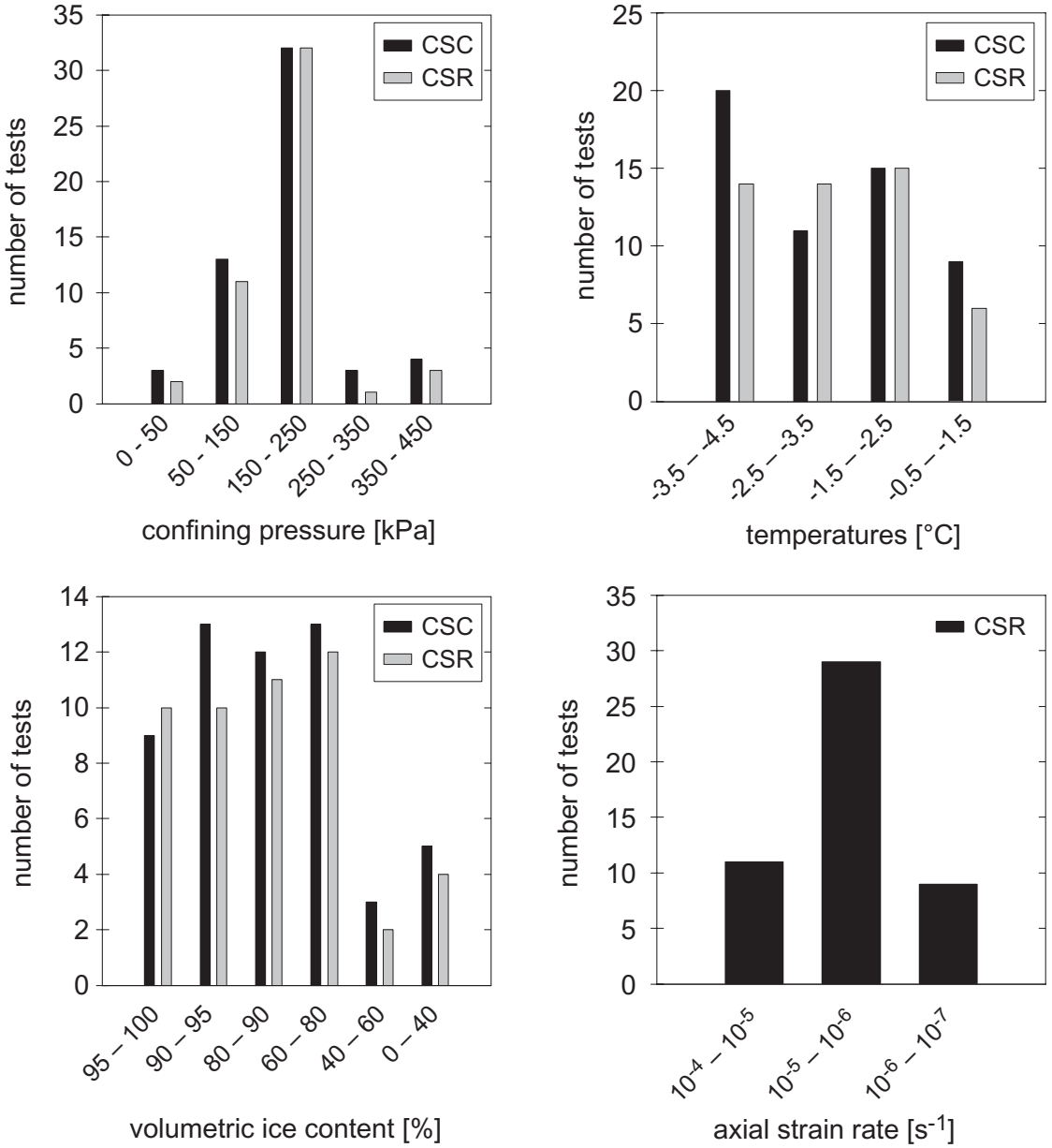

Figure 4-40: *Number of successfully tested samples on artificial as well as original permafrost samples for creep (CSC) and constant strain rate (CSR) tests.*

The major aspects can be summarised as follows:

- creep
  - Minimum axial creep strain rates increase exponentially with the applied deviatoric stress.
  - Axial creep strain rates increase with increasing temperature, the inclination of the logarithm of the creep rate versus applied stress, however, seems to be unaffected.
  - The creep susceptibility decreases with decreasing volumetric ice content, even though this effect was mainly noted for ice contents lower than about 65%. There seems to be no major influence anymore for higher volumetric ice contents.
  - The volumetric air content of the sample influences the volumetric response and mechanisms. The primary creep phases increase in terms of duration and strain with increasing air content.
  - Tertiary creep was only achieved for some samples within test duration, for deviatoric stresses larger than about 400 kPa.
  - Creep strain rates do not appear to be influenced by the applied confining pressure.
- shear strength
  - Peak and residual values of deviatoric stress seem to be independent of the confining pressures applied in this test series.
  - The shear strength mobilised increases with increasing axial strain rate. In addition, the ratio between the peak and the residual approaches a value of unity as axial strain rates decrease, when creep and local stress redistribution starts to dominate the response of the frozen soil, i.e. there is enough time for such a response to develop.
  - The sample appears to undergo a strengthening of the bonds and behaves as if there had been no pre-loading after a period of deviatoric stress relaxation. The effect of self healing of the previously broken bonds is very pronounced in terms of a peak deviatoric stress mobilised above the value reached prior to relaxation.
  - The volumetric sample response is also influenced by the amount and character (trapped, open) of air voids.
- Values of minimum creep strain rates are strongly related to the peak and residual shear strength of the same soil. Both values represent a mechanical response of the soil under a loading condition, dependent of the temperature and composition of the samples.

Finally, the results showed that similar responses can be obtained from artificially frozen and *in situ* samples, assuming that the samples are prepared in an adequate way, i.e. using crushed ice and mixing it with solids at the same temperature.

Chapter 5

Data Analyses

The test results presented in the previous chapter are discussed and analysed in order to prepare them for numerical modelling at some stage in the future. The analyses are based on Glen's flow law, which was adapted to suit the results of the current work. However, factors that might be responsible for the rather large scattering of the test data are also discussed in some of the subsequent sub-sections and are summarised briefly at the end of this chapter.

5.1 Creep Analyses

The analyses were focused mainly on the creep results, even though the test data showed that it is possible to combine constant stress (creep) tests with constant strain rate tests (Chapter 4.4.5). The data presented showed a rather large scattering due to various factors that will be discussed in this chapter. Highly sophisticated models are not recommended for the data analyses, since the variation in response is so large. In addition, major progress on constitutive modelling of creep behaviour, that are presented within the literature review, have been developed for the modelling of the whole creep process including primary and tertiary creep, and therefore are mainly applicable to changes in loading conditions, such as those occurring for a new foundation. The main focus within the current study, however, was the variation of the minimum creep rates, i.e. secondary creep or steady state creep, as a function of the temperature, applied stress and sample composition. Therefore, a *Glen* type approach was selected to link the axial strain rate with a power function of the applied stress. This has been recommended by various authors (cf. Chapter 2.3.5). The exponent *n* was chosen to be independent of the temperature and reasonable results emerged from this assumption, which will be discussed in more detail later. In order to be independent of the confining pressure, which seems to have only a minor influence, and since the data should be comparable to *in situ* pressuremeter test data, the stress invariant σ_e was chosen to be the best representative of the stress state.

$$\dot{\varepsilon} = A(T, w_i)\sigma_e^{n(w_i)} \qquad [5\text{-}1]$$

$\dot{\varepsilon}$ axial strain rate [s^{-1}]

σ_e second stress invariant: $\sigma_e = \frac{\sqrt{2}}{2}q$ [kPa]

q is the deviatoric stress: $q = \sigma_1 - \sigma_3$ (under triaxial conditions)

A, n Creep parameters, which are a function of the composition, volumetric ice content w_i and temperature T

The variation of the creep parameters A and n, in particular with temperature and sample composition, are discussed within the following sections.

5.1.1 Temperature

The data have shown that the temperature has a significant influence on the creep behaviour. The minimum strain rate increases with increasing temperature. This effect has been realised for years and many others have described it using the *Arrhenius equation* (see Chapter 2.3.1). This equation, however, has its limitations at temperatures close to the melting point, since the unfrozen water changes the activation energy (Barnes *et al.*, 1971; Fish, 1985). Sometimes an apparent activation energy was used for tests carried out at temperatures approaching zero centigrade (see Table 2-4).

The creep parameters A and n could be determined for various ranges of ice content. Best fits were performed automatically on the measured data, using an exponential curve fit as a first approach. Very similar curves could be determined although the creep parameters were rather different, since the parameters A and n are highly sensitive. An increase of n resulted in a decrease of A and *vice versa*. The use of a best fit approximation did not reveal a constant value for n and therefore new best fit values for A were calculated applying a constant value for n, assuming that n is only dependent on the structure of the sample. In order to judge the results, the accuracy, which can be expressed as a function of the correlation coefficient R^2, was determined according to [5-2].

$$R^2 = 1 - \frac{\sum_i^n (y_i - \hat{y}_i)^2}{\sum_i^n (y_i)^2 - \frac{\left(\sum_i^n y_i\right)^2}{n}} \qquad [5\text{-}2]$$

y_i logarithm (base 10) of the original value

$\hat{y}_i$ logarithm (base 10) of the calculated value

The scatter of the two creep parameters after using the best fit approach for samples with volumetric ice contents between 90 and 98% are presented in Figure 5-1 and Table 5-1. The mean value of *n* is 2.72 for the presented data and *A* is $2.73 \cdot 10^{-13}$ with standard deviations of 0.78 and $5.16 \cdot 10^{-13}$, respectively.

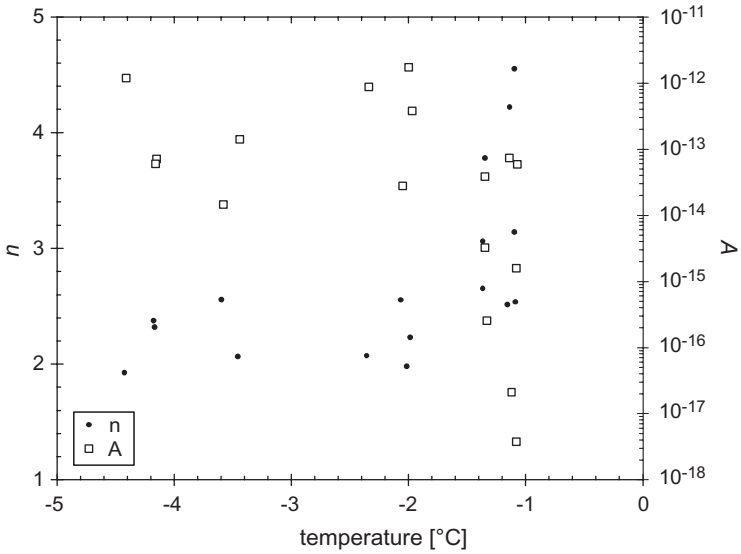

Figure 5-1: *"Unfiltered" creep parameters for samples with a volumetric ice content between 90 and 98%.*

test No.	*n*	*A*	R^2
11	2.54	$1.5 \cdot 10^{-14}$	0.87
24	2.05	$1.4 \cdot 10^{-13}$	0.83
37	2.21	$3.8 \cdot 10^{-13}$	0.91
39	1.96	$1.7 \cdot 10^{-12}$	0.91
41	2.54	$2.8 \cdot 10^{-14}$	0.97
44	2.06	$8.7 \cdot 10^{-13}$	0.99
46	3.12	$1.6 \cdot 10^{-15}$	0.98
47	3.00	$3.2 \cdot 10^{-15}$	0.98
50	2.52	$5.9 \cdot 10^{-14}$	0.99
51	2.64	$3.9 \cdot 10^{-14}$	1.00
52	2.50	$7.4 \cdot 10^{-14}$	1.00
53	4.20	$2.1 \cdot 10^{-17}$	1.00
54	4.53	$3.8 \cdot 10^{-18}$	1.00
55	3.76	$2.6 \cdot 10^{-16}$	1.00
56	2.30	$7.1 \cdot 10^{-14}$	0.94
59	2.36	$6.0 \cdot 10^{-14}$	0.95
60	1.91	$1.2 \cdot 10^{-12}$	0.89

Table 5-1: *Creep parameters for tests shown in Figure 5-1.*

The mean correlation coefficient R^2_{mean}, is an indicator of the quality of the data fitting to the power law. R^2_{mean} was determined as 0.95 with a standard deviation of 0.04.

The scatter of the creep parameters for temperatures colder than about -2°C is much lower than for the data close to -1°C. An individual analysis for these two regions might have been appropriate but was not performed due to following reasons:

- The scatter of the temperature range between -2 and -1°C is very significant and therefore it would have been very difficult to determine a solution or even just a trend. In consequence, the trends observed for colder temperatures were extrapolated for the temperature range between -2 and 0°C and compared with the test data.
- One unique relationship for the whole temperature range also slightly simplifies implementation in a future numerical model.

The value of *n* was kept constant for all tests at the mean value of 2.72 and corresponding *A* values were calculated. The mean correlation coefficient decreased to a value of 0.85 with a standard deviation of 0.11. However, a clearly increasing trend of *A* could be determined with increasing temperature (Figure 5-2) that can be explained by an increase of unfrozen water close to the melting point.

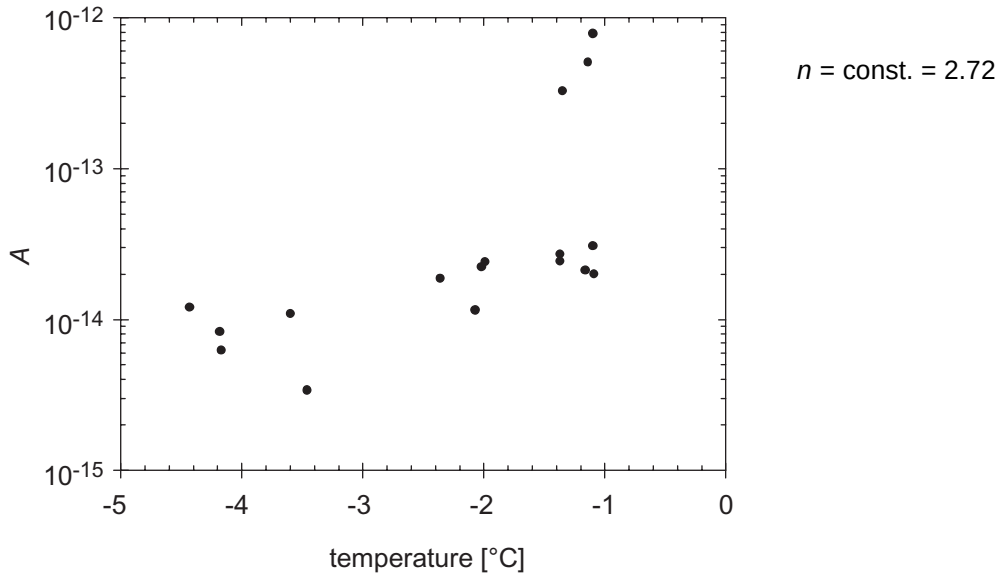

Figure 5-2: *Values of A as a function of temperature for a constant value of n and for samples with a volumetric ice content between 90 and 98%.*

Various other constant values of *n* were used to calculate *A* values and the corresponding correlation coefficients were determined in order to investigate the quality of the approach. A maximum correlation coefficient could then be determined for the mean value of *n*.

The temperature dependency of *A* (Figure 5-2) can be explained by a change in the activation energy *Q* due to a change in the unfrozen water content. Using the relationship [5-3], an apparent activation energy can be determined as a function of the temperature, and indirectly as a function of the unfrozen water content.

$$A = B \cdot e^{\left(-\frac{Q}{R \cdot T}\right)} \quad \text{(see Chapter 2.3.5)} \qquad [5\text{-}3]$$

It is assumed that *B* is a soil parameter and is independent of the temperature *T*. The activation energy *Q* can be calculated from two *A* values, A_1 and A_2 at the corresponding temperatures T_1 and T_2, according to

$$Q = R \cdot \frac{(lnA_1 - lnA_2)}{\frac{1}{T_2} - \frac{1}{T_1}}. \qquad [5\text{-}4]$$

R universal gas constant: 8.314 $J \cdot K^{-1} \cdot mole^{-1}$

Constant activation energies had to be assumed within a definite temperature range, since there was still some scatter in the calculated data. However, these values (Figure 5-3) are very similar to those calculated by various other authors and seem to approach a constant value for temperatures colder than the tested minimum, where the amount of unfrozen water is no longer relevant (see Chapter 2).

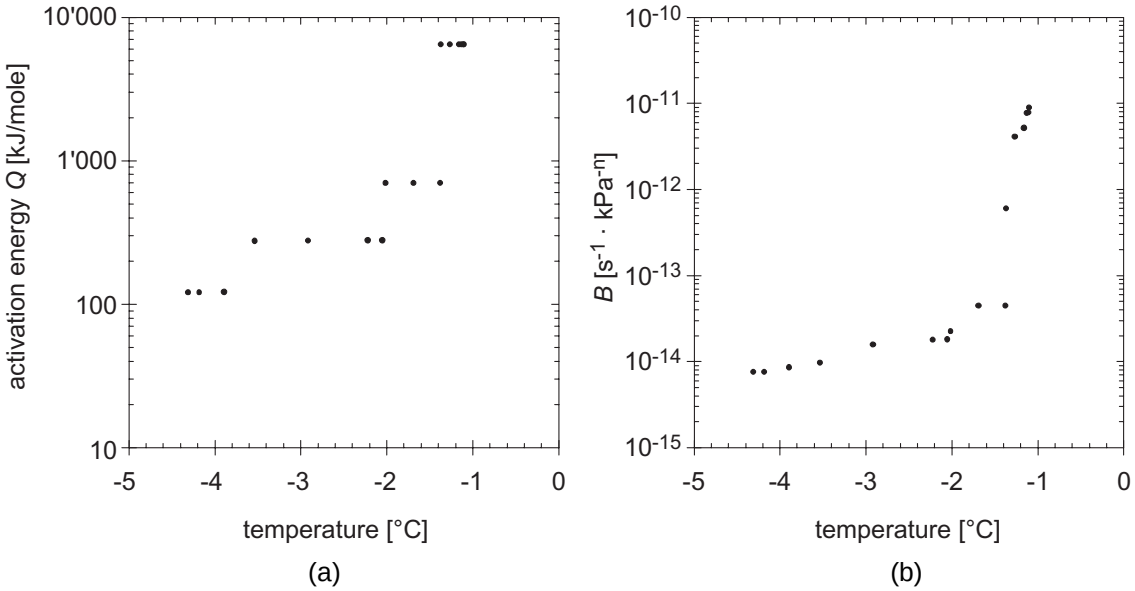

Figure 5-3: *Activation energy Q (a) and creep parameter B (b), as a function of temperature for volumetric ice contents between 90 and 98%.*

5.1.2 Composition

Test results from samples with volumetric ice contents lower then 90% were analysed similar to the proceedings described above. The creep parameters were determined using the *n* value that resulted in the best least square fit R^2 for the selected range of samples (Figure 5-4). An increase in the value of *A* could be

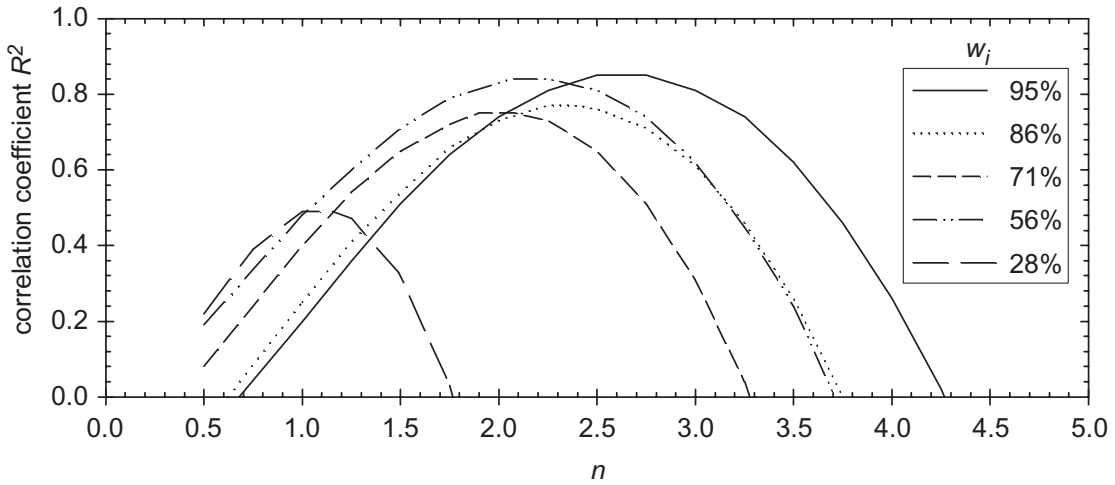

Figure 5-4: *Correlation coefficient for various n values and ranges of mean volumetric ice contents.*

determined for warmer temperatures for all tests. However, this increase was less significant and lower mean values of *n* resulted for samples with an increasing percentage of solid particles. Due to decreasing sample quality as the solid content increased, it was assumed that the accuracy of the power law fit also decreased.

The variation of the activation energy with temperature for various volumetric ice contents is shown in Figure 5-5. The change in activation energy may be more pronounced at temperatures close to the melting point for samples with a larger percentage of solid particles as the percentage of unfrozen water around the particles increases. The ice contents within the tested samples, however, are very high, and therefore this effect is not very apparent.

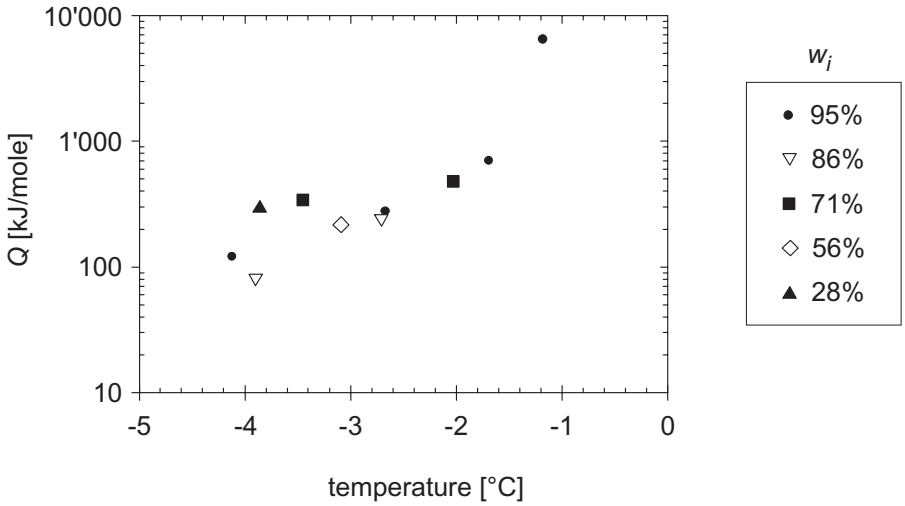

Figure 5-5: *Activation energy as a function of temperature for various volumetric ice contents.*

Nevertheless, clear trends can be determined and these are shown in Figure 5-6a and Table 5-2. The values that were concluded for the highest volumetric ice contents are very similar to those that had been reported by others (e.g Glen, 1955; Cole, 1987). In contrast to the activation energy, the second creep

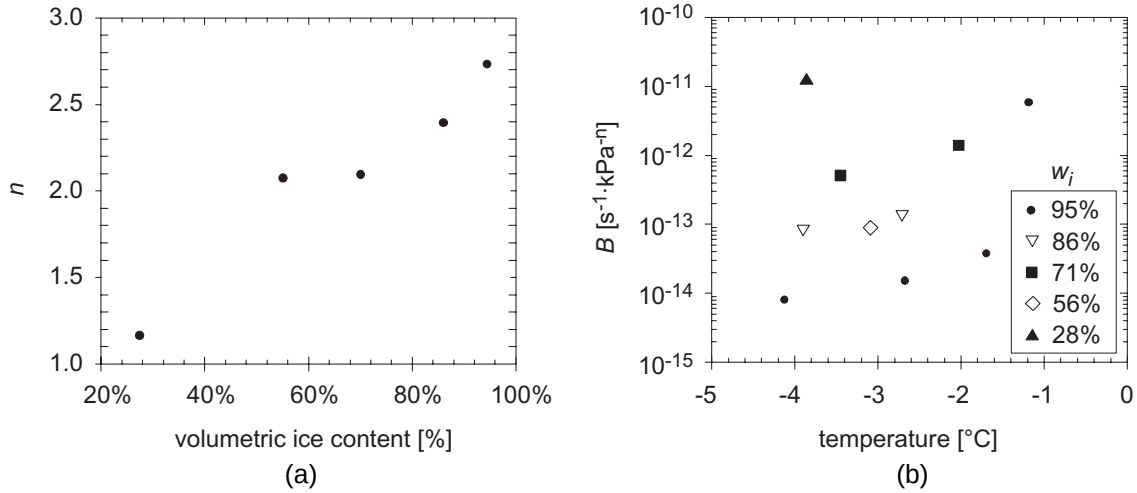

Figure 5-6: *a) Creep parameter n as a function of volumetric ice content.*
b) B as a function of temperature and volumetric ice content.

parameter *B* is clearly structure-dependent (Figure 5-6b). The additional temperature dependency is also an indicator of the change in structure due to an increase in the water phase and a decrease in the solid ice phase. These results might not be as accurate as those determined from high ice contents, since there were few test results for samples with a high percentage of solids. These uncertainties might be a reason why the value of *B* deduced for a mean volumetric ice content w_i of 56% is nearly similar to the values determined from samples with w_i = 86% and smaller than the values for w_i = 71%.

mean vol. ice content	no. of tests	activation energy *Q* [kJ/mole]				*n*		R^2
		~ -4°C	~ -3°C	~ -2°C	~ -1°C	best R^2	standard deviation	
94.8%	17	116	270	670	6200	2.72	0.78	0.85
86.5%	12	82	240	-	-	2.38	0.61	0.77
70.5%	10	-	360	450	-	2.08	0.63	0.75
55.5%	3	-	216	-	-	2.06	0.73	0.84
27.9%	5	190	-	-	-	1.15	0.88	0.49

Table 5-2: *Summary of creep properties.*

The significant decrease of *n* for a volumetric ice content of about 28% can be attributed to structural hindrance that starts to be relevant at ice contents of about 60% for frozen sands (Ting *et al.*, 1983). The particles are in close contact with each other and therefore nearly no creep strains can be developed. In particular, there is a decrease in the stress sensitivity, which is expressed by *n*.

5.1.3 Combination of Creep Parameters

Creep parameters calculated for individual samples can be combined in order to be able to determine the creep strain as a function of various sample composition, temperatures and applied stresses, using the following relationships:

$$n(w_i) = 2.13 \cdot w_i + 0.65 \qquad R^2 = 0.94 \qquad [5\text{-}5]$$

Equation [5-5] is based on Figure 5-6a with w_i as an absolute value, i.e. not in percent. Equation [5-6] was derived for the activation energy *Q* as a function of the temperature *T* in degrees centigrade (Figure 5-5):

$$Q(T) = 5945 \cdot e^{T} \qquad R^2 = 0.71\text{, for } 0°C > T > -4.5°C \qquad [5\text{-}6]$$

The effect of the volumetric ice content on the activation energy was neglected within the presented solution. Although this also omits the influence of the unfrozen water content, it seems to be only of minor importance and can be accounted for with the creep parameter *B*. At colder temperatures, the activation energy remains constant and can be taken as about 68 kJ/mole (Mellor and Testa, 1969).

The last parameter to be determined is *B*, which is primarily a function of the sample composition. However, the composition, i.e. the unfrozen water content changes with temperature and therefore, *B* is also a function of the temperature (Figure 5-6b):

$$B(w_i,T) = \frac{22.04}{ln(1-T)^{7.71} \cdot e^{(7.6 \cdot w_i^2 + 24.8)}} \qquad R^2 = 0.60 \qquad [5\text{-}7]$$

The low correlation coefficient of this relationship is due to the highly non-linear increase of *B* close to the melting point. An extrapolation based on the available results had to be performed, which might not represent the real soil behaviour, since no data were available for temperatures between 0 and -1°C. Several studies on the unfrozen water content and its influence on the activation energy (e.g. Barnes *at al.*, 1971; Anderson and Morgenstern, 1973; Fish, 1985; Stähli and Stadler, 1997) have shown highly non-linear changes close to zero centigrade. Consequently, the author assumes that the formulations of the creep parameters presented are a serviceable approximation of the real behaviour at temperatures lower than -1°C.

The temperature in centigrade was used for the new calculations, in contrast to the Arrhenius' approach, where the activation energy is a factor of the absolute temperature in degrees Kelvin. Since non-linear relationships had to be modelled close to a temperature of 0°C, significant changes were necessary in the derivatives of the functions adopted. This is only possible when the applied variable varies in the range of several tens of percentages (e.g. 0°C – 5°C) instead of only some percentages (273.15°K – 268.15°K).

Two perspectives of equation [5-7] are shown in Figure 5-7 together with the data points determined from analyses of the triaxial creep tests.

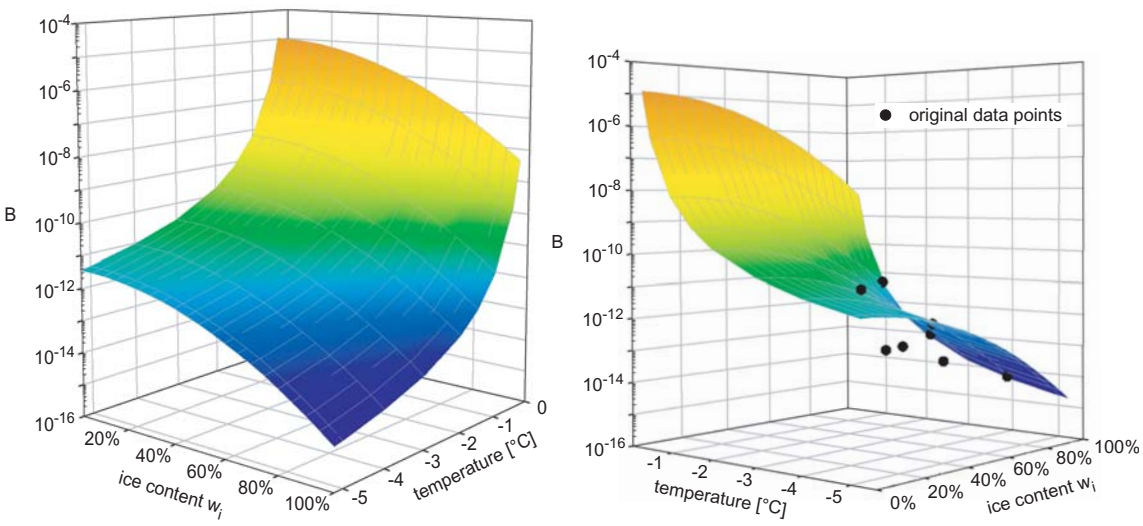

Figure 5-7: *Graphical solution of equation [5-7] without (a) and with (b) original data points.*

The final solution for the strain rate as a function of temperature T, volumetric ice content w_i and the stress invariant σ_e can be determined by combining equations [5-1], [5-3] and [5-5] – [5-7]:

$$\dot{\varepsilon}(w_i, \sigma_e, T) = \frac{22.04}{ln(1-T)^{7.71} e^{(7.6 \cdot w_i^2 + 24.8)}} \cdot e^{\left(-\frac{5945 \cdot e^T}{R \cdot (T + T_0)}\right)} \cdot \sigma_e^{(2.13 \cdot w_i + 0.65)} \quad [5\text{-}8]$$

T_0 absolute temperature: 273.15°C

The increase of the strain rate with increasing temperature is significant, in particular close to the melting point. Close to 0 kPa, a rapid drop-off in creep strain rate can be observed due to the power law of the increase of the strain rate with applied stress.

Equation [5-8] is shown in Figure 5-8 for three different volumetric ice contents w_i.

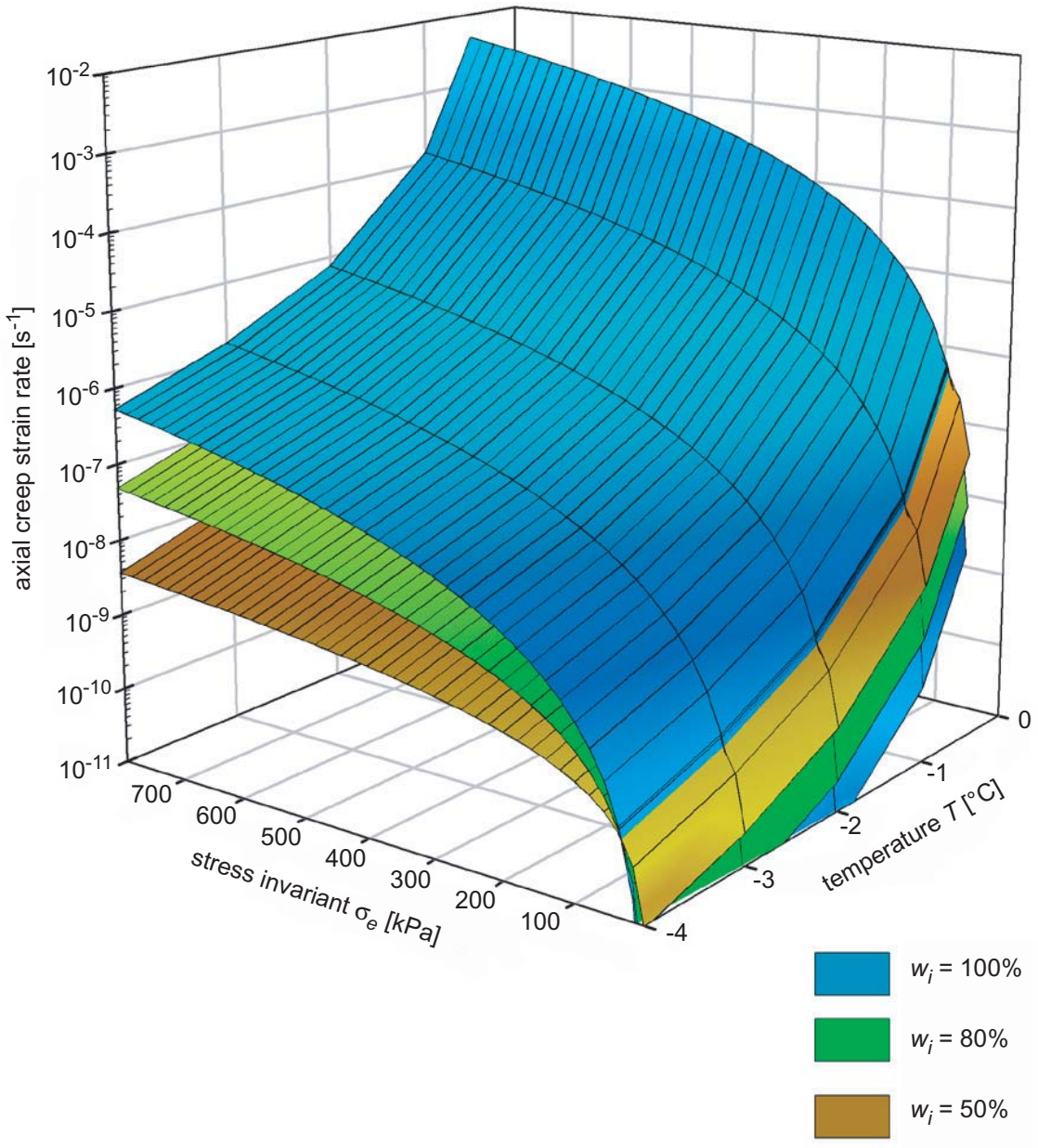

Figure 5-8: *Graphical solution of equation [5-8] for three different values of w_i.*

5.1.4 Judgement of Creep Equation

The solution presented for the calculation of axial creep strain rates (equation [5-8]) incorporates sample composition (i.e. volumetric ice content), temperature and stress state, and is the result of several curve-fits from data derived from original permafrost and artificial samples. As a consequence, various inaccuracies will be inherent in the predictions based on this equation either from the sample quality itself or the test procedure. Furthermore, several assumptions or even hypotheses were necessary in order to determine a relationship for the various components of this general creep equation, such as n, B or Q. Size effects have also to be considered, since the creep test could only be performed on samples that had grains with a maximum diameter of about 70 mm and many larger boulders are present within a rock glacier. In addition, the representation of a test with grain diameters larger than the maximum grain size acceptable for samples under triaxial loading, which is a fifth of the sample diameter, is questionable. However, only some samples had such large solid grains, since most of the cores containing large stones were damaged during the drilling process.

Even though there are many uncertainties, the fact that results from the two rock glaciers, Muragl and Murtèl-Corvatsch, as well as from artificially produced frozen samples, could be combined within the framework presented herein, seems to support that the presented solution is reasonably representative. It can be concluded that this solution can also be used for samples from other sites, at least as a first approximation.

5.2 Shear Strength

The main focus within the current study was the creep response of frozen soils and therefore the samples were only tested for their shear strength followed several creep stages. Consequently, the axial deformation due to creep reduced the height of the sample to a size smaller than is recommended for proper triaxial testing (c.f. Head, 1996). In addition, it is not possible to study small strain behaviour, where an upper yield region can be observed for frozen soils (e.g. Sayles, 1974; Mellor and Cole, 1982; Jones and Parameswaran, 1983; Andersen *et al.*, 1995; Da Re, 2000; Da Re *et al.*, 2001). Arenson *et al.* (submitted, b) showed that samples from borehole 2/1987 from the Murtèl-Corvatsch rock glacier, which were tested recently (Almasi, 2001), displayed an upper yield region, with ongoing strain hardening.

The occurrence of a peak shear strength followed by strain softening was dependent of the volume fraction of solids, and in particular of the percentage of air, and could only be achieved for few tests. The behaviour of the tests presented herein most probably represents a reload behaviour, i.e. the peak strength could only be mobilised because of the previous creep stages and the subsequent relaxation. The Youngs' modulus that could be determined from the inclination of the deviatoric stress against axial strain, is a value for a reload. Only residual states, i.e. deviatoric stresses at large strains at the end of the constant strain rate test were compared with each other, since the relaxation times varied and therefore a comparison for the various peak states would not have been appropriate.

5.2.1 Strain Rate, Confining Pressure and Temperature Dependency of Strength

Dependency of strength on the applied strain rate, confining pressure and temperature could be determined from constant strain rate tests that were carried out at the end of a creep test. Varies studies by Fish (1991; 1993; 1994) showed that the creep strength of frozen soils and ice under triaxial compression can be described by a parabolic failure criterion. Since creep response and strength at constant strain rate are strongly related (Chapter 4.4.5), it was thought that a similar relationship could be obtained for the different axial strain rates applied. Unfortunately, no such trend was found for the tested samples, which might be due to the low stress level or due to the different conditions for each sample. In addition, there were few tests that had different confining pressures, and therefore any such conclusions would not be well proven.

However, an increase of the residual deviatoric stress with increasing mean stress (Figure 5-9) can be estimated using a Mohr-Coulomb failure criterion, but for total and not for effective stress. An angle of friction ϕ[1] and a cohesion c[1] could be determined from the following relationship:

$$sin\phi = \frac{3M}{6 + M} \qquad [5\text{-}9]$$

$$c = \frac{a(3 - sin\phi)}{6\,cos\phi} \qquad [5\text{-}10]$$

M is the inclination of the linear regression and a is the intercept on the q-Axis, i.e. at p = 0.

test Nos.	volumetric ice content	temp.	strain rate	angle of friction ϕ	cohesion c	R^2
39, 41, 44	95%	-2.1°C	$8.2 \cdot 10^{-6}$ s^{-1}	5.9°	520 kPa	0.83
19, 21, 58, 70	85%	-3.9°C	$8.2 \cdot 10^{-6}$ s^{-1}	12.1°	480 kPa	0.65
34, 36, 43	74%	-2.1°C	$8.2 \cdot 10^{-6}$ s^{-1}	17.4°	280 kPa	0.72
10, 18	66%	-3.4°C	$3.8 \cdot 10^{-5}$ s^{-1}	20.7° 38.0°	450 kPa 240 kPa	n/a

Table 5-3: *Parameters for selected test groups with equivalent volumetric ice content.*

1. the ‘ has been omitted from c and ϕ to signify that these parameters are based on total stresses.

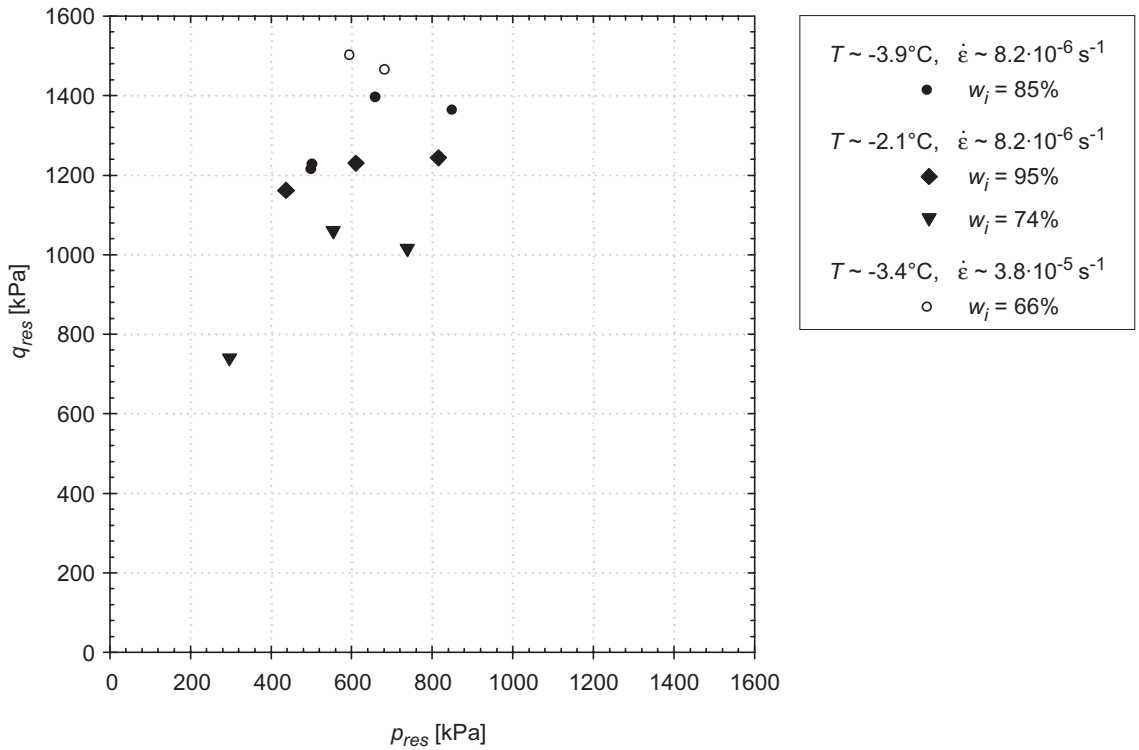

Figure 5-9: *p-q-diagram of various shear tests with different confining stress at the residual state.*

Even though the samples presented in Figure 5-9 vary in temperature, confining pressure and applied strain rate (Table 5-3), the parameters show an interesting trend that is shown in Figure 5-10. This trend was used for the determination of the angle of friction and the cohesion for the two tests with a volumetric ice content of about 66%. Since only two results were available, which, in addition, indicate a completely reversed trend by themselves, it was not possible to determine ϕ and c without an assumption. Two assumptions are proposed:

- Angle of friction is independent of the temperature and the strain rate (• in Figure 5-10).
- The cohesion is independent of the applied strain rate (◦ in Figure 5-10).

In addition to these tests, values for dry material are included (w_i = 0%) with no cohesion (c = 0) and an angle of friction between 30° and 35°.

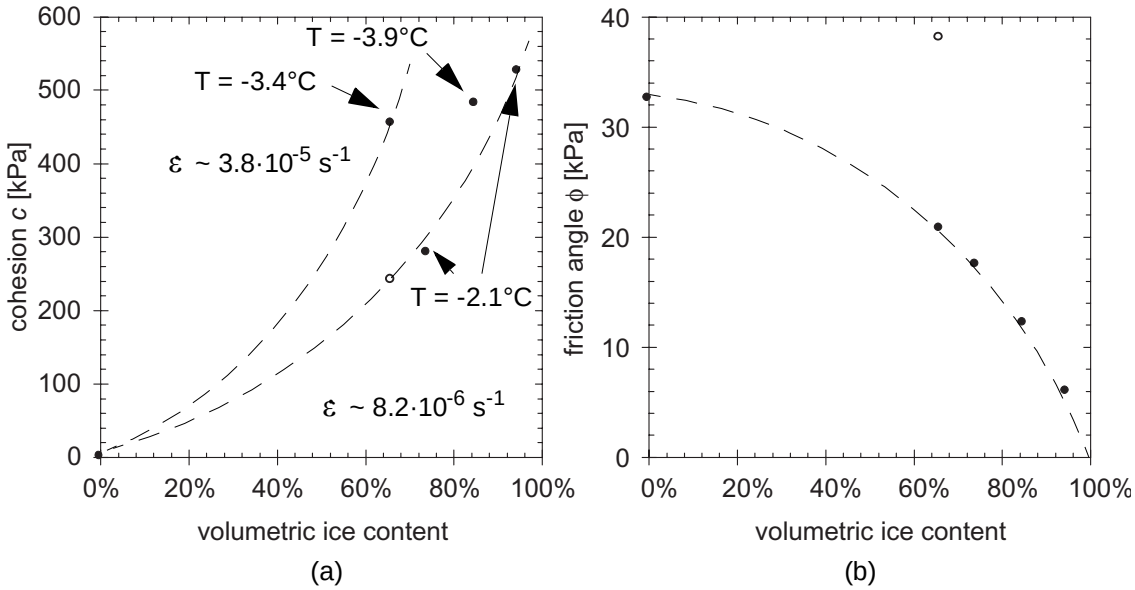

Figure 5-10: *Dependency of the cohesion c (a) and the angle of friction ϕ (b) on the volumetric ice content and temperature.*
∘: c is independent of temperature and strain rate.
•: ϕ is independent of temperature and strain rate.

Trends indicate for the first assumption that the cohesion *c*, which is usually 0 kPa for dry granular uncemented soils (e.g. Schofield and Wroth, 1968), increases with increasing volumetric ice content (Figure 5-10a). The increase is strain rate dependent and probably temperature dependent as well. The strain rate dependency is illustrated by the tests at $w_i \approx$ 66% that showed a high value for the cohesion under the assumed conditions. In addition, the tests at -3.9°C ($w_i \approx$ 85%) also show a slightly higher value for *c* than a smooth fitting curve through the data at T ~ -2.1°C would imply.

The angle of friction on the other hand, decreases with increasing volumetric ice content (Figure 5-10b), but seems to be temperature and strain rate independent, similar to the observations Ladanyi (1972) made about ice-rich, cold frozen soil. The fit in Figure 5-10b is only an assumption and has no mathematical background. However, due to the decreasing amount of solid particles, structural hindrance is reduced and therefore, the strength becomes insensitive to the stress level. It is, nevertheless, questionable if the angle of friction is zero for an ice sample, even though Jones (1982) showed that confining pressures have little effect on the shear strength of polycrystalline ice.

A very high angle of friction ϕ of about 38° can be determined for a volumetric ice content of 66% if a cohesion *c* = 240 kPa is assumed, which would indicate no dependency on temperature and strain rate. An increase of the angle of friction with increasing volumetric ice content is thought to be unrealistic, considering for example Ladanyi (1972) or Jones (1982), and therefore the author concentrates more on the first assumption, even though the true soil response might be somewhere in-between.

In summary, the tests showed that the ice strength, which is both temperature and strain rate dependent, is responsible for the initial strength of the ice-soil-mixture. Additional strength is further dependent upon the percentage of solid particles within this mixture. However, the particles lose their strengthening influence with increasing volumetric ice content and hence, only very low additional components of strength can be mobilised with increasing normal stress (low angle of friction ϕ).

No further analyses have been carried out on this very limited data, but the observations might help for future investigations.

5.2.2 Volumetric Behaviour

The volumetric response varied significantly for the range of applied test conditions and sample compositions (Figure 5-11). However, all tests demonstrated in common that the volumetric changes had not been finished at axial strains of about 10%, even though the deviatoric stress had reached a constant value. It is thought that a continuous change of the sample geometry is going on due to crack propagation throughout the sample. A constant strength is reached at an axial strain of about 6% and this represents the combined strength mobilised by the bonds and frictional shearing between the ice crystals and the solid particles. Refreezing processes occur simultaneously due to ongoing stress distributions within the sample. In addition, bonds fail and reform at a new locations, inducing ongoing volume change.

Samples that showed compression during the shearing have either been sheared at very low strain rates, or have high volumetric air contents, allowing additional compression of the air to occur within the voids instead of leading to dilatant behaviour.

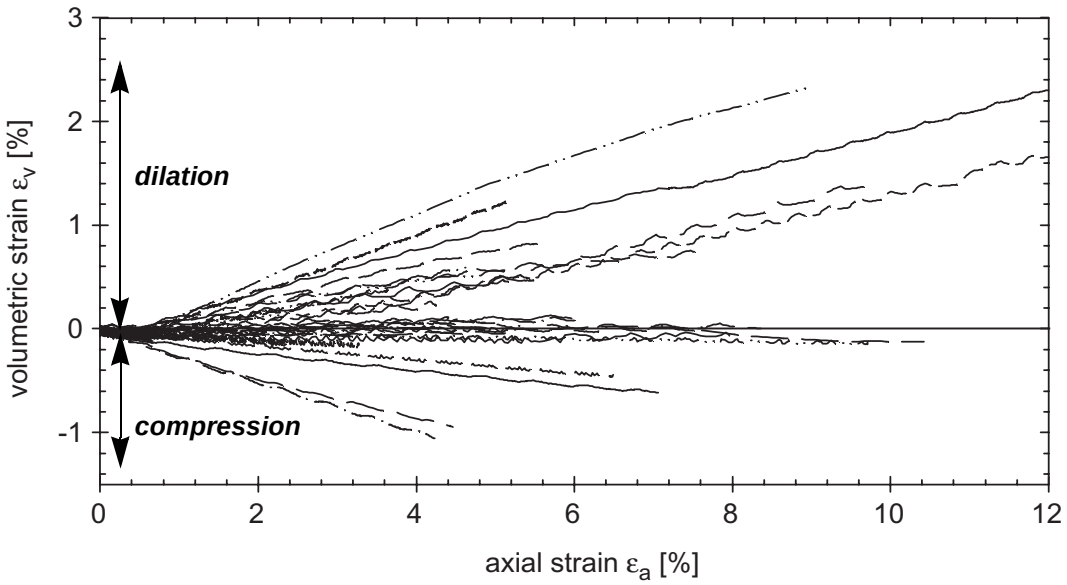

Figure 5-11: *Volumetric changes for all tests on samples from the two rock glaciers: Murtèl-Corvatsch and Muragl.*

Pore pressures were recorded in parallel to the volume changes, and they showed behaviour consistent with the statement above (e.g. Figure 4-27), i.e. decrease of pore pressure (air + water) for most of the tests, which showed volume increase after a short increase at low axial strain and a continuous increase of pore pressure for samples with compressive volumetric change. In addition, the volumetric strain change continued to axial strains larger than 10%, implying that the sample is still adapting the internal structure to resist the applied load.

The author was not able to find a relationship between the strength and the volumetric ice, air or solid content and therefore only trends, as shown in Figure 4-28, could be presented. Further studies are therefore necessary to focus on this particular influence.

5.3 Comparison Between Creep Tests and Shear Tests.

There is evidence of correspondence between the minimum creep strain rate from experimental data on ice and frozen soils, determined from constant stress tests (creep) and the shear response from constant strain rate tests. This effect has also been shown in Chapter 4.4.5 but will now be analysed further.

After Vaid and Campanella (1977), results of constant strain rate compression can be directly compared with the response of a similar sample under constant stress, which is inducing creep, and *vice versa*. The applied axial strain rates for the constant axial strain rate tests, and the applied deviatoric stress for the creep tests have not been in the range in which a comparison would be possible for most of the tests. The need to focus on the creep behaviour at the relatively low stresses expected *in situ* conflicted with the limited time available for the shear tests. Performing shear tests with corresponding axial strain rates would have lasted several weeks for each creep stage. However, the sample used in test No. 35 sheared with a very low strain rate after five creep stages, and it was possible to compare the two test types for the third stage (Figure 5-12).

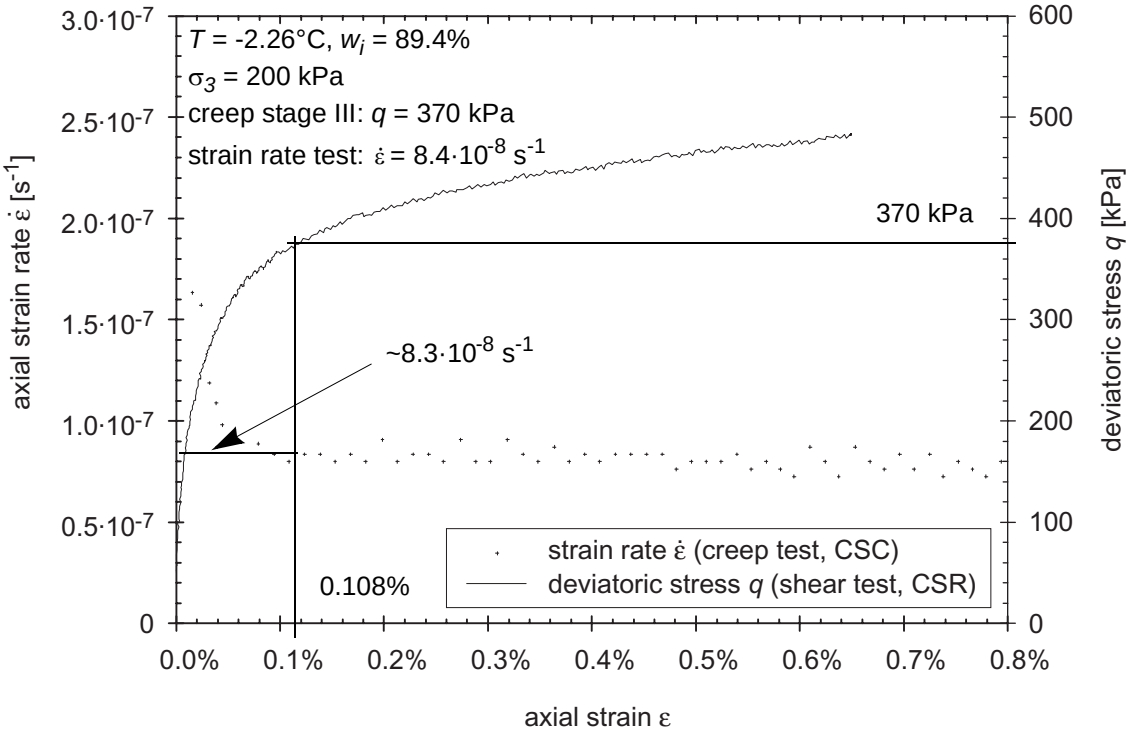

Figure 5-12: *Axial strain rate (creep test) and deviatoric stress q (constant strain rate test) against axial strain ε for test No. 35.*

It was possible to determine the axial strain at which the corresponding axial strain rate would be achieved in a creep test under similar deviatoric stress from the deviator stress – axial strain curve. During the constant strain rate test ($\dot{\varepsilon} = 8.4 \cdot 10^{-8}$ s^{-1}) the deviator stress q reached a value of 370 kPa after about 214 minutes, i.e. at an axial strain of $\varepsilon = 0.108\%$. The creep test also showed an axial strain rate of about $8.3 \cdot 10^{-8}$ s^{-1} for the similar axial creep strain, indicating a good agreement between the two types of test.

This coherence can be now applied for other tests with much higher strain rates, e.g. test No. 47 (Figure 5-13). Two axial strains can be determined for this particular test at an arbitrary deviatoric stress of 1700 kPa that is higher than the residual value: 0.34% and 1.95%. This implies a minimum creep strain rate lower than $8.8 \cdot 10^{-6}$ s^{-1} for such a load on one hand, but it is also an indicator that tertiary creep occurs. Assuming that this occurs in-between the two values of strain (0.34% and 1.95%) and that the applied strain rate is a medium strain rate for the corresponding (imaginary) creep test, tertiary creep would start about 1.5 days after a load of 1700 kPa would have been applied.

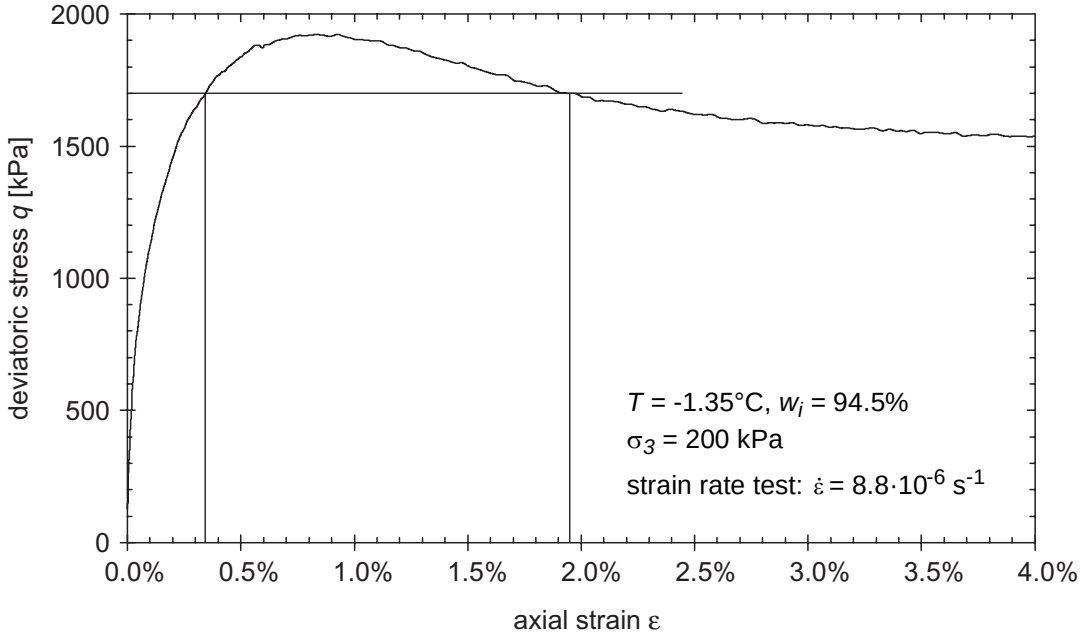

Figure 5-13: *Deviatoric stress and axial strain rate for test No. 47 for the determination of corresponding creep response.*

Even it is not proven, the author doubts that application of a deviatoric stress smaller than the residual strength prevents tertiary creep from developing *per se*, considering the following points:

- The shear response is highly dependent on the applied shear strain rate. Higher deformation rates result in higher residual strengths.
- Triaxial responses at large strains are influenced by boundary conditions, such as restraint due to the rubber membrane or platten friction, and therefore the residual value might be deduced to be higher than in reality.
- The structure within the frozen sample might change during long term creep due to recrystalisation and dislocation effects, and therefore the material properties at the beginning and the end of a creep test may not be similar and may not be compared with a shear test where the soil structure remains approximately constant.
- The method might not be applicable for axial strains smaller than about 0.2% since these can be attained immediately after loading in a creep test, i.e. strain rates approach infinity.

The following exponential relationship could be established for the correspondence shown in Figure 4-37 (Equation [5-11] and Table 5-4), linking the residual strength q_{res} determined from a constant strain rate test at two different axial strain rates with the minimum creep strain rate $\dot{\varepsilon}_{min}$ for a deviatoric load q. Note, that this relationship is independent of the temperature, sample composition and confining pressure.

$$\varepsilon_{min} = a \cdot e^{b \cdot q_{res}} \qquad [5\text{-}11]$$

CSC: q [kPa]	CSR: $\dot{\varepsilon} = 7.9 \cdot 10^{-6}\ s^{-1}$			CSR: $\dot{\varepsilon} = 7.9 \cdot 10^{-7}\ s^{-1}$		
	a	b	R^2	a	b	R^2
200	$6.3 \cdot 10^{-7}$	$-3.0 \cdot 10^{-3}$	0.88	$3.0 \cdot 10^{-6}$	$-7.3 \cdot 10^{-3}$	0.87
400	$3.3 \cdot 10^{-6}$	$-3.2 \cdot 10^{-3}$	0.86	$1.6 \cdot 10^{-5}$	$-7.4 \cdot 10^{-3}$	0.79
600	$1.1 \cdot 10^{-5}$	$-3.3 \cdot 10^{-3}$	0.74	$5.4 \cdot 10^{-5}$	$-7.4 \cdot 10^{-3}$	0.72
800	$2.7 \cdot 10^{-5}$	$-3.4 \cdot 10^{-3}$	0.63	$1.4 \cdot 10^{-4}$	$-7.5 \cdot 10^{-3}$	0.66

Table 5-4: *Parameters for Equation [5-11] for two different strain rates $\dot{\varepsilon}$.*

While the factor b remains nearly constant for all deviatoric stresses q, a increases according to a power law dependent of q. The correlation coefficient is questionable since there are insufficient data available and therefore no further relationships are given. Nevertheless, the data indicate that the exponent b, which relates a to q_{res} from a constant strain rate test, decreases less than a for increasing strain rates:

$a(\dot{\varepsilon} = 7.9 \cdot 10^{-6} \cdot s^{-1}) \approx 0.2 \cdot a(\dot{\varepsilon} = 7.9 \cdot 10^{-7} \cdot s^{-1})$, and

$b(\dot{\varepsilon} = 7.9 \cdot 10^{-6} \cdot s^{-1}) \approx 0.5 \cdot b(\dot{\varepsilon} = 7.9 \cdot 10^{-7} \cdot s^{-1})$.

5.4 Conclusion from the Data Analyses

It was possible to determine a relationship for the minimum, steady state axial creep strain rates as a function of the temperature, volumetric ice content and applied stress that is valid for a large range of warm, i.e. 0 – -5°C, and ice-rich permafrost soils within a legitimate accuracy. The results presented herein are encouraging, considering the differences in sample quality.

It has also been demonstrated that the shear strength is primarily a function of the sample composition and the axial strain rate. It was further possible to detect the influences of various boundary conditions. In addition, it was shown that the creep and strength response are strongly linked.

However, volumetric behaviour could not be analysed properly, mainly due to limitations of the testing equipment. In order to study this effect, special measuring techniques are required in combination with detailed analyses of the structural changes taking place during a test. These will be discussed further in the recommendations for future work (Section 8.3).

Chapter 6

Comparison Between Laboratory and Field Investigations

Determination of an appropriate constitutive model and the relevant parameters is the main goal following on from the laboratory tests performed on real rock glacier samples with a view to numerical modelling of rock glacier behaviour for future predictions and past reconstructions. All analyses are worthless if they do not represent the behaviour experienced in nature. The laboratory results are now compared with the field measurements, which have included deformation measurements taken at both rock glacier locations as well as pressuremeter tests at the Murtèl-Corvatsch rock glacier (see Chapter 3). The comparisons made in the current chapter are very preliminary, and serve only to prove that the laboratory results can be used for future investigations. Consequently, many assumptions had to be made, either to simplify the problem or because of a lack of knowledge. Further investigations are necessary for a better solution of the problem presented here.

6.1 Deformation Measurements

6.1.1 Scenarios

Various different scenarios were chosen in order to demonstrate the influence of the temperature and the volumetric ice content with depth for an imaginary, 35 m layer of frozen soil, which seems to be representative for several Alpine rock glaciers (Barsch, 1996). As a first step, strain rates were calculated with the solution deduced within the previous chapter (equation [5-8]) in order to compare the different scenarios and influences. These values were then normalised by the maximum axial strain rate of the scenario under investigation and summed up from the bottom to the top after multiplying the result with the depth interval for a unit time step. This procedure reveals the extent of influence of the various boundary conditions (Figure 6-1). It is important to note that it is not possible to compare

each scenario directly, since the maximum strain rates vary considerably. The input data for the scenarios are given in Table 6-1, different temperature and earth pressure coefficients based on *total* stresses (*K*-values) are investigated for some specific volumetric ice contents. The *K*-value, which is the ratio between the horizontal stress σ_h and the vertical stress σ_v, is an indicator for the current creep inducing stress. A temperature gradient of 0°C/100 m or various constant *K*-values would have resulted in similar distributions of the virtual deformation and are therefore not presented. Seasonal changes in temperature within the upper part of the ground are neglected and a virtual mean temperature T_M was chosen for the surface. A basic volumetric ice content of 90% was selected. This is a realistic value that differentiates permafrost from an ice glacier.

The scenarios represent the main phenomena as follows:

Scenarios A_1 & A_2

The temperature is constant throughout the whole depth of the permafrost. Although this is not realistic, it serves as a basis for comparisons. An increase in the *K*-value is also more realistic than a constant value, in particular due to the inclined nature of a rock glacier. It must be assumed that the horizontal stresses increase with depth.

Scenarios B_1 – B_6

Various temperatures and temperature gradients are compared within these scenarios. Due to different initial conditions (i.e. temperatures at the surface) and temperature gradients, the depths of the permafrost base *(T* = 0°C) varies. A gradient of 5°C per 100 m is a realistic value (e.g. Corvatsch 2/1987), while 8°C per 100 m is rather large. However, such a gradient might be possible due to thermal irregularities.

Scenarios C_1 – C_3

Constant ice contents were chosen throughout the whole layer and might therefore represent various permafrost conditions. The temperature and the *K*-value are kept constant.

Scenario D

In contrast to the scenarios C, the temperature increases with depth and a 5 m thick layer with a volumetric ice content of 50% as well as a layer with 40% (> depth of 30 m) were included, simulating layered soil conditions. The remainder of the rock glacier above 15 m and between 20 and 30 m contained 90% ice by volume.

Scenario E

The *K*-value was set to 2.0 at a depth of 20 m after increasing linearly from *K* = 1.1 at 15 m depth. Such a scenario represents a possible arching effect in the ground resulting in stress concentrations at a definite depth and might also be typical for layered soils. The value of *K* reduced again to 1.1 over the depth of 20 – 25 m. The volumetric ice content was constant at 90%.

Scenario F

This is probably the most realistic scenario, due to the changes in temperature, volumetric ice content and *K*-value with depth. However, all changes are assumed to be more or less gradual, which may not be correct for natural conditions.

The sum of lateral deformations for the different scenarios as shown in Figure 6-2 is determined as follows:

1. The creep strain rate at a depth *z*, $\dot{\varepsilon}(z)$ is calculated according to Equation [5-8] as a function of the temperature *T*, stresses (σ_v, $\sigma_h = K \cdot \sigma_v$) and volumetric ice content w_i.
2. The relative strain rate is expressed as a function of the maximum strain rate for the whole layer:
   $$\dot{\varepsilon}_{rel.}(z) = \frac{\varepsilon(z)}{\varepsilon_{max}}$$
3. Over a finite depth interval $\Delta z = z_2 - z_1$, the deformation *d* can be calculated according to: $d = \Delta z \cdot \dot{\varepsilon}_{rel.}(z)$.
4. The sum of the normalised deformations shown in Figure 6-2 were subsequently determined by summarising the lateral deformations of the intervals Δz from the bottom to the top.

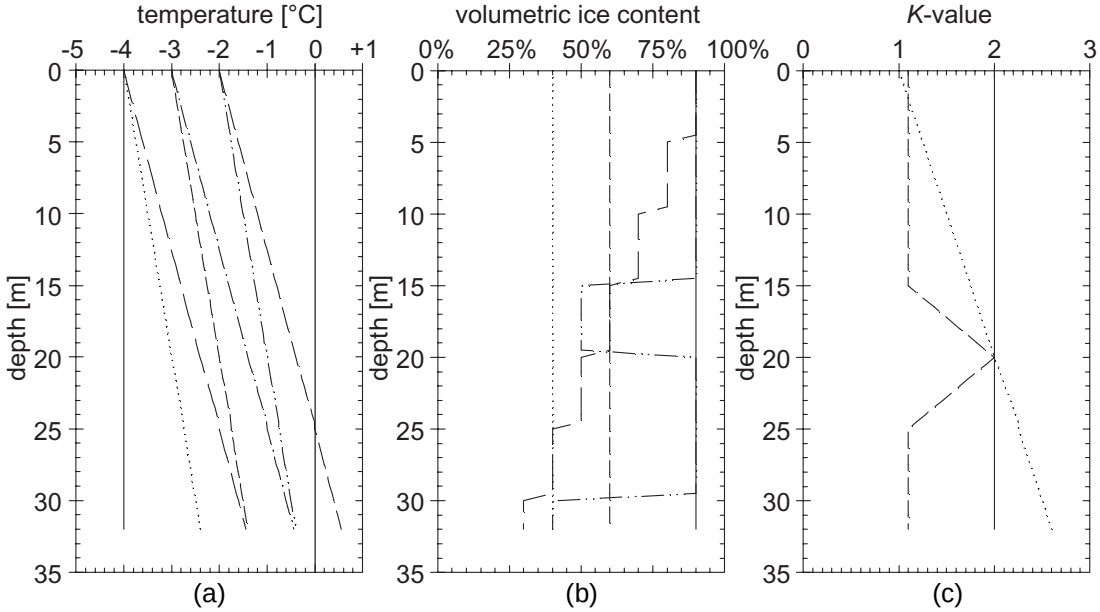

signature	(a)	(b)	(c)
———	A_1, A_2, C	A_1, A_2, B_1–B_6, C_3, E	A_1, B_1–B_6, C, D
·····	B_1, D, E, F	C_1	A_2, F
– – – – –	B_2	C_2	E
—·—·—	B_3	D	
— — —	B_4	F	
—··—··—	B_5		
— — — —	B_6		

$$K = \frac{\sigma_h}{\sigma_v}$$

Figure 6-1: *Various input parameters for the six scenarios.*

	temperature	*K*-value	ice content
Scenarios A	gradient: 0°C/100 m T_M = -4°C	const. (2.0) / linear increase	90%
Scenarios B	gradient: 5°C & 8°C/100 m, T_M = -4°C, -3°C, -2°C	2.0	90%
Scenarios C	gradient: 0°C/100 m T_M = -4°C	2.0	40%, 60%, 90%
Scenario D	gradient: 5°C/100 m T_M = -4°C	2.0	15–20 m: 50% >30 m: 40% rest: 90%
Scenario E	gradient: 5°C/100 m T_M = -4°C	15 – 20 m: 1.1 – 2.0 20 – 25 : 2 – 1.1 rest: 1.1	90%
Scenario F	gradient: 5°C/100 m T_M = -4°C	linear increase	90% – 30%

Table 6-1: *Overview scenarios.*

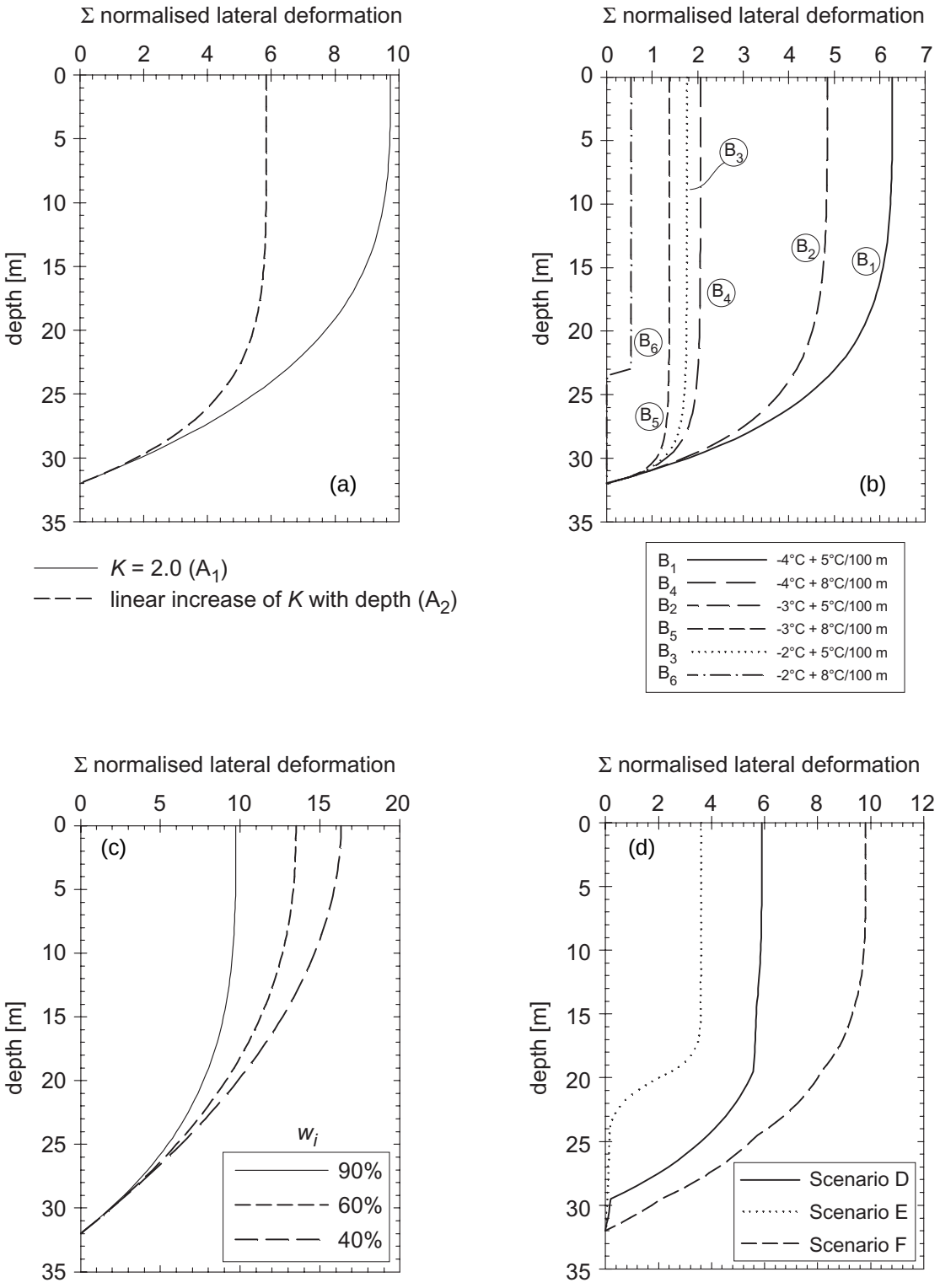

Figure 6-2: *Deformation distribution plots for various scenarios (Table 6-1).*
a) Scenario A (dT/dz = 0, variation in K, w_i = const.)
b) Scenario B (variation in dT/dz, w_i and K = const.)
c) Scenario C (variation in w_i, dT/dz = 0, K = const.)
d) Scenario D (variation in w_i, dT/dz = const., K = const.)
Scenario E (variation in K, dT/dz = const., w_i = const.)
Scenario F (variation in K and w_i, dT/dz = const.)

Some major mechanisms and conclusions can be summarised from the deformation profiles presented:

- Constant conditions in terms of temperature, ice content and *K*-value, result in a smoothly curving deformation profile, i.e. no distinct shear horizon can be determined. This is because only the stresses increase without affecting the creep parameters.
- A variation of the boundary conditions with depth in order to represent more “realistic” states, results in much higher strain rates with depth, and therefore, the deformations tend to be more concentrated near the bottom of the frozen layer.
- Larger temperature gradients have the effect that temperatures become closer to zero centigrade at a shallower depth. Considering the strongly exponential influence of temperatures on the strain rate close to the melting point, it is not surprising that the main part of the deformation occurs within the lowest few metres.
- Low volumetric ice contents reduce the creep susceptibility, and therefore the deformations are more uniformly distributed.
- Distinct shear horizons or zones can only be formed when a sharp difference in the volumetric ice content or stress occurs. The former condition is very typical when considering the stratigraphy of a rock glacier. However, this effect might even act in very thin layers of some millimetres (see also Arenson *et al*., 2002). The latter effect is possibly due to arching effects or porewater that influences local stress conditions, either through seepage or due to high pressures of water trapped within the pores.
- Theoretically, sharp changes in temperature would also evoke a shear horizon. However, numerous temperature measurements have shown that this is not likely to be relevant within the Alpine permafrost under investigation.

6.1.2 *In Situ* Deformation Measurements

The borehole deformations of the two rock glaciers, Muragl and Murtèl-Corvatsch, which were recorded with slope inclinometers, are presented in Chapter 3. As shown in the previous section, the shear horizons observed cannot be explained by smooth changes in the stratigraphy, temperature or stress conditions assumed in this simplified analysis. Temperature profiles (Figure 6-3) with a temperature gradient of 5.8°C/100 m for Muragl and 3.5°C/100 m for Murtèl-Corvatsch were chosen, neglecting seasonal variations within the upper 15 m as recorded during *in situ* monitoring. The volumetric ice contents and densities (Figure 6-4) were determined using sample analyses of the cores.

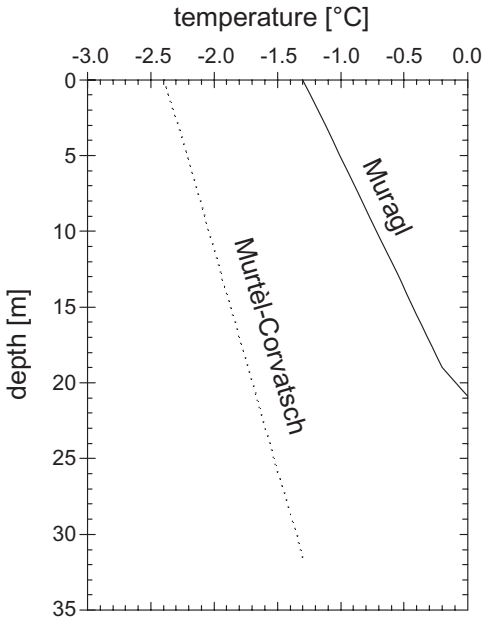

Figure 6-3: *Temperature*

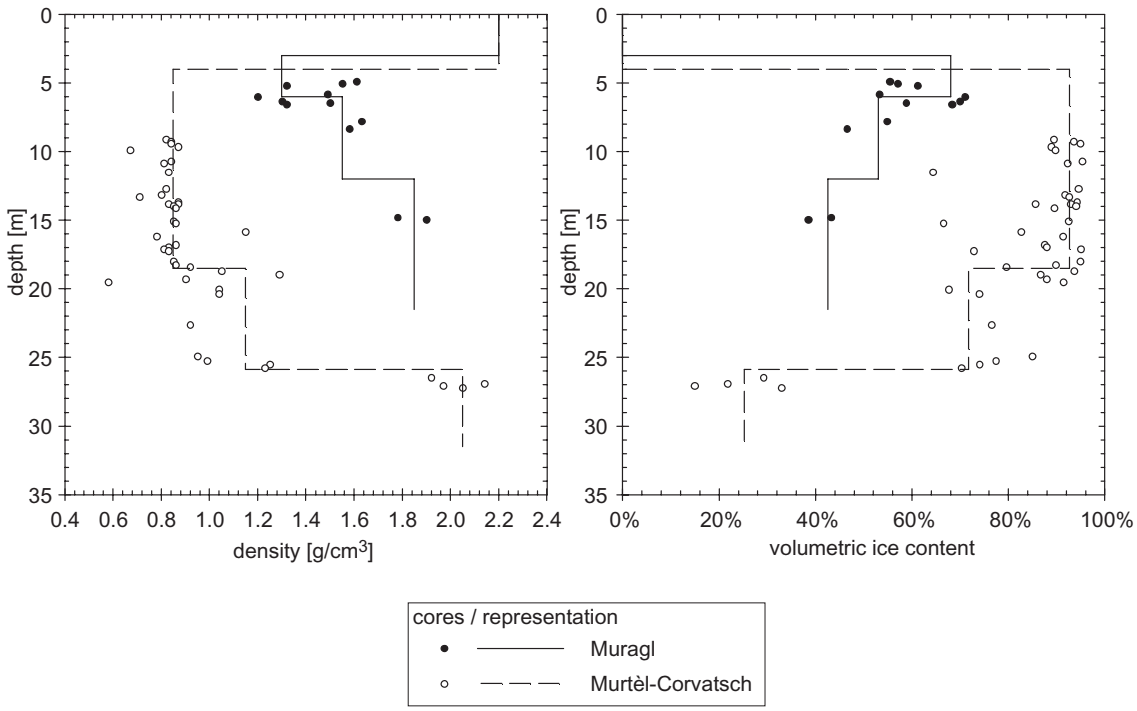

Figure 6-4: *Density and volumetric ice content for the representation used.*

The ratio between the horizontal and vertical stresses, i.e. *K*, was assumed to increase linearly from a value of 1.0 at the surface towards 2.0 at the permafrost base, i.e. 21.5 m for Muragl and the depth of the shear zone within borehole 2/1987, i.e. 31.5 m for Murtèl-Corvatsch

A maximum lateral strain rate could be determined similar to the proceedings described on page 197, from the boundary conditions mentioned above at a depth of about 26 m for Murtèl-Corvatsch and 19 m for Muragl (Figure 6-5). Both maxima can be found in layers that are warm, but still have a considerable amount of ice. The distribution (in percent) also reveals that lateral deformations are more uniform for the colder site (Murtèl-Corvatsch). This is mainly due to the strong increase in strain rate at temperatures close to the melting point, and therefore the strain at 19 m depth is predominant within the Muragl rock glacier.

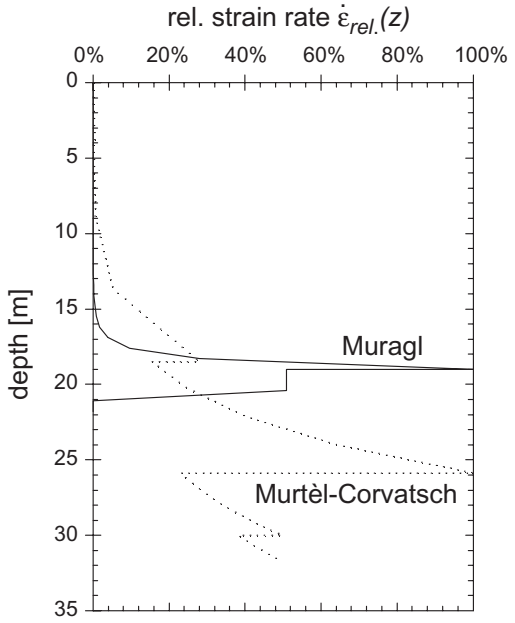

Figure 6-5: *Distribution of the relative strain rate with depth in percent. 100% represents the maximum strain rate determined within the permafrost layer.*

A deformation profile was calculated from the individual strain rates shown in Figure 6-5, and this is presented in Figure 6-6, showing the consequences of the phenomena described above. Typically a very distinct shear zone can be deduced for Muragl, whereas the Murtèl-Corvatsch model shows several distinct layers, which exhibit increased strain rates. However, the top layers show nearly no creep deformations, which is larger due to the cold temperatures. A comparison of the actual numbers is not very appropriate due to a large difference in the maximum strain rate, which was the basis for the calculations. The maximum for Muragl was about five magnitudes higher than for Corvatsch, and since this maximum was calculated for a depth close to the permafrost base, with a rapid decrease for shallower depths due to the temperature decrease, the sum of all deformations was about four magnitudes smaller. Smoothly distributed strain rates result in a larger sum of the deformations, even though the maximum strain rate may be much smaller and *vice versa*.

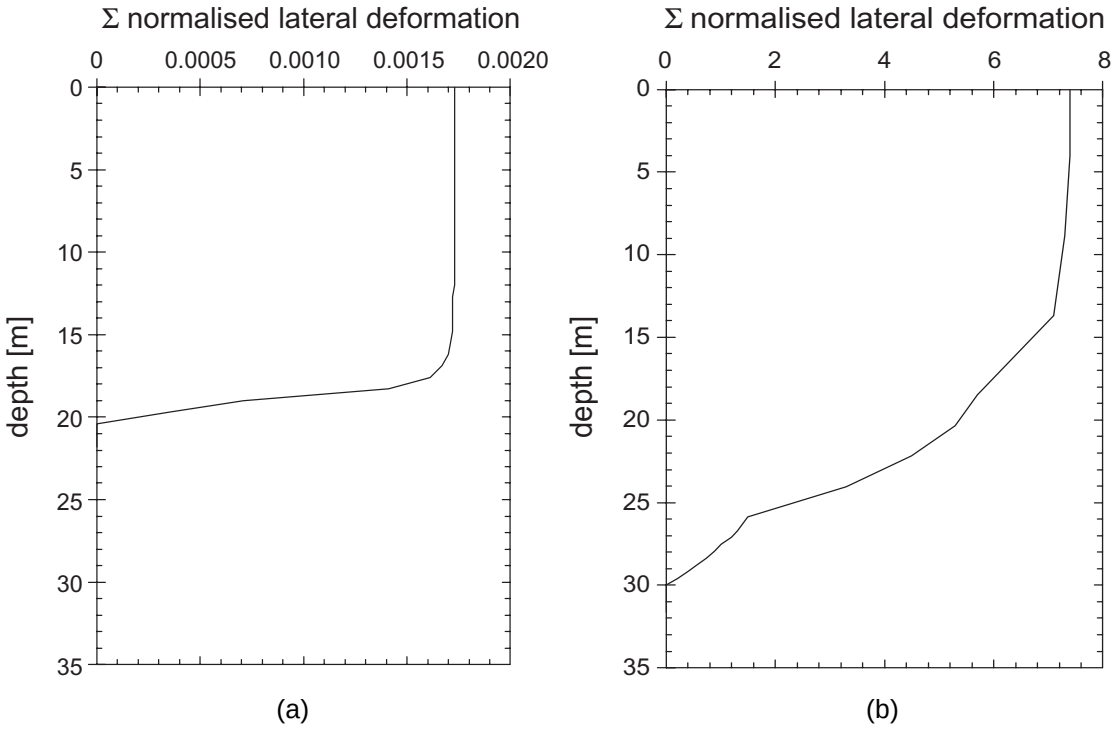

Figure 6-6: *Deformation profiles for (a) the Muragl and (b) the Murtèl-Corvatsch rock glacier.*

Judgement of deformation profiles

Comparing the calculated deformation profiles with those measured *in situ* (Figure 3-24 and Figure 3-39), agreement in terms of shape of the curves can be determined as well as many nonconformities. The distinct shear zone is represented very well for the Muragl site, which is a function of the high temperature. In addition, the stress assumption does not appear to rule the response predominantly. For the colder Murtèl-Corvatsch rock glacier, it was not possible to model a distinct shear zone, since the influence of the temperatures is less dominant. A shear zone similar to the inclinometer data can therefore only be explained by sharp changes in stress conditions. Several arching events within the ground may result in horizontal stresses that cannot be linked to the vertical stress in the same way throughout the whole depth. Some layers may have K-values close to 1 whereas other layers might show values that are closer to passive failure ($K \approx 3$, assuming no cohesion) and hence increasing the strain rate tremendously.

Extrusion effects, such as those observed at Muragl 3/1999 at about 16 m, or at Murtèl-Corvatsch 2/1987 between 22 and 28 m, could not be modelled. As discussed in Arenson and Springman (2000) or Arenson *et al*. (2002), such anomalies might be induced by three dimensional interactions caused by the very heterogeneous nature of rock glaciers and due to deformations within the active layer.

The model used, assumes ice within the lowest part of the Muragl rock glacier at temperatures just below zero centigrade, even though data from the boreholes have shown that no ice was present at temperatures below 0°C, due to sub permafrost air circulation (Vonder Mühll *et al*., submitted) and therefore, the creep should be zero at this depth.

In addition, the author could not determine absolute numbers for the deformations, mainly due to a lack of knowledge of the stresses acting and due to a missing reference length that could be used to multiply the strains in order to obtain displacements.

It was shown that some features can be explained by the solution presented by comparing calculated and measured deformations. A one dimensional analysis, however, is insufficient for modelling rock glacier behaviour due to the very complex structure and stress distribution. Numerical modelling, such as finite element (FEM), finite difference (FDM) or particle flow code (PFC) analysis, are therefore inevitable, even though several drawbacks have to be considered such as

- limitation for large strains with FEM,
- the determination of *in situ* stress conditions, and
- discontinuities and brittle behaviour are difficult or impossible to model with FEM and FDM.

6.2 *In Situ* Pressuremeter Tests

A detailed analysis of the modelling of pressuremeter results and a comparison between creep parameters determined from *in situ* pressuremeter and triaxial tests are given in Arenson *et al.* (submitted, a), and therefore only a brief summary will be given herein. From the two different approaches for the determination of creep parameters, a *primary creep approach* (e.g. Ladanyi and Johnston, 1973) and a *secondary creep approach* (Kjartanson *et al.*, 1988), only the latter will be investigated since this method adopts steady state creep rates and consequently, comparable creep parameters can be determined. It was not possible to investigate the dependency of the field data on the temperature since the number of these tests was limited. Therefore, the basic form of the creep equation was used (see also Chapter 5.1):

$$\dot{\varepsilon} = A \cdot \sigma_e^{\,n} \qquad [6\text{-}1]$$

The radial creep strain rate ε was expressed as a function of the stress invariant σ_e and two creep parameters A and n, which are temperature and structure dependent and are therefore not constant throughout the length of the borehole. The variation of these two creep parameters for the pressuremeter tests and for all triaxial creep tests that were performed on samples from borehole 1/2000, are shown in Figure 6-7. Most of the triaxial creep tests were performed at lower temperatures than those *in situ*, so that greater creep susceptibility would be expected. Only the test on the sample from a depth of 22.8 m (No. 45: T = -1.15°C) was performed at a comparable temperature. The samples from 25.7 and 25.9 m were tested at about -2.1°C, whereas the rest were tested at a temperature of about -4.1°C.

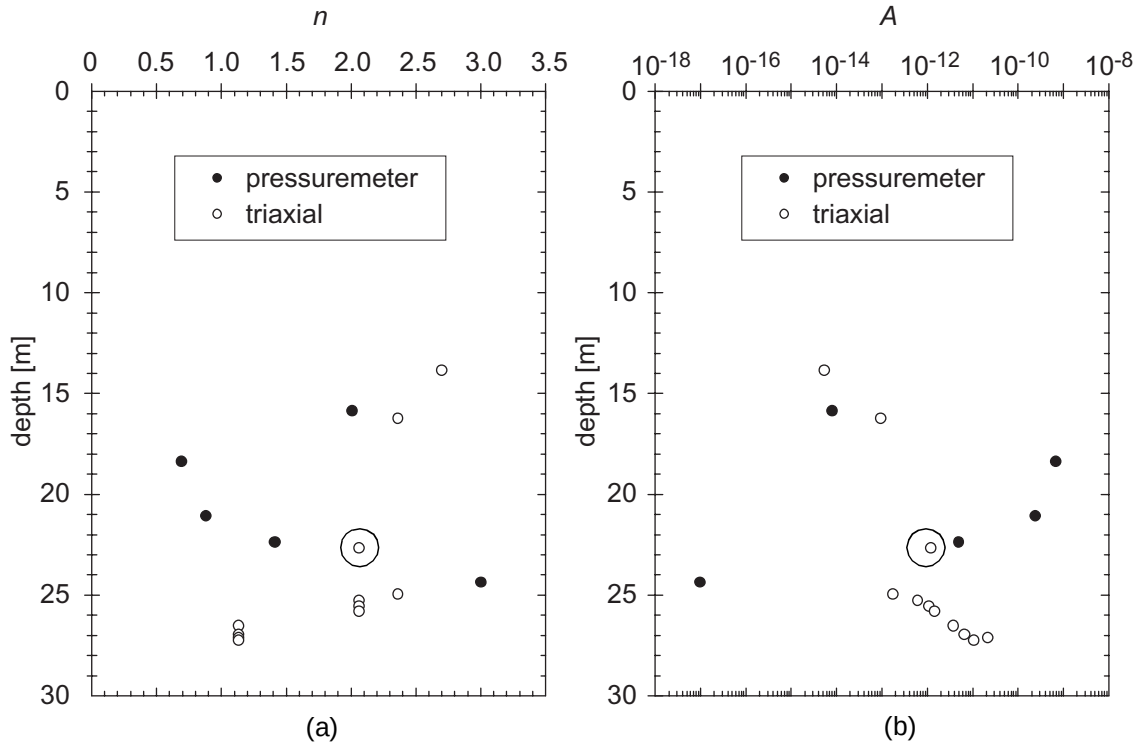

Figure 6-7: *Creep parameters (a) n and (b) A for pressuremeter and triaxial creep tests. Test No. 45 is marked with a circle.*

However, considering the differences in test temperature, the pressuremeter reveals very consistent results that are comparable with the triaxial creep tests and especially that of test No. 45 at a comparable temperature. The very low values of *n* and higher values for *A* at depths between 17 and 22 m indicate a layer with low volumetric ice content. This might have been the cause for the failure in saving cores from that particular zone. The deepest pressuremeter test (24.5 m) indicates a very high ice content, which might not be really true when analysing the triaxial creep test. The 'real' value for *n* might be slightly lower, at maximum 3.0, and *A* higher, since equation [6-1] is very sensitive to small changes in *n* and *A*. Nevertheless, the pressuremeter shows that at the corresponding depth there is a layer with a higher ice content compared to the adjacent layers.

Even though pressuremeter tests can be used as an alternative method of determining creep properties *in situ* for Alpine permafrost and of obtaining some hints about the stratigraphy, the heterogeneity of rock glacier soil conditions make it essential to perform a number of tests at various depths and locations. In addition, exceptional care has to be taken while drilling and preparing the testing probe. Both aspects are responsible for the test quality. While careful drilling results in better borehole stability and a smoother borehole wall, temperature equalisation of the probe minimises thermal disturbances. Furthermore, pressuremeter tests might be able to be carried out under conditions where sampling is nearly impossible.

Discussion

The current discussion includes several aspects from microstructural analyses of frozen soils to rock glacier behaviour in general. In contrast to the construct of the previous chapters, the discussion starts with the fundamentals of frozen soils, which is important for the explanation of the various processes influencing the creep and strength response of ice-soil-air mixtures. Only with an understanding of the mechanisms at micro–scale it is possible to explain meso– and macro–scale behaviour. Therefore, the following chapters try to analyse the mechanisms within a rock glacier on the basis of the findings from the microstructural analyses.

This discussion is primarily based on the laboratory tests and field measurements presented within the current work. Several aspects from literature, that have been summarised in Chapter 2, are also included and discussed.

7.1 Microstructural Mechanisms of Frozen Soils

A range of microstructural mechanisms characterises the response of frozen soils. This work confirmed past findings (cf. Chapter 2) and has thrown new light on the interaction between solid particles, ice crystals and air voids during loading. Various effects are dominant, depending on the temperature, stress conditions and sample composition and are therefore responsible for the sample response and behaviour induced by an external load or deformation.

In contrast to most of the tests that have been presented in the literature, the frozen soil under investigation is characterised by high volumetric ice contents and volumetric air contents up to about 25%. In addition, unfrozen water is present, since the temperature within Alpine rock glaciers is typically close to the melting point of ice, in particular within the zones of major deformation that are of main concern. The structure of an unloaded frozen model soil, which will be used for further description of the microstructural behaviour, is shown in Figure 7-1

and is adopted from Schulson (2001) who demonstrated the formation of a shear fault in polycrystalline ice. This soil consists of a reasonably symmetric ice matrix, that is more or less similarly oriented, i.e. the C-axis of the ice crystals are nearly parallel. This assumption might not be true, but simplifies the various sketches. The grain size of the ice crystals vary and is smaller close to the solid particles. The percentage of solid particles is low and hence, the particles are not in contact with each other from the beginning. A volumetric ice content of about 68%, a particle content of about 28% and an air content of 4% is given within the presented Figure 7-1. Typically, there is a thin layer of unfrozen water around the soil grains that adheres to the solids and forms between them and the ice crystals. This layer might be several μm thick, since the temperature is only just below 0°C. Air bubbles and cracks present within the ice matrix will influence the behaviour significantly. Some of these air voids might be interconnected, when considering a three dimensional expansion, but there are also air voids that are trapped within the ice matrix.

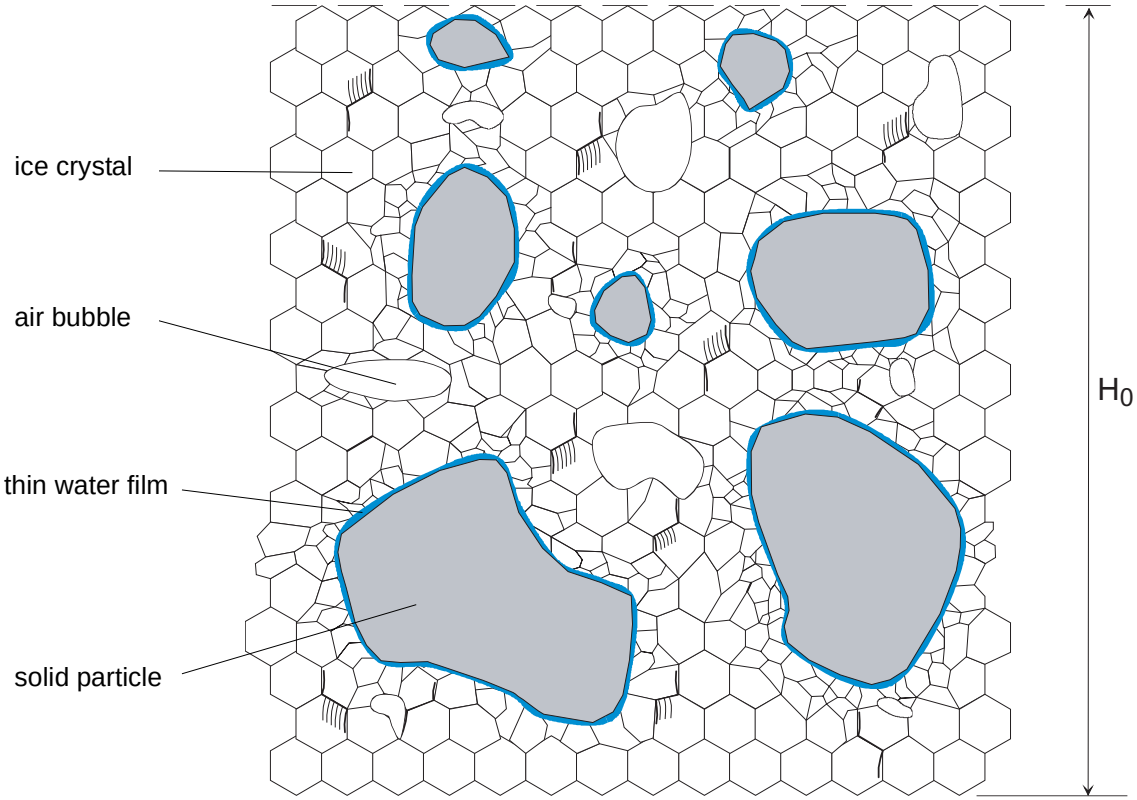

Figure 7-1: *Structure of a model frozen soil, before any loading or deformation occurred.*

The soil will now be loaded. The response will differ depending on the loading rate and the amount of air voids (Figure 7-2). Open air voids will be more compressed than trapped air voids, since the pressure in the air can be adjusted to the overall condition. Within a soil with a high volumetric air content, the pressure within the compressible air increases as the volume reduces. In addition, damping can develop, resulting in enhanced grain boundary sliding instead of ice crystals breaking due to secondary cracks that take effect in the case of a rapid loading (brittle failure). The response of a creep tests might be different, depending on the test procedure used.

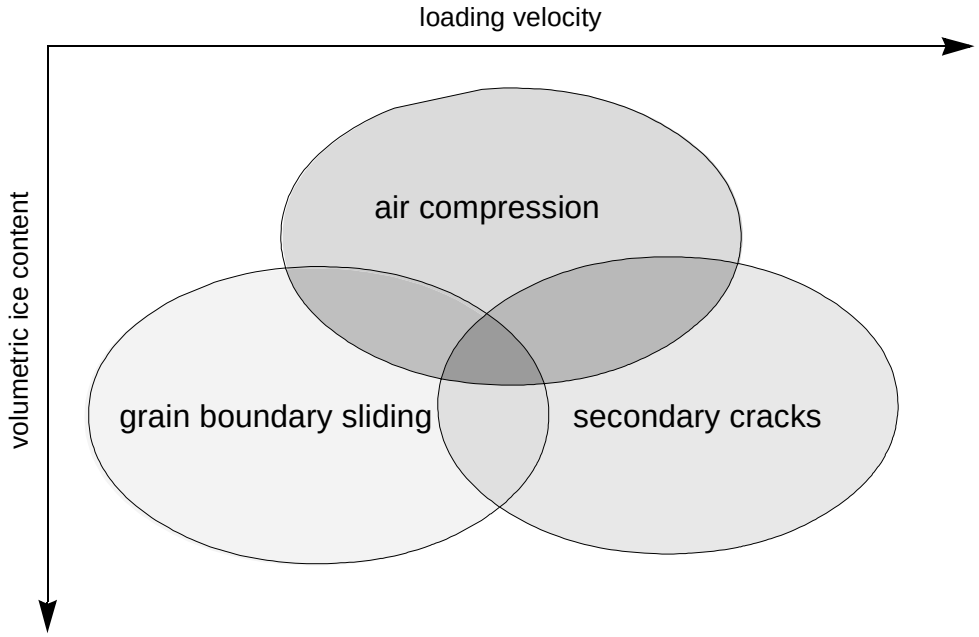

Figure 7-2: *Dependency of the response mechanism of frozen soil on the loading velocity and the volumetric ice content.*

A loading frame with a stepper motor was used in this study, i.e. the load could not be applied immediately, since several steps were necessary to achieve the desired load. Maximum loading velocity was 10 N/s. The time interval between the start of the loading until the full load was acting lasted up to 90 s for a softer sample. In contrast, it is possible to put the sample immediately under the desired stress conditions for creep tests where a dead load can be placed directly on the sample (usually for uniaxial creep tests). This difference in loading rate results in larger primary creep response for the finite loading, since more grain boundary sliding occurs. The nearly infinite loading rate accounts for the stiff behaviour of ice under rapid loading. However, it is assumed that the stresses within the sample are independent of the test procedure after some time, i.e. secondary and tertiary creep responses will be similar.

Four situations of the deformed structure of Figure 7-1, with an initial height of H_0, are shown in Figure 7-3 and described in the following sections. Steps one to four represent situations with an increasing axial compression ΔH.

The deformed soil sample is shown in Figure 7-3 after step 1. The solid particles are still in the same position within the ice matrix, and only very few ice crystals have been broken into smaller pieces. The reduction in the volume of the air voids results in a general volume decrease, i.e. reduction in height (ΔH_1), without affecting the horizontal extension of the sample.

Further loading (Figure 7-3, step 2) prompts more sliding between the ice crystals, which might be promoted by the high pressures within some of the trapped air voids due to a local reduction of the effective stress. The solid particles are now being moved closer together until they come into contact with each other. Some pressure melting must be expected around the particles due to stress concentrations, enhancing the sliding process. The volume of the air voids cannot be decreased similarly to the first loading step and hence the cross

sectional area increases. The dislocation within the crystalline structure also breaks some of the bonds between the crystals, and additional voids can be created, starting with the formation of new wing cracks. Some air voids might also be split into two halves due to compression, and crystals may start to refreeze in areas of stress reduction.

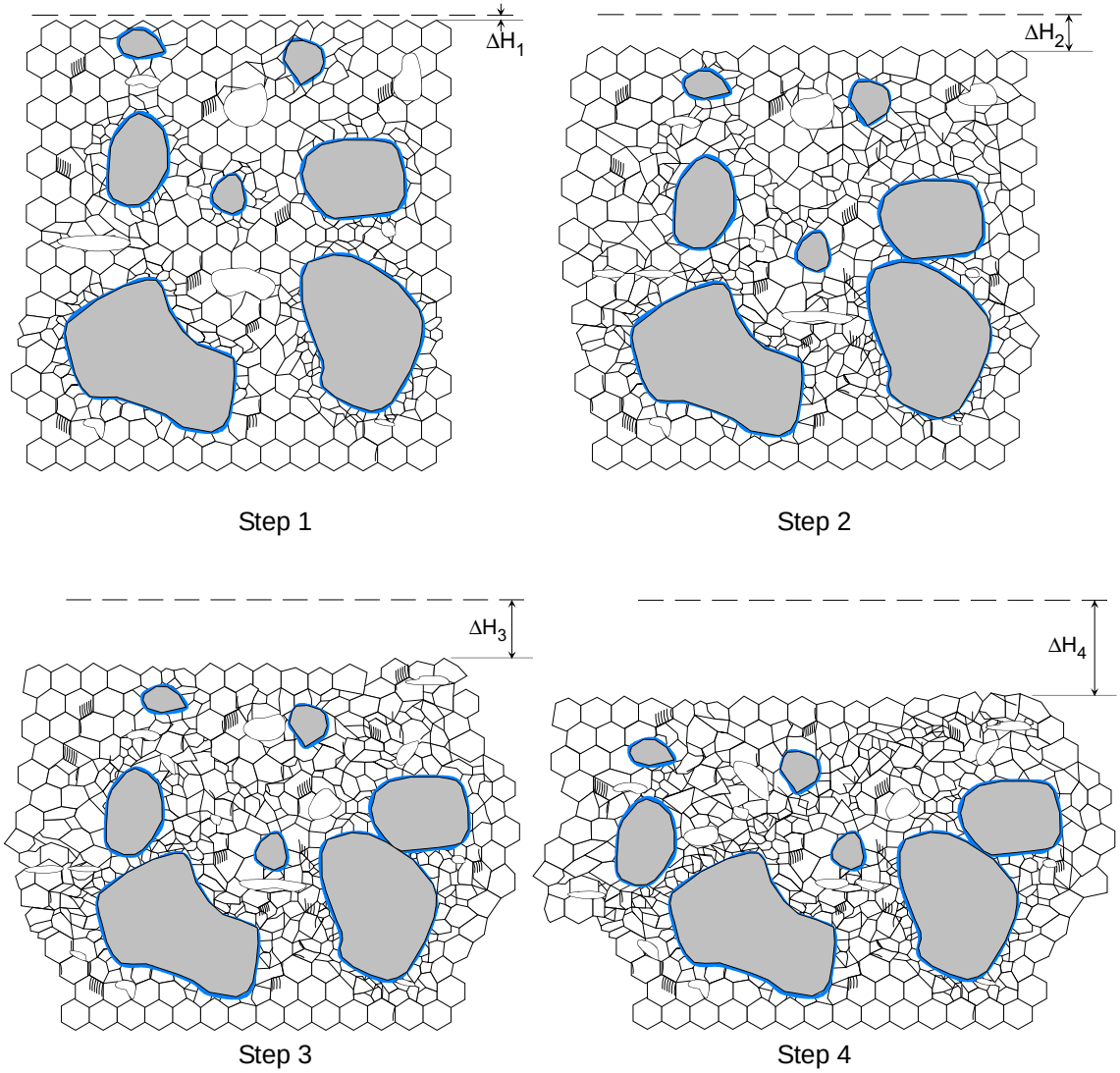

Figure 7-3: *Deformation mechanisms.*

The particles that are in contact have to pass around each other, since the strength of the individual grains is much higher than the strength of the crystalline matrix. The soil will re-structure, accompanied by cracking of bonds and destructuration of ice crystals into smaller pieces. However, smaller crystals enlarge the critical strain necessary for crack initiation (Sinha, 1984), possibly resulting in a slight increase of shearing resistance. This change of the matrix causes the sample to increase in volume. Pore air expands within the opening cracks, and hence pore pressures might decrease within a closed system (Step 3). Stress concentrations through the particles may further result in pressure melting, and ice crystal fracturing occurs between the solid grains.

A preferential shear plane develops for very large deformation, along which smaller ice crystals can be observed (Step 4). The solid particles cannot contribute anymore to the shearing resistance, other than by limiting the degrees of freedom of shearing deformation within the fractured series of ice crystals along the failure plane. The bonds in low-stress areas can refreeze, since deformations are only expected within a thin shear layer. Further volume decrease or change in pore pressures may not develop as long as the air voids remain trapped. The sample has reached a residual state, characterised by constant volume for further shear deformations. However, some voids within the area of concentrated shear might be connected to an open system due to the ongoing deformation, allowing further volume decrease. On the other hand, new fracturing between the bonds or within the ice crystals may as well result in opposing behaviour, i.e. a volume increase.

In terms of deviatoric stress q, pore pressure u and volumetric response V, the steps 1 to 4, shown in Figure 7-3 and described above, can be presented as shown in Figure 7-4.

Step 1 is represented by a steep increase of q up to the primary yield region, where the bonds between the ice crystals start to break and grain boundary sliding occurs (2). Further strength with subsequent strain softening is now mobilised due to structural hindrance, i.e. the particles come into contact with each other and have to move within the ice matrix (3). A peak in strength can therefore only be mobilised if enough solid particles are present (Figure 7-5). The ice crystals within a matrix with a low percentage of solids will keep on sliding at a low strain rate and no peak will be reached at small strains. The behaviour is ductile in contrast to the dilatancy that can be observed for samples with more solid grains.

The volume decreases as the pore pressures reach a maximum before the behaviour becomes dilatant, while mobilising additional strength during the second step. The pore pressures, however, are actuated by a mixture of porewater, that might be present as free water or as water bound to the grains, and pore air, which is trapped within closed voids.

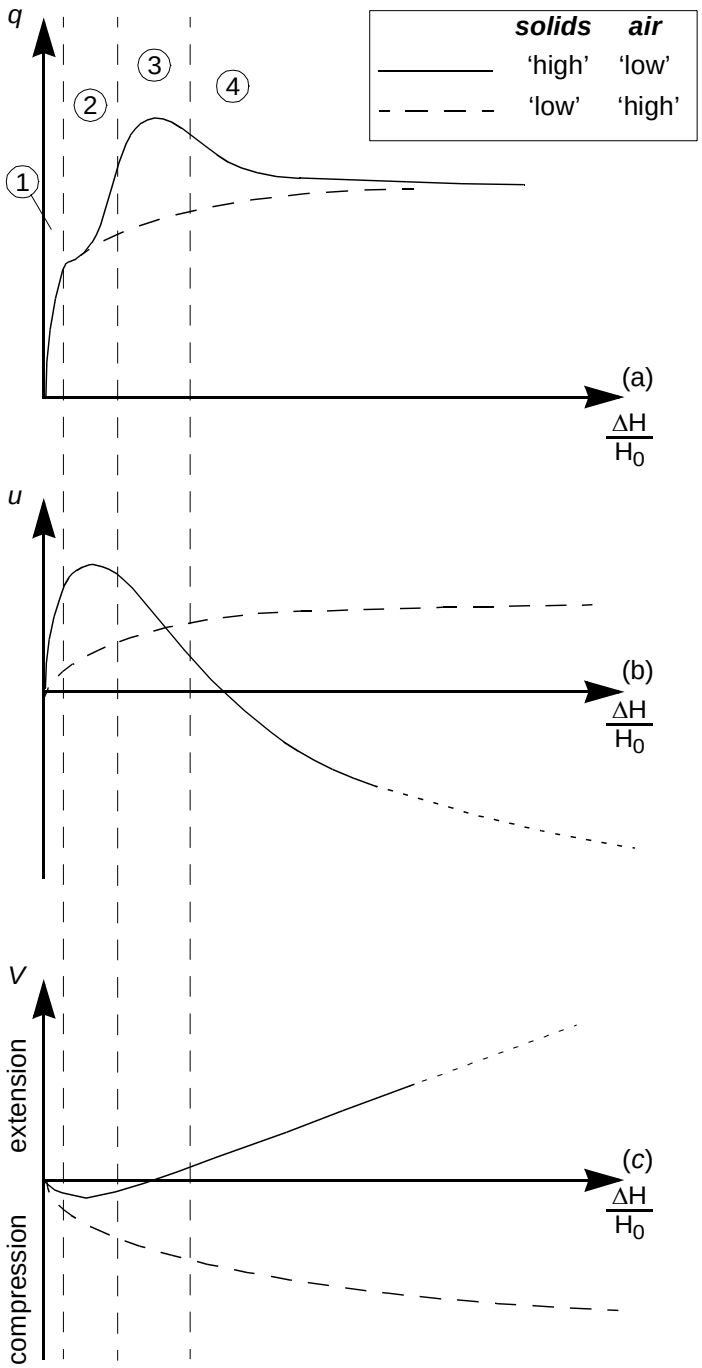

Figure 7-4: *Deviatoric stress q, pore pressure u and volumetric response V during shearing of frozen soils.*
a) deviator stress q against axial strain $\Delta H/H_0$
b) pore pressure u against axial strain $\Delta H/H_0$
c) volume V against axial strain $\Delta H/H_0$

The volume increases again and the pore pressures can even become negative (4) provided that the grains, ice crystals and solids, move further apart from each other. The volume (or under undrained conditions, the pore pressure) approaches a constant value under drained conditions for unfrozen soils, such

as a dense sand. This might be the case for very large strains within a frozen environment, but ongoing melting, refreezing or bond breaking processes may result in continuous change in volume and pore pressure, of which, the former has also been recorded by Shibata *et al*. (1985).

Only a volume decrease, i.e. compression, in combination with an increase in pore pressures can be measured for a very loose soil, which is characterised by high ice and air content. However, for very large strains, even such a material might start to behave similarly to a denser soil. This could be shown from the constant strain rate tests for very loose samples after long lasting creep tests.

Brittle fracture has to be considered in addition to the physical mechanisms leading to a *dilatant* or a *ductile* response (Figure 7-5). Ice can behave very stiffly under rapid loading conditions. A peak shear response will be mobilised within a few micro strain, followed by a sudden decrease in strength due to a collapse of the crystalline structure. Severe fracturing results in the formation of many new, but much smaller ice grains. The volume increases and the pore pressures decrease at the beginning, but change their behaviour immediately at the peak strength due to this 'pulverisation' of the sample. Therefore, nominally ductile soils can also have a peak strength if they are loaded fast enough (Figure 7-5).

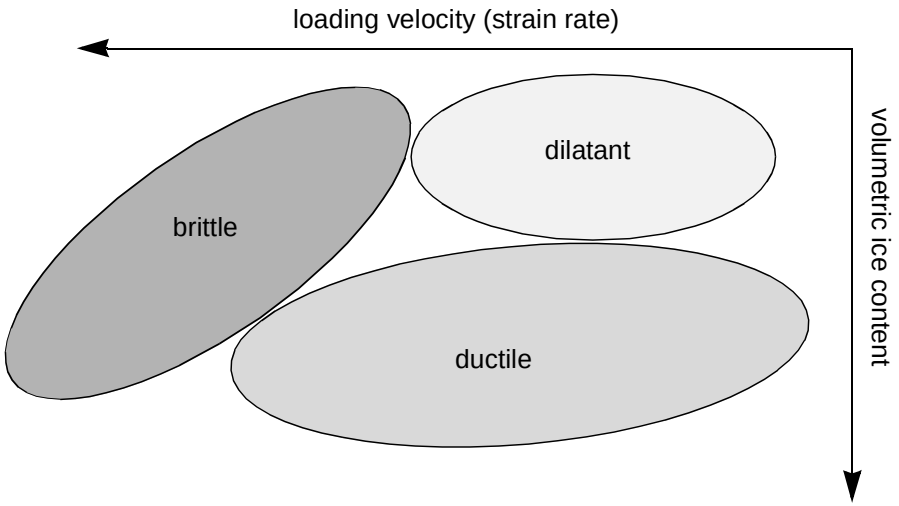

Figure 7-5: *Stress response as a function of the loading velocity and the ice content.*

The transition from dilatancy to ductile behaviour can only be estimated for the current tests and has to be investigated more intensively in the future. The experiments presented reveal that this transition seems to be at around 5% to10% volumetric air content for an axial strain rate of about $8 \cdot 10^{-6}$ s^{-1}. The value might also be dependent on the distribution of the air voids.

On a microstructural level, the mechanisms can be regarded as an ice-structure interaction between the ice and the solid particles. Palmer (1991a) showed that depending on the loading regime, different fragment sizes have to be expected, which may result in the sample responses shown in Figure 7-5.

It also seems to be obvious that mechanisms under shear are similar in a way to mechanisms occurring under conditions of creep, but at a lower deviator stress, since creep tests and constant strain rate tests can be compared directly (e.g. Vaid and Campanella, 1977). Mainly soil compression, i.e. compression of

air voids, accompanied by grain boundary sliding occurs due to the low deviatoric stresses during a creep test. Stress concentrations along the grain boundaries induce these bonds to break, allowing deformation to occur with stress release. This does not happen continuously and that is why most of the creep tests displayed irregularities in their strain-time diagrams. Depending on the sample, a sudden increase in strain rate was measured sometimes for a very short strain period. This can be explained by an increase in stress at various locations within the sample until the bonds break, followed by stress redistribution. Solid particles may come into contact with each other with ongoing compression of the sample during creep, reducing the strain rate due to dilatant processes. A sample with low volumetric ice content that indicated imminent creep failure through the development of tertiary creep, may reduce its creep rate again when particles start to interact and dilatancy must be overcome en route from shearing to failure.

Relaxation tests showed the self healing potential of frozen soils. As a consequence, stress releases, or reductions in deformation, allowed the frozen matrix to reform and broken bonds to refreeze. Recrystallisation can occur, changing the ice matrix. This is a function of the time scale and changes in temperature. Hence, the strength after a stress release increases until the situation is similar to the conditions before the stress decreased in terms of broken bonds, and the response will again be the same. This occurs within the first percentage of further strain, and it is therefore very dangerous to count on such a peak shear strength.

The potential for self healing and recrystallisation might also be very important for the whole creep process. It is assumed that local stress concentrations within the soil result in similar behaviour independent of whether the local stress concentration was induced by loading or a deformation at the boundary. The stress will probably increase due to further displacement during shear, which induces a new stress concentration, whereas local relaxation may act during the creep tests. The crystalline matrix may now reconfigure, appropriate for the new stress conditions during creep or relaxation, until the next stress concentration may result in local grain boundary sliding or even crack formation. Such a mechanism may be similar to the change in stress paths in a granular material that has been measured by means of grains of photoelastic material. The grains translate the contact forces into a second rank tensor and secondly they permit the stress components to be measured (Allersma, 2002).

It must be concluded that the creep process, as well as the loading-unloading-reloading process, are quite similar in terms of microstructural response. The presumption can be made that the ice-soil mixture undergoes ongoing changes, even though the loading conditions remain unchanged, and the overall sample response seems to be continuous. Examples of microscopic flow in polycrystalline ice demonstrate such ongoing crystalline changes during pure shear (e.g. Wilson and Marmo, 2000).

7.2 Constitutive Approach

Several constitutive models for creep of frozen geomaterials are presented within the literature review (Chapter 2.3.5). Most of the more sophisticated models aim to model the entire range of creep behaviour, i.e. primary, secondary (steady state) and tertiary creep. In addition, importance has been attached to creep failure, in particular the time until creep failure occurs (e.g. Fish, 1976; 1984), for which the assumption of reaching the end of secondary creep as an inflection point in the strain rate - time diagram was necessary. Such an assumption opposes the steady state creep theory that follows a Glen (1955) type law, showing a constant strain rate with time. Even though the selection of an inflection point results in a unique solution for creep for all three stages, the question remains if secondary creep really is only an inflection, and if so, where it can be located with respect to time (Gardner *et al.*, 1984). Most of the creep tests, uniaxial or triaxial (cf. Table 2-8) could not give a clear answer since the duration of the tests were either too short, the stress could not been maintained constant during the whole test, or the applied load was so large that the secondary creep phase was very small, i.e. there was only an inflection point. Similar problems occurred during the current study due to problems with the measurement of the sample volume and area. Therefore it was not easy to keep the stress constant. The primary creep phase was enlarged due to the continuous stress decrease associated with increase of sample area and hence a continuous decrease of the strain rate with time. Alternatively, instead of creating tertiary creep, a secondary creep phase with a constant strain rate was provoked.

With respect to the nature of the geomaterial under investigation, it is important to note that the stress conditions within a creeping rock glacier are much lower than the stresses induced due to artificial constructions, for which most of the presented constitutive equations and laboratory investigations have been developed and set up, respectively. Furthermore, rock glacier creep can be considered as a continuous process and not as an initial loading, resulting in a change of the stress conditions, such as would be the case for a new foundation.

As a conclusion, the simple form of steady state creep (Glen, 1955), incorporating the variation in sample condition and temperature directly in the creep parameters, was chosen to be the constitutive approach that accounts best for the natural boundary conditions. Comparisons with published data using a similar approach are not really possible, since sample conditions, stress states or temperatures varied substantially. However, the stress exponent n expected for polycrystalline ice (n = 2.78) can be compared with tests on samples with a volumetric ice content of about 100% (n ~3, see Table 2-3), indicating that the results presented fit well with previous observations.

7.3 Unfrozen Water

The pore water is always a very important element in geotechnical analysis, since it can change the effective stress conditions dramatically and hence may be responsible for significant changes in the mobilisation of shear strength. Liquid water is present within frozen soils at temperatures close to the melting point. This depends both on the amount and size of the solid particles (Williams, 1967b; Anderson and Morgenstern, 1973; Stähli and Stadler, 1997). Weakly and

strongly bonded water have varying effects. The strongly bonded water, is present around the particle, and holds them together due to negative pore water pressure that increases the effective stress and is responsible for the strength of the ice – particle mixture. In order to sustain that bond, the ice matrix has to be present all around the solid grain. If the ice is not present and the water is connected to a positive pressure, such as the atmospheric pressure, the particle will fall out of the ice matrix (Figure 7-6a & b), which could be observed at the edge of various samples (e.g. Figure 7-6c).

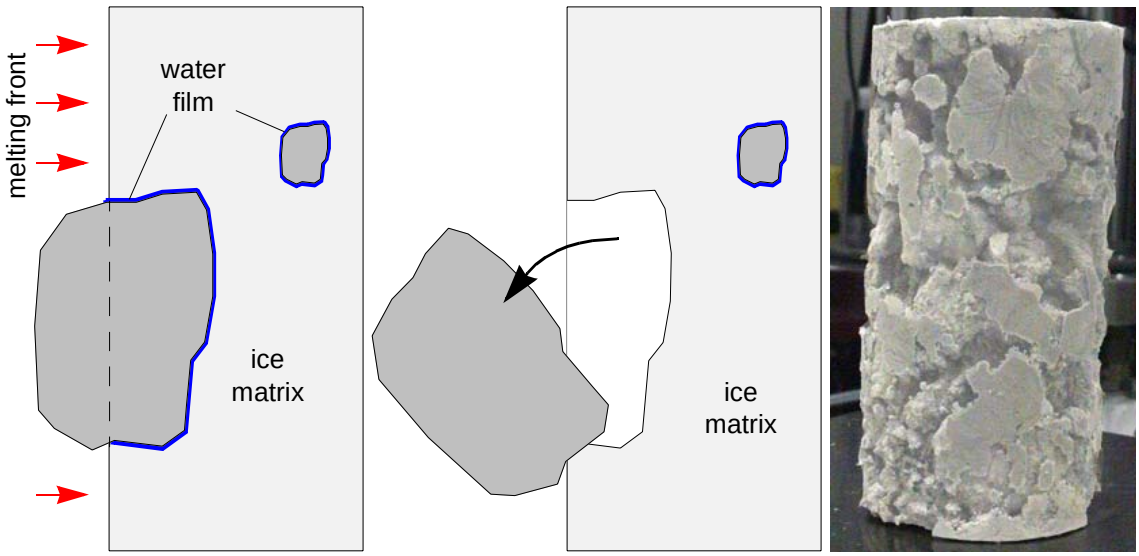

Figure 7-6: *Origin of rough surfaces for samples with low volumetric ice content: a) Some particles may be cut during the drilling process (dashed line) or exposed to a melting front so that the suction in the unfrozen water film dissipated. b) There is no suction in the water film and it cannot retain the particle, which falls out of the ice matrix. c) The sample from the Murtèl-Corvatsch borehole 1/2000 from a depth of 27.4 m shows many surface voids. Such a sample cannot be used for proper triaxial testing (height ≈ 150 mm, diameter ≈ 74 mm).*

The mechanism described can also occur within a frozen soil as soon as a particle comes into contact with air voids that are large enough to change the pressure within the water film. This may be an important mechanism that reduces the strength of a soil with a high volumetric air content.

Weakly bound water may have three central effects:

- reduction of effective stresses,
- increasing effect on grain boundary sliding, and
- thermal disturbances.

The reduction in effective stress is of major concern in unfrozen soils and can, if additional seepage or confined groundwater occurs, cause severe damage. It may also influence the crystalline ice structure. Free water will destroy the connection between the ice matrix and solid particles, similar to air voids that come in contact with strongly bonded water. In addition, water can enter cracks and enhance crack propagation and grain boundary sliding.

Despite these direct mechanical influences, weakly bound water has temperatures typically close to 0°C and can therefore accelerate the warming of the frozen soil, generating more water, reducing the suction and consequently influencing the mechanical response. Seepage through a rock glacier occurs as soon as voids are connected and preferential flow channels from the surface are present. Melt water or water from rainfall with temperatures above zero centigrade changes the thermal conditions due to conduction and convection along these channels. If the flow velocity decreases and the water has reached a temperature of zero centigrade, it can refreeze and formerly open channels will be closed. In addition, the volumetric ice content will be increased.

Even though these investigations have demonstrated more clearly the complexity of these systems, there is a strong need for more research that focuses on that influence, in particular on the rock glacier hydrology and its influence on the thermal regime.

7.4 Field Observations

Seasonal effects on deformations within the active zone have been reported, among others, by Bennett and French (1991) and Wang and French (1995). The variations have been caused by temperature changes, and in particular by the presence of water within these uppermost layers consisting of fine materials.

7.4.1 Muragl Rock Glacier

Seasonal variations in deformation have been measured for the first time for deep seated creep, i.e. within the frozen body of a rock glacier (Arenson *et al*., 2002). This change in velocity can be attributed to the shift in temperature. There will be a phase shift in temperature with depth, so that the warmer temperatures reach the shear zone (16 – 18 m) five to six months later in winter, which is accompanied by an acceleration in strain rate. Vonder Mühll *et al*. (submitted), however, showed seasonal temperature variations of about 0.5°C underneath the permafrost base within borehole 3/1999, indicating an open air system connected to the surface, which might reduce the delay in the temperature change within the shear zone. The main question to be asked is how fast the deformations react to variations in temperatures, since a temperature change has also implications on the composition, i.e. ice content of the soil. The insulating effect of the snow cover (Vonder Mühll *et al.*, 1998) could also be discussed alongside the temperature measurements, even though the measurement of the snow height failed several times due to tilting of the mast. Nevertheless, colder soil temperatures were recorded during the winters 1999/2000 and 2001/2002 than during the year in-between, where a thicker snow cover was measured.

The constant value of about 0°C within borehole 4/2000 is an indicator of the degrading nature of the permafrost within the Muragl rock glacier, where the ice only exists because it has been carried down-slope within the rock glacier. The shearing movements have tended to take place in the lowest part of the frozen zone, where the material was found to be ice-rich (>50 vol.-% ice). If melting from the bottom occurs, the shear zone may move further to the surface, for example due to decreasing ice content or, increasing structural hindrance. The ice in the non-moving layer will melt while the process will slowly proceed and the shear zone might gradually move towards the surface, accompanied by a loss in volume (Figure 7-7).

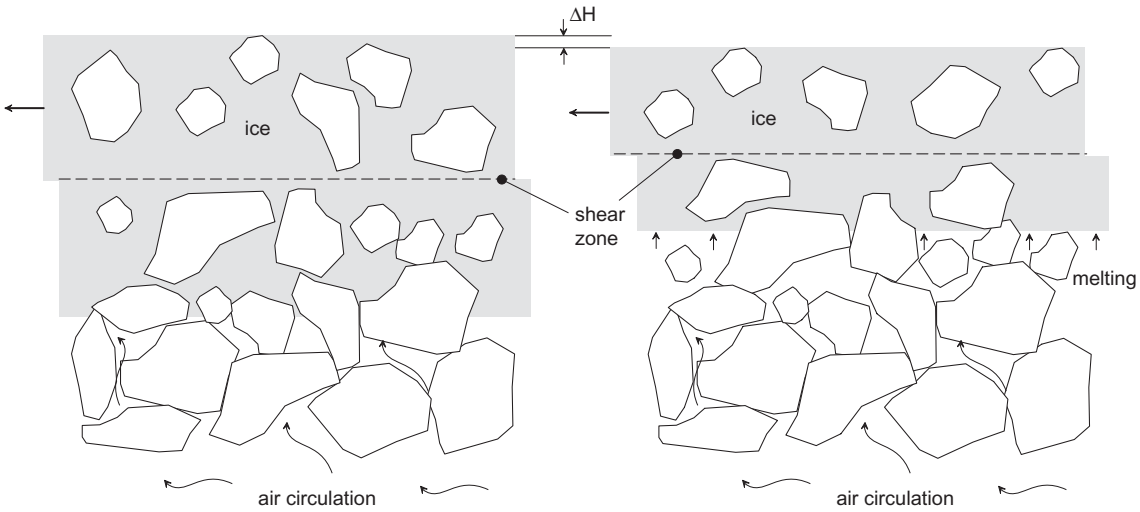

Figure 7-7: *Melting at the permafrost base resulting in a shift of the shear zone to a shallower depth.*

Water accumulation within the layer underneath the permafrost base can be ruled out due to the free draining nature of the soil matrix. Dramatic deformation events, similar to those demonstrated by surging glaciers due to uplift pressures (e.g. Björnsson, 1998), are not likely to occur. The deformations observed seem to be more or less continuous, which has major implications for the slope stability (see below).

Unfortunately, it is not possible to follow up on the borehole deformations due to the large deformation within the shear zone, which destroyed both inclinometer casings within four and nine months, respectively. However, future monitoring of the temperatures might be an indicator of possible changes in the depth of the shear zone if the temperature conditions change in the future. This conclusion can be drawn from the observation that the shear zone within the Muragl rock glacier is currently about 2 – 4 metres above the thermally determined permafrost base.

Velocity and attenuating tomograms were inverted from travel times and amplitudes measured during 22 MHz georadar crosshole experiments (Musil, 2002) for the planes through the boreholes 3/1999 – 4/1999 – 2/1999 and boreholes 3/1999 – 4/1999 – 1/1999. The tomograms can be subdivided into several zones (Figure 7-8), which have been confirmed by the loggings from the drillings presented in Section 3.2.5. The spatial distribution of the frozen material could be determined from the geophysical investigations. The voids within the layer underneath the permafrost are an additional proof that these might have been

filled with ice, which melted only recently. The distinct change in properties between layer B and C is an indicator for the internal deformation process, since creep will only occur within the ice containing layer. However, it is not possible to determine if the deformations are constrained to a shear zone or distributed within the entire layer from the tomograms alone.

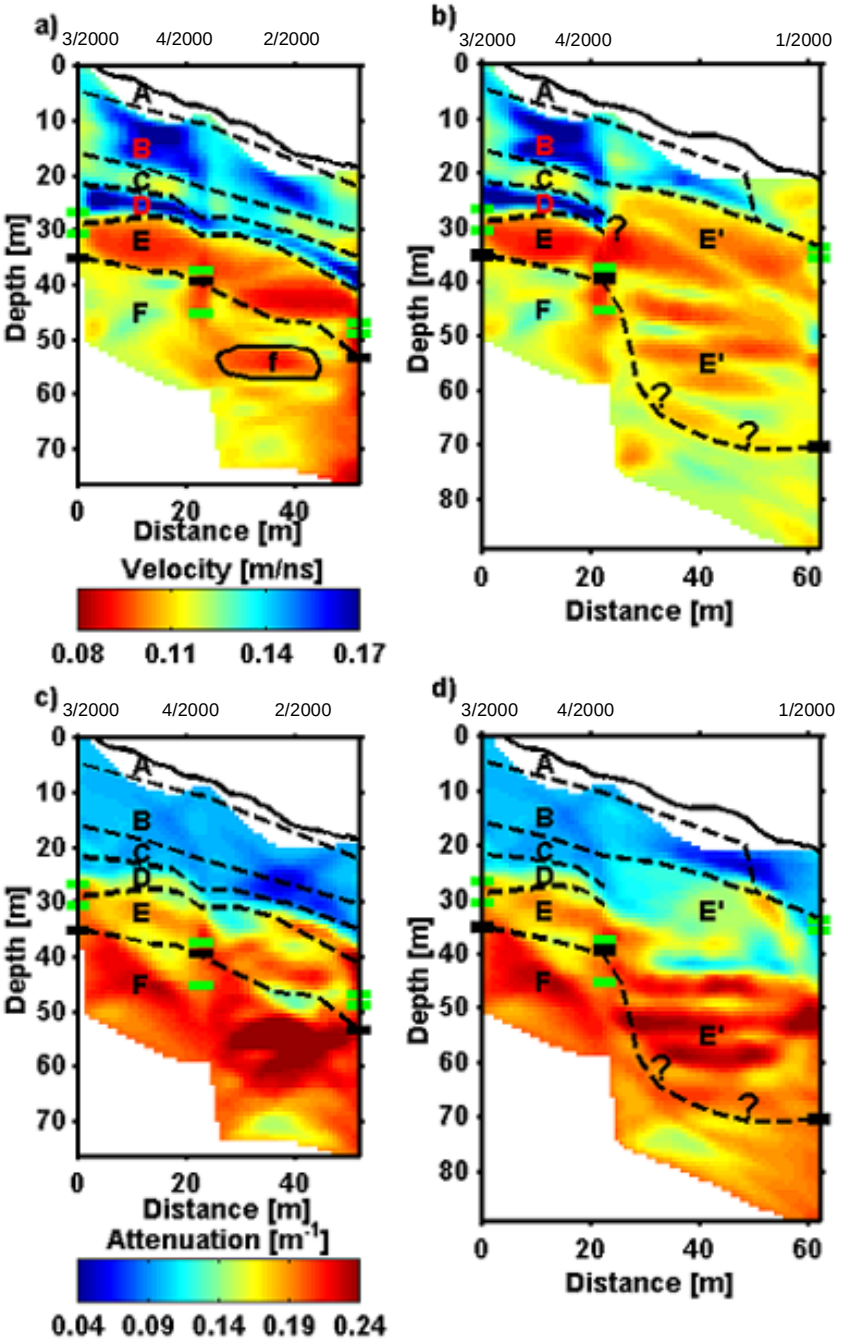

A upper 3-10m, containing mainly large boulders with numerous air voids (active layer).

B 7-11m thick, indicating large amount of ice.

C dry zone of sandy gravel, which is virtually ice-free.

D probably large voids (layer is difficult to interpret).

E low velocity and high attenuations indicate the presence of water.

F bedrock.

Figure 7-8: *Tomographic inversion of Muragl crosshole georadar data. a) and b) show the velocity and c) and d) the attenuation distributions, respectively. Small solid black lines indicate bedrock depth obtained from borehole logs and small green lines indicate the range of groundwater-table depths in the boreholes (Musil, 2002; Maurer et al., submitted).*

7.4.2 Murtèl-Corvatsch Rock Glacier

The deformation processes and the temperature distributions are slightly different for the second rock glacier under investigation. An internal deformation profile was available from early measurements (Wagner, 1992). Since the deformation rate is expected to be about nine times lower than for the boreholes at Muragl, it was assumed that the TDR measurements would not reveal any useful results within the duration of this project, but might deliver interesting data in the future within the framework of PERMOS (Vonder Mühll *et al*., 2001b). However, the strange TDR measurements within borehole 2/2000 can only be explained by the coaxial cable shearing off. The same borehole also shows a temperature distribution that is very different from earlier observations from borehole 2/1987, with temperatures constant at 0°C below about 25 m and with sharp rises and exponential decay with time occurring at shallower depths (Vonder Mühll *et al.*, submitted). Water within the borehole was thought to have entered the casing at a depth of between 20 and 25 m, thereby filling it up. However, the author doubts that a sudden movement of the rock glacier has induced the failure. Local rearrangement of the soil around the boreholes is more likely to be the cause of a possible damage of the casing and the coaxial cable, resulting in the phenomenon measured.

Nevertheless, there is strong proof that there is free water within the rock glacier. Lehmann and Green (2000) attributed their first reflection in the GPR-profile (Figure 3-30) to a shear zone. Georadar detects changes in the dielectricity of the ground, which will be caused by having water filled pores, it is likely that this first reflection actually shows a perched water table due to free water within the rock glacier. Since the ground temperatures at that particular depth are about -1.5°C, it is not very likely that the water can stay there for long without freezing. In addition, the temperature gradient of borehole 2/1987 would change at that particular depth. It must therefore be the case that water flows along a preferential path, which seems to be at the same depth as the shear zone. This is very reasonable, since water reduces effective stresses and may weaken the shearing resistance of the soil and increase its creep susceptibility. The hypothesis of seasonal free water flow is supported further by the temperature readings at depths between 10 and 20 m in borehole 2/2000, that show periodical water run off. Comparison with surface temperatures and precipitation measurements indicate a close relationship to melt water run off (Vonder Mühll *et al.*, submitted).

The talik at the bottom of the rock glacier (Vonder Mühll, 1992), seems to define the location of the permafrost base and consists of very poorly graded boulders and cobbles, and hence large air voids are present, allowing easy water and air circulation. In contrast to the first conclusions from borehole data (2/1987: Haeberli *et al*., 1988) it must be assumed that bedrock is not reached at a depth of 62 m. The recent drillings indicate that the bedrock is deeper with an unfrozen layer of boulders, through which melt water and air from the surface can circulate. This influences the thermal gradient in the frozen body above, similar to the observations made at Muragl. Since the temperature variations reported at a depth of about 55 m (Vonder Mühll, 1992) only vary between -0.15 and +0.10°C, water or air that had been cooled by the permafrost seems to be the most likely thermal source. Air circulation underneath the permafrost base is also supported by observations during the drilling operation, where air rose

through the boreholes due to the *Venturi* effect (Vonder Mühll *et al*., submitted). The cold air temperatures suggest that the air void system is very large and that the connection to the atmosphere is further up-stream of the rock glacier, since the air needs some time to be cooled down to about 0°C during the summer.

7.4.3 Summary

The various field observations at both locations revealed significant new information concerning rock glacier behaviour and response to climatic changes. The internal structure and the temperature profiles of both rock glaciers are quite different from each other, nevertheless, some common general behaviour and observations can be determined:

- Deformation is concentrated within a shear zone.
- In addition to horizontal down-slope movements in the main direction of the rock glacier deformation, only vertical settlements (i.e. no heaving) occurred.
- Soil temperatures are a function of the snow cover, in particular the first snow fall and subsequent melting, rather than of the mean air temperatures.
- Air and water is present within the frozen matrix, either in trapped voids (mostly air) or in a open void system that can be supplied from the surface, such as from melt water.
- The internal water circulation may result in local water accumulations within the frozen layer, reducing effective stresses. This water may freeze and change the flow paths within the permafrost.
- The drainage conditions underneath both rock glaciers are very good, i.e. melt water originating from the lowest icy layers will not accumulate at the base, but will flow away.
- Due to the void system underneath the frozen layers, flow of air and water can influence the thermal conditions of the permafrost from its basis. This results in a change of the thermal gradient and an acceleration of the melting process compared to surface–down temperature stimulation.

Several differences have to be stated:

- Temperatures within the Muragl rock glacier are much warmer than in the Murtèl-Corvatsch rock glacier. The depth of the zero annual amplitude is at about 15 m for Muragl and about 18 m for Murtèl-Corvatsch.
- The warmer conditions within the Muragl rock glacier contribute to a higher creep velocity. In addition, seasonal changes in velocity can be observed due to small temperature variations within the shallower shear zone.
- The topographic conditions of the Muragl rock glacier are steeper (surface inclination in the area of the boreholes: ~22°) than at the Murtèl-Corvatsch rock glacier (~14°), also contributing to higher gravity-driven forces and therefore a higher creep velocity.

- The area under investigation on the Muragl rock glacier seems to be within a zone of degrading permafrost, which is indicated by the 0°C isothermal conditions within borehole 2/1999 and the presence of a relatively thin layer of frozen geomaterial.
- The front of the Muragl rock glacier has advanced into an environment where new permafrost cannot be generated under the current climatic conditions. It only exists because it has been created at higher elevation and carried down-slope within the rock glacier.

7.5 Testing Equipment, Experimental Set-Up and Data Acquisition

7.5.1 Laboratory Testing

The precision of the data cannot be better than the quality of the sampling and the testing techniques will allow. It is crucial to know the limits of a particular testing procedure. This starts with the sampling and ends with the analysis of the melted sample after the test and the accuracy of the data processing. Therefore, the testing equipment, the set-up of the experiments and the data acquisition will be discussed within the following sections.

Testing equipment and conditions

The triaxial test devices that were used herein have their limitations in investigating the microstructural and volumetric behaviour. The accuracy of the measurement of volume change is quite low (variations up to 4% of the sample volume) and is only good for trend analysis. However, in order to determine the axial stress acting on a frozen soil sample more accurately, the area and consequently the volume change should be measured with significantly better resolution. A large increase in the area results in a decrease in the axial stress so that the assumption that the stress remains constant cannot be satisfied. It should be possible to imply the change of the area directly for future tests, which must have a better volumetric change measurement instrument, and hence, the axial load can then be changed continuously, guaranteeing constant stress conditions. The load was increased manually in steps for the current tests according to a guessed change in area that was recalculated after the test was finished. The average stress was then used in order to determine the corresponding minimum strain rate. This approach might lead to slightly lower strain rates because i) stress concentrations might be different and therefore pressure melting, re-freezing or crack inducing and closure might vary from constant stress conditions, ii) different deformations might have developed for stresses under the average value influencing the initial deformed condition of the subsequent loading step. There is, however, no proof of the extent of the influence since no comparison is available. However, the author assumes that the effect of this influence on the final result, in particular the minimum strain rate, is only minor.

The pore pressures measured can only be described as local to the plattens, although the interlinking of the unfrozen voids will increase as the temperature approaches zero centigrade. It might be possible to place several mini pore pressure transducers directly into a frozen sample in order to get pore pressure distributions of a sample during shear for further investigations on artificially fro-

zen soils. However, there are other penalties to be expected in terms of affecting the test outcome in a mechanical sense. This would allow for an analysis of effective stresses, which has to be a major goal in the future.

The temperature conditions during a test, and over the whole test series, are also very important for the data analyses. The temperatures within the cold room varied by about ±1°C and therefore influenced the test apparatuses, even though the temperature of the sample itself could be maintained more or less stable to within ±0.05°C. It was not possible to carry out tests within a temperature range between 0°C and about -1°C because of the loss of efficiency relating to the control of the temperature within the cold room, which would lead to significant temperature variations in the sample. Trends for such temperatures were simply extrapolated from the current analyses and might not be correct given the considerable changes in structure of frozen soils close to 0°C. Secondly, some of the transducers (both pore pressures and the cell pressure) are located outside the cell liquid (cf. Figure 4-3) and are therefore exposed to larger temperature changes than the actual liquid they measure, resulting in an oscillation of the readings around the correct value. Thirdly, the temperature within the cold room was not exactly the same at the three different locations of the triaxial test apparatuses due to the air circulation.

It was decided to use confining pressures that would represent *in situ* conditions and therefore the applied confining pressures were relatively low (up to 400 kPa). It seemed as if there was nearly no influence on the sample response. This is expected to be different if high confining pressures would induce pressure melting or would be able to suppress a dilatant behaviour with strain softening. The behaviour may also move from a sample response with brittle fracture to a more ductile failure regime with strain hardening.

Sample condition and preparation

The major achievement of the current project was the mechanical testing of *real* rock glacier soil samples. Even though these samples have been crucial for the determination of the stratigraphy, the calibration of geophysical investigations, solid and ice grain characteristics, *etc*., mechanical as well as thermal disturbance occurred during the drilling process. The fragile crystalline structure might have been damaged, particularly around the circumferences of the samples for low volumetric ice contents, the shape of the sample was also not a perfect cylinder (e.g. Figure 7-6c) and consequently the stresses are not equally distributed throughout the sample due to the variations in diameter.

The size of the particles in the frozen soils might also be a crucial factor for the behaviour of the frozen soil. Small particles have a larger specific surface and therefore more water is able to adhere. In addition, structural hindrance might be prevalent for mixtures with larger particles since fine particles will move more easily around each other. It must therefore be expected that a frozen soil with large solid particles is less creep susceptible than a sample with a similar volumetric ice content but smaller particles. Within the current study, however, this effect could not be shown since the particles within the original permafrost samples looked very similar for comparable volumetric ice contents, and only very few samples with different grain sizes were prepared and tested artificially.

The samples were cut to length using a circular saw, which also added some disturbance. It was important to level off the surfaces at each end of the sample so that axial stress was applied perpendicular to the planes, and therefore any holes were filled with water, which was frozen and ground to smooth parallel horizontal planes.

Recrystallisation must be expected during transportation and storage of the sample at about -18°C and this might not be completely reversed while warming up the sample to the test temperature. In particular, the amount of unfrozen water might be slightly different, since the unfrozen water content during freezing is not the same as the unfrozen water content during thawing (Stähli and Stadler, 1997). This replicates the hysteretic water retention curves obtained from wetting and drying cycles for unsaturated soils (e.g. Fredlund and Xing, 1994; Fredlund, 2000). For similar temperatures, there is likely to be more unfrozen water present during the freezing stage than during the thawing stage. Consequently, it is important to know the actual state of the permafrost samples taken from the field. It must be assumed that the amount of unfrozen water is lower than in nature for the sample tested, since they were transported and stored at a temperature of about -18°C and only brought to the test temperature some days before the test started. The author is not aware of a study about the time effects, i.e. whether the unfrozen water content may stabilise at a single value for freezing and thawing if the sample is kept for a long enough time at the corresponding temperature.

Additional recrystallisation might also take place due to a change in stress conditions after bringing the sample out of the ground. Since the samples were stored in the inner plastic liner that was used during the triple tube drilling, horizontal expansion was not possible. However, stress release might have caused expansion along the vertical axes and refreezing of formerly melted areas due to local stress concentrations.

Probably the most important fact concerning the sample condition was the extreme difference in composition and condition. Every sample was quite unique, and consequently it was not possible to produce several samples, which were exactly the same, to obtain absolute redundancies by repeating all aspects of some of the tests, which is very important for scientific work. Even though some samples showed similar composition, the *in situ* stress conditions, temperatures, the stress history or the sample might have been different and therefore the response might differ. This problem, which is typical when testing real soil samples, can only be eliminated when samples similar to the natural ones are prepared artificially.

Data analysis

The sensitivity of the equations describing the stress–strain response is shown in Chapter 5. Nevertheless, reasonable results could be presented, by taking the various effects that may influence the sample response into consideration. This fit to the data is only valid for creep tests at temperatures colder than about -1°C and for deviatoric stresses greater than 50 kPa. The former limitation is due to assumptions about the activation energy, which become invalid close to the melting point. This also calls the use of Equation 2-31 into question. In addition,

no data are available at warmer temperatures due to problems with test temperatures close to the melting point (cf. above) and because the number of good quality samples was limited. The restriction concerning low deviatoric stresses can be solved by carrying out creep tests over a period of several months, judging by the creep response of the tests at a deviatoric stress of 100 kPa, where it was very difficult to obtain steady state creep within a few days to weeks. The facility at the Institute for Geotechnical Engineering has only three test units and therefore the author had to concentrate on creep tests at higher deviatoric stresses. In addition, it would make not much sense in extensively studying that particular behaviour since most of the long term creep tests showed that the most of the samples never reached a steady state creep phase, they approached a constant value for the deformation, i.e. the strain rate approached zero.

The analysis about the mobilised shear strengths was very rudimentary, largely because the creep response was considered to be more important and so the triaxial tests were designed to take this into account. Most of the samples were exposed to several creep stages before they were sheared, so the response was primarily that of a dense frozen soil. A more advanced model linking strain behaviour with mobilised strength could not be determined, last but not least because of the problems with the volume measurements.

Summary

The results presented from the laboratory investigations help in arriving at a general understanding of the mechanisms that are important in frozen soil behaviour. The degree of accuracy of these interpretations are consistent with the sample quality and the sophistication of the measurement techniques. For future investigations, however, it is recommended that the accuracy of the testing apparatus is improved to permit a focus to be made on testing thoroughly specific aspects of frozen soil response. Artificial samples are thought to be ideal to focus on particular points of interest in a more detailed manner. It might also be useful to develop optical methods of investigation into frozen soil behaviour, similar to those presented in ice mechanics (e.g. Wilson and Marmo, 2000), which might reveal more information on the effect of solid grains on the crack propagation and ice crystal boundary sliding. Additional recommendations for future investigations are given in Chapter 8.3.1.

7.5.2 Field Measurements and Testing

Several different field measurement and monitoring instruments were used within this project. These had to be synchronised with each other, and as it was not possible to use the best technique for each individual measurement, compromises had to be made and accepted.

All these measurements were dependent on having a borehole causing minimal disturbance in the surrounding soil. This has to be drilled under very difficult conditions into an active rock glacier. Despite the mechanical and thermal disturbances of the samples and the adjacent ground, drilling through such a hetero-

geneous soil might alter the existing connectivity of water and air channels within the rock glacier and therefore change the current hydrological and thermal conditions.

In-situ pressuremeter

There was no previous experience of performing pressuremeter tests within an active rock glacier. Despite the mechanical and thermal disturbances of the ground close to the borehole wall, the results are very promising and reasonable creep parameters could be determined because the time span between finishing drilling and starting testing was kept within three to five hours (pressuremeter probe assimilation). Pressuremeter tests might even be the only possible test that is able to deliver creep parameters within layers of low volumetric ice contents, where the borehole stability is difficult to maintain for a longer period of time (Arenson *et al*., submitted, a). The use of cased drilling with preliminary percussion drilling might be a solution. Underneath the casing, the borehole only needs to be stable for a length of about 2 m.

The pressuremeter tests should be performed with caution, ensuring that there is temperature stabilisation of the probe and that enough time has to be allowed for the individual creep stages. Even though the test is difficult to perform, stress relaxation tests may be a good alternative to reduce the test duration (e.g. Ladanyi and Huneault, 1987).

Deformation monitoring

The different systems used to measure vertical and horizontal deformations have been presented and discussed in Chapter 3. All systems need a plastic tube to be grouted into a borehole. These include slope inclinometers, USBR-type settlement hooks or magnet extensometers. They have several advantages as well as disantvantages. On one hand, the systems are very accurate (1 – 5 mm per 30 m depth), the direction of the deformation can be determined, measurements may be carried out relatively easily and the instruments are not very expensive. On the other hand, it is not possible to obtain continuous readings and the installation of a plastic tube into heterogeneous and unstable ground, that might have large air voids and cavities, is quite difficult. Local deformations cannot be detected with these techniques, since differences are only recorded over a fixed length. The stiff plastic tube might also not be as flexible as the ground in which it is embedded and therefore the real deformation may be larger in zones where the slope changes significantly over each fixed length. Therefore, fine shear bands cannot be identified, even though they might be important for deformation processes.

Time domain reflectometry (TDR) allows continuous readings to be made and thin shear zones to be detected. In addition, the cable is extremely flexible and will deform much better with the soil. On the other hand, it is not possible to determine absolute deformations or directions of deformation and the cables has to be grouted into the ground, hence, it is not possible to lower other monitoring or testing devices into the borehole at some time in the future.

Table 7-1 summarises some of the borehole deformation techniques used for a range of applications in permafrost monitoring, in particular of creeping soil masses, such as rock glaciers.

instrument	direction of meas.	range of application
slope inclinometer	horizontal	Very accurate (±1 mm/30 m) and horizontal directions can be determined along the whole borehole. Requires human intervention to read data. It is a snap-reading method and it is not possible to have an automatic alarm system.
in-place slope inclinometer	horizontal	Continuous deformation measurements are possible but due to their costs they are only recommended for selected depths.
TDR	-	Continuous reading is possible and sudden events can be measured. It is, however, not possible to measure absolute deformations and directions. This would be ideal as a warning system up to the point that the TDR cable has been severed. It may be installed in an inclinometer casing that cannot be accessed any more using a probe (Kane *et al*., 2001).
magnet extensometer	vertical	Good for trend measurements (±3 - 5 mm per reading). Requires human intervention to obtain data. Only a snap-reading method.
settlement hook	vertical	Similar to magnet extensometers with a slightly higher accuracy if installed properly (±1 mm per 30 m). Since the diameter of the probe is larger, the lifetime is much shorter than for magnet extensometers. Only momentary readings and requires human intervention to obtain data.
sliding micrometer sliding deformeter	vertical	High accuracy instrument (±0.01 mm/1 m). Only momentary readings and very time consuming over large depths. Requires human intervention to obtain data.
Trivec	horizontal/ vertical	Combination of slope inclinometer and sliding micrometer with a very good accuracy (±0.003 mm/m vert., ±0.05 mm/m horiz.). Since measurements are very time consuming and no continuous readings are possible, it is not recommended for these purposes. Expensive installation and operation. Requires human intervention to obtain data.

Table 7-1: *Deformation monitoring in permafrost.*

instrument	direction of meas.	range of application
fibre optic sensors	-	Might be a good alternative to TDR measurements since continuous readings are possible and therefore sudden changes can be recognised. However, the accuracy and the costs for long cables under changing temperatures are not known.

Table 7-1: *Deformation monitoring in permafrost.*

Concentrated deformations within a borehole, induced by sharp shear horizons might lead to a relatively short measuring time within the borehole by rendering the measurement system unserviceable. It is therefore highly recommended also to measure surface deformations. Possible movements at the bottom of the borehole are recognised, and it is essential to correct for this in obtaining the rock glacier deformation profile.

Temperature monitoring

In general, thermistors were mounted on a cable at predetermined spacings (i.e. thermistor strings) and used for temperature monitoring. Automatic data logging allows continuous readings of temperatures at the thermistor depths within a borehole. Thermistor strings lowered into a plastic casing, might be subject to a different temperature regime than that in the surrounding ground, since new water channels might be created or a 'Venturi' effect might be imposed (Vonder Mühll *et al*., submitted), unless the string is either grouted or frozen into position. However, additional measurements within the borehole and recalibrations of the thermistors are not possible any longer. A faster response to changes in temperature may occur in an air or water filled borehole, than would be the case for equivalent depths within the rock glacier. The depth of the various thermistors should represent the main thermal features, i.e. it is important to be able to measure the depth of the active layer within the first few metres, as well as the depth of the zero annual amplitude, which is at about 12 – 18 m. It is also very important to be able to determine the permafrost base. It is therefore recommended to increase the distances between the thermistors with depth.

It is known that the temporal, spatial and geometrical details concerning the snow cover strongly influence the temperature regime within Alpine permafrost. It is recommended that the snow height should be measured at the location of a borehole in addition to the air temperature.

Geophysical borehole logging

Geophysical borehole loggings have delivered some useful results concerning ice content or density of the soil around the boreholes during previous drilling campaigns. However, it was necessary to install a metal casing in most of the boreholes to ensure stability of the wall and this eliminated the use of some methods (e.g. geoelectric, georadar). Furthermore several of the remaining methods require the borehole to be filled with water. This was not possible due to the very porous layer directly below the permafrost. Despite the cross-hole geo-

radar measurements that were performed in the plastic casing, which was placed into the boreholes before the steel casing was pulled out of the ground (Musil, 2002), the results that were obtained from Muragl were not very meaningful.

Organic material

The cores from the borehole Murtèl-Corvatsch 2/1987 contained some organic materials at depths down to 25.7 m (Haeberli *et al.,* 1999b; Almasi, 2001). All samples from all boreholes were carefully melted and inspected after the mechanical testing. No organic material was found within the Muragl rock glacier and only very little was present within the two recent boreholes at Murtèl-Corvatsch (borehole 1/2000, at a depth of about 14.0 m and within borehole 2/2000 at depths between 9.2 and 15.4 m). The weight of the moss within a 15 cm sample was less than 0.2 mg, except for a sample from borehole 2/2000, 13.77 – 13.92 m depth, where a larger piece was discovered (2.5 mg: Figure 7-9). The amount, however, was not enough for dating the organic remains using the ^{14}C method.

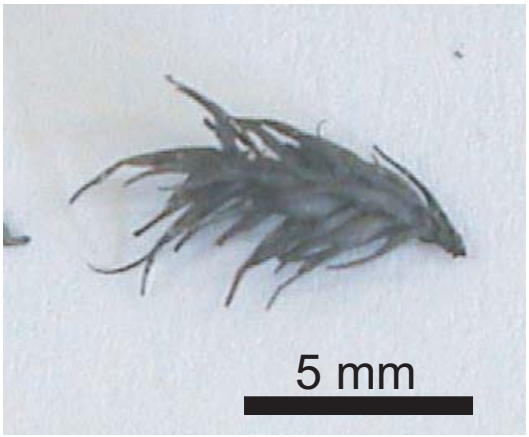

Figure 7-9: *Organic material: borehole 2/2000, 13.8 m.*

7.6 Implications for Rock Glaciers

Within Alpine mountain areas, where the temperatures inside the permafrost lies between 0°C and about -2°C, the deformation behaviour of rock glaciers is influenced by the ice content, the size and distribution of the soil particles, the confining pressure and the temperature. The laboratory tests have shown that low ice contents and larger particles strengthen the frozen material due to interlocking of the soil particles on one hand and change the behaviour from brittle to more ductile on the other hand. In addition, there is enough cold energy stored within the permafrost body in order to refreeze water and to induce recrystallisation in zones of low stress within the ground.

The horizontal deformation measurements show that the layers within a rock glacier have a different susceptibility to creep. Extrusion beneath the active layer was observed for all sites. This gravity-driven effect, which is induced by the different equivalent shear stiffnesses of these layers, including the rate effects from creep has been described by Arenson *et al*. (2002). The conditions are slightly different within the shear zone (temperature, amount of soil particles, unfrozen water content, grain size distribution, *etc*.) than in the layer above and therefore, this layer is more creep-susceptible.

7.6.1 Shear Strength

The mobilisation of the strengthening mechanisms will be summarised briefly in order to analyse failure and deformation processes that determine rock glacier stability. Shear strength may be thought to derive from friction and cohesion (Coulomb, 1776). For permafrost containing particles in contact with each other, the shear strength is based on the former mechanism and is a function of the angle of friction and the effective normal stress mobilised between these particles, where pore pressure is positive if it acts to push the soil particles apart from each other. The angle of friction of the soil matrix may be judged approximately by the angle of repose of a dry body of this soil. Additional components of shear strength may be mobilised due to interlocking and the accompanying dilatancy in densely packed soil matrixes (e.g. Bolton, 1986), which has first been described and named by Osborne Reynolds (1885, 1886).

The shear strength within the ice-rich zones is mainly due to cohesion. This was shown to be nearly independent of the confining pressure within the stress range tested, which was similar to conditions assumed to act in the natural environment. The shear strength and therefore also the susceptibility to creep will vary principally as a function of the structure and the temperature. Changes to either of these may be one of the triggers leading to transition from secondary to accelerating tertiary creep and failure.

Stability analyses depend on the determination of driving forces as well as resisting forces acting on possible failure planes. The latter are usually quantified based on mobilised shear resistance. This may be affected by influences at the micro-scale and so unfrozen water is thought to play an important role in adding to or detracting from the stability of the rock glacier in terms of slip failure, since it is likely to influence the effective stresses at temperatures close to zero centigrade. With decreasing temperature, the unfrozen water content is reduced and suction is generated between the particles. This increases the effective stresses and hence the frictional component of the shearing resistance. However, the thickness of the unfrozen water film around the particles will increase as the permafrost approaches 0°C. When the water-filled voids increase further in extent, positive porewater pressures will develop, reducing the effective stresses to the detriment of the frictional shearing resistance.

7.6.2 Stability

It is possible to consider the stability of a rock glacier based on the observations presented herein. It is clear that creep processes dominate within the potential shear zone. The main question to be asked is whether the creep mode will develop towards the tertiary stage - which implies an acceleration of the velocity until this local element 'fails'. For slope failure to occur, a sufficient number of elements must lose shearing resistance along a potential failure zone. The laboratory tests on specimens under triaxial conditions, as well as the *in situ* pressuremeter tests, have demonstrated tertiary creep, but only at shear stress levels significantly higher (3 – 4 times) than are thought to be relevant for Alpine rock glaciers.

A rock glacier can have a large system permeability due to inter-linked air voids and cavities, even though the ice matrix itself is almost impermeable. Significant bodies of unfrozen water can also be locked into cavities within the frozen body for some time, and can influence the deformation behaviour due to local reduction in effective stress. Additional factors affecting the shearing resistance within a rock glacier, and hence the stability, can be condensed as follows:

- When ice is present, slopes can be stable at angles steeper than the angle of repose of the dry granular mass, representing the friction angle of the soil mass. However, the possibility of tertiary creep should be considered.
- Infiltrating water generates positive increments of porewater pressure, which then reduce the effective stress and hence the shearing resistance of the soil. The angle of the stable slope is reduced to less than the friction angle of the soil under conditions of water flow within a saturated regime. This is a more dangerous scenario and is much more likely to lead to slip failure or debris flows, particularly within the active layer.
- If the density of the packing (solid particles per volume) increases above a critical ratio, interlocking and dilatancy occur, increasing the shearing resistance. The melting of the ice matrix within a frozen soil can increase the relative density of the soil matrix, which would then mobilise greater shear resistance.

Several stability mechanisms can be determined from these conclusions. These are shown in Figure 7-10 and are discussed in the following section.

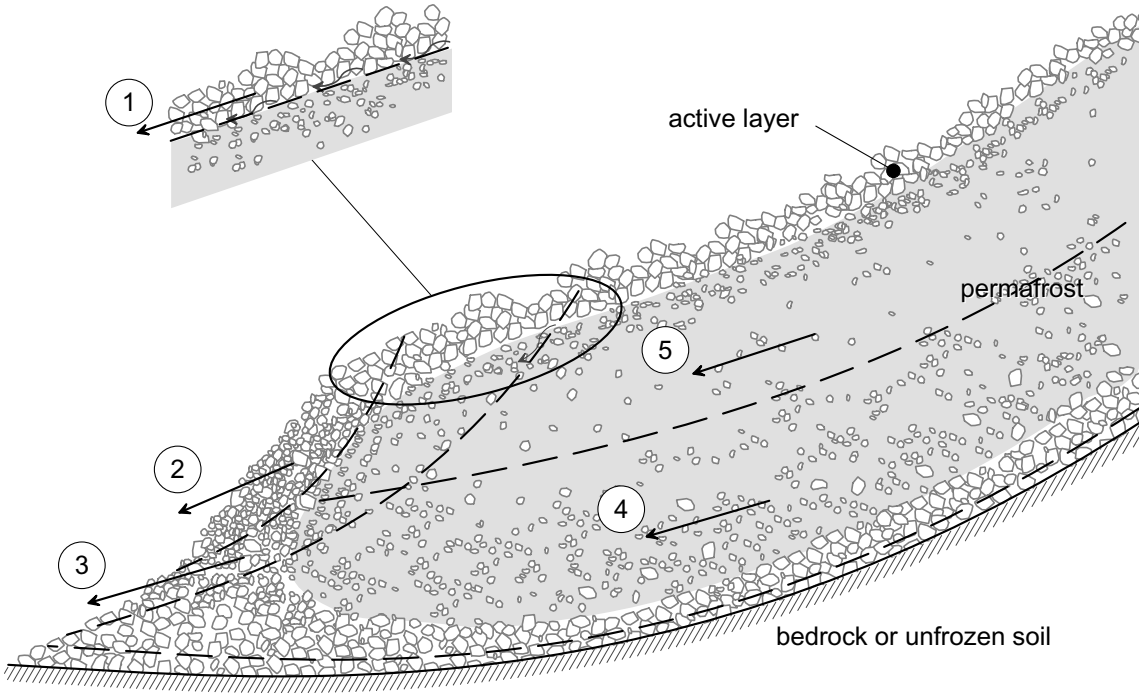

1) surface instability
2) front instability
3) toe instability
4) failure at permafrost base
5) failure in shear zone

Figure 7-10: *Possible stability problems within active rock glaciers.*

Surface instability (1)

Instabilities can occur in combination with seepage within the active layer for steep slopes. The water flows on the permafrost table and reduces the effective stresses within the unfrozen active layer, triggering debris flows.

Front instability (2)

Rock glacier fronts are usually steep (>40°) and consist primarily of fine surficial materials over the majority of the slope, i.e. gravel to silt size. Large stones and boulders, which had been carried on top of the rock glacier, usually roll down the front and end up at the foot or in the fore-field (Figure 7-11).

Figure 7-11: *Front of Muragl rock glacier.*

A humid environment can be expected due to vapour exchange between the ice, water and air phases within the rock glacier, resulting in partially saturated soil conditions. Suctions develop between the particles and therefore increase the shearing strength. However, a retreat of the ice-rich layer in combination with either complete drying or complete saturation during and following rainfalls results in destruction of the negative pore pressures and hence may lead to slope failure in the front (Springman *et al*., in press). Such minor failures are very likely to occur, since the front is likely to be in a state of incipient failure. In addition to possible damage further below the front due to the run out of the debris flow, such a slip failure enhances warming and melting of the frozen core within the tongue of the rock glacier.

Toe instability (3)

Slope failure may emerge through the frozen body and the toe of the rock glacier. This may only be dangerous if water can enter the permafrost through a large void system inducing high water pressures along the slip circle or generate sufficient high pore pressure or exit flow rates to cause uplift or erosion.

Failure at permafrost base (4)

Sudden deformations at the basis of the permafrost, or more precisely below the frozen material, is not very likely to occur for the two rock glaciers under investigation. Higher temperatures within the lowest frozen layers might increase creep velocities, but a reduction of the volumetric ice content, that accompanies melting from the bottom, increase the strength of the material and reduces its creep susceptibility. In addition, stresses are too low to either develop tertiary creep failure or even crushing of the solid particles (e.g. Bowman and Soga, 2002), and are likely to be consistent over long periods of time (i.e. no further deposition).

The high permeability of the layers underneath the frozen soils rules out the possibility of high pore pressures developing to reduce the strength sufficiently to cause failure.

Failure in shear zone (5)

A shear zone may develop within the frozen ground (e.g. Murtèl-Corvatsch), depending on the internal composition and geometry of the rock glacier. Water might also accumulate within such a shear zone due to the heterogeneity of the frozen soil matrix, increasing its creep susceptibility. However, it is very unlikely that a failure occurs throughout the whole rock glacier within such a layer, since the stresses are generally very low. Temperature increase within the frozen mass, that will take effect very slowly, results in a dislocation of the shear zone towards the surface together with volume reduction of the rock glacier mass, but rapid failure is unlikely to occur.

Tensile creep failure (6)

The topography can also be very important in the development of an instability. Tensile creep is induced within steep slopes due to gravity forces, which might result in tensile creep failure similar to hanging glaciers (e.g. Alean, 1985). Since the rock glaciers under investigation are not located in such a steep environment, tensile creep properties have not been investigated within this study. It is also questionable whether a rock glacier could be sustained on a steep slope. It must be assumed that melting of the ice at the front will cause ongoing instabilities of mode 2 until the unfrozen front is stable so that no tensile forces can be developed within the rock glacier to cause failure of the whole permafrost body.

It is known from various studies, performed mainly on frozen silts (e.g. Bragg and Andersland, 1980; Zhu and Carbee,1987), that tensile creep is less temperature dependent than compression creep and therefore a change in climatic conditions would be less damaging for these zones.

If a rock glacier is located in such an environment, surface deformation measurements can help in determining a potential failure since an acceleration of the deformation can be expected and recorded.

Summary

In conclusion it can be said that failure modes 1 and 2 are probable and such instabilities also have a damage potential for the environment below, even though the amount of material released is limited relative to the mass of the entire rock glacier. However, depending on the location of the rock glacier, large debris flows can be triggered with severe consequences further downhill. Failure mode 3 is not very likely to occur due to the low stress conditions within the tongue of a rock glacier and the high permeability of the large boulders at the toe. Modes 4 and 5 are also very unlikely to occur considering the large permeability of the layers below the frozen body of known rock glaciers. And since it is very unlikely that a rock glacier can sustain steep slopes, it is also very doubtful that instability mode 6 will develop and in addition it can be measured with appropriate deformation measurements.

Chapter 8

Summary, Conclusions and Recommendations

A total of six boreholes were drilled into two different Alpine rock glaciers in the Engadin, Swiss Alps. The geomechanical aspects of the investigations included an array of field as well as laboratory tests in order to determine the thermo-mechanical response of frozen soils and associated parameters relating to creep and failure. Field investigations were performed in all six boreholes, and from the surface, for the purpose of determining the spatial distribution of the rock glacier material and to monitor rock glacier behaviour. These data form the basis for an assessment of slope stability processes. Numerical models may be adopted in future to evaluate the impact of ongoing climate changes.

Several mechanisms might be responsible for the micromechanical behaviour of frozen geomaterials. These have been reviewed extensively with respect to the general behaviour of creeping ice-rich permafrost within the discussion from the previous chapter. The current chapter presents major conclusions from the laboratory tests and field investigations and their major influence on general rock glacier behaviour is summarised.

An additional section will deal with recommendations for further investigations in the laboratory as well as in the field. Monitoring and preventative measures will be illustrated briefly with respect to the natural hazard potential of melting Alpine permafrost.

8.1 Mechanical Response of Frozen Soils

The response of original permafrost samples to loading under temperature and stress conditions similar to their natural environment has been the main focus of the triaxial creep tests. Sudden major changes of these boundary conditions could be excluded and therefore the steady state long-term behaviour was

investigated using triaxial test equipment that has been developed and manufactured at the Institute for Geotechnical Engineering at the Swiss Federal Institute of Technology, Zurich. Failure processes, creep failure and shear failure induced at constant stress and constant strain rate, respectively, have been investigated revealing a range of responses that could be incorporated into a general understanding of the micromechanical behaviour of frozen soils, in particular of Alpine permafrost. Additional tests were conducted on artificially frozen samples in order to compare the behaviour of natural and artificial samples, since the extraction, transport and storage of naturally frozen samples comes with many technical, logistic and financial challenges. The range of the sample conditions and the test set up are as follows:

- artificial samples:
  - volumetric ice content: 61 – 100%; volumetric air content: 0 – 19%
  - grain size: 0 – 16 mm
  - crushed ice, columnar grained ice
- rock glacier samples:
  - volumetric ice content: 39 – 96%; volumetric air content: 0 – 25% (generally lower ice contents within the Muragl rock glacier)
  - grain size: 0 – >80 mm (mainly silty sand, well graded; however, some tests had large piece of stones that might have influenced the sample response)
- confining pressure: 50 – 400 kPa
- temperatures: -4.5 – -1.0°C
- deviatoric stress (in creep tests): 60 – 1300 kPa
- creep stages: 1 – 7
- axial strain rates (in constant strain rate tests): $1 \cdot 10^{-7} – 7 \cdot 10^{-5}$ s^{-1}

Minimum creep rates were assumed to be constant with time and can be considered as steady state creep. Therefore, a Glen type flow law was used to describe the secondary axial creep rate as a function of the applied deviatoric stress based on triaxial compression test results. The creep parameters, however, are not constant for the selected test conditions, i.e. the influence of temperature and sample composition had to be incorporated. Below about -1.5°C the effect of the temperature could be modelled with an Arrhenius approach. Close to the melting point of the ice, however, the temperature severely affects the sample composition, i.e. phase changes occur from ice to water, which influences the behaviour. This could be accounted for by an exponential increase of the activation energy with temperature approaching zero centigrade. In addition, the creep parameter *B* (multiplier of the exponential components) also appears to be a function of the temperature. On the other hand, the stress exponent *n* was only a function of the initial volumetric ice content and showed good consistency with values from literature for pure ice samples.

The results of the creep tests showed the very high sensitivity to the various sample conditions. Generally it can be stated that the temperature influences the creep more than does the volumetric ice content for low stress conditions. The

creep rate may vary by an order of magnitude, even for small temperature changes close to the melting point, due to the exponential nature of the influence of the activation energy. Decreasing ice contents reduce the creep susceptibility at large, but the stress dependency increases, i.e. the gradient of the creep rate normalised by the initial creep rate increases faster for a frozen soil with a low volumetric ice content compared to a sample with high ice content.

Tests under constant strain rate loading as well as constant stress (creep) conditions seemed to indicate similar response at a microstructural level, which is extremely strain rate dependent. Fast loading results in more brittle behaviour whereas very slow loading tends to induce a ductile response, although this is also a function of the volumetric ice content. Structural hindrance will cause dilatancy for frozen soils with dense packing of the solid phase and low air contents.

The stress distribution within the sample will not be uniform, with preferential stress paths developing and enforcing local phenomena such as pressure melting, crack formation (wing cracks, secondary cracks) or re-freezing in connection with recrystalllisation of the ice. It must therefore be assumed that the structure of the sample keeps on changing during the entire experiment. Even though the shear tests showed some indication of a residual state, because the deviatoric stress reached a value that was quite constant for large strains, ongoing volumetric changes were observed. These were mainly compressive, but for some tests, dilation was measured. It is possible that air voids are compressed due to the high volumetric air content and the density of the samples increase in combination with the development of a shear zone, on which the residual shear strength is mobilised. This may provoke a different mechanism to dominate the ongoing response to shearing. A loose sample would show a ductile behaviour initially accompanied by volumetric compression to form a denser mixture of ice crystals and soil particles along a failure plane, and this may then lead to dilation at large strains.

The creep, as well as the shear response of the samples tested did not show significant influence of the applied confining pressure, which was chosen to be of the order of the magnitude of the *in situ* stresses. Larger confining pressures than expected for Alpine rock glaciers will tend to suppress dilatancy and crack formation, and pressure melting is more likely to be induced.

No triaxial tests were performed close to the melting point of the ice, i.e. 0 – -0.5°C, even though this is the most sensitive temperature range in terms of stability, since the unfrozen water content increases with temperature. The constitutive approach might therefore slightly underestimate the creep rates because an extrapolation was based on the results carried out at colder temperatures. An increase in temperature combined with an increase in unfrozen water content results in a decrease of the volumetric ice content and a change in volume. On the other hand, negative pore pressures in combination with an increased structural hindrance due to particle interaction reduces the creep susceptibility. Therefore, the proposed solution may also be applicable close to 0°C, even though further investigations are strongly recommended with tests to be performed on artificially frozen samples since the response seems to be quite similar. Precautions are necessary with the sample preparation. It is of particular importance that the particles are uniformly distributed and a volumetric air content resembling natural observations is essential.

8.2 Slope Stability and General Movements of Rock Glaciers

The analyses of measured borehole deformations within active rock glaciers in combination with the results from field and laboratory tests investigating the thermo-mechanical response of ice-rich frozen soils leads to the conclusion that rock glaciers are relatively stable in general. This might also be the reason why rock glaciers are relatively old compared to temperate glaciers, since sudden dramatic events that may change their general morphology have not occurred very often.

However, smaller instabilities can be induced by thawing processes within the active layer, most probably in combination with seepage from melt water or rainfall. Such relatively small mass movements, compared with the steady creep of the whole rock glacier, may nevertheless be the trigger for larger debris flows, depending on the environment around the rock glacier. These local instabilities also change the thermal regime, e.g. erosion of the active layer, and accelerated permafrost degradation can be induced. Mass movements induced by models reviewed in McRoberts and Morgenstern (1974), such as the thaw-consolidation model or the ablation model are not of importance for rock glaciers, but might be relevant for other permafrost sites in a mountain environment that are less ice-rich and consists of uniform finer grains (e.g. silts).

Seasonal changes in the creeping movements of active rock glaciers may be observed, depending on the depth of the shear zone. For shallow shear horizons at depths above the zero annual amplitude (Alpine environment: 16-20 m), seasonal differences have to be expected, with a phase shift depending on thermal properties, and hence, heat propagation within the ground. At greater depths, changes in velocity can be induced by long-term variations of climatic conditions, which influence the permafrost temperature through changes in the mean annual air temperature, the snow cover or the solar radiation. Additional stratigraphical effects, such as layers with high permeability underneath the permafrost, that are likely to be connected to the atmosphere, also influence the thermal regime and hence the deformation process. However, such influences can be strongly retarded.

The majority of both the vertical and the horizontal deformations were measured within the shear zone. Even though compressive flow occurs down-slope in the areas under investigation, only settlements, i.e. a decrease in thickness of the rock glacier, were observed. These deformations were an order of magnitude smaller than the vertical deformations. Air voids and cavities were noted within the permafrost body during the drilling operations. Subsequent analysis of the core samples indicated an average value of about 5% to 10% from the zones in which it was feasible to take nominally undisturbed samples. These voids may allow the soil mass to deform horizontally in regions of compressive flow within the rock glacier, without any effect in the orthogonal direction, due to volume reduction of the soil-ice-air matrix.

The movements of a rock glacier can be described by three major zones (Figure 8-1). The advance of rock glaciers is induced by gravitational forces. Near the front there is a general volume reduction probably due to melting of interstitial ice and an ongoing compaction of loose soil due to compression. Boulders that had been carried along on top of the rock glacier will fall off the front

and accumulate in the forefield of the rock glacier. Further up-slope there is a compression zone, which is signified by furrows and ridges. Mainly creep deformation due to compression occurs within this zone, which is accompanied by a volume reduction due to the compressibility of the air voids within the very heterogeneous nature of the ground. Even though a general settlement of the rock glacier is recorded it must be assumed that the ridges are formed due to local heave or movements at the transition between the compressive and the extensive creep zones, possibly in connection to additional shear zones. However, the formation of the ridges is still not clear and further investigations are necessary.

The upper zone of a rock glacier is dominated by extensive flow due to the steep slope. It is characterised by a smooth surface and higher surface velocities than within the compression zone (e.g. Kääb, 1998). However, no internal deformation or stress measurements are available within this zone and therefore several assumptions are based on speculations. Nevertheless, it can be assumed that a decrease of the horizontal stresses occurs within this zone due to the inclination of the slope, resulting in extension of a soil element. Close to the surface this might even result in negative stresses, i.e. tension. Due to this stress decreases, cracks could be created or enlarged, increasing the average volumetric air content. These cavities will again be compressed and closed within the adjacent region of compression. In consequence, a volume increase may be expected in the direction of the rock glacier flow, i.e. down-slope.

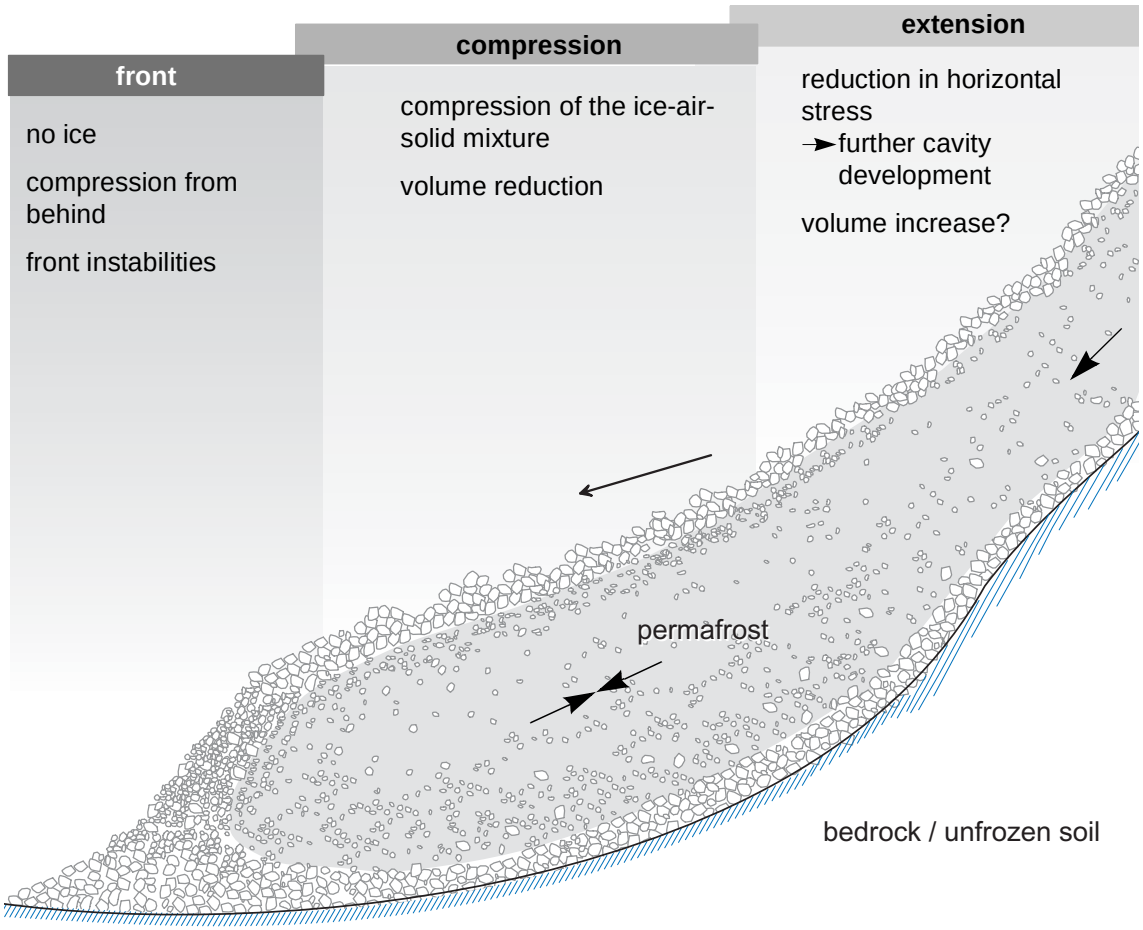

Figure 8-1: *Stages of rock glacier deformation.*

8.3 Recommendations for Further Research

8.3.1 Laboratory Investigation

Several limitations had to be accepted due to the testing equipment. These have been mentioned already during the data analysis and the discussion. Despite unproven details concerning mechanisms on a microstructural level during creep and shear, the major problem in frozen soil mechanics is the uncertainty about the effective stresses. Therefore there is a strong need for more sophisticated testing equipment and instrumentation. The current research showed that it is possible to use artificially frozen samples, and hence, further laboratory investigations can be carried out on samples, of which the composition is known and reproducibility can be guaranteed. The following improvements are recommended for the determination of effective stresses:

- Mini-pore pressure transducers (e.g. Muraleetharan and Granger, 1999): It should be possible to place several transducers in a frozen sample for a spatial determination of pore pressures (air and water).
- Pressure pads (Garnier *et al.*, 1999; Laue *et al*., 2002) can be placed between the top and the bottom platten. Eventually it might even be possible to spot miniature pressure pads directly in a sample without disturbing its response too much.

The volumetric behaviour as well as the crack formation has to be investigated more intensively for a better understanding of the mechanisms. The following methods, most of which have already been used in geotechnical testing, would lead to improved characterisation:

- Optical determination of the sample volume during the test (digital imaging techniques: e.g. Macari *et al*., 1997; summary of various methods: Geiser *et al*., 2000).
- Pore volume determination with air similar to the triaxial tests performed on snow (von Moos, 2002) or on partially saturated soils (e.g. Geiser *et al*., 2000).
- Determination of acoustic waves, which are induced by breaking bonds (e.g. Fish and Sayles, 1981; Glaser and Hand, 1998; Weiss *et al*., 1998). Fracturing and sliding effects could be distinguished as a function of the ice content.
- Computer tomography (e.g. Desrues *et al*., 1996; Walters *et al*., 1998; Alshibli *et al.*, 2000) during a test. This would allow for a determination of compressing and dilating zones as well as of crack development within a sample. Special treatment of the samples before the tests may be required depending on the applied method. The influence of such additives has to be investigated previously.
- DC resistivity (e.g. Hauck, 2001) or TDR (Stähli and Stadler, 1997) measurements during the test should allow for a determination of the volumetric amount of unfrozen water subject to the condition that the method is carefully calibrated.

- Optical investigations of samples under shear stress with microscopes and polarised light similar to Wilson and Marmo (2000) may reveal development of stress paths and changes in ice crystal geometry.

An improvement of the volume measurement would also help in maintaining constant stresses during a creep test at large strains. However, all recommendations presented have to be tested very carefully to establish the extent of their influence on the thermo-mechanical behaviour of the frozen sample under investigation. Instruments that are inserted into the soil may change its response severely.

The tests presented showed that there is still a need for further tests at warmer temperatures, i.e. > -1°C, at low deviatoric stresses, with volumetric ice contents lower than about 40% and under triaxial extension. These tests should help to improve the formulation herein and in particular for soils with more unfrozen water. Investigations on creep deformations under low stresses can also be problematic because such tests might last several months before any conclusions can be drawn. Last but not least, the effect of the grain size distribution should be investigated more intensively, since the amount of small grains will influence the unfrozen water content (e.g. Anderson and Morgenstern, 1973). Triaxial testing has its limits for larger grain sizes (e.g. Head, 1996). In order to gain feasible results, the maximum grain size may not be larger than a fifth of the sample diameter. This was exceeded for some of the original samples extracted from the rock glaciers.

Different testing approaches have to be considered to solve such a problem. One possibility may be a geotechnical centrifuge (e.g. Schofield, 1980; Springman *et al.*, 2001). Due to the scaling effects, relatively large parts of a slope can be modelled effectively and long-term behaviour could be investigated due to the scaling effects on time. In addition, failure can be induced due to a warming at the surface or the bottom, without endangering populated areas. Solifluction processes have already been modelled successfully and are described in Irving *et al.* (2000) or Harris *et al.* (2000a; b; 2002). The modelling of models, i.e. similar tests carried out under different acceleration levels, would also allow grain size effects to be studied. If the processes are not viscosity-controlled, no conflicts should emerge due to the scaling in the centrifuge (Harris *et al.*, 2002). However, fracturing effects, such as brittle behaviour, have to be interpreted with caution since the fracture toughness will not be modelled linearly with the acceleration of the centrifuge (Palmer, 1991b). The sample preparation for centrifuge testing also has to be investigated since the ratio between sample grains and ice crystals should be maintained in the model compared to the prototype.

Instead of triaxial tests, direct shear box tests at various scales (e.g. Yasufuku *et al.*, submitted) may also be very useful in the determination of frozen soil behaviour under load or deformation. The stress paths experienced in a rock glacier are more akin to direct shear than to triaxial compression. Similar to the recommendations for better triaxial testing mentioned above, improvements have to be made to a direct shear box in order to study the volumetric and effective stress behaviour. Larger sample size might even reduce the effect due to the insertion of the instrumentation on the thermo-mechanical response.

Oedometer tests with large samples may be an important additional source of information, since the response of frozen soils under compression can be studied with TDR, DC resistivity or Bender elements (e.g. Bates, 1989). The former two might help in determining the unfrozen water content under various stress conditions. Bender elements allow the elastic properties (shear modulus) of the sample to be measured during the test.

In conclusion, the author also thinks that a unified testing system for frozen soils under triaxial as well as direct shear conditions, that considers sample geometry, grain size, strain rates, creep stages, deformation measurements, pore pressure determination and volume determination, would be desirable.

8.3.2 Field Investigations and Monitoring

Slope instabilities, that may have severe consequences for the environment below a rock glacier are the main threat in connection with global warming in densely populated areas in the Swiss Alps. This has been the major force in pushing permafrost research in Switzerland. Even though it could be shown that sudden collapses of Alpine permafrost may not be expected for these two rock glaciers, there is a potential for inducing debris flows depending on the geometry, hydrology, exposure, *etc*.

Temperature changes and variation in composition within a frozen mass only happen very slowly. Therefore a change in movement, resulting from internal structural changes, also develops gradually. Terrestrial surface deformation measurements may therefore be the most effective method to determine irregularities such as a possible acceleration in movement. Such measurements can be performed automatically and the data can be viewed on-line. Fixed points have to be positioned where no deformation occurs and the possibility of performing measurements when there is a snow cover has to be considered in order to obtain reasonable results.

There are still several unanswered problems concerning the morphology and the history of rock glaciers that may be answered when performing additional field investigations:

Rock glacier hydrology

The drilling and the temperature measurements revealed that water flow within a rock glacier is very likely. Seasonal GPR-measurements, for example on the Murtèl-Corvatsch rock glacier, may reveal changes of the water flow during the year. Additional tracer measurements might expose preferential water flows and mean macro permeability within the connected channels. Such measurements are also necessary in the modelling of thermal regimes within Alpine rock glaciers. Installation of pore pressure transducers (e.g. piezometer) at several locations within a rock glacier may also assist in determining seasonal water flow and can then be linked to surface processes, such as melt water or rainfall. Such installations have to be performed very carefully without creating new open channels.

In addition to the network of channels of water within the rock glaciers, air circulation was also observed during the drilling process within and underneath the rock glaciers. Unfortunately, the author is not aware of any reasonable method concerning a measurement of the extent of air circulation, however, in terms of thermal modelling, it might be useful to have a better knowledge of the spatial variation of the temperature with time for correlation with surface conditions.

Stress states within a rock glacier

The very heterogeneous rock glaciers under investigations may have highly complex stress conditions. Arching effects and local failure processes in combination with time-dependent deformations result in a non-uniform stress distribution. Field investigations can help in a better understanding of these stresses. Pressure sensors may give some hints about stress distributions, even though it might not be trivial to install them (e.g. Pfeffer *et al*., 2000) and there are always questions posed about precisely what is being measured (e.g. Burland, 1967).

Pressuremeter tests may be a more useful tool for determining *in situ* stress conditions. However, the tests have to be carried out very carefully in order not to disturb the ground during drilling and installation of the probe (c.f. Arenson *et al.*, submitted, a).

Rock glacier deformation

The borehole deformation measurements within the Muragl rock glacier confirmed previous observations within Alpine rock glaciers: that a zone exhibiting higher local shear deformations than the surrounding soil may be found. However, the measurement techniques used did not allow for a detailed analysis of this zone. More advanced methods, based on TDR or fibre optic cables are promising in terms of obtaining a better understanding of this zone as well as long-term alterations, such as change in depth and seasonal variations. In addition, continuous measurements are possible.

Borehole deformation measurements that are distributed over a larger area of a rock glacier may help in determining the spatial geometry of the shear zone(s). Such an investigation would reveal if there is only one shear zone throughout the whole rock glacier and how its depth may change. An indirect determination of the shear zone distribution might be possible with GPR measurements from the surface as soon as water is present in such a zone (e.g. Murtèl-Corvatsch rock glacier).

Stratigraphy

A proper knowledge of the stratigraphy is not only of scientific interest, it is also crucial for proper modelling. Improved geophysical investigations from the surface and from borehole-to-borehole (Musil, 2002) might deliver the appropriate information. In distinct cases, additional boreholes have to be drilled for calibration. Cores are indispensable. Unfortunately, cone penetration tests, that have been used extensively in Arctic permafrost (e.g. Ladanyi and Huneault, 1989)

are not appropriate in an Alpine environment since the mixture of ice and hard rocks would be impenetrable, even though such a method would be much faster and more economical.

Temperature measurements

Permafrost is a thermal phenomenon. Temperature monitoring is very important in terms of studying the reaction to climate change. However, several studies showed that it is not only the mean air temperature that influences the soil temperature, but also the snow cover. Therefore, every temperature profile should be compared with the daily mean air temperature and the snow height. Thermal modelling also has to account for this insulating effect.

8.3.3 Numerical Modelling

Numerical modelling of rock glacier behaviour and its influence on the environment has to be the final goal of the current emphasis on permafrost research in Switzerland with special focus on the consequences of climate change. Thermal and mechanical processes need to be coupled. The field investigations also showed that the hydrology of a rock glacier is much more complex than originally thought and since water influences the mechanical as well as the thermal responses, it has to be modelled as well. Temperature measurements with depth showed that one-dimensional thermal approaches are not sufficient since warmer air temperatures within cavities underneath the permafrost base have a major influence on the thermal gradient and may accelerate melting processes.

Finite element or finite difference methods, which are very widespread in geotechnical engineering, may have their limitations in rock glacier modelling in terms of representing the thermo-mechanical behaviour, since rock glacier ‘soils’ should not be modelled as a continuum. However, a first approach could be implemented in such a code if temperature distributions can be modelled and suitable constitutive relationships are available. Discrete or distinct element modelling is considered to be considerably more promising (Cundall and Strack, 1979). A particle flow code could be adopted to model the interrelationship between solid and either air or liquid phases. The inclusion of cementation effects could also be modelled although further development would be required to replicate phase changes and grain boundary sliding during creep with ongoing temperature variations. However, the author assumes that this can be best modelled when accounting for the various phases of a frozen soil individually instead of using a single constitutive relationship for the whole mixture. Consequently, this should be the focus of future numerical modelling of aspects of frozen soils, which may then be extended to reproduce the whole rock glacier behaviour under changing environmental boundary conditions, such as temperature or topography.

Increasing computational power and improvements in particle flow code modelling (e.g. Thavalingam *et al*., 2001; McDowell and Bolton, 2001; McDowell and Harireche, 2002) might probably soon allow for the modelling of rock glacier behaviour more accurately than today and may help in determining their future stability.

References

Ackert, R.P. (1998). A rock glacier/debris-covered glacier system at Galena Creek, Absaroka Mountains, Wyoming. *Geografiska Annaler, Vol. 80*A, 267-276.

Adachi, T., Oka F. and Poorooshasb, H.B. (1990). A constitutive model for frozen sand. *Journal of Energy Resources Technology, ASME, Vol. 112*, 208-212.

Adachi, T., Oka, F. and Mimura, M. (1996). Modeling aspects associated with time dependent behavior of soils. *Measuring and Modeling Time Dependent Soil Behavior, ASCE, Geotechnical Special Publication, No. 61*, 61-95.

Aldrich, H.P. Jr. (1956). Frost penetration below highway and airfield pavements. In *Factors Influencing Ground Freezing. Publ. 425. Washington D.C.: National Academy of Sciences–National Research Council*, 124-149.

Alean, J. (1985). Ice avalanche activity and mass balance of a high-altitude hanging glacier in the Swiss Alps. *Annals of Glaciology, Vol. 6*, 248-249.

Alkire, B.D. and Andersland, O.B. (1973). The effect of confining pressure on the mechanical properties of sand-ice materials. *Journal of Glaciology, Vol. 12*, 469-481.

Allersma, H.G.B. (2002). http://dutcgeo.ct.tudelft.nl/allersma/hgball.htm.

Almasi, N. (2001). Permafrost. Diplomarbeit in Geotechnik, *Institut für Geotechnik, ETH Zürich*, 64p.

Alshibli, K.A., Sture, S., Costes, N.C., Frank, M.L., Lankton, M.R., Batiste, S.N. and Swanson, R.A. (2000). Assessment of localized deformations in sand using X-ray computed tomography. *Geotechnical Testing Journal, ASTM, Vol. 23*, 274-299.

Andersen, G.R., Swan, C.W., Ladd, C.C. and Germain, J.T. (1995). Small-strain behavior of frozen sand in triaxial compression. *Canadian Geotechnical Journal, Vol. 32*, 428-451.

Andersland, O.B. and Akili, W. (1967). Stress effect on creep rates of a frozen clay soil. *Géotechnique, Vol. 17*, 27-39.

Andersland, O.B. and AlNouri, I. (1970). Time-dependent strength behavior of frozen soils. *Journal of the Soil Mechanics and Foundation Division, ASCE, Vol. 96*, 1249-1265.

Andersland, O.B. and Anderson, D.M. (1978). Geotechnical engineering for cold regions. *McGraw-Hill, New York*, 566p.

Andersland, O.B. and Ladanyi, B. (1994). An introduction to frozen ground engineering. *Chapmann & Hall, New York*, 352p.

Anderson, D.M. and Morgenstern, N.R. (1973). Physics, chemistry, and mechanics of frozen ground: A review. In *Proceedings of the 2nd International Conference on Permafrost, Yakutsk, U.S.S.R.,* 257-288.

Anderson, D.M., Tice, A.R. and McKim, H.L. (1973). The unfrozen water and the apparent specific heat capacity of frozen soils. In *Proceedings of the 2nd International Conference on Permafrost, Yakutsk, U.S.S.R.,* 289-295.

Andrews, R.M. (1985). Measurements of the fracture toughness of glacier ice. *Journal of Glaciology, Vol. 31*, 171-176.

Anisimov, O.A. and Nelson, F.E. (1996). Permafrost distribution in the northern hemisphere under scenarios of climatic change. *Global and Planetary Change, Vol. 14*, 59-72.

Arakawa, M. and Maeno, N. (1997). Mechanical strength of polycrystalline ice under uniaxial compression. *Cold Region Science and Technology, Vol. 26*, 215-229.

Arenson, L. (2000). Verformungsmessung im Blockgletscher Muragl, Installation der Inklinometerrohre. *Institut für Geotechnik, Bericht Nr. I 451/1*, 23p.

Arenson, L. and Springman, S.M. (2000). Slope stability and related problems of Alpine permafrost. In *Proceedings of the International Workshop on Permafrost Engineering, Longyearbyen, Svalbard, Norway*, 185-196.

Arenson, L.U., Hoelzle, M. and Springman, S.M. (2002). Borehole deformation measurements and internal structure of some rock glaciers in Switzerland. *Permafrost and Periglacial Processes, Vol. 13,* 117-135.

Arenson, L.U., Hawkins, P. and Springman, S.M (submitted, a). Pressuremeter tests within an active rock glacier in the Swiss Alps. In *Proceedings of the 8th International Conference on Permafrost, Zurich, Switzerland*.

Arenson, L.U., Almasi, N. and Springman, S.M (submitted, b). Shearing response of ice-rich rock glacier material. In *Proceedings of the 8th International Conference on Permafrost, Zurich, Switzerland*.

Ashby, M.F. and Duval, P. (1985). The creep of polycrystalline ice. *Cold Regions Science and Technology, Vol. 11*, 285-300.

Baker, T.H.W. and Konrad, J.M. (1985). Effect of sample preparation in the strength of artificially frozen sand. In *Proceedings of the 4th International Symposium on Ground Freezing, Sapporo,* 171-176.

Baker, T.H.W. and Kurfurst, P.J. (1985). Acoustic and mechanical properties of frozen sand. In *Proceedings of the 4th International Symposium on Ground Freezing, Sapporo, Japan*, 227-234.

Barnes, P., Tabor, D. and Walker, J.C.F. (1971). The friction and creep of polycrystalline ice. *Proceedings of the Royal Society of London, Series A. Mathematical and Physical Science, Vol. 324*, 127-155.

Barsch, D. (1969). Studien und Messungen an Blockgletscher in Macun, Unterengadin. *Zeitschrift für Geomorphologie, Supplementband 8*, 11-30.

Barsch, D. (1973). Refraktionsseismische Bestimmung der Obergrenze des gefrorenen Schuttkörpers in verschiedenen Blockgletschern Graubündens, Schweizer Alpen. *Zeitschrift für Gletscherkunde und Glaziologie, Vol. 9,* 143-167.

Barsch, D. (1977). Ein Permafrostprofil aus Graubünden, Schweizer Alpen. *Zeitschrift für Geomorphologie, NF 21*, 79-86.

Barsch, D. (1978). Active rockglaciers as indicators of discontinuous permafrost: an example from the Swiss Alps. In *Proceedings of the 3rd International Conference on Permafrost, Ottawa*, 349-352.

Barsch, D. (1996). Rockglaciers, Indicators for the Present and Former Geoecology in High Mountain Environments, *Springer Verlag, Heidelberg*, 331p.

Barsch, D. and Hell, G. (1975). Photogrammetrische Bewegungsmessungen am Blockgletscher Murtèl I Oberengadin, Schweizer Alpen. *Zeitschrift für Gletscherkunde und Glazialgeologie, Vol. 11,* 111-142.

Barsch, D., Fierz, H. and Haeberli, W. (1979). Shallow core drilling and borehole measurements in the permafrost of an active rock glacier near the Grubengletscher, Wallis, Swiss Alps. *Arctic and Alpine Research, Vol. 11*, 215-228.

Bartelt, P. and von Moos, M. (2000). Triaxial tests to determine a microstructure-based snow viscosity law. *Annals of Glaciology, Vol. 31*, 457-462.

Bates, C.R. (1989). Dynamic soil property measurements during triaxial testing. *Géotechnique, Vol. 39*, 721-726.

Bedford, A. and Drumheller, D.S. (1983). Theories of immiscible and structured mixtures, *International Journal of Engineering Science, Vol. 21*, 863-960.

Bennett, L.P. and French, H.M. (1991). Solifluction and the role of permafrost creep, Eastern Melville Island, N.W.T. Canada, *Permafrost and Periglacial Processes, Vol. 2*, 95-102.

Berthling, I., Etzelmüller, B., Eiken, T. and Sollid, J.K. (1998). Rock glacier on Prins Karls Forland, Svalbard. I: internal structure, flow velocity and morphology. *Permafrost and Periglacial Processes, Vol. 9*, 135-145.

Berthling, I., Etzelmüller, B., Isaksen, K. and Sollid, J.K. (2000). Rock glacier on Prins Karls Forland, Svalbard. II: GPR soundings and development of internal structure. *Permafrost and Periglacial Processes, Vol. 13*, 357-370.

Björnsson, H. (1998). Hydrological characteristics of the drainage system beneath a surging glacier. *Nature, Vol. 395*, 771-774.

Blatter, H. and Hutter, K. (1991). Polythermal conditions in arctic glaciers. *Journal of Glaciology, Vol. 37*, 261-269.

Bockheim, J.G. (1995). Permafrost distribution in the southern circumpolar region and its relation to the environment: a review and recommendations for further research. *Permafrost and Periglacial Processes, Vol. 6*, 27-45.

Bolton, M.D. (1986). The strength and dilatancy of sands. *Géotechnique, Vol. 30*, 65-78.

Bourbonnais, J. and Ladanyi, B. (1985). The mechanical behavior of frozen sand down to cryogenic temperatures. In *Proceedings of the 4th International Symposium on Ground Freezing, Sapporo, Japan,* 235-244.

Bowmann, E.T. and Soga, K. (2002). Time effects in creep of sands. In *Proceedings of the International Workshop on Constitutive and Centrifuge Geotechnical Modelling: Two Extremes, S. Springman (ed.), A.A. Balkema*.

Bragg, R.A. and Andersland, O.B. (1980). Strain rate, temperature, and sample size effects on compression and tensile properties of frozen sand. In *Proceedings of the 2nd International Symposium on Ground Freezing, Trondheim, Norway,* 34-47.

Briaud, J.-L. (1992). The pressuremeter. *A.A. Balkema, Rotterdam*, 322p.

Bridgman, P.W. (1912). Water, in the liquid and five solid forms, under pressure. In *Proceedings of the American Academy of Arts and Sciences, Vol. 47*, 441-558.

Brown, J. (1997). Disturbance and recovery of permafrost terrain. *Disturbance and Recovery in Arctic Lands*, 167-178.

Brown, J., Ferrians, O.J., Heginbottom, J.A. and Melnikov, E.S. (1998). Circum-Arctic map of permafrost and ground ice conditions. Scale 1:10'000'000. *Circum-Pacific map series, CP-45, Washington, D.C.: United States Geological Survey.*

Brown, R.J.E. and Kupsch W.O. (1974). Permafrost terminology. *Canadian National Research Council, Assoc. Comm. on Geotechnical Research Tech. Mem. III,* 62p.

Brown, R.J.E., Johnston, G.H., Mackay, J.R, Morgenstern, N.R. and Shilts, W.W. (1981). Permafrost distribution and terrain characteristics. *Chap. 2 in Permafrost Engineering Design and Construction, ed. G.H. Johnston. New York: Wiley*, 31-77.

Brown, W.H. (1925). A probable fossil glacier. *Journal of Geology, Vol. 33*, 464-466.

Budd, W.F. and Jacka, T.H. (1989). A review of ice rheology for ice sheet modelling. *Cold Regions Science and Technology, Vol. 16*, 107-144.

Burger, K.C., Degenhardt Jr., J.J. and Giardino, J.R. (1999). Engineering geomorphology of rock glaciers. *Geomorphology, Vol. 31*, 93-132.

Burland, J.B. (1967). Deformation of soft clay. *Dissertation, University of Cambridge*.

Calkin, P.E., Kaufmann, D.S., Przybyl, B.J., Whitford, W.B. and Peck, B.J. (1998). Glacier regimes, periglacial landforms, and Holocene climate change in the Kigluaik Mountains, Sward Peninsula, Alaska, USA. *Arctic and Alpine Research, Vol. 30*, 154-165.

Capps, S.R. (1910). Rock glaciers in Alaska. *Journal of Geology, Vol. 18*, 359-375.

Chamberlain, E.J., Groves, E. and Perham, R. (1972). The mechanical behaviour of frozen earth materials under high pressure triaxial tests conditions. *Géotechnique, Vol. 22*, 469-483.

Cheng, G. and Dramis, F. (1992). Distribution of mountain permafrost and climate. *Permafrost and Periglacial Processes, Vol. 3*, 83-91.

Clark, D.H., Steig, E.J., Potter, N. Jr., Fitzpatrick, J., Updike, A.B. and Clarke, G.M. (1996). Old ice in rock glaciers may provide long-term climate records. *EOS (Transactions, American Geophysical Union), Vol. 77*, 217&221-222.

Cole, D.M. (1983). The relationship between creep and strength behavior of ice at failure. *Cold Regions Science and Technology, Vol. 8*, 189-197.

Cole, D.M. (1987). Strain-rate and grain-size effects in ice. *Journal of Glaciology, Vol. 33*, 274-280.

Cole, D.M. (2001). The microstructure of ice and its influence on mechanical properties. *Engineering Fracture Mechanics, Vol. 68*, 1797-1822.

Corte, A.E. (1987). Rock glacier taxonomy. In *Rock Glaciers. eds: J.R. Giardino, J.F. Shroeder Jr. and J.D. Vitek. Allen & Unwin, Winchester*, 27-39.

Coulomb, C.A. (1776). Essai sur une application des règles, de maximis et minims à quelque problèmes de statique, relatifs à l'architecture. *Academy Royales des Sciences: Memoires de mathématique et physique par divers savants, Vol. 7*, 343-382.

Cross, C.V. and How, E. (1903). Geography and general geology of the quadrangle in Silverton folio. *U.S Geological Survey Folio 120*, 1-25.

Cundall, P.A. and Strack, O.D.L. (1979). A discrete numerical model for granular assemblies. *Géotechnique, Vol. 29,* 47-65.

Da Re, G. (2000). Physical mechanisms controlling the pre-failure stress-strain behavior of frozen sand. *PhD, Department of Civil and Environmental Engineering, Massachusetts Institute of Technology, Cambridge*, 569p.

Da Re, G., Santagata, M.C. and Germaine, J.T. (2001). LVDT based system for the measurement of the prefailure behavior of geomaterials. *Geotechnical Testing Journal, Vol. 24*, 288-298.

Dash, J.G., Fu, H. and Wettlaufer, J.S. (1995). The premelting of ice and its environmental consequences. *Reports on Progress in Physics, Vol. 58*, 115-167.

Davies, M.C.R., Hamza, O., Lumsden, B. and Harris, C. (2000). Laboratory measurements of the shear strength of ice-filled rock joints. *Annals of Glaciology, Vol. 31*, 463-467.

Davies, M.C.R., Hamza, O. and Harris, C. (2001). The effect of rise in mean annual temperature on the stability of rock slopes containing ice-filled discontinuities. *Permafrost and Periglacial Processes, Vol. 12*, 137-144.

Dempsey, J.P. (1991). The fracture toughness of ice. In *Ice-Structure Interaction, Proceedings of the IUTAM Symposium, St. John's, Newfoundland, Canada*, 109-142.

Dempsey, J.P., Palmer, A.C. and Sodhi, D.S. (2001). High pressure zone formation during compressive ice failure. *Engineering Fracture Mechanics, Vol. 68*, 1961-1974.

Deque, M., Marquet, P. and Jones, R.G. (1998). Simulation of climate change over Europe using a global variable resolution general circulation model. *Climate Dynamics, Vol. 14*, 173-189.

Derradji-Aouat, A. and Evign, E. (2001). A constitutive model for isotropic freshwater ice. *Canadian Geotechnical Journal, Vol. 38*, 818-827.

Desrues, J., Chambon, R., Mokni, M. and Mazerolle, F. (1996). Void ratio evolution inside shear bands in triaxial sand specimens studied by computed tomography. *Géotechnique, Vol. 46*, 529-546.

Dickinson, W., Cooper, P., Webster, B. and Ashby, J. (1999). A portable drilling rig for coring permafrost sediments. *Journal of Sedimentary Research, Vol. 69*, 518-527.

Dillon, H.B. and Andersland, O.B. (1967). Deformation rates of polycrystalline ice. In *Physics of Snow and Ice, Proceedings of the International Conference on Low Temperature Science, Sapporo, Vol. I*, 313-327.

Domaradzki, J. (1951). Blockströme im Kanton Graubünden. Ergebnisse der wissenschaftlichen Untersuchung des schweizerischen Nationalparks. *Kommission der Schweizerischen Naturforschenden Gesellschaft. III/24,* 177-235.

Domaschuk, L., Shields, D.H. and Rahman, M. (1991). A model for attenuating creep of frozen sand. *Cold Regions Science and Technology, Vol. 19*, 145-161.

Dowding, C.H., Cole, R.G. and Pierce, C.E. (2001). Detection of shear in soft soils with compliantly grouted TDR cables. In *Proceedings of the 2nd International Symposium and Workshop on Time Domain Reflectometry for Innovative Geotechnical Applications*.

Dramis, F., Govi, M., Guglielmin, M. and Mortara, G. (1995). Mountain permafrost and slope instability in the Italian Alps. The Val Pola landslide. *Permafrost and Periglacial Processes, Vol. 6*, 73-81.

Drucker, D.C. and Prager, W. (1952). Soil mechanics and plastic analysis of limit design. *Quarterly of Applied Mathematics*, *Vol. 10*, 157-165.

Duval, P., Ashby, M.F. and Anderman, I. (1983). Rate-controlling processes in the creep of polycrystalline ice, *Journal of Physical Chemistry, Vol. 87*, 4066-4074.

Ebinuma, T. and Maeno, N. (1992). Mechanical behaviors of polycrystalline ice containing pressurized gas enclosures. In *Physics and Chemistry of Ice, ed. N. Maeno and T. Hondoh, Sapporo, Japan: Hokkaido University Press,* 428-433.

EGS (1999). European Geophysical Services sa, Report: Borehole logging Muragl.

Elconin, R.F. and La Chapelle, E.R. (1997). Flow and internal structure of a rock glacier. *Journal of Glaciology, Vol. 43*, 238-244.

Elvin, A.A. and Shyam Sunder, S. (1996). Microcracking due to grain boundary sliding in polycrystalline ice under uniaxial compression. *Acta Materialia, Vol. 44*, 43-56.

Etzelmüller, B., Ødegård, R.S., Berthling, I. and Sollid, J.L. (2001). Terrain parameters and remote sensing data in the analysis of permafrost distribution and periglacial processes: Principles and examples from southern Norway. *Permafrost and Periglacial Processes, Vol. 12,* 79-92.

Feda, J. (1992). Creep of soils and related phenomena, *Elesevier, Amsterdam*, 422p.

Fisch, W. Sr., Fisch, W. Jr. and Haeberli, W. (1977). Electrical D.C. resistivity soundings with long profiles on rock glaciers and moraines in the Alps of Switzerland. *Zeitschrift für Gletscherkunde und Glazialgeologie, Vol. 13,* 239-260.

Fish, A.M. (1976). An acoustic and pressure meter method for investigation of the rheological properties of ice, *Cand. Sci. thesis, CRREL*, 205p.

Fish, A.M. (1983). Comparison of U.S.S.R. codes and US. Army manual for design of foundation on permafrost. *Cold Regions Science and Technology, Vol. 8*, 3-24.

Fish, A.M. (1984). Thermodynamic model of creep at constant stress and constant strain rate. *Cold Regions Science and Technology, Vol. 45*, 143-161.

Fish, A.M. (1985). Creep strength, strain rate, temparature and unfrozen water relationship in frozen soil. In *Proceedings of the 4th International Symposium on Ground Freezing, Sapporo*, 29-36.

Fish, A.M. (1991). Strength of frozen soil under a combined stress sate. In *Proceedings of the 6th International Symposium on Ground Freezing, Beijing*, 135-145.

Fish, A.M. (1993). Combined creep and yield model of ice under multiaxial stress. *International Journal of Offshore and Polar Engineering, Vol. 3; No.2*, 130-138.

Fish, A.M. (1994). Creep strength of Ottawa frozen sand under varying mean stress. In *Proceedings of the 7th International Symposium on Ground Freezing, Nancy*, 103-108.

Fish, A.M. and Sayles, F.H. (1981). Acoustic emissions during creep of frozen soils. *Acoustic Emissions in Geotechnical Engineering Practice, ASTM STP 750*, 194-206.

Fish, A.M. and Zaretsky, Y.K. (1997a). Ice strength as a function of hydrostatic pressure and temperature. *CRREL Report 97-6*, 23p.

Fish, A.M. and Zaretsky, Y.K. (1997b). Temperature effect on strength of ice under triaxial compression. In *Proceedings of the 7th International Offshore and Polar Engineering Conference, Honolulu*, 415-422.

Fowler, A.C. (1997). Mathematical Models in the Applied Sciences. *Cambridge University Press*, 402p.

Francke, J.L., Terrill, L.J. and Francke, C.T. (1994). Time domain reflectometry study at the waste isolation pilot plant. In *Proceedings of the Symposium on Time Domain Reflectometry in Environmental, Infrastructure, and Mining Applications, Evanston, IL, USA*, 555-567.

Fredlund, D.G. (2000). The implementation of unsaturated soil mechanics into geotechnical engineering. *Canadian Geotechnical Journal, Vol. 37*, 963-986.

Fredlund, D.G. and Rahardjo, H. (1993). Soil mechanics for unsaturated soils. *Wiley, New York*, 517p.

Fredlund, D.G. and Xing, A. (1994). Equations for the soil-water retention curve. *Canadian Geotechnical Journal, Vol. 31*, 521-532;1026.

Freitag, D.R. and McFadden, T.T. (1997). Introduction to cold regions engineering. *ASCE Press, USA*, 760p.

French, H.M. (1996). The periglacial environment. *Addison Wesles Longman Ltd., Essex , 2nd edition*, 341p.

French, H.M. (1999). Past and present permafrost as an indicator of climate change. *Polar Research, Vol. 18*, 269-274.

Frost, H.J. and Ashby, M.F. (1982). Deformation mechanisms maps. *Pergamon Press, Oxford*, 166p.

Fujii, Y. and Higuchi, K. (1972). On the permafrost at the summit of Mt. Fuji. *Seppyo 34*, 173-186.

Funk, M., Eichelmeyer, K. and Iken, A. (1994). Mechanisms of fast flow in Jacobshavns Isbrae, West Greenland: art II. Modeling of englacial temperatures. *Journal of Glaciology, Vol. 40*, 569-585.

Gagnon, R.E. and Gammon, P.H. (1995). Triaxial experiments in iceberg and glacier ice. *Journal of Glaciology, Vol. 41*, 528-540.

Gardner, A.R., Jones, R.H. and Harris, J.S. (1982). Strength and creep testing of frozen soils. In *Proceedings of the 3rd International Symposium on Ground Freezing, Hanover*.

Gardner, A.R., Jones, R.H. and Harris, J.S. (1984). A new creep equation for frozen soils and ice. *Cold Regions Science and Technology, Vol. 9,* 271-275.

Garnier, J., Ternet, O., Cottineau, L.-M. and Brown, C.J. (1999). Placement of embedded pressure cells. *Géotechnique, Vol. 49*, 405-414.

Geiser, F., Laloui, L. and Vulliet, L. (2000). On the volume measurement in unsaturated triaxial test. *Unsaturated Soils in Asia*, *Rahardjo, Toll & Leong (eds), Balkema*, 669-674.

GEOTEST (2000). Blockgletscher Muragl: Geophysikalische Bohrlochmessungen. *Bericht GEOTEST Nr. 99192.1, Rüegg F. and Holub P. (eds.)*, 12p.

Giardino, J.R. (1979). Rock glacier mechanics and chronologies: Mount Mestas, Colorado, *unpublished PhD Dissertation, University of Nebraska, Lincoln*, 244p.

Giardino, J.R. and Vick, S.G. (1985). Engineering hazards of rock glaciers. *Bulletin of the Association of Engineering Geologists, Vol. 22*, 201-216.

Giardino, J.R. and Vitek, J.D. (1988). The significance of rock glaciers in the glacial-periglacial landscape continuum. *Journal of Quaternary Science, Vol. 3*, 97-103.

Giardino, J.R., Shroeder, J.F. Jr. and Vitek, J.D. (1987). Rock Glaciers. *Allen & Unwin, Winchester*, 355p.

Gieck, R. (1989). Technische Formelsammlung. 29. Auflage, *Gieck Verlag, Germering, Germany*.

Glaser, S.D. and Hand, M.K. (1998). Imaging of rock fractures with low-frequency ultrasonic reflection/diffraction. *Geotechnical Testing Journal, ASTM, Vol. 21*, 317-327.

Glasstone, S., Laidler, K. and Eyring, H. (1941). The theory of rate process, *McGraw Hill, New York*, 611p.

Glen, B.J. (1955). The creep of polycrystalline ice. *Proceedings of the Royal Society of London, Series A. Mathematical and Physical Science, Vol. 228*, 519-538.

Glen, B.J. (1958). The mechanical properties of ice I: The plastic properties of ice. *Advances in Physics, Vol. 7*, 254-256.

Gold, L.W. (1977). Engineering properties of fresh-water ice. *Journal of Glaciology, Vol. 19,* 197-212.

Goldstein, R.J., Eckert, E.R.G., Ibele, W.E., Patankar, S.V., Simon, T.W., Kuehn, T.H., Strykowski, P.J., Tamma, K.K., Bar-Cohen, A., Heberlein, J.V.R., Davidson, J.H., Bischof, J., Kulacki, F.A., Kortshagen, U. and Garrick, S. (2002). Heat transfer – a review of 2000 literature. *International Journal of Heat and Mass Transfer, Vol. 45*, 2853-2957.

Goodman, D.J. (1980). Critical stress intensity factor (K_{Ic}) measurements at high loading rates for polycrystalline ice. In *Physics and Mechanics of ice, Proceedings of the IUTAM Symposium, Copenhagen, Denmark*, 129-146.

Goodman, D.J., Frost, H.J. and Ashby, M.F. (1981). The plasticity of polycrystalline ice. *Philosophical Magazine A, Vol. 43*, 665-695.

Goughner, R.R. and Andersland, O.B. (1968). Mechanical properties of a sand-ice system. *Journal of the Soil Mechanics and Foundation Division, ASCE, Vol. 94*, 923-950.

Greve, R., Weis, M. and Hutter, K. (1998). Paleoclimatic evolution and present conditions of the Greenland Ice Sheet in the vicinity of Summit: an approach by large-scale modelling. *Paleoclimates, Vol. 2*, 133-161.

Gruber, S. and Hoelzle, M. (2001). Statistical modelling of mountain permafrost distribution: local calibration and incorporation of remotely sensed data. *Permafrost and Periglacial Processes, Vol. 12*, 69-77.

Guodong, C. and Dramis, F. (1992). Distribution of Mountain Permafrost and Climate. *Permafrost and Periglacial Processes, Vol. 3*, 83-91.

Haeberli, W. (1973). Die Basis-Temperatur der winterlichen Schneedecke als möglicher Indikator für die Verbreitung von Permafrost in den Alpen. *Zeitschrift für Gletscherkunde und Glazialgeologie, Vol. 9*, 221-227.

Haeberli, W. (1975). Untersuchungen zur Verbreitung von Permafrost zwischen Flüelapass und Piz Grialetsch (Graubünden). *Versuchsanstalt für Wasserbau, Hydrologie und Glaziologie, ETH Zürich, Mitteilung Nr. 17*, 221p.

Haeberli, W. (1985). Creep of mountain permafrost: internal structure and flow of Alpine rock glaciers. *Versuchsanstalt für Wasserbau, Hydrologie und Glaziologie, ETH Zürich, Mitteilung Nr. 77, 142p.*

Haeberli, W. (1992). Construction, environmental problems and natural hazards in periglacial mountain belts. *Permafrost and Periglacial Processes, Vol. 3*, 111-124.

Haeberli, W. (1999). Consequences of global change effects on cryospheric processes and hydrology in alpine environments. In *Europe's cold regions: scenarios for landscape responses to global change, Grabherr, G., Heal, O.W., Gottfried, M., Pauli, H. and Reiter, K. (eds), Third Workshop of ARTERI, Dept. of Vegetation Ecology and Conservation Biology, University of Vienna, 13*.

Haeberli, W. (2000). Modern research perspectives relating to permafrost creep and rock glaciers: A discussion. *Permafrost and Periglacial Processes, Vol. 11*, 290-294.

Haeberli, W. and Vonder Mühll, D. (1996). On the characteristics and possible origins of ice in rock glacier permafrost. *Zeitschrift für Geomorphologie N.F., Vol. 104*, 43-57.

Haeberli, W., Huder, J., Keusen, H.-R., Pika, J. and Röthlisberger, H. (1988): Core drilling through rock glacier-permafrost. In *Proceedings of the 5th International Conference on Permafrost, Trondheim, Vol. 2*, 937-942.

Haeberli, W., Rickenmann, D., Zimmermann, M. and Rösli, U. (1990a). Investigation of 1987 debris flows in the Swiss Alps: General concept and geophysical soundings. *Hydrology in Mountain Regions. II - Artificial Reservoirs; Water and Slopes, IAHS Publ. No. 194,* 303-310.

Haeberli, W., Baltensperger, U., Bösch, H., Gäggeler, H., Gloor, M., Hoehn, E., Hofer, A., Holub, P., Keil, R., Keusen, H.R., Rössler, E., Schmid W., Stauffer, B., Vonder Mühll, D., Wagenbach, D., Wagner, S. and Zoller, H. (1990b). Pilot Analyses of permafrost cores from the active rock glacier Murtèl I, Piz Corvatsch, Eastern Swiss Alps. *A Workshop Report, VAW Arbeitsheft Nr. 9*, 38p.

Haeberli, W., Guodong, C., Gorbunov, A. P. and Harris, S. A. (1993). Mountain permafrost and climatic change. *Permafrost and Periglacial Processes, Vol. 4*, 165-174.

Haeberli, W., Wegmann, M. and Vonder Mühll, D. (1997). Slope stability problems related to glacier shrinkage and permafrost degradation in the Alps. *Eclogea Geologicae Helveticae 90*, 407-414.

Haeberli, W., Hoelzle, M., Kääb, A., Keller, F., Vonder Mühll, D. and Wagner, S. (1998). Ten years after drilling through the permafrost of the active rock glacier Murtèl, eastern Swiss Alps: Answered questions and new perspectives. *Proceedings of the 7th International Conference on Permafrost, Yellowknife, Canada,* 403-410.

Haeberli, W., Kääb, A., Hoelzle, M., Bösch, H., Funk, M., Vonder Mühll, D. and Keller, F. (1999a). Eisschwund und Naturkatastrophen im Hochgebirge. *Zürich: vdf, Hochschulverlag an der ETH*, 190p.

Haeberli, W., Kääb, A., Wagner, S., Vonder Mühll, D., Geissler, P., Haas, J.N., Glatzel-Mattheier, H. and Wagenbach, D. (1999b). Pollen analysis and ^{14}C age of moss remains in a permafrost core recovered from the active rock glacier Murtèl-Corvatsch, Swiss Alps: geomorphological and glaciological implications. *Journal of Glaciology, Vol. 45*, 1-8.

Hamilton, S.J. and Whalle, W.B. (1995). Rock glacier nomenclature: A re-assessment. *Geomorphology, Vol. 14*, 73-88.

Hampton, C.N., Jones, R.H. and Harris, J.S. (1988). The time response of frozen soils subjected to triaxial stress. In *Proceedings of the 5th International Symposium on Ground Freezing, Nottinghman, England,* 559-560.

Harris, C. and Davies, M.C.R. (2000). Gelifluction: Observations from large-scale laboratory simulations. *Arctic, Antarctic and Alpine Research, Vol. 32*, 202-207.

Harris, C. and Lewkowicz, A.G. (2000). An analysis of the stability of thawing slopes, Ellesmere Island, Nunavut, Canada. *Canadian Geotechnical Journal, Vol. 37*, 449-462.

Harris, C., Davies, M.C.R. and Coutard, J.-P. (1995). Laboratory simulation of periglacial solifluction: Significance of porewater pressures, moisture contents and undrained shear strengths during soil thawing. *Permafrost and Periglacial Processes, Vol. 6*, 293-311.

Harris, C., Rea, B.R. and Davies, M.C.R. (2000a). Geotechnical centrifuge modelling of gelifluction processes: validation of a new approach to periglacial slope studies. *Annals of Glaciology, Vol. 31*, 263-268.

Harris, C., Murton, J. and Davies, M.C.R. (2000b). Soft-sediment deformation during thawing of ice-rich frozen soils: results of scaled centrifuge modelling experiments. *Sedimentology, Vol. 47*, 687-700.

Harris, C., Davies, M.C.R. and Etzelmüller, B. (2001a). The assessment of potential hazards associated with mountain permafrost in a warming global climate. *Permafrost and Periglacial Processes, Vol. 12, 145-156.*

Harris, C., Haeberli, W., Vonder Mühll, D. and King, L. (2001b). Permafrost monitoring in the high mountains of Europe: the PACE project in the global context. *Permafrost and Periglacial Processes, Vol. 12, 3-11.*

Harris, C., Davies, M.C.R. and Rea, B. (2002). Centrifuge modeling of slope processes in thawing ice-rich soils. In *Proceedings of the International Conference on Physical Modelling in Geotechnics: ICPMG '02, Phillips, Guo & Popescu (eds), Balkema*, 297-302.

Hauck, C. (2001). Geophysical methods for detecting permafrost in high mountains. *Versuchsanstalt für Wasserbau, Hydrologie und Glaziologie, ETH Zürich, Mitteilung Nr. 171*, 204p.

Hauck, C., Guglielmin, M., Isaksen, K. and Vonder Mühll, D. (2001). Applicability of frequency-domain and time-domain electromagnetic methods for mountain permafrost studies. *Permafrost and Periglacial Processes, Vol. 12*, 39-52.

Haynes, F.D. and Karalius, J.A. (1977). Effect of temperature on the strength of frozen silt. *CRREL Report 77-3*, 27p.

He, P., Zhu, Y. and Cheng, G. (2000). Constitutive models of frozen soil. *Canadian Geotechnical Journal, Vol. 37*, 811-816.

Head, K.H. (1996). Manual of soil laboratory testing, Vol. 3: Effective Stress Tests. *John Wiley & Sons*, 454p.

Heginbottom, J.A., Brown, J., Melnikov, E.S. and Ferriens, O.J. (1993). Circumarctic map of permafrost and ground ice conditions. In *Proceedings of the 6th International Conference on Permafrost, Beijing,* 1132-1136.

Henry, K.S. (2000). A review of the thermodynamics of frost heave. *CRREL - Technical Report, TR-00-16,* 25p.

Herzog, P. and Ramholt, T. (1979). Deformations- und Festigkeitsuntersuchungen an Material aus dem Milchbucktunnel. *Mitteilungen der Schweizerischen Gesellschaft für Boden- und Felsmechanik, Nr. 112*, 6p.

Hobbs, P.V. (1974). Ice physics. *Impressum Oxford: Clarendon Press,* 837p.

Hoelzle, M., Wagner, S., Kääb, A. and Vonder Mühll, D. (1998). Surface movements and internal deformation of ice-rock mixtures within rock glaciers at Pontresina-Schafberg, Upper Engadin, Switzerland. In *Proceedings of the 7th International Conference on Permafrost, Yellowknife, Canada,* 465-471.

Hoelzle, M., Mittaz, C., Etzelmüller, B. and Haeberli, W. (2001). Surface energy fluxes and distribution models of permafrost in European mountain areas: an overview of current developments. *Permafrost and Periglacial Processes, Vol. 12*, 53-68.

Holdsworth, G., Kulvinen, K.C. and Rand, J.H. (1984). Ice drilling Technology. *CRREL - Special Report, 84-34,* 142p.

Hooke, R., Le, B., Dahlin, B.B. and Kauper, M.T. (1972). Creep of ice containing dispersed fine sand. *Journal of Glaciology, Vol. 11*, 327-336.

Hulme, M., Mitchell, J.F.B., Ingram, W.J., Lowe, J., Johns, T.C., New, M. and Viner, D. (1999). Climate change scenarios for global impact studies. *Global Environmental Change, Vol. 9*, S3-S19.

Hult, J.A.H. (1966). Creep in engineering structures. *Blaisdel Publishing Company, Waltham, MA*, 115p.

Humlum, O. (1982). Rock glacier types on Diski, central west Greenland. *Geografisk Tidsskrift, Vol. 82*, 59-66.

Humlum, O. (1998). The climatic significance of rock glaciers. *Permafrost and Periglacial Processes, Vol. 9*, 375-395.

Hutter, K., Laloui, L. and Vulliet, L. (1999). Thermodynamically based mixture models of saturated and unsaturated soils. *Mechanics of cohesive - frictional materials, Vol. 4*, 295-338.

Hutter, K. and Svendsen, B. (2000). Classical mixture models for polythermal ice. *Advances in cold-region thermal engineering and sciences : technological, environmental, and climatological impact, K. Hutter (ed.)*, 197-214.

Hvorslev, M.J. and Goode, T.B. (1963). Core drilling in frozen soils. In *Proceedings of the International Conference on Permafrost, Edmonton, Canada*, 364-371.

Ikeda, A. and Matsuoka, N. (2002). Degradation of talus-derived rock glaciers in the Upper Engadin, Swiss Alps. *Permafrost and Periglacial Processes, Vol. 13*, 145-161.

IPCC (2001). Contribution of working group II to the third assessment report of the intergovernmental panel on climate change (IPCC). *James J. McCarthy, Osvaldo F. Canziani, Neil A. Leary, David J. Dokken and Kasey S. White (Eds.), Cambridge University Press, UK,* 1000p.

Irving, D.H.B., Rea, B.R. and Harris, C. (2000). Physical modelling of the rheology of clean and sediment-rich polycrystalline ice using a geotechnical centrifuge: potential applications. *Deformation of Glacial Materials, Special Publication of the Geological Society, London, 176*, 47-55.

Isaksen, K., Odegard, R.S., Eiken, T. and Sollid, J.L. (2000). Composition, flow and development of two tongue-shaped rock glaciers in the permafrost of Svalbard. *Permafrost and Periglacial Processes, Vol. 11,* 241-257.

Isaksen, K., Holmlund, P. and Sollid, J.L. (2001). Three deep alpine permafrost boreholes in Svalbard and Scandinavia. *Permafrost and Periglacial Processes, Vol. 12,* 13-25.

Jacka, T.H. (1983). The time and strain required for the development of minimum strain-rate in ice. *Cold Regions Science and Technology, Vol. 8*, 261-268.

Jäckli, H. (1957). Gegenwartsgeologie des bündnerischen Rheingebietes. *Beiträge zur Geologie der Schweiz, geotechnische Serie, 36.*

Jessberger, H.L. (1996). Bodenvereisung. In *Grundbautaschenbuch: Teil 2, 5. Auflage, Ernst & Sohn, Berlin*, 109-136.

Johnson, J.P. (1978). Rock glacier types and their drainage systems, Grizzly Creek, Yukon Territory, *Canadian Journal of Earth Sciences, Vol. 15,* 1496-1507.

Johnson, J.P. (1984a). Periglacial conditions of instability and mass movement: A discussion. *Zeitschrift für Geomorphologie, Vol. 28*, 235-250.

Johnson, J.P. (1984b). Rock glacier formation by high-magnitude, low-frequency slope processes in the southern Yukon. *Annals of the Association of American Geographers, Vol. 74,* 408-419.

Johnson, J.P. and Nickling, W.G. (1979). Englacial temperature and deformation of a rock glacier in the Kluane Range, Yukon Territory, Canada. *Canadian Journal of Earth Sciences, Vol. 16*, 2275-2283.

Johnston, G.H. (1981). Permafrost Engineering Design and Construction. *Wiley, Toronto*, 540p.

Joly, M. (1970). Comportement rhéologique des liquides et suspensions. *Cahiers du Group Français du Rhéologie – No. Spécial "Rhéologie et hydrotechnique"*, 397-405.

Jones, S.J. (1982). The confined compressive strength of polycrystalline ice. *Journal of Glaciology, Vol. 28*, 171-177.

Jones, S.J. and Parameswaran, V.R. (1983). Deformation behavior of frozen sand-ice materials under triaxial compression. In *Proceedings* of *the 4th International Conference on Permafrost*, *Fairbanks, Alaska*, 560-565.

Kääb, A. (1998). Oberflächenkinematik ausgewählter Blockgletscher des Oberengadins. In *Beiträge aus der Gebirgs-Geomorphologie, Jahrestagung 1997 der Schweizerischen Geomorphologischen Gesellschaft. Versuchsanstalt für Wasserbau, Hydrologie und Glaziologie, ETH Zürich, Mitteilung Nr. 158*, 121-140.

Kääb, A. and Vollmer, M. (2000). Surface geometry, thickness changes and flow fields on creeping mountain permafrost: Automatic extraction by digital image analysis. *Permafrost and Periglacial Processes, Vol. 11*, 315-326.

Kääb, A., Haeberli, W. and Gudmundsson, G.H. (1997). Analysing the creep of mountain permafrost using high precision aerial photogrammetry: 25 years of monitoring Gruben rock glacier, Swiss Alps. *Permafrost and Periglacial Processes, Vol. 3*, 409-426.

Kääb, A., Gudmundsson, G.H. and Hoelzle, M. (1998). Surface deformation of creeping mountain permafrost. Photogrammetric investigations on Murtèl rock glacier, Swiss Alps. In *Proceedings of the 7th International Conference on Permafrost, Yellowknife, Canada,* 531-538.

Kääb, A., Isaksen, K., Eiken, T. and Farbrot, H. (2002). Geometry and dynamics of two lobe-shaped rock glaciers in the permafrost of Svalbard. *Norsk Geografisk Tidsskrift – Norwegian Journal of Geography, Vol. 56*, 152-160.

Kalifa, P., Ouillon G., and Duval, P. (1992). Microcracking and the failure of polycrystalline ice under triaxial compression. *Journal of Glaciology, Vol. 38*, 65-76.

Kane, W.F. (2000). Monitoring slope movement with time domain reflectometry (TDR). *Geotechnical Field Instrumentation: Applications for Engineers and Geologists. Sponsored by: ASCE Seattle Section Geotechnical Group Spring Seminar and the University of Washington Department of Civil Engineering, Seattle, Washington*.

Kane, W.F., Beck, T.J. and Hughes, J.J. (2001). Applications of the time domain reflectometry to landslide and slope monitoring. In *Proceedings of the 2nd International Symposium and Workshop on Time Domain Reflectometry for Innovative Geotechnical Applications*, 305-314.

Kaplar, C.W: (1963). Laboratory determination on the dynamic moduli of frozen soils and of ice. In *Proceedings of the first International Conference on Permafrost, Lafayette, Canada,* 293-301.

Keller, F. (1990). Permafrost im Baugrund. *Berichte und Forschungen, Geographisches Institut Freiburg, 3*, 115.

Keller, F. (1992). Automated mapping of mountain permafrost using the program PERMAKART within the geographical information system ARC/INFO. *Permafrost and Periglacial Processes, Vol. 3*, 133-138.

Keller, F. and Gubler, H.U. (1993). Interaction between snow cover and high mountain permafrost Murtèl/Corvatsch, Swiss Alps, In *Proceedings of the 6th International Conference on Permafrost, Beijing*, 332-337.

Keller, F., Frauenfelder, R., Gardaz, J.-M., Hoelzle, M., Kneisel, C., Lugon, R., Phillips, M., Reynard, E. and Wenker, L. (1998). Permafrost map of Switzerland. In *Proceedings of the 7th International Conference on Permafrost, Yellowknife, Canada,* 557-562.

King, L., Fisch, W.W., Haeberli, W. and Waechter, H.P. (1987). Comparison of resistivity and radio-echo soundings on rock glacier permafrost. *Zeitschrift für Gletscherkunde und Glaziologie, Vol. 23*, 77-97.

Kjartanson, B.H., Shields, D.H. Domaschuk, L. and Man, C-S. (1988). The creep of ice with the pressuremeter. *Canadian Geotechnical Journal, Vol. 25*, 250-261.

Kjartanson, B.H., Shields, D.H. and Domaschuk, L. (1990). Pressuremeter creep testing in ice: calibration and test procedures. *Geotechnical Testing Journal, Vol. 13*, 3-9.

Knutti, R., Stocker, T.F., Joos, F. and Plattner, G.K. (2002). Constraints on radiative forcing and future climate change from observations and climate model ensembles. *Nature, Vol. 416*, 719-723.

Konrad, S.K., Humphrey, N.F., Steig, E.J., Clark, D.H., Potter Jr., N. and Pfeffer, W.T. (1999). Rock glacier dynamics and paleoclimatic implications. *Geology, Vol. 27*, 1131-1134.

Koster, E.A. and Nieuwenhuijzen, M.E. (1992). Permafrost response to climatic change. *Catena Supplement, Vol. 22*, 37-58.

Kudryashov, B.B. and Yakovlev, A.M. (1991). Drilling in the permafrost. *Russian Translation Series: 84, Balkema, Rotterdam*, 318p.

Lachenbruch, A.H., Cladouhos, T.T. and Saltus, R.W. (1988). Permafrost temperature and the changing climate. In *Proceedings of the 5th International Conference on Permafrost, Trondheim*, 9-17.

Ladanyi, B. (1972). An engineering theory of creep of frozen soils. *Canadian Geotechnical Journal, Vol. 9*, 63-80.

Ladanyi, B. (1980). Stress- and strain-rate-controlled borehole dilatometer tests in permafrost. In *Proceedings of the Workshop on Permafrost Engineering, Quebec City*, 57-69.

Ladanyi, B. (1981). Mechanical behaviour of frozen soils. *Mechanics of Structured Media, Part B*, 205-245.

Ladanyi, B. (1982). Borehole and creep relaxation tests in ice-rich permafrost. In *Proceedings of the 4th Canadian Permafrost Conference, Calgary, Alberta*, 406-415.

Ladanyi, B. (1985). Stress transfer mechanism in frozen soils. In *Proceedings of the 10th Canadian Congress of Applied Mechanics*, 11-23.

Ladanyi, B. (2002). Behavior of ice/rock mixtures on slopes. In *Proceedings of the 11th International Conference on Cold Regions Engineering, ASCE, Anchorage, Alaska*.

Ladanyi, B. and Benyamina, M.B. (1995). Triaxial relaxation testing of a frozen sand. *Canadian Geotechnical Journal, Vol. 32*, 496-511.

Ladanyi, B. and Huneault, P. (1987). Use of the borehole dilatometer stress-relaxation test for determining the creep properties of ice. In *Proceedings of the 6th International Offshore Mechanics and Arctic Engineering Symposium, Houston, Texas*, 253-259.

Ladanyi, B. and Huneault, P. (1989). Cone penetrometer tests in permafrost - The Fox Tunnel, Alaska. *Mining in the Arctic*, 75-82.

Ladanyi, B. and Johnston G.H. (1973). Evaluation of in situ creep properties of frozen soils with pressuremeter. In *Proceedings of the 2nd International Conference on Permafrost, Yakutsk, U.S.S.R.*, 310-318.

Ladanyi, B. and Melouki, M. (1993). Determination of creep properties of frozen soils by means of the borehole stress relaxation test. *Canadian Geotechnical Journal, Vol. 30*, 170-186.

Ladanyi, B. and Morel, J.F. (1989). Effect of internal confinement on compression strength of frozen sand. *Canadian Geotechnical Journal, Vol. 27*, 8-18.

Landauer, J.K. (1955). Stress-strain relations in snow under uniaxial compression. *Journal of Applied Physics, Vol. 26*, 1493-1497.

Lange, R.G. (1968). Rotary drilling and coring in permafrost, Part I, Preliminary investigations, Fort Churchill, Manitoba. *CRREL - Technical Report, 95*, 22p.

Lange, R.G. (1973a). Investigation of sampling perennially frozen alluvial gravel by core drilling. In *Proceedings of the 2nd International Conference on Permafrost, Yakutsk,* U.S.S.R., 535-541.

Lange, R.G. (1973b). Deep rotary core drilling in ice. *CRREL - Technical Report, 94*, 48p.

Lange, R.G. and Smith, T.K. (1972). Rotary drilling and coring in permafrost, Part III, Deep core drilling, core analysis and borehole thermometry at Cape Thopson, Alaska. *CRREL - Technical Report, 95 III*, 24p.

Laue, J., Nater., P., Chikatamarla, R. and Springman, S.M. (2002). Der Einsatz von "pressure pads" in geotechnischen Labor- und Modellversuchen. *Messen in der Geotechnik; Braunschweig*.

Lehmann, F. and Green, A. (2000). Topographic migration of georadar data: Implications for acquisition and processing. *Geophysics, Vol. 65*, 836-848.

Lewkowicz, A.G. (1992). Factors influencing the distribution and initiation of active layer detachment slides on Ellesmere Island, Arctic Canada. *Periglacial Geomorphology*, 223-250.

Leysinger Vieli, G.J.-M.C. and Gudmundsson, G.H. (2001). Overriding or plug-flow: the advance of rock glaciers over different grounds. *EOS Trans. of the American Geophysical Union (AGU), Vol. 82, Fall Meet. Suppl*.

Lovell, C.W. (1957). Temperature effects on phase composition and strength of partially frozen soils. *Highway Research Board Bulletin, 168*, 74-95.

Lunardini, V.J. (2000). Climatic warming and permafrost. *Advances in Cold-Region Thermal Engineering and Science*, 483-502.

Ma, W., Wu, Z., Chang, X. and Sheng, Y. (1997). Effects of shear stress strength and the average normal stress on deformation of frozen soil. *Progress in Natural Science, Vol. 7*, 594-599.

Macari, E.J., Parker, J.K. and Costes, N.C (1997). Measurement of volume changes in triaxial tests using digital imaging techniques. *Geotechnical Testing Journal, ASTM, Vol. 20*, 103-109.

Madura, J.F. (1994). Ice coordinates. *http://www.ibiblio.org/water/wsn-archive/msg00037.html (Jun. '02)*.

Maisch, M., Wipf, A., Denneler, B., Battaglia, J. and Benz, C. (1998). Auswirkungen von Klimaänderungen auf die Gletscher und deren Vorfelder. *Projekt-Schlussbericht NFP 31*.

Manley, M.E. and Schulson, E.M. (1997). On the strain-rate sensitivity of columnar ice. *Journal of Glaciology, Vol. 43*, 408-410.

Martin, H.E. and Whalley, W.B. (1987). Rock glaciers I: rock glacier morphology: classification and distribution. *Progress in Physical Geography, Vol. 11*, 261-282.

Matsuoka, N. (2001). Solifluction rates, processes and landforms: a global review. *Earth-Science Reviews, Vol. 55*, 107-134.

Maurer, H.R., Springman, S.M., Arenson, L.U., Musil, M. and Vonder Mühll, D. (submitted). Characterisation of potentially unstable mountain permafrost - A multidisciplinary approach. In *Proceedings of the 8th International Conference on Permafrost, Zurich, Switzerland*.

McDowell, G.R. and Bolton, M.D. (2001). Micro mechanics of elastic soil. *Soils and Foundations, Vol. 41*, 147-152.

McDowell, G.R. and Harireche, O. (2002). Discrete element modelling of yielding and normal compression of sand. *Géotechnique, Vol. 52*, 299-304.

McRoberts, E.C. and Morgenstern, N.R. (1974). The stability of thawing slopes. *Canadian Geotechnical Journal, Vol. 11*, 447-469.

Meglis, I.L., Melanson, P.M. and Jordaan, I.J. (1999). Microstructural change in ice: II. Creep behaviour under triaxial stress conditions. *Journal of Glaciology, Vol. 45*, 438-448.

Melanson, P.M., Meglis, I.L., Jordaan, I.J. and Stone, B.M. (1999). Microstructural change in ice: I. Constant-deformation rate tests under triaxial stress conditions. *Journal of Glaciology, Vol. 45*, 417-437.

Mellor, M. (1972). Strength and deformability of rocks at low temperatures. *CRREL - Research Report, 294*.

Mellor, M. (1980). Mechanical properties of polycrystalline ice. In *Physics and Mechanics of Ice, Proceedings of the IUTAM Symposium, Copenhagen, Denmark*, 217-245.

Mellor, M. and Cole, D.M. (1982). Deformation and failure of ice under constant stress or constant strain-rate. *Cold Regions Science and Technology, Vol. 5*, 201-219.

Mellor, M. and Cole, D.M. (1983). Stress/strain/time relationship for ice under uniaxial compression. *Cold Regions Science and Technology, Vol. 6*, 207-230.

Mellor, M. and Sellmann, P.V. (1975). General considerations for drill system design. *CRREL - Technical Report, 264*, 40p.

Mellor, M. and Testa, R. (1969). Effect of temperature on the creep of ice. *Journal of Glaciology, Vol. 8*, 131-145.

Michel, B. (1978). The strength of polycrystalline ice. *Canadian Journal of Civil Engineering, Vol. 5*, 285-300.

Michel, B. (1980). Mechanical model of creep of polycrystalline ice with crack activity. In *Physics and Mechanics of ice, Proceedings of the IUTAM Symposium, Copenhagen, Denmark*, 1979 -264.

Mitchell, J.K. (1964). Shearing resistance of soils as a rate process. *Journal of the Soil Mechanics and Foundation Division, ASCE, Vol. 90*, 29-61.

Mitchell, J.K. (1976). Fundamentals of soil behaviour. *John Wiley & Sons, Inc., New York,* 422p.

Mitchell, J.K. and Campanella, R.G. (1968). Soil creep as a rate process. *Journal of the Soil Mechanics and Foundation Division, ASCE, Vol. 94*, 231-253.

Mittaz, C. Hoelzle, M. and Haeberli, W. (2000). First results and interpretation of energy-flux measurements over Alpine permafrost. *Annals of Glaciology, Vol. 31*, 275-280.

Mizuno, Y. (1998). Effect of hydrostatic confining pressure on the failure mode and compressive strength of polycrystalline ice, *The Journal of Physical Chemistry B, Vol. 102*, 376-381.

Moore, D.W. and Friedmann, I. (1991). Longitudinal section of an alpine rock glacier exposed south of Berthoud Pass, central Colorado Front Range. *Geol. Soc. Am. Abstr. Programms, Vol. 23*, 50.

Morgan, V.I. (1991). High-temperature ice creep tests. *Cold Regions Science and Technology, Vol. 19*, 295-300.

Muller, S.W. (1947). Permafrost or permanently frozen ground and related engineering problems. *Ann Arbor, Mich., J.W. Edwards,* 231p.

Muraleetharan, K.K. and Granger, K.K. (1999). The use of miniature pore pressure transducers in measuring matric suction in unsaturated soils. *Geotechnical Testing Journal, ASTM, Vol. 22*, 226-234.

Murat, J.R., Ladanyi, B. and Huneault, P. (1989). In situ determination of creep properties of sea ice with the pressuremeter. *Canadian Geotechnical Journal, Vol. 26*, 575-594.

Murayama, S. and Shibata, T. (1961). Rheological properties of clays, In *Proceedings of the 5th International Congress on Soil Mechanics and Foundation Engineering, Paris*, 269-273.

Musil, M. (2002). Inverting seismic and georadar data with applications to the Muragl rock glacier. *PhD, Institute for Geophysics, Swiss Federal Institute of Technology, Zurich, No. 14581*, 191p.

Musil, M., Maurer, H.R., Green, A.G., Horstmeyer, H., Nitsche, F.O., Vonder Mühll, D. and Springman, S. (submitted, a). Shallow seismic surveying of an alpine rock glacier. *Geophysics*.

Musil, M., Maurer, H.R., Holliger, K. and Green, A.G. (submitted, b). Internal structure of an alpine rock glacier based on crosshole georadar traveltimes and amplitudes. *Geophysics*.

Neaupane, K.M. and Yamabe, T. (2001). A fully coupled thermo-hydro-mechanical nonlinear model for a frozen medium. *Computers and Geotechnics, Vol. 28*, 613-637.

Nelson, F.E., Anisimov, O.A. and Shiklomanov, N.I. (2001). Subsidence risk from thawing permafrost. *Nature, Vol. 410*, 889-890.

Nicholas, J.W. and Butler, D.R. (1996). Application of relative age-dating techniques on rock glaciers on the La Sal Mountains, Utah – an interpretation of Holocene paleoclimates. *Geografiska Annaler Series A – Physical Geography, Vol. 78*, 1-18.

Nyberg, L., Stähli, M., Mellander, P.E. and Bishop, K.H. (2001). Soil frost effects on soil water and runoff dynamics along a boreal forest transect: 1. Field investigations. *Hydrological Processes, Vol. 15*, 909-926.

Nye J.F. (1953). The flow law of ice from measurements in glacier tunnels, laboratory experiments and the Jungfraufirn borehole experiment. *Proceedings of the Royal Society of London, Series A. Mathematical and Physical Science, Vol. 219*, 477-489.

O'Connor, K.M. and Dowding, C.H. (1999). GeoMeasurements by Pulsing TDR Cables and Probes. *CRC Press, Boca Raton, Florida*, 352p.

Oka, F., Adachi, T., Yashima, A. and Chu, L.L. (1994). Strain localization analysis by elasto-viscoplastic softening model for frozen sand. *International Journal for Numerical Methods in Geomechanics, Vol. 18*, 813-832.

Olyphant, G.A. (1983). Computer simulation of rock-glacier development under viscous and pseudoplastic flow. *The Geological Society of America bulletin, Vol. 94*, 499-505.

Osokin, N.I., Samoylov, R.S., Sosnovskiy, A.V., Sokratov, S.A. and Zhidkov, V.A. (2000). Model of the influence of snow cover on soil freezing. *Annals of Glaciology, Vol. 31*, 417-421.

Osterkamp, T.E. and Rommanovsky, V.E. (1999). Evidence for warming and thawing of discontinuous permafrost in Alaska. *Permafrost and Periglacial Processes, Vol. 10*, 17-37.

Oswell, J.M. and Hanna, A.J. (1997). Aspects of Geotechnical Engineering in Permafrost Regions. In *Innovative Design and Construction for Foundations and Substructures Subject to Freezing and Frost. ASCE Geotechnical Special Publication, No. 73*, 32-50.

Outcalt, S.I., Nelson, F.E. and Hinkel, K.M. (1990). The zero-curtain effect: Heat and mass transfer across an isothermal region in freezing soil, *Water Resources Research, Vol. 26*, 1509–1516.

Ouvry, J.F. (1985). Results of triaxial compression tests and triaxial creep tests on an artificially frozen stiff clay. In *Proceedings of the 4th International Symposium on Ground Freezing, Sapporo,* 207-212.

Palmer, A.C. (1972). Undrained plane-strain expansion of a cylindrical cavity in clay: a simple interpretation of the pressuremeter test. *Géotechnique, Vol. 22*, 451-457.

Palmer, A.C. (1991a). Fracture mechanics models of ice-structure interaction. In *Ice-Structure Interaction, Proceedings of the IUTAM Symposium, St. John's, Newfoundland, Canada*, 93-106.

Palmer, A.C. (1991b). Centrifuge modelling of ice and brittle materials. *Canadian Geotechnical Journal, Vol. 28*, 896-898.

Palmer, A.C. and Sanderson, T.J.O. (1991). Fractal crushing of ice. *Proceedings of the Royal Society London, A, Vol. 433*, 469-477.

Parameswaran, V.R. and Jones, S.J. (1981). Triaxial testing of frozen sand. *Journal of Glaciology, Vol. 27*, 147-155.

Perzyna, P. (1963). The constitutive equations for work hardening and rate sensitive plastic materials. In *Proceedings of Vibrational Problems, Warsaw, Vol. 4*, 281-290.

Petrenko, V.F. and Whitworth, R.W. (1999). Physics of ice. *Oxford University Press*, 373p.

Pfeffer, W.T., Humphrey, N.F., Amadei, B., Harper, J.T., and Wegmann, J. (2000). In-situ stress tensor measured in an Alaskan glacier. *Annals of Glaciology, Vol. 31*, 229-235.

Phillips, M., Bartelt, P. and Christen, M. (2000). Influences of avalanche-defence snow-supporting structures on ground temperature in Alpine permafrost. *Annals of Glaciology, Vol. 31*, 422-426.

Phukan, A. (1985). Frozen ground Engineering. *Englewood Cliffs - N.J.: Prentice-Hall*, 336p.

Pusch, R. and Feltham, P. (1980). A stochastic model of the creep of soils. *Géotechnique, Vol. 30*, 497-506.

Puswewala, U.G.A. and Rajapakse, R.K.N.D. (1993). Computation analysis of creep in ice and frozen soil based on Fish's unified model. *Canadian Journal of Civil Engineering, Vol. 20*, 120-132.

Randolph, M.F. (1983). Design consideration for offshore piles. In *Proceedings of the Conference on Geotechnical Practice In Offshore Engineering, Austin, Texas*, 422-439.

Rein, R.G., Vidyutkumar, V.H. and Sliepcevich, C.M. (1975). Creep of sand-ice system. *Journal of the Geotechnical Engineering Division, ASCE, Vol. 101*, 115-128.

Reynolds, O. (1885). On the dilatancy of media composed of rigid particles in contact. With experimental illustrations. *Philosophical Magazine, December*.

Reynolds, O. (1886). Experiments showing dilatancy, a property of granular material, possibly connected with gravitation. In *Proceedings of the Royal Institution of Great Britain, February*.

Riedel, H. and Rice, J.R. (1980). Tensile cracks in creeping solids. In *Fracture Mechanics: 12th Conference, Special Technical Publication 700, ASTM, Philadelphia*, 112-130.

Riseborough, D.W. and Smith, M.W. (1993). Modelling permafrost response to climate change and climate variability. In *Proceedings of the 4th International Symposium on Thermal Engineering Science of Cold Regions, Special Report 93-22*, 179-187.

Rist, M.A. and Murrell, S.A.F. (1994). Ice triaxial deformation and fracture. *Journal of Glaciology, Vol. 40*, 305-318.

Rist, M.A., Sammonds, P.R. and Murrell, S.A.F. (1991). Strain rate control during deformation of ice: An assessment of the performance of a new servo-controlled triaxial testing system. *Cold Regions Science and Technology, Vol. 19*, 189-200.

Rist, M.A., Jones, S.J. and Slade, T.D. (1994). Microcracking and shear fracture in ice. *Annals of Glaciology, Vol. 19*, 131-137.

Romanovsky, V.E. and Osterkamp, T.E. (2000). Effects of unfrozen water on heat mass transport processes in the active layer and permafrost. *Permafrost and Periglacial Processes, Vol. 11*, 219-239.

Salomon, W. (1929). Arktische Bodenformen in den Alpen. *Sitzungsbericht der Heidelberger Akademie der Wissenschaften. Mathematisch-naturwissenschaftliche Klasse 5. Abhandlungen Walter de Gruyter, No. 31.*

Savigny, K.W. and Morgenstern, N.R. (1986a). In situ creep properties in ice-rich permafrost soil. *Canadian Geotechnical Journal, Vol. 23*, 504-514.

Savigny, K.W. and Morgenstern, N.R. (1986b). Creep behaviour of undisturbed clay permafrost. *Canadian Geotechnical Journal, Vol. 23*, 515-527.

Sayles, F.H. (1966). Low temperature soil mechanics. CRREL Technical Note.

Sayles, F.H. (1968). Creep of frozen sands. CRREL Technical Report 190, 60p.

Sayles, F.H. (1973). Triaxial and creep tests on frozen Ottawa sand. In *Proceedings of the 2nd International Conference on Permafrost, Yakutsk, U.S.S.R.,* 384-391.

Sayles, F.H. (1974). Triaxial constant strain rate tests and triaxial creep tests on frozen Ottawa sand. *CRREL Technical Report 253*, 32p.

Sayles, F.H. (1988). State-of-the-art: mechanical properties of frozen soil. In *Proceedings of the 5th International Symposium on Ground Freezing, Nottingham, England,* 143-165.

Sayles, F.H. and Carbee, D.K. (1981). Strength of frozen silt as a function of ice content and dry unit weight. *Engineering Geology, Vol. 18*, 55-66.

Sayles, F.H. and Haines, D. (1974), Creep of frozen silt and clay. *CRREL Technical Report 252*, 54p.

Sayles, F.H., Baker, T.H.W., Gallavres, F., Jessberger, H.L., Kinosita, S., Sadocskiy, A.V., Sego, D. and Vyalov, S.S. (1987). Classification and laboratory testing of artificially frozen ground. *Journal of Cold Regions Engineering, Vol. 1*, 22-48.

Schofield, A.N. (1980). Cambridge geotechnical centrifuge operations. *Géotechnique, Vol. 30*, 227-268.

Schofield, A.N. and Wroth, C.P. (1968). Critical state soil mechanics. *McGraw-Hill Book, Company (UK) Limited, London*, 310p.

Schofield, R.K. (1935). The *pF* of the water in soil. In *Proceedings of the 3rd International Congress of Soil Science, Vol. 2*, 37-48 *and Vol. 3*, 182-186.

Schulson, E.M. (1990). The brittle compressive fracture of ice. *Acta Metallurgica et Materialia, Vol. 38*, 1963-1976.

Schulson, E.M. (2001). Brittle failure of ice. *Engineering Fracture Mechanics, Vol. 68*, 1839-1887.

Schulson, E.M. and Nickolayev, O.Y. (1995). Failure of columnar saline ice under biaxial compression: Failure envelops and brittle-to-ductile transition. *Journal of Geophysical Research, Vol. 100*, 22383-22400.

Schulson, E.M., Jones, D.E. and Kuehn, G.A. (1991). The effect of confinement on brittle compressive fracture of ice. *Annals of Glaciology, Vol. 15*, 216-221.

Sellmann, P.V. and Mellor, M. (1986). Drill bits for frozen fine-grained soils. *CRREL - Special Report, 86-27*, 33p.

Shibata, T., Adachi, T., Yashima, A., Takahashi, T. and Yoshioka, I. (1985). Time-dependence and volumetric change characteristic of frozen sand under triaxial stress condition. In *Proceedings of the 4th International Symposium on Ground Freezing, Sapporo,* 173-179.

Singh, A. and Mitchell, J.K. (1968). General stress-strain-time function for soils, *Journal of the Soil Mechanics and Foundation Division, ASCE, Vol. 94*, 21-46.

Singh, A. and Mitchell, J.K. (1969). Creep potential and creep rupture of soils. In *Proceedings of the 7th International Conference on Soil Mechanics and Foundation Engineering, Mexico*, 379-384.

Singh, S.K. and Jordaan, I.J. (1996). Triaxial tests on crushed ice. *Cold Regions Science and Technology, Vol. 24*, 153-165.

Sinha, N.K. (1978). Short term rheology of polycrystalline ice. *Journal of Glaciology, Vol. 21*, 457-473.

Sinha, N.K. (1979). Grain boundary sliding in polycrystalline materials. *Philosophical Magazine A, Vol. 40*, 825-842.

Sinha, N.K. (1984). Intercrystalline cracking, grain-boundary sliding, and delayed elasticity at high temperatures. *Journal of Material Science, Vol. 19*, 359-376.

Sinha, N.K. (1988). Crack-enhanced creep in polycrystalline material: strain-rate sensitive strength and deformation of ice. *Journal of Material Science, Vol. 23*, 4415-4428.

Sinha, N.K. (1989a). Elasticity of natural types of polycrystalline ice. *Cold Regions Science and Technology, Vol. 17*, 127-135.

Sinha, N.K. (1989b). Microcrack-enhanced creep in polycrystalline material at elevated temperature. *Acta Metallurgica, Vol. 37*, 3107-3118.

Slopeindicator (2002). Settlement probes for inclinometer casing. *http://www.slopeindicator.com (Jun. '02).*

SN 670 008a (1997). Identifikation der Lockergesteine: Labormethode mit Klassifikation nach USCS, *Schweizer Norm, Vereinigung Schweizerischer Strassenfachleute, VSS*, 16p.

Sokratov, S.A. and Barry, R.G.. (2001). Parameterization of an inter-seasonal variation in the thermo-insulation effect of snow cover on soil temperatures and energy balance. *www.breiling.org/snow/snowpubl/sokrat/Barrow.pdf, (Oct. '01)*.

Sollid, J.L. and Sørbel, L. (1992). Rock glaciers in Svbalbard and Norway. *Permafrost and Periglacial Processes, Vol. 3*, 215-220.

Sollid, J.L., Holmlund, P. Isaksen, K. and Harris, C. (2000). Deep permafrost boreholes in western Svalbard, northern Sweden and southern Norway. *Norsk Geografisk Tidsskrift – Norwegian Journal of Geography, Vol. 54*, 186-191.

Springman, S.M., Laue, J., Boyle, R., White, J. and Zweidler, A. (2001). The ETH Zurich Geotechnical Drum Centrifuge. *International Journal of Physical Modelling in Geotechnics, Vol. 1*, 59-71.

Springman, S.M., Jommi, C. and Teysseire, P. (in press). Instabilities on moraine slopes induced by loss of suction: a case history. *Géotechnique (Apr./May 2003)*.

Stähli, M. and Stadler, D. (1997). Measurement of water solute dynamics in freezing soil columns with time domain reflectometry. *Journal of Hydrology, Vol. 195*, 352-369.

Stearns, S.R. (1966). Permafrost (perennially frozen ground). *US Army Cold Regions Research and Engineering Laboratory, I-A2,* 72p.

Steinemann, S. (1958). Experimentelle Untersuchungen zur Plastizität von Eis. *Beiträge zur Geologie der Schweiz, Hydrologie Nr.10*, 72p.

Steig, E.J., Fitzpatrick, J.J., Clark, D.H. and Potter, N. Jr. (1998). The geochemical record in rock glaciers. *Geografiska Annaler, Vol. 80*A, 277-268.

Stoffel, L. (1995). Bautechnische Grundlagen für das Erstellen von Lawinenverbauungen im alpinen Permafrost. *Mitteilungen des Eidgenössischen Institutes für Schnee- und Lawinenforschung, Nr. 52,* 173p.

Swan, C.W. (1996). Behaviour of a sand in frozen and unfrozen states. In *Proceedings of the 8th International Conference on Cold Regions Engineering*, 483-493.

Szyszkowski, W. and Glockner, P.G. (1985). Modelling the time-dependent behaviour of ice. *Cold Regions Science and Technology, Vol. 11*, 3-21.

Tammann, G. (1900). Über die Grenzen des festen Zustandes IV. *Annalen der Physik, Serie 4, 2*, 1-31.

Tektronix, Inc. (1992). 1502B metallic time domain reflectometer, operator Manual.

Thalparpan, P. (2000). Lawinenverbauungen im Permafrost: Schlussbericht und Erläuterungen zu den Kapiteln IV und V der Richtlinien für den Lawinenverbau im Anbruchgebiet. *Eidgenössisches Institut für Schnee- und Lawinenforschung, Davos*, 92p.

Thavalingam, A., Bicanic, N. Robinson, J.I. and Ponniah, D.A. (2001). Computational framework for discontinuous modelling of masonry arch bridges. *Computers and Structures, Vol. 79*, 1821-1830.

Thorsteinsson, T. (2001). An analytical approach to deformation of anisotropic ice-crystal aggregates. *Journal of Glaciology, Vol. 47*, 507-516.

Ting, J.M. (1981). The creep of frozen sands: Qualitative and quantitative models. Research Report R81-5, Dept. of Civil Engineering, MIT, Cambridge, Massachusetts.

Ting, J.M. (1983a). Tertiary creep model for frozen sands. *Journal of the Geotechnical Engineering Division, ASCE, Vol. 109*, 932-945.

Ting, J.M. (1983b). On the nature of the minimum creep rate – time correlation for soil, ice, and frozen soil. *Canadian Geotechnical Journal, Vol. 20*, 176-181.

Ting, J.M., Martin, R.T. and Ladd, C.C. (1983). Mechanisms of strength for frozen sand. *Journal of the Geotechnical Engineering Division, ASCE, Vol. 109*, 1286-1302.

Toope, T.A., Arunachalam, V.M. and Muggeridge, D.B. (1991). Effect of bubble concentration on the tensile creep and fracture of granular T_1 ice. In *Proceedings of the 11th International Conference on Port and Ocean engineering und Arctic Conditions, St. John's*, 556-570.

Trausch-Giudici, J. (in prep.) Verformungsverhalten von Seebodenlehm. *Dissertation, Institute for Geotechnical Engineering, ETH Zurich*.

Tresca, H. (1869). Mémoire sur le poinçonnage et la théorie mécanique de la déformation des métaux. *Comptes rendues hebdomadaires des Séances de l'Académie des Sciences, Paris Vol. 68*, 1197-1201.

Truesdell, C.A., and R. Toupin. (1960). The classical field theories. In *Flügge's Handbuch der Physik, vol. 3, part 1, Springer-Verlag, Berlin*, 226-793.

Vaid, Y.P. and Campanella, R.G. (1977). Time-dependent behavior of undisturbed clay. *Journal of the Geotechnical Engineering Division, ASCE, Vol. 103*, 693-709.

Vinson, T. (1978). Parameter effects on dynamic properties of frozen soils. *Journal of the Geotechnical Engineering Division, ASCE, Vol. 104*, 1289-1306.

von Moos, M. (2002). Untersuchungen über das visko-elastische Verhalten von Schnee auf der Grundlage von triaxialen Kriechversuchen Zürich. *(ETH-Dissertation Nr. 13725, Zürich, 2000) Veröffentlichungen des Instituts für Geotechnik (IGT) der ETH Zürich, Band 214, vdf*, 141p.

Vonder Mühll, D. (1992). Evidence of intrapermafrost groundwater flow beneath an active rock glacier in the Swiss Alps. *Permafrost and Periglacial Processes, Vol. 3*, 169-173.

Vonder Mühll, D. (1993). Geophysikalische Untersuchungen im Permafrost des Oberengadins. *Versuchsanstalt für Wasserbau, Hydrologie und Glaziologie, ETH Zürich, Mitteilung Nr. 122*, 222p.

Vonder Mühll, D. (1996). Drilling in Alpine permafrost. *Norsk Geografisk Tidsskrift – Norwegian Journal of Geography, Vol. 50*, 17-24.

Vonder Mühll, D. (1999). Permafrost – Verbreitung und ausgewählte Aspekte. *Hydrologischer Atlas der Schweiz, Blatt 3.9*.

Vonder Mühll, D. (2002). Personal communications.

Vonder Mühll, D. and Holub, P. (1992). Borehole logging in Alpine permafrost, Upper Engadin, Swiss Alps, *Permafrost and Periglacial Processes, Vol. 3*, 125-132.

Vonder Mühll, D. and Klingelé, E.E. (1994). Gravimetrical investigation of ice-rich permafrost within the rock glacier Murtèl-Corvatsch (Upper Engadin, Swiss Alps). *Permafrost and Periglacial Processes, Vol. 5*, 13-24.

Vonder Mühll, D. and Schmid, W. (1993). Geophysical and photogrammetrical investigation of rock glacier Muragl I, Upper Engadin, Swiss Alps. In *Proceedings of the 6th International Conference on Permafrost, Beijing, China,* 1089-1095.

Vonder Mühll, D., Stucki, T., and Haeberli, W. (1998). Borehole temperatures in Alpine permafrost: a ten year series. In *Proceedings of the 7th International Conference on Permafrost, Yellowknife, Canada,* 1089-1095.

Vonder Mühll, D., Hauck, C., Gubler, H., McDonald, R. and Russill, N. (2001a). New geophysical methods of investigating the nature and distribution of mountain permafrost with special reference to radiometry techniques. *Permafrost and Periglacial Processes, Vol. 12*, 27-38.

Vonder Mühll, D., Delaloye, R., Haeberli, W., Hoelzle, M. and Krummenacher, B. (2001b). Permafrost Monitoring Switzerland PERMOS, *1. Jahresbericht 1999/2000*, *www.unibas.ch/vr-forschung/PERMOS (Jun. '02)*, 32p.

Vonder Mühll, D., Arenson, L. and Springman, S. (submitted). Temperature conditions in two Alpine rock glaciers. In *Proceedings of the 8th International Conference on Permafrost, Zurich*.

Vyalov, S.S., Gmoshinskii, V.G., Gorodetskii, S.E., Grigorieva, V.G., Zaretskii, I.K., Pekarskaia, N.K. and Shusherina, E.P. (1962). The strength and creep of frozen soils and calculations for ice-retaining structures. *CRREL Translation, No. 76*, 301p.

Wagner, S. (1990). Ice fabrics and air bubbles. *VAW Arbeitsheft Nr. 9*, 16-21.

Wagner, S. (1992). Creep of Alpine permafrost, investigated on the Murtèl rock glacier. *Permafrost and Periglacial Processes, Vol. 3*, 157-162.

Wagner, S. (1996a). DC resistivity and seismic refraction soundings on rock glacier permafrost in northwestern Svalbard. *Norsk Geografisk Tidsskrift – Norwegian Journal of Geography, Vol. 50*, 25-36.

Wagner, S. (1996b). Dreidimensionale Modellierungen zweier Gletscher und Deformationsanalyse von eisreichem Permafrost. *Versuchsanstalt für Wasserbau, Hydrologie und Glaziologie, ETH Zürich, Mitteilung Nr. 146*, 135p.

Wagner, W., Saul, A. and Pruss, A. (1994). International equations for the pressure along the melting and along the sublimation curve of ordinary water substance. *Journal of Physical and Chemical Reference Data, Vol. 23*, 515-527.

Wahrhaftig, C. and Cox, A. (1959). Rock glacier in the Alaska Range. *Bulletin of the Geological Society of America, 70*, 383-436.

Walters, D.A., Wong, R.C.K. and Kantzas, A. (1998). The application of computer-assisted tomography in the analysis of fracture geometry. *Geotechnical Testing Journal, ASTM, Vol. 21*, 328-335.

Wang, B. and French, H.M. (1995). In situ creep of frozen soil, Fenghuo Shan, Tibet Plateau, China. *Canadian Geotechnical Journal, Vol. 32*, 545-552.

Washburn, A.L. (1979). Geocryology. *Edward Arnold, London,* 406p.

Watanabe, K. and Mizoguchi, M. (2002). Amount of unfrozen water in frozen porous media saturated with solution. *Cold Regions Science and Technology, Vol. 34*, 103-110.

Wegmann, M., Gudmundsson, G.H. and Haeberli, W. (1998). Permafrost change in rock walls and the retreat of Alpine glaciers: a thermal modelling approach. *Permafrost and Periglacial Processes, Vol. 9*, 23-33.

Weiss, J., Grasso, J.-R. and Martin, R. (1998). AE and scaling laws in microstructurally controlled ice sample. In *Proceedings of the 6th Conference on Acoustic Emission/ Microseismic Activity in Geologic Structures and Materials*, 583-595.

Whalley W.B. and Martin, H.E. (1992). Rock glaciers: II models and mechanisms. *Progress in Physical Geography, Vol. 16*, 127-186

Wijeweera, H. and Joshi, R.C. (1991). Creep behavior of fine-grained frozen soils. *Canadian Geotechnical Journal, Vol. 28*, 489-502.

Williams, P.J. (1967a), Unfrozen water content of frozen soils and soil moisture suction. *Norwegian Geotechnical Institute, Publication No. 72*, 11-26.

Williams, P.J. (1967b). Unfrozen water in frozen soils: pore size – freezing temperature – pressure relationship. *Norwegian Geotechnical Institute, Publication No. 72*, 37-48.

Williams, P.J. (1967c). Suction and its effect in unfrozen water or frozen soils. *Norwegian Geotechnical Institute, Publication No. 72*, 27-35.

Williams, P.J. (1995). Permafrost and climate change: geotechnical implications. *Philosophical Transactions of the Royal Society London A: Physical Sciences and Engineering, Vol. 352*, 347-358.

Wilson, C. and Marmo, B. (2000). Flow in polycrystalline ice. *http://www.virtualexplorer.com.au/VEjournal/2000Volumes/Volume2/www/contribs/wilson/index.html, (Jun.'02) Vol. 2*.

Yasufuku, N., Springman, S.M. and Omine, K. (2001). Stress-strain relationship of frozen sand as a composite geomaterial. *Soils and Foundations, Vol. 41*, 17-30.

Yasufuku, N., Springman, S.M., Arenson, L.U. and Ramholt, T. (submitted). Stress-dilatancy behaviour of frozen sand in direct shear. In *Proceedings of the 8th International Conference on Permafrost, Zurich, Switzerland*.

Yershov, E.D. (1998). General Geocryology. *Cambridge University Press*, 580p.

Yu, H.S. and Collins, I.F. (1998). Analysis of self-boring pressuremeter tests in overconsolidated clays, *Géotechnique, Vol. 48*, 689-693.

Zhang, T. and Stamnes, K. (1998). Impact of climatic factors on the active layer and permafrost at Barrow, Alaska. *Permafrost and Periglacial Processes, Vol. 9*, 229-246.

Zhu Yuanlin and Carbee, D.L. (1983). Creep behaviour of frozen silt under constant uniaxial stress. In *Proceedings* of *the 4th International Conference on Permafrost*, *Fairbanks, Alaska*, 1507-1512.

Zhu Yuanlin and Carbee, D.L. (1984). Uniaxial compressive strength of frozen silt under constant deformation rates. *Cold Regions Science and Technology, Vol. 9*, 3-15.

Zhu Yuanlin and Carbee, D.L. (1987). Tensile strength of frozen silt. *CRREL Report 87-15*.

Zhu Yuanlin, He, P., Zhang, J. and Wang, J. (1997). Triaxial creep model of frozen soil under dynamic loading. *Progress in Natural Science. Vol. 7*, 465-468.

Zimmermann, M. (1990). Debris flows 1987 in Switzerland: geomorphological and meteorological aspects. *Hydrology in Mountain Regions. II - Artificial Reservoirs; Water and Slopes, IAHS Publ. No. 194,* 387-393.

Zimmermann, M. and Haeberli, W. (1992). Climatic change and debris flow activity in high-mountain areas – A case study in the Swiss Alps. *Catena Supplement, Vol. 22*, 59-72.

Acknowledgements

It must have been October 1991 when I saw the buildings of the Swiss Federal Institute of Technology (ETH) for the first time as an undergraduate student. And now, about eleven years later I have finally managed to leave ETH, most of which I never thought could be so fascinating. During all those years I met many people who (voluntarily and involuntarily) got involved in this project and in my additional work within the Institute for Geotechnical Engineering (IGT) and the ETH. There is a large number of colleagues, students, field helpers, mentors and friends who have played a part in my thesis, and whom I really would like to thank for their encouragement and sympathy during the time of my doctoral work in Zurich.

My special thanks go to SARAH SPRINGMAN for giving me the opportunity to work in the Institute and for the very interesting project (ETH grant: 0-20-509-98), which is (hopefully was) not a typical field of activity in geotechnical engineering here in Zurich. I also thank her very much for creating English sentences out of my sequences of English words for this thesis. And as her first official assistant (she actually had no choice...), I learned a lot concerning the setting-up of her group, about scientific working and about new methods of teaching students. Furthermore, I gained a lot from the many discussions we had during the years, including useful recommendations for my running activities.

I gratefully acknowledge the work and the recommendations of my two co-examiners: Prof. MICHAEL DAVIES (University of Dundee) and Prof. ANDREW PALMER (University of Cambridge), who gave me very useful hints about the weak points of my thesis. In addition, I would like to thank JAN LAUE and DANIEL VONDER MÜHLL for reading parts of an earlier version of this manuscript and JITENDRA SHARMA for additional corrections.

Since there had been no previous experience with permafrost within our Institute before I started, and it was not taught during my undergraduate study at ETH, I had to learn the basics for myself. Luckily, I had a couple of experts, who helped me during that process (and even beyond), and through several discussions with them I probably learned much more than what I could from hours of lectures. First of all, I thank DANIEL VONDER MÜHLL very much for his support and the open door he always had for every silly question. His additional invaluable experience in organising field campaigns and his extensive group of

acquaintances made life within our project much easier. In addition, members of the Glaciology and Geomorphodynamics group at the University of Zurich have always been a source of support. Luckily, Professor WILFRIED HAEBERLI, REGULA FRAUENFELDER, ANDI KÄÄB, CATHRINE MITTAZ and MARTIN HOELZLE were always interested in my work and therefore, synergy could be used and many interesting discussions emerged.

I would like to acknowledge the additional support that I received from the SLF (Swiss Federal Institute for Snow and Avalanche Research) in Davos. MARTIN SCHNEEBELI and GEORG KRÜSI helped me with the preparation of thin sections and MARCIA PHILLIPS kindly made the temperature data from Pontresina Schafberg available. MANFRED STÄHLI and HANNES WYDLER of the Institute of Terrestrial Ecology, ETH, offered their support with the TDR measurements and the physics of frozen soils.

I found a lot of support during the field investigations, which formed the basis for this work. Many, many people helped during different stages of the project, who I would like to thank sincerely for their commitment. I know that the conditions have sometimes been very difficult and therefore I appreciate their help even more. Surprisingly I never had problems in finding persons willing to help with the field investigations. These are in alphabetic order (in addition to several others mentioned within the acknowledgements): ANDRÉ BLANCHARD, MICHELE COSTA, PATRICE CRON, MICHAEL FUCHS, RALF GROSS, DANIELA HEITZ, CHARIS and FELIX KELLER, FRANK LEHMANN, SEPP LUTHIGER, HANSRUEDI MAURER, ROGER MEIER, MARTIN MUSIL, PHILIPPE NATER, ROCCO PANDURRI, DOMINIK PEYER, OLIVER PFEIFFER, MELANIE REYMOND, MYRIAM RUDOLF VON ROHR, MARTIN SCHUSTER, AUREL SCHWERZMANN, CORNELIUS SENN, STEPHAN SUTER, MARKUS VON MOOS and THOMAS WEBER.

The Institute of Biochemistry, University of Zurich, kindly offered their cold room for the storage of the valuable permafrost samples. Thanks to BAS VAN WIERINGEN, I knew that the samples were stored safely. Sadly, he lost his fight against cancer before I could show him the results. His dedication will always be remembered within this work.

I am very grateful for the support from various companies that have often shown interest in what we were doing: Oberengadiner Bergbahnen (Mr. MEILI), Celeriner Bergbahnen (BRUNO PAGANINI, GERD MÜLLER), Muragl Bergbahn (Mr. GROTHLO), Stump Bohr AG (FRANCO SALIS, HITCH and ROGER MEIER, CLAUDIO BAIADA, ULRICH SAMBETH), Heli Bernina (Fam. BÄRFUSS and their crew), Cambridge Insitu (PHILIP HAWKINS), Néstle Frisco Findus (Mr. ROHNER, Mr. BAUMGARTNER), Academia Engiadina (FELIX KELLER), Samedan (Mr. ITEN) and the Swiss Army.

For the successful laboratory testing, I am thankful to the workshop and the electronic lab of our Institute for the design and construction of the apparatus and the Swiss National Science Foundation for the funding (R'EQUIP programme: Nr. 21-53302.98). ADRIAN ZWEIDLER designed the triaxial test devices, which were then manufactured with great care by HEINZ BUSCHOR and FREDY EHRBAR. ERNST BLEIKER then programmed the software for the test control. He also was responsible for the successful data collection in the field. I appreciate the work of the workshop and the electronic lab very much, since they also helped me with various other difficulties that occurred during my time at the

Institute. A special thank you goes to MARCO SPERL who helped in every situation and found a solution for every problem, in the laboratory as well as in the field. And thanks to MARCO, we never feared starving.

Since our workshop had been completely absorbed with the construction of the triaxial test devices, I had to outsource the manufacturing of the mount for the positioning of the sample. DAVID GREEN of the mechanical workshop of the Cambridge University Engineering Department made a perfect job, which is gratefully acknowledged.

ANDREAS MEIER of the Institute of Cell Biology, ETH, helped with production of crushed ice and TOM JAGGI of the Institute for Building Materials, ETH, provided the cutting room of his Institute for my sample preparation. I appreciate their support very much.

Many thanks to all other colleagues at the IGT for a wonderful time. The experience in laboratory testing from DUSAN BYSTRICKY and TOM RAMHOLT are irreplaceable. With JOLANDA TRAUSCH GIUDICI I could always exchange the latest experiences with the new triaxial apparatus. And during the many discussions with other assistants in which I had to explain what I'm actually doing, I learned to analyse my data carefully, since the toughest questions came from people who have not been involved in permafrost research at all. And thanks to CHRISTIAN MÜLLER I learned that the crystalline structure of ice is not as simple as I thought at the beginning.

I could profit a lot from the diploma and semester theses carried out at our Institute that have been related to permafrost during the last three years, and I therefore have to thank NADINE ALMASI, MARTHA JOHANSEN and ERIK ANDERSEN for their questions and problems which I had to answer and solve.

Last but not least there was my family and BARBARA, who showed interest in what I'm doing and gave support throughout this time. I have to emphasise BARBARA's understanding and tremendous patience during all the years I worked hard for this project. But I also got numerous inputs and ideas from her while discussing problems during different stages or while she had to listen to my practice of presentations. She even understood that some of the questions had to be answered in the middle of the night and why I had to visit the rock glaciers in Wrangle National Park (Alaska) during our holidays. However, BARBARA managed to lead me through difficult periods and showed me that there is a life outside the ETH, and it seems as if I got caught by her love for the mountains.